**BOLU ABANT IZZET BAYSAL UNIVERSITY**

**THE GRADUATE SCHOOL OF NATURAL AND APPLIED SCIENCES**

**USE OF A SEMIFLUORINATED ACRYLIC COMPOUND**

**IN**

**REINFORCEMENT OF HIGH DENSITY POLYETHYLENE**

**AND**

**SOME MICROSPHERE PREPARATION STUDIES**

**DOCTOR OF PHILOSOPHY**

**UĞUR SOYKAN**

**BOLU, JANUARY 2019**

**BOLU ABANT İZZET BAYSAL UNIVERSITY**

**THE GRADUATE SCHOOL OF NATURAL AND APPLIED SCIENCES**

**DEPARTMENT OF CHEMISTRY**

**USE OF A SEMIFLUORINATED ACRYLIC COMPOUND**

**IN**

**REINFORCEMENT OF HIGH DENSITY POLYETHYLENE**

**AND**

**SOME MICROSPHERE PREPARATION STUDIES**

**DOCTOR OF PHILOSOPHY**

**UĞUR SOYKAN**

**BOLU, JANUARY 2019**

# APPROVAL OF THE THESIS

**USE OF A SEMIFLUORINATED ACRYLIC COMPOUND IN REINFORCEMENT OF HIGH DENSITY POLYETHYLENE AND SOME MICROSPHERE PREPARATION STUDIES** submitted by **Uğur SOYKAN** in partial fulfillment of the requirements for the degree of **Doctor of Philosophy** in **Department of Chemistry, The Graduate School of Natural and Applied Sciences of BOLU ABANT IZZET BAYSAL UNIVERSITY in 28/01/2019** by

**Examining Committee Members**                    **Signature**

Supervisor
Assoc. Prof. Dr. Sedat ÇETİN
Bolu Abant İzzet Baysal University

Member
Prof. Dr. Uğur YAHŞİ
Marmara University

Member
Prof. Dr. Özdemir ÖZARSLAN
Bolu Abant İzzet Baysal University

Member
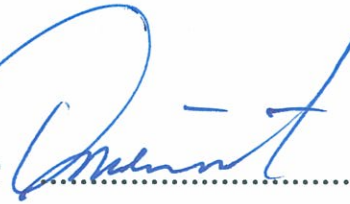Assoc. Prof. Dr. Gürcan YILDIRIM
Bolu Abant İzzet Baysal University

Member
Assist. Prof. Dr. Yasin KANBUR
Karabük University


**Graduation Date**                    :


Prof. Dr.  Ömer ÖZYURT

Director of Graduate School of Natural and Applied Sciences

THIS DISSERTATION IS DEVOTED TO MY LOVELY SON !!!

**DECLARATION**

I hereby declare that all information in this document has been obtained and presented in accordance with academic rules and ethical conduct. I also declare that, as required by these rules and conduct, I have fully cited and referenced all material and results that are not original to this work.

Uğur SOYKAN

_____

# ABSTRACT

USE OF A SEMIFLUORINATED ACRYLIC COMPOUND IN
REINFORCEMENT OF HIGH DENSITY POLYETHYLENE AND SOME
MICROSPHERE PREPARATION STUDIES
PHD THESIS
UĞUR SOYKAN
BOLU ABANT IZZET BAYSAL UNIVERSITY GRADUATE SCHOOL OF
NATURAL AND APPLIED SCIENCES
DEPARTMENT OF CHEMISTRY
(SUPERVISOR: ASSOC. PROF. DR. SEDAT ÇETİN)

BOLU, JANUARY 2019

In this dissertation, a novel semifluorinated acrylic compound, 3,3,4,4,5,5,6,6,7,7,8,8,8-dodecafluoro-5-methyloctyl-4-(acryloyloxy) benzoate (ABCF13) was synthesized, and it was used in the reinforcement of high density polyethylene (HDPE) by graft copolymerization and in the preparation of crosslinked microspheres by suspension polymerization. The prepared microspheres were then used in the preparation of blends with HDPE. The thermal, microstructural, mechanical and morphological properties of all the graft coproducts and the blends were investigated.

The monomer, ABCF13 was synthesized by the reaction of 3,3,4,4,5,5,6,6,7,7,8,8,8-dodecafluoro-1-octanol with p-acryloyloxybenzoyl chloride (ABC) in ethyl acetate containing triethylamine. ABC was precedingly synthesized by refluxing p-acryloyloxybenzoic acid, prepared by the reaction of acryloylchloride with p-hydroxybenzoic acid in basic medium, in thionly chloride.

The graft copolymerization of ABCF13 onto the HDPE was conducted by bulk-melt polymerization at 140°C by using benzoyl peroxide initiator in evacuated tubes. The products involving poly(ABCF13) units at varying percentages were prepared by employing ABCF13 at the concentrations of 5, 10, 15, 20, 30 and 40% in the reaction mixtures. The content of poly(ABCF13) in the products and percent conversion of the reactions were determined gravimetrically. The percent conversion exhibited consistent rise with the increase of monomer concentration in the reaction mixture and reached the maximum value, 97.9% at 40% ABCF13 yielding the product including 39.18% poly(ABCF13).

The DSC analyses of the coproducts displayed that there existed considerable and significant increases in both the melting temperature of crystalline domains and crystallinity in the HDPE matrix, consistent with the graft content. Maximum melting temperature 134.2°C was recorded with 13.96% poly(ABCF13), which was followed by decreases with the increasing of content. The XRD analyses revealed that the graft copolymerization gave rise to significant expansions in lateral dimensions of orthorhombic unit cells in crystalline domains of HDPE. The maxima, 7.420 Å in the parameter $a$ (0.84% increase) and 4,957 Å in the parameter $b$ (0.98% increase) were recorded with the product again involving 13.96% poly(ABCF13). The maxima were then followed by contractions. The parameter $c$, however, remained relatively unchanged. The grain (crystal) size increased initially, and after reaching maximum at 9.15% poly(ABCF13) reduced gradually with the content to sizes even smaller than that

of pure HDPE. The PALS analyses showed that the size of the free volumes increased almost linearly with the percentage of poly(ABCF13) while the free volume fraction in the products exhibited a decrease tendency with the content. Remarkable improvements were achieved in the mechanical behaviors of the products. The maximum tensile strength 43.75 MPa and elastic modulus 393 MPa (133% and 9% improvement, respectively) were achieved with the product comprising 9.15% poly(ABCF13). Moreover, the absorbed energy in the impact tests exhibited 100% increase in the same product. The SEM images of the tensile and impact fractured surfaces of the products showed that the samples possessed completely homogeneous structure without any phase separation. A gradual transition from ductile behavior to brittle nature was observed as poly(ABCF13) percentage increased in the matrix.

The well-shaped, crosslinked poly(ABCF13) microspheres with the size in the range of 10-100 µm were prepared by using ethylene glycol dimethacrylate (1%) (crosslinking agent), potassium persulfate (1.3%) (water soluble initiator), 0.2 g ABCF13 monomer in 150 mL of water at 70°C for 24 h reaction time and with the stirring rate of 500 rpm. Structure and morphology of the products were monitored by SEM. The poly(ABCF13) microsphere-HDPE blends involving the microspheres at varying ratios (1, 3, 5, 7 and 10%) were prepared by direct mixing of the components, and molded by microinjection molding for characterizations. The processing with the microspheres led to decrease in the melting temperature of HDPE in consistence with the content of microsphere. The $a$ and $b$ unit cell parameters increased initially and reached maxima with the sample including 5% microsphere, which were followed by dramatic decreases. The $c$ parameter remained relatively unchanged. The mechanical tests of the products displayed that there existed considerable improvements in tensile strength, modulus and impact strength. The maximum tensile strength 25.66 MPa, elastic modulus 499 MPa and maximum absorbed energy in the impact test 26.84 kJ/m$^2$ (29%, 42% and 41% improvement, respectively) were achieved with the blend involving 5% microsphere. After the maxima, the mechanical characters depicted weakening trend as the microsphere content increased in the matrix. The SEM analyses revealed that although there existed fibrillar formations in all samples, the extensions decreased with the increase of the microsphere content. While ductile behavior was observed with the formation of long-bulky extensions at low contents, brittleness started to prevail at high contents with some short and thin fibrils.

**KEYWORDS:** High Density Polyethylene, Semi-fluorinated Compound, Graft Copolymerization, Reinforcement, Unit Cell Parameters, Free Volume, Crosslinked Microsphere

# ÖZET

**YÜKSEK YOĞUNLUKLU POLİETİLENİN GÜÇLENDİRİLMESİNDE
YARIFLORLU AKRİLİK BİR BİLEŞİĞİN KULLANIMI VE BAZI
MİKROKÜRECİK HAZIRLAMA ÇALIŞMALARI
DOKTORA TEZİ
UĞUR SOYKAN
BOLU ABANT İZZET BAYSAL ÜNİVERSİTESİ
FEN BİLİMLERİ ENSTİTÜSÜ
KİMYA ANABİLİM DALI
(TEZ DANIŞMANI: DOÇ. DR. SEDAT ÇETİN)**

**BOLU, OCAK - 2019**

Bu tezde, yeni bir yarı-florlu akrilik bileşik, 3,3,4,4,5,5,6,6,7,7,8,8,8-dodekafloro-5-metiloktil-4-(akriloiloksi) benzoat (ABCF13) sentezlenmiştir. Bu bileşik aşı kopolimerizasyonu ile yüksek yoğunluklu polietilen (YYPE)'in güçlendirilmesinde ve süspansiyon polimerizasyonu ile çapraz bağlı mikrokürecikler mikrokürecikler hazırlanmasında kullanılmıştır. Hazırlanan mikrokürecikler ile daha sonra YYPE blendleri hazırlanmıştır. Tüm aşı ürünlerinin ve blendlerin termal, mikroyapısal, mekanik ve morfolojik özellikleri incelenmiştir.

ABCF13 monomeri trietilamin içeren etil asetat çözeltisi içerisinde 3,3,4,4,5,5,6,6,7,7,8,8,8-dodekafluoro-1-oktanolün p-akriloiloksibenzoil klorür (ABC) ile tepkimesiyle sentezlenmiştir. ABC, bazik ortamda akriloilklorürün p-hidroksibenzoik asit ile tepkimesiyle hazırlanan p-akriloiloksibenzoik asidin tiyonil klorür içerisinde geri soğutucu altında kaynatılmasıyla sentezlenmiştir.

ABCF13'ün YYPE üzerine aşı kopolimerleşmesi 140°C'de benzoil peroksit başlatıcısı kullanılarak vakumlu tüpler içinde kütle polimerleşmesiyle gerçekleştirilmiştir. Değişen yüzdelerde poli(ABCF13) birimleri içeren ürünler, ABCF13'ün tepkime ortamındaki %5, 10, 15, 20, 30 ve 40'lık derişimleri kullanılarak hazırlanmıştır. Ürünlerdeki poli(ABCF13) içeriği ve tepkimelerin yüzde dönüşümü gravimetrik olarak belirlenmiştir. Dönüşüm yüzdesi, tepkime ortamında monomer derişiminin artmasıyla artmış ve %40 ABCF13'de %39.18 poli(ABCF13) içeren ürün ile maksimum dönüşüme (%97,9) ulaşmıştır.

Ürünlerin DSC analizleri, hem kristalin bölgelerin erime sıcaklığında ve hem de YYPE matrisin kristallik yüzdesinde aşı içeriği ile orantılı olarak anlamlı ve önemli artışların olduğunu göstermiştir. Erime sıcaklığı %13.96 poli(ABCF13) içeren örnekte 134.2°C ile maksimuma ulaştıktan sonra aşı içeriğinin artmasıyla azalmıştır. XRD analizleri, aşı kopolimerleşmesinin, YYPE'nin kristalin bölgelerindeki ortorombik birim hücrelerinin yanal boyutlarında kayda değer genişlemelere sebep olduğunu göstermiştir. Maksimum değerler, $a$ parametresinde 7.420Å (%0.84 artış) ve $b$ parametresinde 4.957Å (%0.98 artış), yine %13.96 poli(ABCF13) içeren üründe kaydedilmiştir. Maksimum değerlerden sonra birim hücre parametrelerinde daralmalar olmuştur. Fakat, $c$ parametresinde önemli bir değişim kaydedilmemiştir. Tane (kristal) büyüklüğü başlangıçta artmıştır ve %9.15 poli(ABCF13) içeren örnekte maksimuma ulaştıktan sonra, aşı içeriğinin artması ile saf YYPE'den bile daha küçük kristal büyüklüklerine ulaşmıştır.

PALS analizleri, serbest hacmin poli(ABCF13) yüzdesiyle neredeyse doğrusal olarak arttığını gösterirken, ürünlerdeki serbest hacim oranın ise, aşı içeriğiyle azalma eğiliminde olduğunu göstermiştir. Ürünlerin mekanik davranışlarında anlamlı gelişmeler görülmüştür. %9.15 poli(ABCF13) içeren ürün ile maksimum gerilim direncine (43.75 MPa) ve elastik modülüne (393 MPa) (sırasıyla %133 ve %9 gelişme) ulaşılmıştır. Ayrıca, darbe testlerinde emilen enerji aynı üründe %100 artış göstermiştir. Ürünlerin gerilim ve çarpma ile kırılmış yüzeylerinin SEM görüntüleri herhangi bir faz ayrımı olmaksızın örneklerin tamamen homojen yapılara sahip olduğunu göstermiştir. Matris içerisinde poli(ABCF13) yüzdesinin artmasıyla sünek davranıştan kırılgan yapıya doğru kademeli bir geçiş olduğu da gözlenmiştir.

Boyutları 10-100 µm arasında iyi-şekilli, çapraz bağlı poli(ABCF13) mikrokürecikler, etilen glikol dimetakrilat (%1) (çapraz bağlayıcı), potasyum persülfat (%1.3) (suda çözünür başlatıcı), 0.2 g ABCF13 monomeri kullanılarak 150 mL su içinde 500 rpm karıştırma hızı ile 70°C'de 24 saat reaksiyon süresinde sentezlenmiştir. Ürünlerin yapısı ve morfolojisi SEM ile görüntülenerek incelenmiştir. Değişen oranlarda (%1, 3, 5, 7 ve 10) mikrokürecik içeren poli(ABCF13)-YYPE blendleri bileşenlerin doğrudan karıştırılmasıyla hazırlanmıştır ve ürünlerin karakterizasyonu için mikroenjeksiyon kalıplama ile kalıplanmıştır. Mikrokürecikler ile yapılan bu işlem, mikrokürecik içeriğinin artışı ile orantılı olarak YYPE'nin erime sıcaklığının azalmasına neden olmuştur. *a* ve *b* birim hücre parametreleri başlangıçta artmıştır ve %5 mikrokürecik içeren örnekle maksimum değerlere ulaştıktan sonra azalmıştır. *c* parametresi ise nispeten değişmeden kalmıştır. Ürünlerin mekanik testleri gerilme direncinde, modülde ve darbe dayanımda önemli gelişmeler olduğunu göstermiştir. Maksimum gerilme direnci (25.66 MPa), elastik modül (499 MPa) ve darbe testindeki maksimum absorbe edilen enerji (26.84 kJ/m$^2$) (sırasıyla %29, %42 ve %41 iyileştirme) %5 mikrokürecik içeren örnek ile elde edilmiştir. Maksimum değerlerden sonra, mekanik karakterler matristeki mikrokürecik içeriğinin artmasıyla azalma eğilimi göstermiştir. SEM analizleri, tüm numunelerde fibril oluşumları olmasına rağmen, mikrokürecik içeriğinin artmasıyla uzamaların azaldığını ortaya çıkarmıştır. Düşük içeriklerde uzun hacimli uzamaların oluşumu ile sünek davranış gözlenirken, yüksek içeriklerde bazı kısa ve ince fibriller ile kırılganlık hakim olmaya başlamıştır.


**ANAHTAR KELİMELER:** Yüksek Yoğunluklu Polietilen, Yarı-florlu bileşikler, Aşı Kopolimerleşmesi, Güçlendirme, Birim Hücre Parametreleri, Serbest Hacim, Çaprazbağlı Mikrokürecik.

# TABLE OF CONTENTS

# LIST OF FIGURES

xiii

# LIST OF TABLES

# LIST OF ABBREVIATIONS AND SYMBOLS

**TPs** : Thermoplastics

**PE** : Polyethylene

**HDPE** : High Density Polyethylene

**UHMWPE** : Ultra High Molecular Weight Polyethylene

**PP** : Polypropylene

**FPs** : Fluoropolymers

**SFP** : Semifluorinated Polymer

**FA** : Fluoroalkyl Acrylate

**CED** : Cohesive Energy Density

**LC** : Liquid Crystal

**LCPs** : Liquid Crystal Polymers

**TPE** : Thermoplastic Elastomer

**PSD** : Particle Size Distribution

**PVA** : Poly Vinyl Alcohol

**CNTs** : Carbon Nanotubes

**ATRP** : Atom Transfer Radical Polymerization

**ABCF13** : 3,3,4,4,5,5,6,6,7,7,8,8,8-trideca fluorooctyl 4-(acrloyloxy) benzoate

**ABA** : p-Acryloyloxybenzoic acid,

**ABC** : p-Acryloyloxybenzoyl chloride

**poly(ABCF13):** poly (3,3,4,4,5,5,6,6,7,7,8,8,8-trideca fluorooctyl 4-(acrloyloxy) benzoate)

**BPO** : Benzoyl Peroxide

**KPS** : Potassium Persulfate

**EGDMA** : Ethylene Glycol Dimethacrylate

**PTFE** : Polytetrafluoroethylene

**CDCl$_3$** : Deuterated Chloroform

**TMS** : Tetramethylsilane

**KBr** : Potassium Bromide

**MHz** : Megahertz

**$^o$C** : Celsius

**h** : Hour

***a, b, c*** : Lattice Parameters

| | |
|---|---|
| **µm** | **:** Micrometer |
| **nm** | **:** Nanometer |
| **min** | **:** Minute |
| **ppm** | **:** Parts Per Million |
| **λ** | **:** Wavelenght |
| **psi** | **:** Pounds Per Square Inch |
| **cal** | **:** Calorie |
| *T* | **:** Temperature |
| **rpm** | **:** Revoluations Per Minute |
| **mm** | **:** Millimeter |
| **g** | **:** Gram |
| **MPa** | : Mega Pascal |
| $\mathbf{V_f}$ | : Free Volume |
| $\mathbf{V_{occ}}$ | : Occupied Volume |
| $\mathbf{V_w}$ | : Van der Waals Volume |
| **V** | : Total Volume |
| **p-Ps** | : Para Positronium |
| **o-Ps** | : Ortho Positronium |
| **τ** | : Mean Lifetime |
| **λ** | : Annihilation Rate |
| **I** | : Intensity |
| **R** | : Free Volume Hole Radius |
| $\mathbf{\tau_1}$ | : Para Positronium Lifetime |
| $\mathbf{\tau_2}$ | : Free Positron Lifetime |
| $\mathbf{\tau_3}$ | : Ortho Positronium Lifetime |
| **FWHM** | **:** Full Width at Half Maximum |
| **d** | : Crystal Thickness |
| $\mathbf{\theta_B}$ | : Bragg Angle |
| **PALS** | : Positron Annihilation Lifetime Spectroscopy |
| **XRD** | **:** X-Ray of X-Ray Diffraction |
| **SEM** | **:** Scanning Electron Microscopy |
| **DSC** | **:** Differential Scanning Calorimetry |
| **FTIR** | **:** Fourier Transform Infrared Spectrometry |
| **NMR** | **:** Nuclear Magnetic Resonance |

# ACKNOWLEDGEMENTS

# 1. INTRODUCTION

Polymers defined as the macromolecules formed by linking together of the hundreds, thousands or more small molecules are indispensible materials which we encountered in all parts of our life. The imparting welcome properties into polymers is becoming more essential occupied issue for science due to the specific needs changing continuously. Therefore, the modification of the polymer materials so as to obtain desired, favorable and superior  characteristics has been widely interested by several scientists in many years (Swift et all., 1997). These engineered, modified and functionalized polymeric materials possessed vital importance in the field of polymer industry because of the large application areas and huge commercial demands (Teegarden, 2004).

There exists many types of valuable synthetic approaches for the polymer modification and designing. Especially surface modifications of polymers were performed by chemical, physical and biological routes ( Jasso-Gastinel and Kenny, 2017). The graft polymerization is known as chemical and common used surface modification method and the grafting allows to change in mechanical, thermal, photochemical, adhesion characteristics of polymer without any  structure deteriorations of polymer backbone (Cetin, 2004).

During the last two decades, a considerable progress has been came out in the preparation and modification of the polymer microsparticles. Polymer microparticles with diameters ranging from 1µm to 1000 µm have presented large platform for applications in the controlled drug carrying and releasing, electronic materials, coating, adhesives, catalysis, medicals as well as adsorbents (Guo et al., 2005; Saralidze et al., 2010 ; Yang et al. 2009).

# 2. GENERAL CHARACTERISTICS OF POLYMER BLENDS

## 2.1 General View on Polyolefins and HDPE

### 2.1.1 Polyolefins

Polyolefins are the most commonly used commodity thermoplastics with a wide variety of applications in polymer industry. The production of polyolefins is continuously increasing in the world day by day due to their particular and favorable physical and chemical properties and their distinct advantages such as lower cost, easy processing, good compatibility for obtaining desired properties, recyclability etc (Nwabunma and Kyu, 2008). The properties of polyolefins are highly affected by great number of parameters such as molecular weight, molecular weight distribution, tacticity, molecular structure and so on (Vasile, 2000a). Polyethylene and polypropylene are the major commercial polyolefins.

Polyethylene (PE) is a simple macromolecule with long backbone consisting of carbon atoms bonded covalently to one another with the double hydrogen atoms attached to each carbon. After the discovery of PE by Reginald Gibson and Eric Fawcett in 1933, PE has been still very vibrant, attractive and promising material over the past 80 years. The things making it important is its excellent and outstanding properties such as toughness, cheapness, flexibility, durability, chemical and impact resistivity, easy processing, near-zero moisture absorption, low coefficient of friction, broad density range, good flow behavior and thermal stability during processing etc. These mentioned properties made PE possessing broad application spectrum in many fields (Vasile and Pascu, 2005). On the other hand, there exists some disadvantages of PE. Namely, the properties such as the absence of the chemical functional groups in its structure, hardness in dyeing, insufficient compatibility with other components in combinations with polar polymers, sticking during processing, low surface energy etc. limit its practical uses (Soykan, 2013).

2

There exists many types of polyethylene, all having essentially the same polymer backbone. The variations arises mainly from branches and, to a lesser extent, defects in the backbone such as vinyl groups often located at chain ends. Branches and other defects modify the nature of the material and play a dominant role in sample's density and crystallinity level. In general, an increase in the concentration of branches results in lower density of the material. A better packaging in crystalline regions leads to higher density as well as an increase in the degree of crystallinity (Peacock, 2000).

The commercial types of PE can be ranked as follows: LDPE (low density PE), LLDPE (linear low density PE), HDPE (high density PE), HMWPE (high molecular weight polyethylene), UHMWPE (ultra high molecular weight polyethylene), HDXLPE (high density cross-linked PE), PEX (cross-linked PE), MDPE (medium density PE), and VLDPE (very low density PE) (Eriman, 2008). Some types of PE with branching structure and density were demonstrated in Figure 2.1.



| LDPE | LLDPE/VLDPE | HDPE |
|---|---|---|
| $0.910–0.940$ g cm$^{-3}$ | $0.915–0.94$ g cm$^{-3}$/ $0.88–0.915$ g cm$^{-3}$ | $0.941–0.97$ g cm$^{-3}$ |
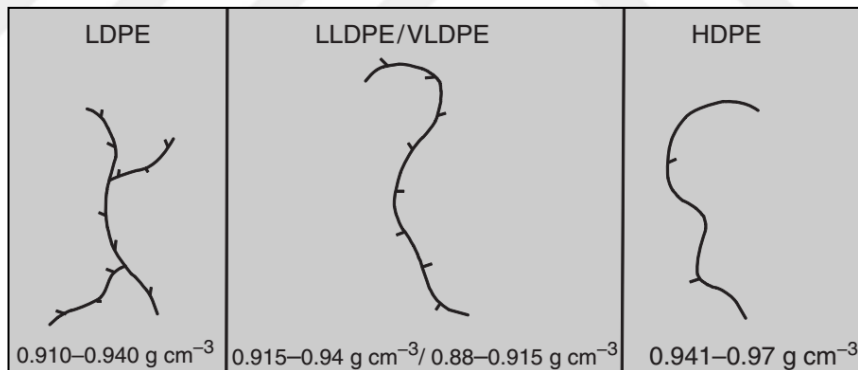
**Figure 2.1.** The simple demonstration of LDPE, LLDPE, VLDPE and HDPE molecules.

### 2.1.2   HDPE

HDPE  is chief part of the polyolefin family with the vast application fields in many industries (daily bottles, fuel tanks of cars, packaging container, toys, carrier bag, wire coating, cable insulation, pipes etc). Therefore, HDPE and their derived coproducts have attracted much attention by scientists for many years to produce

3

materials having superior properties. Among the types of PE, HDPE is clearly the closest in structure to pure PE and is basically composed of unbranched molecules with a few defects in structure without damaging its linearity. Therefore typical HDPE, knows as semi-crystalline polymer, possesses a greater proportion of crystalline regions (its degree of crystallinity ranges from 62 to 82%) thanks to extremely low level of flaws hindering the organization. Due to its linearity with a little entanglements in the melt, HDPE molecules have a tendency to be aligned through the flow direction during processing in melt. HDPE is also vulnerable to warpage due to higher crystallinity and shrinked due to orientation while cooling (Solomon, 1996; Billmeyer, 1984). Furthermore, HDPE has not only larger rigidity and hardness compared to lower density materials with a molecular weight below 300,000 g/mol but also high compressive and tensile strengths. Moreover, HDPE acquire a good reputation in polymer industry due to abrasion-resistant characteristics to scuffing, gouging and scraping. Water, moisture, acids (exception of strong oxidizing acids at certain temperature) and most alkalis have no effects on HDPE because of its good chemical resistance to corrosion (Vesile and Pascu, 2005b).

HDPE can be produced by four methods; (I) Ziegler (II) Philips (III) Standard Oil and (IV) Union Carbide processes. While Union Carbide processes is carried out in gas phase via organochromium compounds employed in polymerization, the other processes are conducted in solution or slurry phases by using different nature catalysts (Azapagic et all., 2003)  The princible properties of HDPE are illustrated in Table 2.1.

HDPE is a semi-crystalline polymer with the formation of spherulites consisting of both crystalline and amorphous regions. The crystal structures are modified by the addition of the nucleating agents, which brings about the formation of either uniform and different shaped or the defective and damaged spherulites. The main factors governing development of the HDPE spherulites are molecular weight and crystallization temperature as well as molecular weight distribution and impurities. Crystalline regions of HDPE is characterized greatly ordered, neatly folded, layered (in parallel), dense and packed molecular chains. The PE chains are principally folded in the growing planes with a lamellar structures. Within the crystal regions, HDPE includes orthorhombic crystal cell with the extended chain

4

conformations (planar zigzag) (Pierra et all., 1997). The simple orthorhombic unit cells of HDPE is demonstrated in Figure 2.2. The unit cell parameters of HDPE highly commensurate with packing properties to be effected by interaction between molecules comprising the polymer chains.

**Table 2.1.** Principle properties of HDPE (Peacock, 2000).

| Property | HDPE |
|---|---|
| Density (g/cm3) | 0.94–0.97 |
| Degree of crystallinity (% from density) | 62–82 |
| Degree of crystallinity (% from calorimetry) | 55-77 |
| Flexural modulus (psi @ 73°) | 1450,000 - 225,000 |
| Tensile modulus (psi) | 155,000 - 200,000 |
| Tensile yield stress (psi) | 2,600 - 4,5000 |
| Tensile strength at break (psi) | 3,200 - 4,500 |
| Tensile elongation at break (%) | 10 - 1,500 |
| Shore hardness Type D | 66 - 73 |
| Izod impact strength (ft-lb/in. of notch) | 0.4 - 4.0 |
| Melting temperature (°C) | 125 - 132 |
| Heat distortion temperature (°C@66 psi) | 80 - 90 |
| Heat of fusion (cal/g) | 38 - 53 |
| Thermal expansivity (106 in/in/°C) | 60 - 110 |
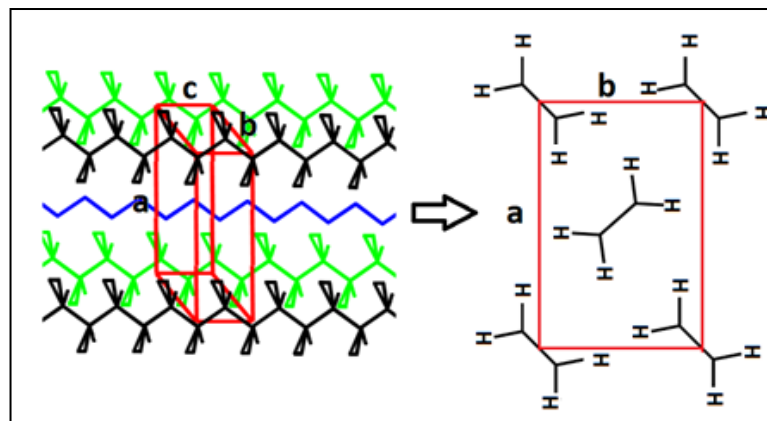


**Figure 2.2.** Orthorhombic unit cells of HDPE.

5

## 2.2    Fluoropolymers (FPs)

Since poly(tetrafluoroethylene) (PTFE) was serendipitously discovered by scientists at DuPont in 1938, polymers including fluorine atom with lower steric hindrance have a continuously growing role in the material sciences. Fluoropolymers are vastly preferred due to the characteristics of chemical resistance, high thermal stability, insulating ability, low refractive index and surface energy (Iacono, 2008). These unique, favorable and impressive characteristics, make fluoropolymers poineer in polymer industry, and they have been utilized in a large number of application areas such as coating industry, production of different types of membranes, housewares for cooking or baking, fabrication of high performance thermoplastics and elastomers for automotive industry, aeroscope, military and biomedical technology (Scheirs, 1997). Moreover, fluorinated polymers possess inert and durable nature because of C-F bond having larger dissociation energy comparing to polymer containing hydrogen instead of fluorine. The substituting fluorine for hydrogen in a number of fully or partially fluorinated polymer molecules cause three main useful corridors; (I) increase in service temperature and reduction in flammability (II) lower surface energy, supporting anti-adhesiveness, lower friction coefficient, self-lubricating and (III) impressive optical and electrical properties (Ameduri and Sawada, 2017). The change in their properties with the increase of fluorine content is shown in Table 2.2 (Ebnesajjad, 2013). Furthermore, in order to understand another effect of fluorine atoms on physical properties of the polymers, Marchionni et all. investigated the cohesive energy density (CED) of  perfluorinated and hydrogenated paraffins and ethers with respect to its dependence on oxygen content and chain length. CED implies the energy gained by arranging the atoms in a crystalline state per unit volume. The findings revealed that the perfluorocarbons with sufficiently high molecular weight possessed  much lower CED value (0.6 times) comparing to that of the relative hydrocarbons when neglecting the presence of oxygen atoms in the main chain. The higher Van der Waals radius of fluorine and the larger polarity of the C-F bond are resposible for the formation of this CED diffcence (Marchionni et all., 1993).

**Table 2.2.** The some effects of increasing fluorine concentration of polymer.

| Property | Impact |
|---|---|
| Chemical Resistance | Increases |
| Melting Point | Increases |
| Coefficient of Friction | Decreases |
| Thermal Stability | Increases |
| Dieletric constant | Decreases |
| Dissipation factor | Decreases |
| Volume and Surface Resistivity | Increases |
| Flame Resistance | Increases |

### 2.2.1 Partially Fluorinated Polymers

Fluoropolymers can be divided into two categories: (I)fully fluorinated (perfluorinated) and (II) partially fluorinated polymer. Conventionally, partially fluorinated polymer can be defined as a polymer containing other atoms (H, O, Cl etc.) in their structures as well as carbon (C) and fluorine (F) and they become homopolymer, copolymer or pendant units in a polymer. Polyvinylidene fluoride (PVDF), ethylene tetrafluoro ethylene copolymer (ETFE), ethylene chlorotrifluoroethylene copolymer (ECTFE) are the most important and common examples of the partially fluorinated polymer (Ebnesajjad, 2013). Since the practical utilities of fluoropolymers are highly restricted because of both compatibility trouble between fluorocarbon polymer and other conventional hydrocarbon polymer and difficulties in processability, the synthesis of copolymers cooperated with more fluorinated groups is required to impart unique features to polymers. In the light of this purpose, the numerous researcher focused on the both production and design of partially fluorinated polymer (Yao et all., 2014). Especially, flouroalkyl acrylate (FA) polymers attracted much interests thanks to considerably low compatibility with common solvents, remarkable low surface energy and friction coefficient, excellent chemical and thermal stability, low refractive index, high transmittance and self-organization (Erol I, 2009; Thomas RR, 1997). Moreover, FA polymers are utilized as fluorine based oil and water repellents for varying materials such as carpet, paper, textile etc. (Ameduri and Sawada, 2017). The molecular design concept of flouroalkyl acrylate polymer is depicted in Figure 2.3.
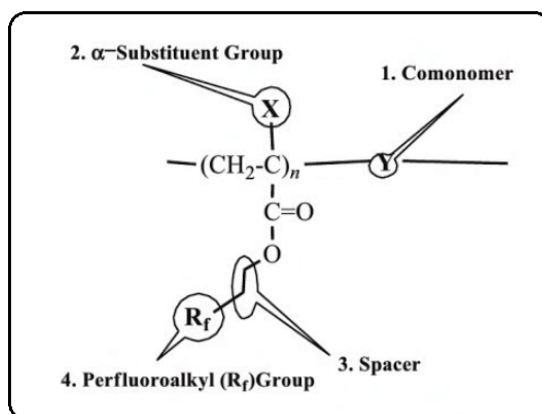
**Figure 2.3.** Molecular design concept of FA polymer.

The hydrocarbon main chain is clearly responsible for mechanical properties and thermal stability of the poly(fluoroalkyl acrylate)s, while surface characters of the polymers highly depended on structures of the side chain $R_f$, which is usually a perfluorinated unit including carbon and fluorine (Honda, 2005). In literature, studies performed in detail in order to control the mobility of $R_f$ units, many types of spacer groups such as methylene (-CH$_2$-) with varying chain lengths, ether (-O-), sulfone (-SO$_2$-), phenyl (-C$_6$H$_6$), sulfonamide and triazole groups have been reported (Ameduri and Sawada, 2017). Furthermore, synthesis of the fluorinated poly(meth)acrylates were performed by (I) random copolymerization via radical polymerization, controlled/"living" radical polymerization and polymers bearing activated groups, (II) block copolymerization via sequential polymerization, functionalization of as-prepared block copolymer and obtained from commercially available polymers, (III) graft and star fluorinated copolymerizations (Yao et all., 2014). Although large number of studies on the surface structures of fluorinated poly(meth)acrylate-based block copolymers, chain-end-functionalized polymers with well-defined perfluorinated and semifluorinated group(s), there are little reported on fluorinated poly(meth)acrylate-based graft and star copolymers in literature (Hirao et all., 2007). Additionally, flouroalkyl acrylate polymers were indispensible for the modification and designing of some polymer properties such as surfaces (Ren et all, 1995; Abrakhi et all., 2013), electro-optics and morphological (Zheng et all., 2008; Schulte et all., 2000), coating (Verweire et all., 2000), membrane etc (Nagai et all., 2001).

### 2.2.2 Liquid Crystalline Properties of Fluoropolymers

#### 2.2.2.1 Liquid Crytalline Polymers (LCPs)

At the beginning of 1900, German physicist Otto Lehmann announced new distinct state of maters rather than solid, liquid and gaseous phases and he named this matter as the liquid crystal. The term of liquid crystal obviously signifies the intermediate state between the isotropic (liquid) and crystalline (solid) states being neither crystalline nor liquid as depicted in Figure 2.4 (Wang XJ and Zhou QF, 2004).
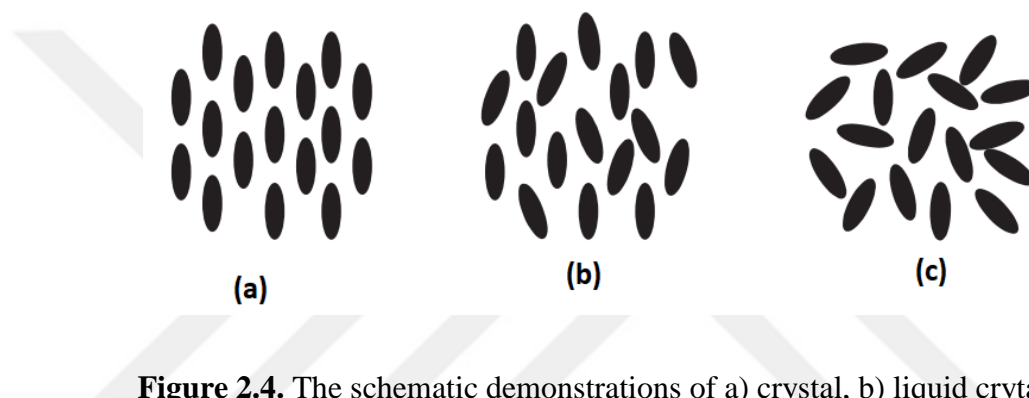


**Figure 2.4.** The schematic demonstrations of a) crystal, b) liquid crytal and c) liquid.

The main chemical structures of liquid crystals could be classified as rodic liquid crystals (regarded as highly anisotropic rigid rod-like molecules), discotic liquid crystals (regarded as rigid flat aromatic core connected with flexible side chains bonded different possitions) and amphiphilic liquid crystals (regarded as tadpole like molecules composed of both hydrophilic and hydrophobic groups located at one end and at another end of the molecule, respectively). There also exists the two or three dimensional polymers depicting highly anisotropic property in both solid and liquid crystal phases, which called as liquid crystal polymer (LCPs). They are made up of basically repeating structural small mesogenic units being rod like, disc like or rod-disc like together in one. Mesogen units can be chemically bonded in the backbone (known as main chain LCPs) or attached to the main chain as a side pendant unit (known side chain LCPs). Furthermore LCPs can have crosslinked network structures. (Wang XJ and Zhou QF, 2004). Figure 2.5 illustrates the some kinds of main chain and side chain LCPs structures.

9
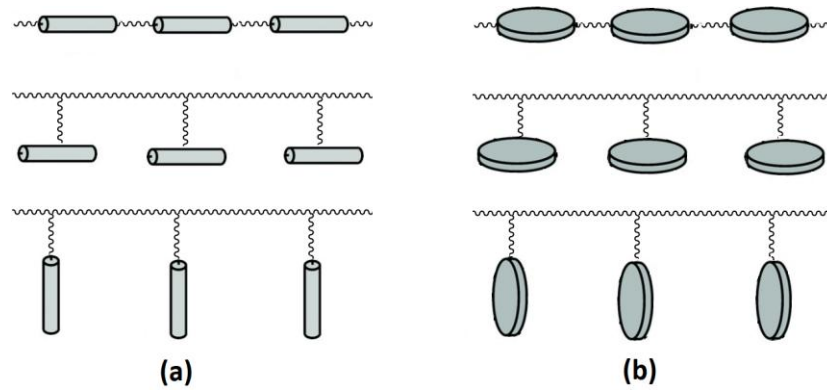
**Figure 2.5.** Schematic representations of a)rod-like and b)disc like LCP presented as main and side chain.

Moreover, some LCPs show liquid crystal organized phase when applied the heat in the certain range of temperature, which called as thermotropic LCPs, while some of them exhibit liquid crystal phase when dissolved in a certain solvent which termed as lyotropic LCPs (Colling and Hird, 1997). This mentioned ordered structures within the thermotropic LCPs domain brings anisotropy both in the fluid and solid states, which giving rise to considerable orientation and extension when processing (Kenig, 1987). Accordingly, LCPs with stiff molecular backbone and ordered manner, when used as a in-situ minor phase in polymer melt, orient itself in TPs matrix to form a fibrillar structure creating effective mechanical reinforcements (Saengsuwan at all., 2003; Ivanova et all., 2011). The fibrils of LCPs formed under proper processing conditions allows the thermoplastic matrix to be developed mechanical performance with elongated domain and gained fibre-reinforced properties (Odonnell and Baird, 1995). The mechanical improvements of these blends depends on the ratio of fibrillar phase of LCP and the load capacity of LCPs fibrils (Tjong and Meng, 1997). The another function of LCPs with a property of the low melt viscosities compared to TPs in blends is to reduce the melt viscosity of the blend in order to get easier processability with desired melt flow (Kayaisang et all., 2009).

10

### 2.2.2.2 Fluorinated Liquid Crystals and Their Polymers

Fluorinated liquid crystalline polymers have been broadly studied over the past few decades due to their interesting, particular and unique properties such as low refractive index, low dielectric constant, low surface energy and high performance (Scheirs, 1997). The fluoro subtituents with the small size allow the corporation with the all kinds of liquid crystals without any destructions in the nature of the liquid crystal materials. Fluoro substituent can be bonded to many varying positions in molecule (Hird, 2007). Namely, fluorine atoms can be introduced on (I) the main aliphatic backbone as perfluorinated, semi-fluorinated ( Janulis et all., 1992), (II) the rigid core located either between the ring ( Roussel, 1999) or on the aromatic rings (Milles et all., 1998), (III) in the chiral centre (Aoki, 1999) and (IV) near the chiral centre or as a polar head group (Kitazume et all., 1993) as illustrated in Figure 2.6.
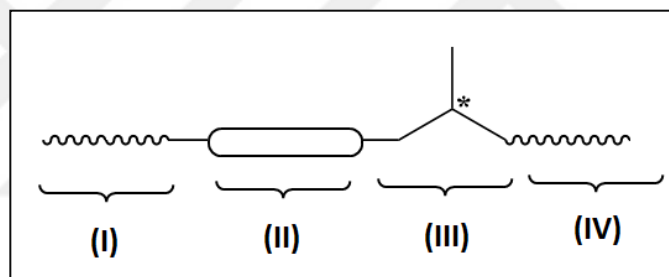


**Figure 2.6.** Representation of the classical rod-like liquid crystal.

Wherever it located in liquid crystal , it was reported (Hird and Toyne, 1988) that fluorine atoms substituted remarkably affect on the    phase transition temperatures, dipole moment, optical anisotropy, viscosity dielectric anisotropy, mesophase morphology, elastic constants and melting temperature properties, which enables to design the mesogens in order to improve the characteristics of molecules. In addition to that, the small fluorinated chains provide a positive dielectric anisotropy to molecules and have a tendency to show nematic phase.

The long chain fluorinated alkyl groups give the extra ordering ability and stability to liquid crystal molecules. Correspondingly, Koden et all. investigated the effects of fluorinated alkyl group on mesophase thermal stabilities and they concluded that the $S_C$-$S_A$ and $S_{A-I}$ transition temperatures of liquid crystals containing a fluorinated alkyl group were higher compared to its related non-

fluorinated compound and they observed that this increase maintained with the increment in the chain length of fluorinated alkyl group. These behavior was attributed to high linearity and rigidity of the fluorinated alkyl group, which meaning that the presence of more extensive fluorination located at terminal position caused a stiffening of the compound. This rigidity assists a lamellar packing and improves the stability of the smectic phase which is increased by the polarity of the fluoro substituentions, which resulting in enhancement in lateral intermolecular attraction forces between a hydrocarbon chainand a perfluorocarbon chains (Koden et all, 1989; Hird and Toyne, 1988). Furthermore, the fluorinated segment of the fluorinated alkyl groups has helical conformation because this fluorinated segment having helix structure is more rigid than the hydrogenated unit due to the considerably steric hindrance effects of fluoro subtituents. Hydrogenated segments have the lowest energy of planar zig-zag conformation (Khairuddean, 2008). The simplified representation of above mentioned model is illustrated in Figure 2.7.
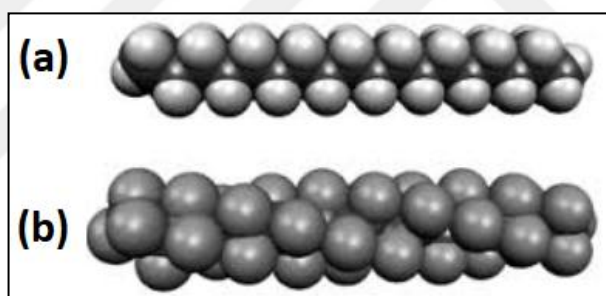


**Figure 2.7.** Model of a) planar zig-zag conformation of the hydrogenated segment and b) helical conformation of the fluorinated segment.

The function of methylene group (-CH$_2$-) used as a spacer between rigid core and extensive fluorinated alkyl tail has been examined by Shelyazhenko et all. in details. They announced that the adequate numbers of methylene groups allow the liquid crystals to show mesomorphic property (Shelyazhenko, 1988). When the perfluorinated alkly group is directly bonded to rigid core part of the liquid crytal, no mesomorphic characteristic was obtained (Fialkov, 1983). Moreover there exists the liquid crystals including the ester (-OCO-), ether, imine and thioester groups as a spacer located between mesogen core and fluorinated tail (Guittard, 1999).

The another important issue struggled with many scientists is obviously synthesis of fluorinated liquid crystal polymers as well as fluorinated liquid crystals. Liquid crystalline fluorinated polymers become an interesting route of material science with a wealth of peculiar properties. The rigid and rod like conformation properties of perfluoro alkenes enables the polymer to show liquid crystal behavior. It is deduced from the researches that semifluorinated alkyl linked as a side pendant units and semifluorinated alkanes have a large tendency to form smectic phase and they are clearly alternative to the phenyl mesogens so as to design liquid crystal polymers (Mahler et all., 1985; Wang et all., 1997). The synthesis of the block copolymers with semifluorinated 2 or 3 armed monodendron side groups were performed by Xiang et all. and they revealed that the obtained polymers formed a smectic B mesophase at room temperature (Xiang et all., 2000). Moreover, Andruzzi et all. investigated both the effects of the fluorocarbon chains bonded to B block of polystyrene (PS) on ABA triblock copolymers with PS and synthetic routes to obtain fluorinated liquid crystalline polymers. They observed different morphologies as depending on the number of fluorinated carbons in the side chains and also the increment in the intermolecular interactions between mesogenic groups owing to the presence of the phenyl group, which caused larger order parameter in obtained polymers (Andruzzi, 2002). Genzer et al. observed the surface molecular orientation of a liquid crystalline uniform layer composed of $CF_3(CF_2)_m(CH_2)_n$-side groups in their thin polymer films consisting of polystyrene and fluorinated block copolymer and revealed that surface structure comprised of smectic B phase and liquid crystalline side group was tilted in block copolymer products with the angle 28°-46° due to -$CF_2$ and -$CH_2$ segments as shown in Figure 2.8 (Genzer et al., 2000a and b).
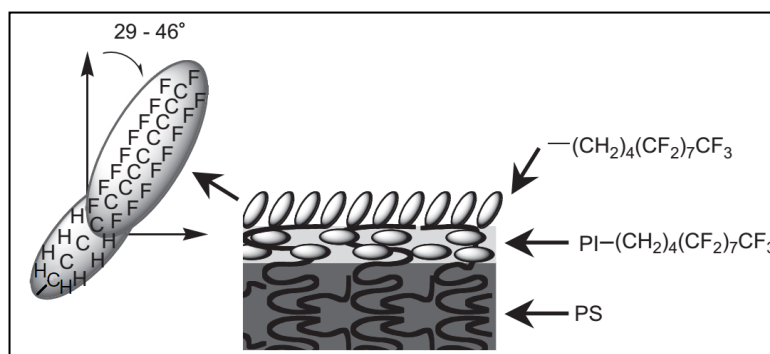


**Figure 2.8.** Schematic illustration for orientation, the surface and bulk structures of fluorinated block copolymer (Genzer et al., 2000).

## 2.3    Polymer Blends

Polymer blends can be described as macromolecules composed of the at least two species and they were formed by combination of thermoplastic–thermoplastic; thermoplastic–rubber; thermoplastic–thermosetting; rubber– thermosetting; or polymer–filler. The aspects of the mixing polymers having different structures have been attractive method promising option for upgrading characteristics of polymers and taking a leader part to obtain satisfied materials with wide application areas. The most important key benefits expected from polymer blends are clearly enhancement in physical properties (especially mechanical, thermal and optical properties) and designing processability, dyeability, flammability of the any polymer. It is well known that the characteristics of the crystalline phases and morphology, the size of crystallites, overall crystallinity property and the size of the spherulites affecting directly yield stress and ultimate strength determines the mechanical properties of blends (Kocsis, 1995). The most popular approaches in order to achieve mechanically improved polymers is blending of LCPs with the thermoplastics (TPs) because of the fact that LCPs depicts unusual mechanical performances owing to not only their rigid and stiff molecular backbones but also their relatively orientation thanks to mesogen groups containing. (Hsu et all., 1993; Machiels et all., 1997; Postema and Fennis, 1997). In the light of this goal, Filipe et. all announced that the highly fibrils in blends containing Rodrun LC3000 as LC and polypropylene as TP with or without compatibilizers were observed with the increments in LCP contents, resulted in mechanical reinforcement of obtained products (Filipe et all., 2006). On the other hand, the blends containing perfluorinated or semi-fluorinated liquid crystals show different behaviors in terms of mechanical properties. Perfluorinations given rise to a dramatic decrements in CED value and increment in line via polarity. CED and dipole moment are highly responsible for the intermolecular (secondary) interactions playing significant role in figuring out the mechanical properties of polymers at temperature below Tg (Giannetti, 2001). Conversely, semifluorinated alkyl linked as a side pendant units brings about positive impact on increasing of crystallinity and interactions between entities.

### 2.3.1 Reinforcement of Polymers

The demand for the reinforced polymer (especially polyolefins) in the world is continuously growing day by day. It is well-known the fact that mechanical reinforcement of polymeric materials is commonly performed by means of fibers (polymeric, carbon, graphite, glass etc.) to increase stiffness, fillers (wood flour, kaolin, talc, silica and calcium carbonate, ash etc.) to improve scratching resistance, dimensional stability and mechanical performance, nanotechnologies (nanotubes in different shapes such as halloysite, carbon nanotubes, nanoclays) and natural reinforcer (sisal fiber, flour, cellulose etc.) (Murphy, 2001). In literature, there exists large number of studies dealing with improvement of polyolefins especially by using LCPs because of their rod like and rigid properties as mentioned above. As an example, the blends formed by combination of ester-amide type LCP (Vectra B-950)/the isotactic stereoregular polypropylene (PP) and their mechanical, morphological and thermal properties were studied by Mandal et all. The obtained findings indicated that the steady increments in both tensile strength and the Young's moduli of the products were detected with the increment in LCP contents. The maximum values in tensile strength and Young's moduli were obtained with the products containing 10% and 15% LCP, respectively. This results was attributed to effective heterogeneous phase nucleating action in the form of fibrils exerted by the LCP rigid moieties (Mandal et all., 2004). As for filler, Lee indicated that the nanosilica coupled with the LCPs with fibrillar formation both created dual reinforcement effects and imparted superior mechanical strength to TP/LCP/Silica matrix (Lee et all., 2003). Similarly, Chae et all. observed 10% increment in storage Modulus of HDPE in the low frequency range by means of silicate-1 nanoparticle used as a filler (Chae et all., 2006).

On the other hand, the another approach introduced into the literature about reinforcement of polymeric materials is the usage of the semi or perfluorinated compounds. It is well-known that semi or perfluorinated segments as a side chain or main chain impart the ability of not only self-organization but also behaving like liquid-crystal segment due to rigid, rod-like, linear and stiff chain nature of the fluorocarbon with helical conformation. Therefore, fluorinated segment can be regarded as unusual alternative mesogen differing from the traditional liquid crystals

having and can be used instead of phenyl segments by designing of LCP. Furthermore, when alky tail(s) attaches to this unconventional mesogen, the segment gains the flexibility character in blends to contribute to orientation of other polymer chains (Andruzzi et al., 2001). The another advantage of the presence of the fluorinated segments in matrix is easier sliding effect of chains because of lower CED value between perfluorinated chains (CED ~150 Jcm$^{-3}$) compared with hydrocarbon analogues (CED ~240 Jcm$^{-3}$), which causing reinforcement of polymer matrix (Hartman et al., 2004). However, in same practical application, the mechanical performance of fluorinated polymers are weak due to the poor intermolecular cohesion between fluorinated chains (Kahraman M and Uçar T, 2016). Andruzzi et al. solved this weak cohesion problem between the perfluorinated groups by substituting biphenyl molecule cores possessing ability to initiate self-organization (Andruzzi et al., 2001). In addition to that, the impact of the fluorinated segment content in polymer matrix on free volume  were investigated by Choi et al. by using the copolymers of methyl methacrylate (MMA) and fluoroacrylate (FA) with different FA content (0–100 wt%). The results depicted that the increase in the content of the floroacrylate polymers in copolymers gave rise to increment of the free volume of the molecules  with decreasing of Tg of the copolymers (Choi et al., 2004). It is clear that the mechanical properties of polymeric materials is directly related to free volume describing as empty microscopic space between molecules, which highly depending on length and the size of the pendant groups. Molecular motions and physical behaviors of glassy and liquid states can be explained by free volume theory and also the increasing of the movement capability of polymer chains and segments in certain size of free volume at glassy state provides mechanical reinforcements (Qi et al., 2015). Similarly, Cengiz et al. reported that thermal and mechanical characteristics of perfluoroalkyl ethyl methacrylate(Zonyl-TM)/methyl methacrylate (MMA) statistical copolymers. It is clear from the results that the free volume fraction of copolymers increases with the increasing of Zonyl-TM contents because of introducing of the long, rigid and dense side chains and at high content of Zonly-TM, the dipole–dipole interactions between $CF_3(CF_2)nCH_2CH_2O-$ groups was observed (Cengiz et al., 2011). Moreover, Kharitonov et al. studied the reinforcement of  ultrahigh molecular weight polyethylene (UHMWPE) with the additional of fluorinated single-walled carbon nanotubess (SWCNT) into the polymer matrix. It is found to be that the tensile strength and Modulus of the materials increased with the

16

increment of fluorinated CNTs. The fluorine atom effects on mechanical improvement of UHMWPE polymer was observed clearly by comparing the pristine CNT and fluorinated CNT at the same contents. This mechanical reinforcement was caused that the inserted fluorinated CNTs acted as crystallization centers, enhanced the adhesion in polymer matrix and also formed high concentration of nanofibrils (Kharitonov et al., 2015).

### 2.3.2 Miscibility in Polymer Blends

The miscibility term obviously signifies a single phase system expecting to be formed by mixture of polymers. The main drawback of blends is the inherent immiscibility among the entities, which depending on the nature of polymer components (morphology, crystallinity, intermolecular interaction and surface tension), compositions and mixing temperature (Strathmann and Lipson, 1999). This phenomena forces out to academic and industrial researcher to investigate the miscibility nature of polymer blends and improve the novel methods to enhance the miscibility. Basically, the miscibility term is directly depended on the molar Gibbs free energy of mixing ($\Delta G_m$). The provision for the spontaneously miscibility is clearly that the change in $\Delta G_m$ must be negative (Vasile and Kulshreshtha, 2003). The thermodynamically equation governing the miscibility nature of the mixtures is $\Delta G_m = \Delta H_m - T\Delta S_m$ ,where T, $\Delta S_m$ and $\Delta H_m$ state the temperature, molar entropy and enthalpy of mixing, respectively (Cetin, 2004). In other word, the increase in $\Delta S_m$ and decrease in $\Delta H_m$ (unfortunately, in many case, both of them are positive) are required for the homogenous mixing. But, the enthalpy becomes more dominated for blends miscibility compared to entropy whose value depicts little positive change (He and Liu, 1997). In order to minimize the molar enthalpy, physical and chemical interactions must exist between components of the mixture as described by Flory-Huggins Theory for modeling the binary polymer mixtures (Robeson, 2007), which favors the mixing. When two entities are mixed, either, most frequently, the system shows a phase separation because of repulsive forces of components or the system is fully miscible due to attractive intermolecular forces. The common attractive encountered forces between pairs is illustrated in Figure 2.9 (Coleman et al., 1991).

| Type of Molecule | Type of Interaction | Interaction Strength |
|---|---|---|
| Non-polar "small" molecules or polymers | | |
| "Weakly" polar molecules or polymers | PHYSICAL | WEAK |
| "Strongly" polar molecules or polymers | | INTERMEDIATE |
| Hydrogen bonded molecules or polymers | | |
| Molecules or polymers that interact by the formation of charge transfer complexes | CHEMICAL | STRONG |
| Ionomers - hydrocarbon polymers containing ionic groups | | |

**Figure 2.9.** Frequent attractive forces between molecules or segments in matrix.

In terms of mechanical properties, partially or fully miscible systems in many blends shows better strengths than totally immiscible system and the lower interfacial tension between components in blends brings about higher performance (Zhuang et al., 1988; Kozlowski and La Mantia 1997). In order to increase the stability of the matrix and achieve desired degree of miscibility between components, the third entity whose equivalent name is compatibilizing agents may be utilized in polymer blends. In literature, graft copolymers, newly synthesized LCP polymers with flexible groups, the modified block copolymers and the addition of catalysts or acids were widely used to achieve desired compatibility (Zhang and He, 2001; Zhao et al., 2000; Kobayashi et al., 1994; He et al., 2004; Thurber et al. 2015). Santos et. al. reported the study on the usage of prepared EPDMSDD as compatibilizer agent for EPDM/waste EPDMR blends and examined the mechanical and rheological properties of the blends. The results obtained from this research showed that the products with addition of 5% of EPDMSDD were found to be best combination for tensile strength at break and elongation values. It is clear that EPDMSDD reduced the interfacial tension and supplied a better dispersion and adhesion between polymers, which resulting in better mechanical properties (Santos et al., 2011). Similarly, the maleic anhydride gafted thermoplastic elastomer ($TPE_g$) as a interfacial modifier for polypropylene(PP)/polyamide 6 (PA6) blends were investigated by Ou et. al. The results obtained from this study indicated that $TPE_g$ improved both compatibility between PP and PA6 and toughness, but caused slightly decrease in tensile strength and modulus of blends at 15 wt% TPEg (Ou et al., 2004).

18

### 2.3.3 Graft Copolymerization

Copolymers can be described as a polymer composed of two or more chemically different constituent entities and they were divided into three groups (block, alternating and random) depending on the arrangements of these structural units throughout the polymer chain. The graft polymerization regards as a chemical method to form segmented polymers possessing the side chains composed of randomly attached different monomers to the main linear backbone. The grafting is a well-known and practical polymer modification technique used with the purpose of the enhancing adhesion, improving tensile strength and other mechanical properties, compatibilizing blends and composites, mold easily etc. and graft polymers consist of both main chain backbone and long branched segments (grafts) linked to backbone. The presence of covalent bonded between polymeric structures separates graft copolymers from other common polymer mixtures. There are lots of graft copolymerization method as following; (I) grafting initiated by chemical means (free-radical grafting, grafting through living polymerization and ionic grafting), (II) grafting initiated by radiation technique, (III) photochemical grafting, (IV) plasma radiation induced grafting and (V) enzymatic grafting (Bhattacharya and Misra, 2004). Figure 2.10 shows the schematically structures of graft copolymer, three types of copolymers and methods for synthesizing graft copolymers.
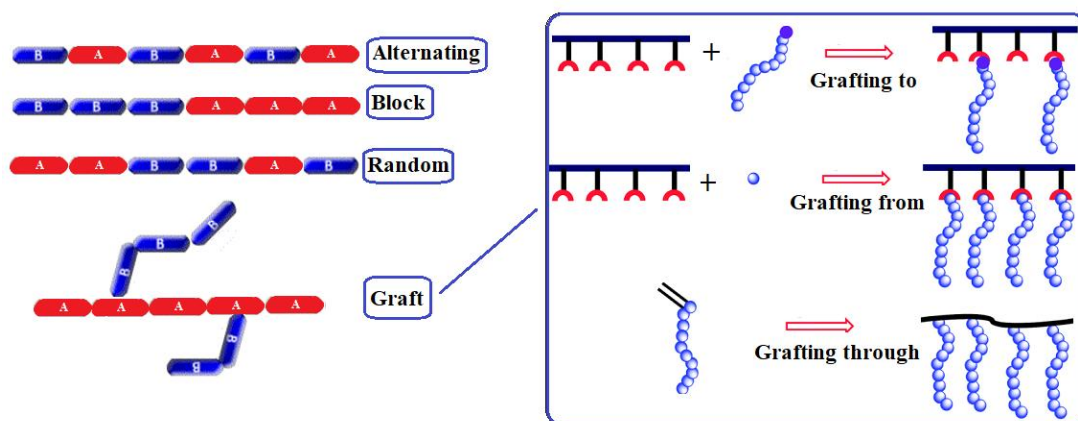


**Figure 2.10.** Simplified representation of the kinds of copolymers and three methods for synthesizing graft copolymers.

Odonnell and Baird  stated that the grafted side chain rigid, rod-like units bring about extra fibrils, orientations and alignments in the produced coproduct matrix  due to highly ordered structure of side segment,  which resulting in significant mechanical reinforcements in polymer blends (Odonnell and Baird, 1995). Durmaz et al. reported the preparation of a novel poly(p-phenylene) (PP) with regularly alternating fluorinated and nonfluorinated polymer side chains along the aromatic polymer backbone. The obtained complex macromolecule composed of both block and graft polymer substitutions  exhibited excellent solubility in frequent organic solvent although PPs have the solubility problem limiting their processability (Durmaz et al., 2012). Although the fluorinated molecules possess unique and particular properties in order to modify the polymers , there are a few studies on graft copolymerization of organo-fluorinated compound onto polyolefins in literature.

## 2.4     Free Volume and PALS Concepts

### 2.4.1   Free Volume

It is impossible that the solids and liquids volumes have not been filled to 100% by the atoms due to their spherical in shapes. Therefore, the free volume concept has becoming the critical research topic in science for examining and understanding the physical characteristics of the  produced materials. The free volume, $V_f$  (also called as total free volume) can be defined as the unoccupied microscopic spaces existing between a solids or liquids molecules. In another explanation of the free volume is the mathematical value obtained from the subtraction of the specific occupied volume ($V_{occ}$) from the total volume  ($V_t$, $cm^3/g$) as depicted in Equation 2.1. $V_{occ}$ is also known as Van der Walls volume ($V_w$) calculated from the Bondi's method and $V_w$ is called as the occupied space where other molecules cannot penetrate via normal thermally energies. In addition to that, the free volume properties obviously depend upon the crystal, semicrystal or amorphous properties that the materials have, as depicted in Figure 2.11. The free volume is identified as the interstitial volume ($V_{fi}$) in a crystal structure, but in amorphous materials, the excess or additional free space come outs in the form of the

disorderly local free volume in subnanometer size because of irregular structures, which resulted in decrement by roundly 10% in density of the materials when compared to crystal. These formed local free volume ($V_{fh}$) are commonly termed as holes (or vacancy). Herein, the $V_{fh}$ can be obtained from the Eguation 2.2, but here, $V_{occ}$ includes both $V_w$ and $V_{fi}$. The hole free volume clearly manages the small molecule diffusion into the materials matrix and molecular mobility (Yang Y, 2011). The another free volume terms encountered in literature is obviously the fractional free volume $f$ described as the ratio of free volume (Vf) to the total volume (Vt), as shown in Equation 2.4.

$$Vf = Vt - \text{Vocc} \tag{2.1}$$

$$Vfh \equiv Vf = Vt - Vocc \tag{2.2}$$

$$Vocc = Vw + Vfi \tag{2.3}$$

$$f = \frac{Vf}{Vt} \tag{2.4}$$
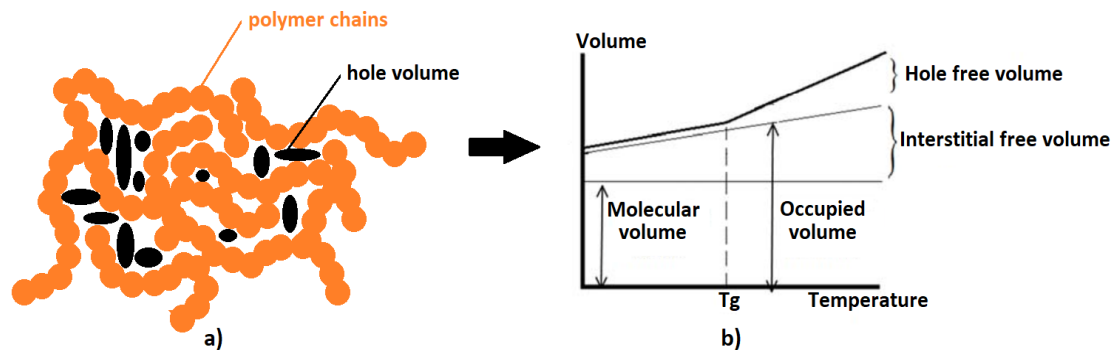


**Figure 2.11.** Schematically representation of a) hole volume in polymer matrix (black one) and b) relative volumes.

It is clear that the various free volume theory models have been developed to describes the micro-structure properties of the polymers due to the fact that lots of physical and chemical characteristics of polymeric compounds considerably are governed by free volume (Sharma et al., 2017a; Ozturk, 2018). Namely, Bamford et. al. and Cohen et al. interpreted that the transport phenomena in polymers have been stated in terms of the free volume arisen from structural disorders in amorphous

21

polymers (Bamford et al., 2001; Cohen and Turnbull, 1959). To interpret the ionic-conductivity mechanism, Yahsi et. al. proposed a model in terms of temperature and pressure depended hole fraction as a measure of the free volume fraction (Yahsi et all., 2008). Furthermore, the free volume indubitably effects the mechanical properties of the polymers (Hosseinabadi et al., 2018; Zhang et al., 2017; Kumar et al., 2005). The free-volume and mechanical properties of the polymers possesses the anti-correlated relationship due to the fact that the formation of excess amount of holes in matrix damages the microscopic structure of polymers (Altaweel et al., 2009). That is, the molecular motions and mobility of polymer chains in the bulk state are directly related to the presence of the holes, spaces and places where there existing voids and vacancies (Roussenova et al., 2014). Burgess et al. investigated the dependence of the addition of the small molecules to PET on both chain mobility and free volume. They concluded that the presence of the caffeine gave rise to decrement in chain motions and free volume (Burgess et al., 2015). As the molecules in matrix are in motion into the holes, the molecules exchanges the place with the holes and the more holes can be needed for this movement of the polymer chains (Qi et al., 2015; Jean et al., 2003) . Therefore the critical free volume must exist in polymer matrix for supplying the optimum molecular motion of the polymeric segments. Moreover, the local free volumes or the molecular and atomic dimensional cavities in polymers increases because of both the disordered packing of the polymer chains in amorphous phase (static state)  and  molecular relaxation of chains and terminal ends (dynamic and transient states) (Jean et al., 2003). However, Zekriardehani et al. found that the free volume in amorphous fraction decreases with the increment in the crystallinity level by means of PALS measurements, which resulting in not only decreasing the relaxation activation energy (meaning the measure of freedom of segmental motion of the polymer) but also more restricting of the motions of polymer chain with orientation (Zekriardehani et al., 2017). Also, Xia et al. reported the relationships between  the relaxation of the free volume holes and molecular orientations with varying levels by using poly(methyl methacrylate) and polycarbonate via PALS. They observed from the results that the free-volume holes and  polymer chain alignments enforce molecular restrictions on the mobility of both PC and PMMA molecules in glassy states (Xia et al., 2014). In addition to the effect of free volume on mechanical properties, the free volume approaches illuminates the thermal (especially Tg) , rheological, crystal properties of the polymeric materials

(Aramoon et al., 2017; White and Lipson, 2016; Lue et al., 2008; Hsieh et al., 1998; Steller and Zuchowska, 1991). It is known that the mismatching between cooling rates and the relaxation of polymer chains brings about entrapment of the unoccupied volume, which leads to form free volume holes (Riande et al., 2000). The local conformational motions are only allowed when the temperature becomes lower than Tg or the certain relaxation temperature and fractional free volume remains roundly constant, but the free volume increases with the increasing of the temperature since the free volume is more sensitive to temperature changes (Struik, 1977).

In addition to that, the chemical modification of the polymers such as grafting, crosslinking etc. have a significant role so as to control the free volume characteristics of the polymeric materials. At this point, Chen et al. studied how the free volume changes with the graft polymerization yield by using maleic anhydride (MA) grafted HDPE. They revealed that the distribution of the free volume became more broader with the increment in degree of grafting in samples, which caused by the presence of the larger concentration of MA polar groups (Chen et al., 2008). Furthermore, Mahmoud et al. founded that the mean free volume of the uncrosslinked polymer samples were generally somewhat lower than those of crosslinked polymer samples and this result derived from the more packing structure of uncrosslinked samples (Mahmoud et al., 2006). Moreover, it was observed in literature that the properties of polymers like permeability (Yampolskii et al., 2001), electrical (Ningaraju et al., 2018), viscosity etc. (Utracki and Sedlacek, 2007; Yang Y, 2011) can be modified by controlling the free volume of the materials.

### 2.4.2 Positron and Positronium Phenomenons

In order to understand free volume phenomenon, the positron and positronium concepts must be examined meticulously. Positron, $\mathbf{e}^+$ can be termed as the antiparticle or antimatter of the electron. This antielectron created the high impression in science world because of the fact that not only it was a first evidence related to the presence of the antimatter but also its physical characteristics were nearly similar (the rest mass related to 511 keV and its spin is 1/2) to the electron with the exception of electric charge. It is well-known the fact that the positron has a positive (+) charge. Positron is scare in nature and has a shorter lifetime due to

unstable character when comparing with the electron. In order to generate positron, there mainly exists two ways; (I) pair production and (II) radioactive decay. The pair production method based on the Einstein's mass-energy equation ($E= m.c^2$). Namely, by the time the energy of photon achieves more energy than 1.022 MeV (this value is twice of the rest of the electrons), the photon generates a positron and an electron by following the conservation law of energy, charge and angular momentum (Yang Y, 2011). The radioactive decay can be defined as the method that the positron is generated from the certain positron sources via radioactive decay. The positron is $\beta^+$ particle and although all of the known elements possesses $\beta^+$ radioactive isotopes, a few elements such as $^{22}$Na, $^{21}$Na, $^{68}$Ge, $^{58}$Co, $^{64}$Cu, $^{44}$Ti are mostly used in applications as positron sources due to the economic aspect, appropriate half-lifetime and proper emitting signals (Kansy J, 2008; Yang Y, 2011; Ozturk B, 2018). The generated positron annihilates with the electron by conserving the momentum and energy. Positronium atom, **Ps** is an intermediate state with the formation of the lightest hydrogen-like bounded state consisting of an electron and a positron by annihilating each other. The atomic mass of positronium and diameter meaning the distance between electron and positron are 0.0011 amu and 3 classical-Bohr radius, respectively. The electron and positron rotate around the common center of mass since they have roundly equal mass (Yang Y, 2011). Both the positron of positronium and the relative electron spin orientations brings about the formation of two possible arrangements of the positronium; (I) para-positronium (**singlet spin state, p-Ps, $^1$S$_0$**); (II) ortho-positronium (**triplet spin state, o-Ps, $^3$S$_1$**). At p-Ps, the spin directions of positron and electron are opposite and spin angular momentum is equal to zero (S=0), while , at o-Ps, the spin directions of electron and positron are parallel one another and the angular momentum is clearly has a value (Mostafa et al., 2009). Moreover the self-annihilation lifetimes of o-Ps and p-Ps in vacuum are equal to 142 ns and 0.125 ns, respectively (Thraenert et al., 2006). The formation of o-Ps take places in the free volume areas of the material where there exists the electrons around. The positron belonging to o-Ps annihilates with the another opposite spin direction electron existing around, which resulting in emission of two photons instead of tree photons. This annihilation type is described as pick-off annihilation. The o-Ps lifetime (inverse of annihilation rate) highly depends on the electron density in the open hole where o-Ps is localized (Yang Y, 2011). That is, the annihilation lifetime of o-Ps decreases considerably with the increments in interaction with host

materials electrons. Therefore, the lifetime of o-Ps includes useful information about the prediction of the hole pore size, crystallinity, functional groups, electron affinity etc. properties of the materials (Thraenert et al., 2006; Mostafa et al., 2009; Ozturk B, 2018).

### 2.4.3 Positron Annihilation Lifetime Spectroscopy (PALS)

There exists lots of application areas showing the importance of the positron usage. These methods can be ranked as Positron Annihilation Lifetime Spectroscopy (PALS), Scanning Positron Microscopy (SPM, Positron Emission Tomography (PET), Transmission Positron Microscopy (TPM), Angular Correction of Annihilation Radiation (ACAR), Positron Diffraction Technique, Positron-Annihilation Induced Auger Electron Spectroscopy (PAES), Coincidence Doppler Broadening (CDB) and Slow Positron Beam (SPL) (Ozturk B, 2018). Among them, PALS is the most robust one donating the most detailed characterization of free volume cavities and the size of the voids. Namely, PALS bases on the interaction between positrons and electrons, which presents the good correlation with the free volume properties of the materials. So, the determination of the o-Ps lifetime ($\tau_3$) and intensity ($I_3$, relative amount of annihilations) is performed thanks to PALS by bombarding the samples with positrons obtained from $Na_{22}$ isotope decay to form positronium complex (Callander DB, 2005). In another words, PALS measures the time difference between the annihilation and birth of the positron by means of the fast–fast coincidence setup coupled with two scintillation detectors (Sharma and Pujari, 2017b; Yahsi et al., 2018). This time difference is highly influenced by the density of the electrons around the positron. So it can be say that the mean lifetime, $\tau$ is the reciprocal of the annihilation rate ($\lambda$), meaning that the increments in $\tau$ brings about the increments in the free volume of the sample. Moreover PALS method gives the snapshot of the hole volume of the polymer materials in certain time (1-4 ns) when is the shorter than the relaxation time of the movements of the polymer segments. The lifetime concept of PALS experiment is divided into three phenomenons; $\tau_1$, $\tau_2$ ($\tau_{free}$) and $\tau_3$ as following descriptions with Equations 2.5, 2.6 and 2.7 (Yang Y, 2011);

➢      p-Ps (channel 1) , $\tau_1$ or $\tau_{p\text{-}Ps}$ , para-positronium lifetime;

$$\tau_{p\text{-}Ps} = \cfrac{1}{\cfrac{\eta}{\tau^O_{p-P_S}} + \cfrac{1}{\tau_{po}}} = 125 \text{ ps} \tag{2.5}$$

➢      If the positron don't form the positronium, Ps (channel 2), $\tau_{free}$ or $\tau_{2,}$ free positron lifetime;

$$\tau_{free} = \tau_p \approx 350 \text{ to } 500 \text{ ps} \tag{2.6}$$

➢      o-Ps (channel 3), $\tau_3$ or $\tau_{o\text{-}Ps}$ , orto-positronium lifetime;

$$\tau_{o\text{-}Ps} = \cfrac{1}{\cfrac{\eta}{\tau^O_{o-P_S}} + \cfrac{1}{\tau_{po}}} \approx 1\text{- } 4 \text{ ns} \tag{2.7}$$

Herein, ɳ donates the contact density (relaxation parameter) and $\tau_{p0}$ describes the pick-of annihilation lifetime. Moreover the intensity can be defined as the following Equation 2.8;

➢      $I_{free} = 1\text{- } (I_{p\text{-}Ps} + I_{o\text{-}Ps})$                                    (2.8)

In polymeric materials, p-Ps lifetime does not depend on the polymer properties, however o-Ps lifetime is directly related to free volume of the polymers. Furthermore, as the electron density of the polymeric samples increases, the direct annihilation of the positron becomes more favorable rather than the tendency to form a positronium. $I_3$ has straight correlation with the number of free volume and $\tau_3$ gives the information about the size of the free volume (Hsieh et al., 2000; Yener et al., 2018; Yu et al., 1994). Although three lifetime concepts are generally recorded in the polymers, HDPE can have four lifetime components with fulfilling fine statics condition, which caused by semi-crystalline characteristics of HDPE (Suziki et al., 1996). For the HDPE, $\tau_1$, $\tau_2$ ($\tau_{free}$) and $\tau_3$ lifetime components are designated as about 250-320 ps, 650-800 ps and 2.5 ns with the intensity $I_1$, $I_2$ and $I_3$, respectively (Brusa et al., 1995).

# 3. GENERAL VIEW ON MICROSPHERES

It is uncontestable that the importance of microparticles in the science and industry due to their charming characteristics and usage in the wide range of application areas enhancing progressively all over the world (Kawaguchi, 2000). Microspheres, which referred to microparticles, can be defined as small spherical particles whose diameters commonly ranging from 1 μm to 1000 μm (Ma and Su, 2013). Especially, the remarkable developments in these micrometric particles have paved the new way for many areas such as medical applications ( Saralidze et al., 2010), ophthalmic, gene, intratumoral, local, oral nassal, buccal etc. drug delivery (Yin et al., 1996; Sahil et al., 2011), electrical applications (Han et al., 2008), optical applications (Fu et al., 2010), membrane production (Prasanth et al., 2011) etc. Recent advancement in microspheres encountered in literature are the usage of chitosan polymer in order to reduce cholesterol-lowering (Kalyan et al., 2010), increasing stability of drugs, utilization for orthopaedic patients, using for cosmetics industry and dental medicine etc. (Sahil et al., 2011). Moreover microspheres are classified into five fundamental types; (I) bioadhesive (Kumar et al., 2013; Thummar et al., 2013) (II)magnetic (Batra et al., 2012) (III) floating (Mukund et al., 2012) (IV) radioactive and (V) polymeric microspheres utilized as a fillers, bulking agents, embolic particles, delivery vehicles for drugs etc. (Ramteke et al., 2012) The different kinds of polymeric microspheres can be described as shown in Figure 3.1.
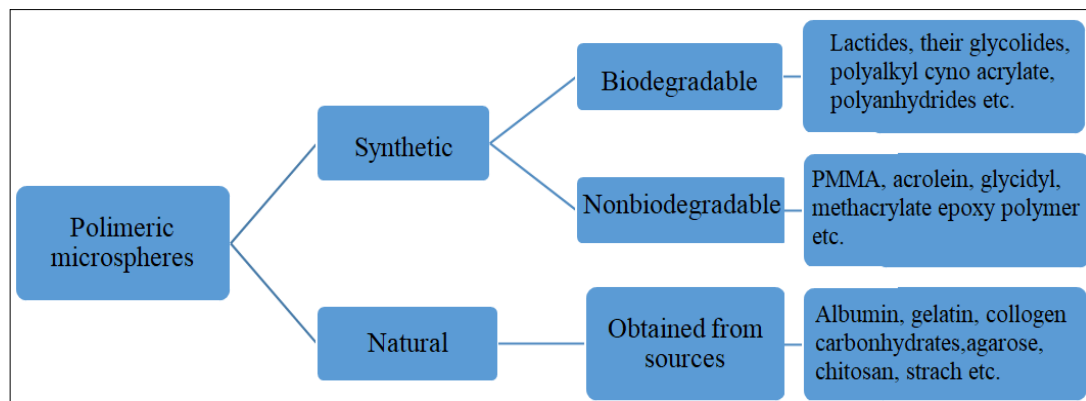


**Figure 3.1.** Schematic demonstration of kinds of polymer microspheres and common examples (Ramteke et al., 2012).

Polymeric microspheres have reached a good reputation due to both their easily production with the distinct chemical and physical properties and presenting to straightforward control over the size range of particles. Moreover, the chromatographic packings, functional coatings, additives for food, cosmetics, medicine, inks and toners, carriers for cells, proteins and enzymes, supports for catalysts, reagents for immunological diagnostics, controlled-release or target-specific drugs and so further are common known applications areas of the polymeric microspheres (Chai et al., 2003).

## 3.1    Preparation Methods for Polymeric Microspheres

Non-polymeric microspheres are mostly fabricated from a simple methods such as using aqueous phase to form spheres, sintering, drying etc.(Hong et al., 2009; Yaparpalvi et al., 1994), whereas the preparation of the polymeric microspheres were conducted by the following frequent methods; (I) solvent evaporation, (II) spray drying, (III) emulsion (IV) dispersion (V) sedimentation (VI) bulk and (VI) suspension polymerizations (Saralidze et al., 2010). The particle size and shape, morphological properties, density of particles, efficiency of particle in some application, isoelectric point, contact angle and swelling index characteristics highly depend on the preparation method chosen (Prasanth et al., 2011). In solvent evaporation technique, the polymer dissolved well or slightly in volatile solvent is dropped into immiscible fluid (continuous phase) comprising the stabilizer to provide the formation and maintenance of spherical state. After the solvent is evaporated slowly, a solid microspheres are obtained as dispersed state following washing, which applied in some researches (Saralidze et al., 2003; Freiberg and Zhu, 2004; Li et al., 2008; Singh and Chaudhary, 2011). The advantages of solvent evaporation method to synthesize  microspheres are clearly simplicity, high yield and applicability for soluble polymers, while the disadvantage of this process are the complication in controlling the particle size, necessity for washing bringing about wastes. As for spray drying method, which alternative for solvent evaporation, the volatile solvent is utilized to dissolve the polymer under pressure and a well-defined spray is produced. These obtained particle from the spray is dried under high power heating, which resulting ending up unconstrained spherical particle (Bitz and

Doelkar, 1996; Witschi and Doelkar, 1998). Both the high polydispersity and the impairments of the highly sensitive bioactive molecules due to upper heating are the disadvantages of the spray drying process ( Giunchedi et al., 1998). Although these two techniques are carried out by using polymer, the alternative methods such as emulsion, dispersion, suspension and sedimentation polymerizations are based on the monomer mixture containing necessary components for polymerization formation. In the emulsion polymerization, there exists a solution that includes stabilizer, emulsifier in order to obtain micelle droplet with monomer and initiator dissolved in water phase. In order to fabricate microspheres with diameters in the micrometer range 0.1-10 μm with the high yield and low polydispersity, the emulsion polymerization is clearly preferable technique (Arshady, 1988; Watts et al., 1990). The another method used to generate microsphere particle is dispersion polymerization conducted by the existence of a solution comprising monomer and initiator with the stabilizer molecules to prevent aggregations. The obtained sphere polymers become insoluble in the chosen solvent for dispersion. Namely, the soluble monomers are progressively transformed into insoluble polymer microspheres with 1-10 μm diameters (Ahmad et al., 2006; Chu and Pan, 2015). However,the only difference between dispersion and precipitation polymerizations is directly related to how soluble the polymer is in the used solvent. The formed polymers by precipitation polymerization depict no tendency to swell in polymerization medium, while the obtained polymers from dispersion polymerization tend to swell in a solution (Kurt, 2010). Also, sphere sizes are considerable effected by stirring speed and heat of polymerization (Piskin et al., 1994). As one can see, the final technique mentioned in this part is rarely used sedimentation polymerization suiting for fabrication of microspheres with large size ( 400-2000μm) and low polydispersity. In this method, the mixture consisting of monomer and initiator is dripped into the mineral oil column heated as a drops whose sizes are determined accurately. The obtained microsphere accumulates at the bottom of the column without any adhesion and sticking together (Ruckenstein and Hong, 1995; Ruckenstein and Sun, 1996). Regarding to bulk polymerization, the polymer produced by mostly radical polymerization is molded as microspheres.

### 3.2 Suspension and Inverse Suspension Polymerizations

Suspension polymerization (equivalently pearl and bead polymerization) is a known polymerization technique proceeding via a free-radical mechanism to form microsphere polymers. As for this method, a liquid monomer (oil phase) including initiator is dripped into a immiscible phase (water phase) that becomes mostly water with a stabilizers such as surfactants and detergents and vigorous stirring maintained during polymerization. (Sivakumar and Panduranga, 2002; Kamiyama et al., 1993). By the time the initiator is activated, the radical polymerization proceeds in drops until the termination. The advantages of the suspension polymerization are simplicity and the obtaining wide range of microsphere size (40-1000 μm but, in many cases, drop diameter lies between 10 and 100 µm) whereas that the fabricated microspheres show relatively high polydispersity is the main disadvantage. So as to obtained well-defined size of the microspheres, micro sieving is necessary, which causing yield reduction (Saralizde et al., 2010). Furthermore, suspension polymerization generally needs the large reactor volumes since the vessels are mostly half full with water (Brooks, 2010). Inverse suspension polymerization can be described as a process which an aqueous solution including molecule having polymerizing capability is dispersed as droplets in a water immiscible phase with the stabilizer. In recent years, the inverse-suspension polymerization technique has became favorable for the preparation of water soluble/swellable materials such as thickeners, flocculating agents (Omidian et al., 2002) superabsorbent hydrogels (Petrusic et al., 2012; Mayoux et al.,2000; Zhou et al., 2012), ion-imprinting polymer (Meouche et al., 2012) etc. Moreover this method is unique aspect due to easy separation, removal heat of reaction, temperature control and low level of impurities and additives and easily controlled particle size by changing reaction parameters.

### 3.3 The Parameter Effecting Suspension Polymerization

It is recognized phenomenon that partial size distribution (PSD) in a suspension polymerization is considerable effected by many significant factors such as continuous/dispersed (monomer) phase ratio, crosslinking agent content, reaction temperature, kinds of stabilizer , vessel geometry and size, stirring rate etc. ( Lima et

al., 1997; Uguzdogan, 2013; Mao et al., 2008; Hamilec and Tobita, 1992). As the Sherrington and Hodge say, suspension polymerization is  an art (Sherrington and Hodge, 1988). In fact, the two fundamental difficulties appear in suspension polymerization; (I) the reactor design and the choice of stirrer and (II) the changes in the system parameters due to high increment of viscosity in organic phase. As the continuous phase/monomer ratio increases, the smaller spheres are obtained. The size of particles decreasing with the increment of the crosslinking agent. The another factor influences the suspension polymerization is clearly the temperature in which polymerization reaction proceed with the radical formation from initiator. Whereas the lower temperature (approximately 50°C) is preferred in the acrylic monomers, the relatively high temperature ( 80°C and above) is chosen for the styrene based monomers. The presence of the stabilizer in suspension polymerization not only provides the stability by sticking the formed polymers in suspension drops but also prevent the coalescence. Poly(vinyl alcohol) (PVA), gum Arabic and surfactants such as sodium dodecyl sulfate are commonly used examples of stabilizers to obtain microsphere with the range of diameter 100-200μm, 250-500 μm and 10-100μm, respectively (Kurt, 2010). Additionally, the drop elasticity improves until the *critical surface-coverage* as the concentration of the stabilizer increases in the medium, further increment influences very little on drop stability. The large vessels for the suspension polymerization is preferable in order to regulate internal liquid flow. The batch, continuous-flow tubular, loop and oscillatory baffled reactors are frequently utilized reactor types for suspension polymerization. Moreover enough agitation is obviously necessary both to help heat transfer and to keep up the dispersion of two phase (Brooks, 2010). Furthermore both the uniform distribution of the mixing force and relative turbulent-free are provided from the spiral stirring arrangements, which reducing the possibility of the inadvertent particle coagulations. The most convenient factor effecting particle size is undoubtedly agitation rate. It is clear that the particle sizes of the microspheres decreases with the increment of the stirring rate (Arshady, 1992; Ravi et al., 2008). The coalescence and sedimentation become inevitable in the case that the axial reactor mixing  is not enough (Brooks, 2010). All in all, the following equation, Eq. (3.1) gives the empirical relationships between  suspension polymerization parameters.

$$\bar{d} \equiv k \ \frac{D_V.\vartheta_d.R.\varepsilon}{D_S.\vartheta_m.C_S.N} \tag{3.1}$$

where $\bar{d}$ = average particle size; k = parameter depending on design, stirrer type etc.; $D_v$ = vessel diameter; $D_s$ = stirrer diameter ; R= volume ratio of droplet phase to suspension phase; N= agitation rate; $\upsilon_d$ =droplet phase viscosity ; $\upsilon_m$ = suspension phase viscosity; $\varepsilon$ = interfacial tension between two phases; $C_s$ = concentration of stabilizer (Arshady, 1992).

### 3.4    Microspheres with Functional Group

During the last two decades, the polymer microspheres bearing functional group have presented large platform for applications in the biomedicines, electronic materials, coating, adhesives, catalysis, and carrier etc. (Kawaguchi, 2000; Horak and Shapoval, 2000; Haragucchi et al., 2010; Zhang et al., 2011; Steinke et al., 1996). Therefore the production of polymer microspheres containing the reactive groups in their structures becomes more important in order to impart the desired and peculiar characteristics into the non-functional polymeric materials. Many reactive groups such as epoxy and amino (Song et al., 2015; Denizli et al., 1999; Cai et al., 2016) amidoxime (Chen et al., 2010; Caykara et al., 2007), carboxylic acid, pyridyl, amide (Huang et al., 2010; Abdelrahman et al., 2006; Guo et al., 2009), hydroxy (Bai et al., 2006), oxide-based (Breed et al., 2009), haloalkly (Karagöz et al., 2010) and thiol (Wang et al., 2014) functional groups have been used in order that desired properties and functionalities are introduced into the polymer microspheres under favorable conditions with proper agents. As mentioned above, the commonly utilized ways to prepare functional polymer microspheres are emulsion, dispersion, suspension and inverse suspension polymerization. Moreover it was reported the existence of the copolymers with reactive functional groups. Poly(glycidyl methacrylate-co-poly(ethylene glycol) methacrylate) monodispersed microsphere copolymers were produced by atom transfer radical polymerization (ATRP) method at room temperature (Yu et al., 2015).

### 3.5 Crosslinking Agents

Crosslinking reagents includes two or more reactive and specific functional ends having capable of reacting with another polymer molecules. That is, two polymer chains join together by means of a branch referred to as a crosslink. Crosslinked plastics are considerably preferred in development of engineering materials due to not only their excellent stability toward physical stress and elevated temperatures but also dimensionally stability under a wide variety of conditions because of their rigid network structure (Odian, 2004). The most widely used crosslinkers can be ranked as are divinylbenzene (DVB), ethylene gylcol dimethacrylate (EGDMA), N,N'-methylene bisacrylamide (MDAA), 1,4-phenylene diacrylamide, tetramethylene dimethacrylate (TDMA) etc. Moreover, bead polymers could be prepared via crosslinkers with the use of the proper synthesis techniques . It is clear that crosslinking characteristic has a big role in improvement of the mechanical strength, insolubility, stiffness, rigidity and shape of polymer microbeads. In addition particle size of the microspheres can be modified by crosslinking agent (Mane et al., 2015).

# 4. AIM AND SCOPE OF THE STUDY

This dissertation is comprised of the investigations on the synthesis of a semifluorinated acrylic compound, 3,3,4,4,5,5,6,6,7,7,8,8,8-dodecafluoro-5-methyloctyl-4-(acryloyloxy) benzoate (ABCF13), graft copolymerization of the compound onto density polyethylene and on the studies of preparation of crosslinked poly(ABCF13) microspheres and their blends with HDPE. It is well-known that the presence of the mesogenic groups in polymer molecular structures brings about arranged and organized behavior with considerable orientations at molecular level. By taking into consideration of the distinctive properties of the fluoroalkly acrylate compounds such as self-organizing ability with rigid, rod-like and stiff perfluorinated segments, providing flexibility, chain sliding effect, having tendency to exhibit smectic phase, the improvements in the properties of HDPE were mainly aimed by the graft copolymerization. By presuming that the microspheres in HDPE matrix would assist the alignment and orientations of the chains along the draw direction in an application of a load, it was also planned to improve the properties of HDPE, especially mechanical characteristics, by preparation of the blends with the microspheres. In addition, there exists many factors effecting the structure and morphology of microspheres. Therefore, the studies also involve determination of the optimum synthesis conditions to prepare the microspheres with desired morphology.

# 5. MATERIAL AND METHODS

## 5.1 Chemicals and Used Materials

### 5.1.1 Solvents and Reagents

Xylene, acetone, dichloromethane, dimethyl formamide, ethanol, hexane, trietylamine and pyridine (Merck A.G.), methanol and dimethyl sulfoxide (VWR A.G.) and ethyl acetate (Sigma Aldrich) were used without any purification.

p-Hydroxybenzoic acid (HBA), acryloyl chloride (AC), thionyl chloride and ethylene diamine (EDA) (Merck A.G.), 3,3,4,4,5,5,6,6,7,7,8,8,8-dodecafluoro-1-octanol (97%) (Alfa Aesar), the major chemicals for the preparation of the monomer, 3,3,4,4,5,5,6,6,7,7,8,8,8-tridecafluorooctyl-4-(acrloyloxy) benzoate, (ABCF13) were used without any purification. Ethylene glycol dimethacrylate (EGDMA) (Merck A.G.) was used as the crosslinking agent for the preparation of microspheres. Benzoyl peroxide (BP) and dicumyl peroxide (DCP) (Merck A.G.), and potassium persulfate (Sigma Aldrich), the initiators used in the homopolymerization, graft copolymerization and microsphere preparation experiments, were used as received.

### 5.1.2 Preparation of Powder HDPE

Granular high density polyethylene (HDPE) (coded as S 0464) supplied from Turkish Petrochemical Industry (PETKIM) was used to prepare PE powder. The HDPE granules were dissolved in boiling xylene at 138-139°C by refluxing for 3-4 days. The polymer was precipitated adding ethanol, collected by filtering and dried in vacuum at 50°C. The polymer was then ground by cooling in liquid nitrogen to obtain in powder form. The powdered HDPE was used in the graft copolymerization experiments. The simple schemic steps of the preparation of powder HDPE is depicted in Figure 5.1.
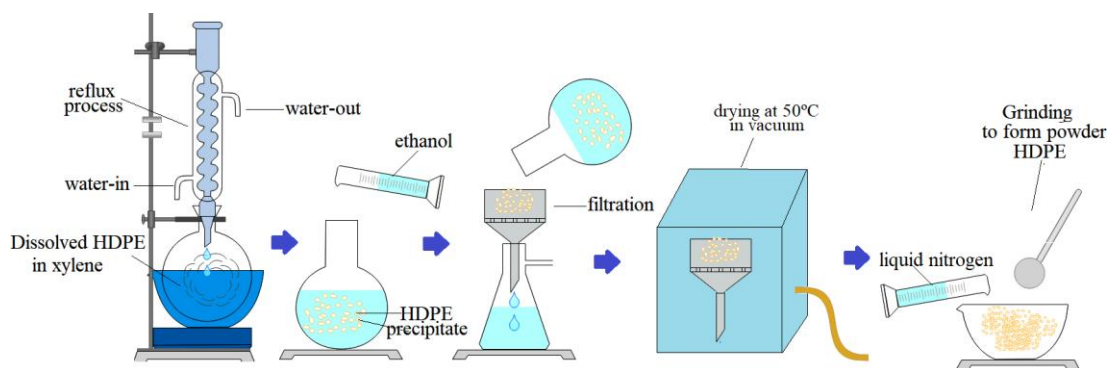
**Figure 5.1.** Simplified preparation steps of powder HDPE.

## 5.2 Synthesis of 3,3,4,4,5,5,6,6,7,7,8,8,8-tridecafluorooctyl-4-(acrloyloxy) benzoate, ABCF13

The synthesis of monomer, ABCF13 was accomplished in three stages: (I) Preparation of p-acryloyloxybenzoic Acid, ABA, (II) Preparation of p-acryloyloxybenzoyl chloride, ABC and (III) Preparation of ABCF13..

### 5.2.1 Preparation of p-Acryloyloxybenzoic Acid, ABA

The synthesis of p-Acryloyloxybenzoic acid, ABA was carried out by the condensation reaction between p-hydroxybenzoic acid and acryloyl chloride in basic medium as previously described by Soykan and coworkers (Soykan et al., 2013). Typically, 34.5 g (0.25 mol) of p- hydroxybenzoic acid was dissolved in 250 ml of NaOH solution (2 molar) prepared previously in a flask equipped with a magnetic stirrer. After cooling the solution to 0 - 5°C in ice bath, 21.5 ml (0.25 mol) of acryloyl chloride was added drop by drop by stirring concurrently. The stirring of the solution was continued for further 1 hour at room temperature. The product formed, ABA was  precipitated by adding diluted and cooled HCl solution, collected by filtering and washed with distilled water excessively. The last product was then recrystallized repeatedly from acetone to obtain pure ABA. The yield found was 77 wt%, in good agreement with the literature (Soykan et al., 2013). The simplified demonstration of the reaction between p-hydroxybenzoic acid and acryloyl chloride was given in Figure 5.2.
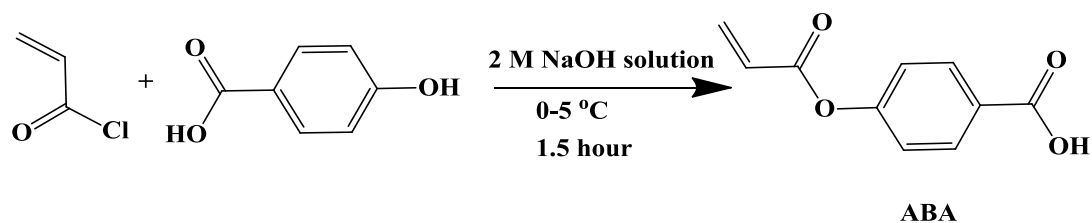
**Figure 5.2.** The simplified demonstration of the reaction between acryloylchloride and p-hydroxybenzoic acid.

### 5.2.2 Preparation of p-Acryloyloxybenzoyl Chloride, ABC

p-Acryloyloxybenzoyl chloride (ABC) required in the synthesis of ABCF13 was prepared by refluxing ABA with thionyl chloride as reported by Sainath and coworkers (Sainath et al, 2000). Typically, 25 g of ABA was refluxed with 250 ml of thionyl chloride containing trace amount of dimethyl formamide for about 8 hours. The product ABC was obtained by removing the excess thionyl chloride with vacuum distillation, and purified by repeated recrystallizations from dichloromethane. During the recrystallizations the solubility was lowered by adding hexane until turbidity. The reaction yield was 98 wt%. The reaction between p-acryloyloxybenzoic acid and thionyl chloride was depicted in Figure 5.3.
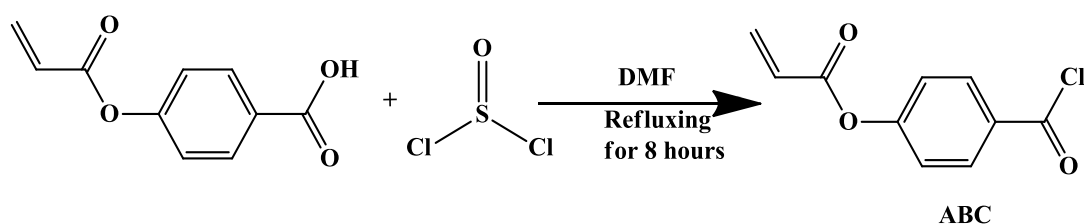


**Figure 5.3.** Simple demonstration of the reaction between p-acryloyloxy benzoic acid and thionyl chloride.

### 5.2.3 Preparation of ABCF13 Monomer

The monomer was prepared by the condensation reaction between 3,3,4,4,5,5,6,6,7,7,8,8,8-dodecafluoro-1-octanol (DFO) and ABC, previously prepared, in basic medium. Typically, 4.75 mmol of DFO and 4.75 mmol of

37

triethylamine was dissolved in 100 mL of EtOAc in a flask equipped with a magnetic stirrer. 4.75 mmol of ABC dissolved in 100 mL of EtOAc was added dropwise at room temperature by stirring the mixture simultaneously. After the reaction was completed, triethylamine hydrochloride salt formed during the reaction was extracted from the product by successive washings (3-4 times) with water. The product was then dissolved in EtOAc. The remaining water in the solution was removed by adding $Na_2SO_4$ as drying agent and then by filtering off. Finally, the solvent was evaporated and the product was purified by repeated recrystallizations from methanol, and dried in vacuum at the room temperature. The synthesis of ABCF13 was also examined by using the solvents DMSO and xylene, but the maximum reaction yield of 81 wt.%, was achieved with EtOAc. The simplified steps and plain reaction were illustrated in Figure 5.4 and 5.5, respetively. FTIR, DSC and ^{1}H-NMR techniques were used for the characterization of the monomer obtained.
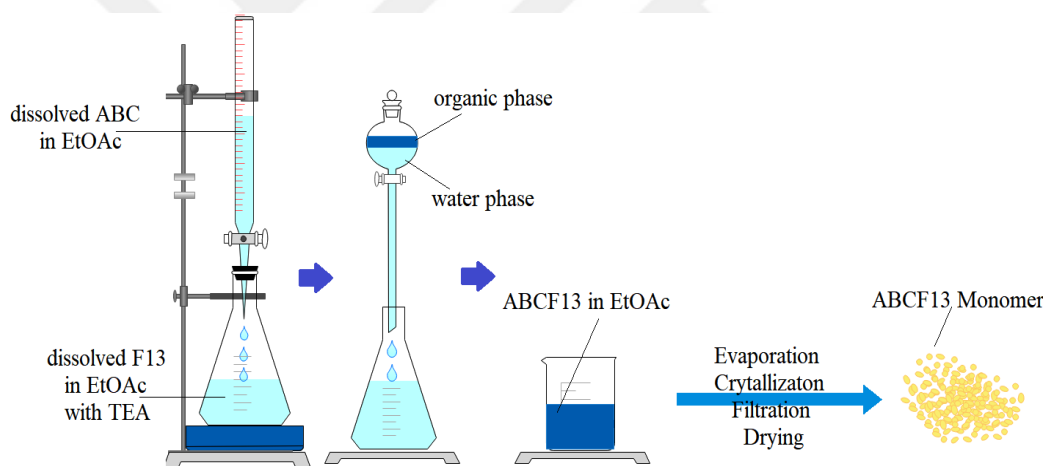


**Figure 5.4.** Preparation stages of ABCF13 monomer.
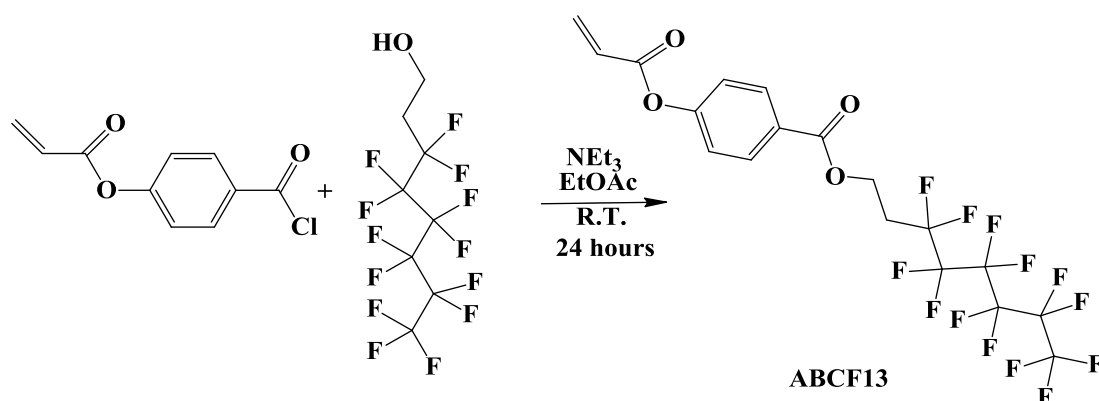


**Figure 5.5**. Simple demonstration of the reaction between ABC and DFO.

A similar route was also followed in order to synthesize another flouroalkyl acrylate monomer by reacting acryloyl chloride with DFO. However, the synthesis was not successful in spite of several attempts at different reaction conditions and use of different solvents. The solvents ethyl acetate, dichloromethane, dimethyl sulfoxide, chloroform with triethylamine and, acetone with sodium hydroxide were examined at varying temperatures (between 0 and 40°C) in order to accomplish the reaction, however, the desired target product, could not be obtained.

### 5.3    Homo and Graft Polymerization of ABCF13

Homopolymerization of the monomer ABCF13 was conducted by bulk-melt polymerization method. The homopolymerization was performed by annealing the mixture of ABCF13 and benzoyl peroxide (BPO, 2% weight of monomer) in vacuum tube at constant temperature of 140°C for an hour. The product, poly(ABCF13) was washed repeatedly with DCM to remove monomer residual, low molecular weight products and products formed during the homopolymerization, and then dried under vacuum. The yield was 96.3%. The product poly(ABCF13) was not soluble in common solvents such as DMF, DMSO, NMP, acetonitrile and dioxane, even when heated in them.

Graft copolymerization of ABCF13 onto the HDPE was also carried out by bulk-melt polymerization. Mixtures composed of HDPE powder, ABCF13 monomer in fine granular form (5, 10, 15, 20, 30, 40% of the mixture) and benzoyl peroxide (BPO) initiator (2% with respect to weight of ABCF13) were prepared by hand grinding in mortar. The mixtures were then heated to 140°C being kept constant for an hour in vacuum ampules. The products were then washed extensively with EMK to remove monomer residual, low molecular weight products and products formed during the polymerization. Because of insolubility of poly(ABCF13) in common solvents, poly(ABCF13) molecules formed during the graft copolymerizations but ungrafted onto HDPE chains could not be removed from the products by washings even with hot DMF, DMSO, NMP, acetonitrile and dioxane. Thus, the extent of graftings could not be determined via gravimetric analysis, and the results, the percentage of poly(ABCF13) in the products were recorded as the total percentage of

poly(ABCF13) involving both grafted and ungrafted poly(ABCF13) units in the products. The experimental set-up for the preparation of glass reaction ampules, and the possible graft copolymerization reaction are shown in Figure 5.6. and Figure 5.7., respectively.
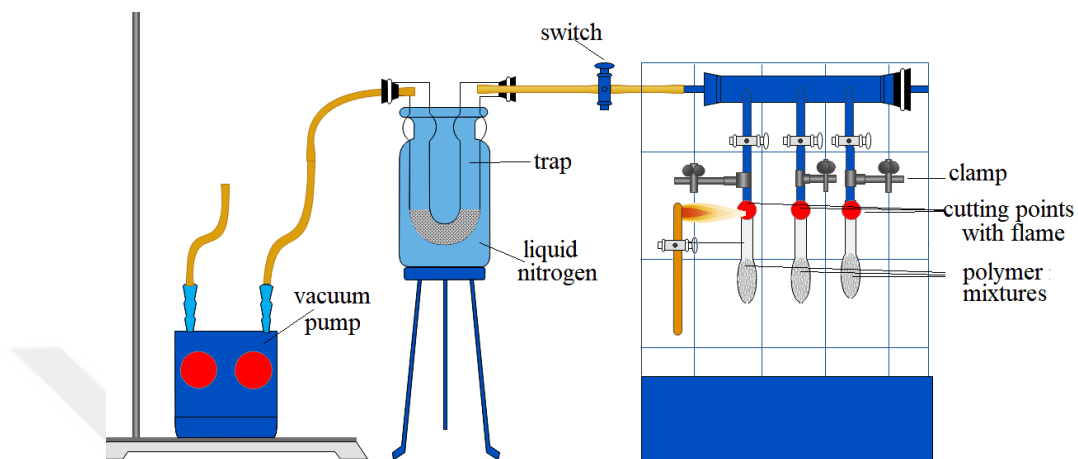


**Figure 5.6**. Schematic represantation of the preparation of glass reaction ampules.
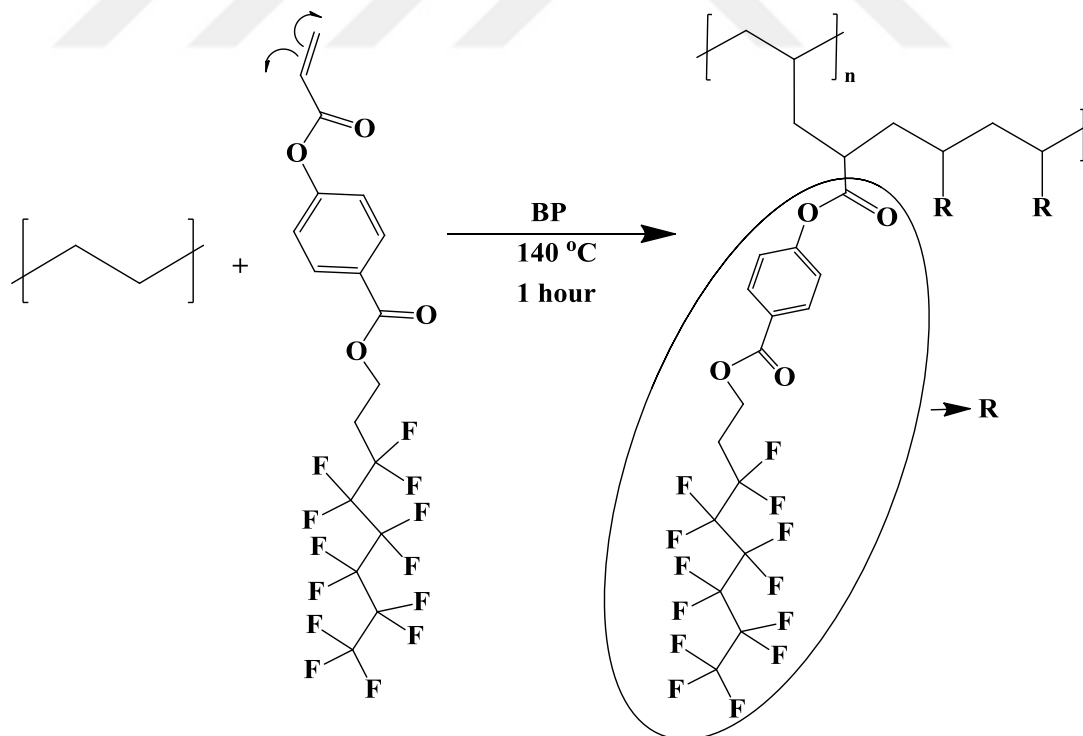


**Figure 5.7.** Possible graft copolymerization of ABCF13 onto HDPE.

## 5.4    Preparation of Crosslinked poly(ABCF13) Microspheres

Crosslinked poly(ABCF13) microspheres were prepared via suspension polymerization. Mixture of ABCF13 melt and the crosslinking agent with predetermined ratio was dripped in certain amount of water at 70°C, as a continuous liquid phase, in two necked cylindirical reaction vessel placed in an oil bath for temperature control, and equipped with a nitrogen gas supply and flat blade turbine type stirrer. The mixture was stirred with the rate of 500 rpm at 70°C until the drop equilibrium was established. After the addition of the initiator KPS, 1.3% with respect to weight of the monomer, the stirring of the suspension mixture was continued for 24 hours to accomplish the polymerization reaction in the drops. The product, crosslinked microspheres, was collected by filtration, washed successively with pure water, and then dried in vacuum oven at 40°C for 12 hours. The average yield of the reaction, determined gravimetrically, was found as 93%. The morphological properties of the microspheres were investigated by using SEM after the samples located on carbon conductive adhesive tape were sputter-coated with Au film. The schematic demonstration of microsphere preparation steps was given in Figure 5.8.
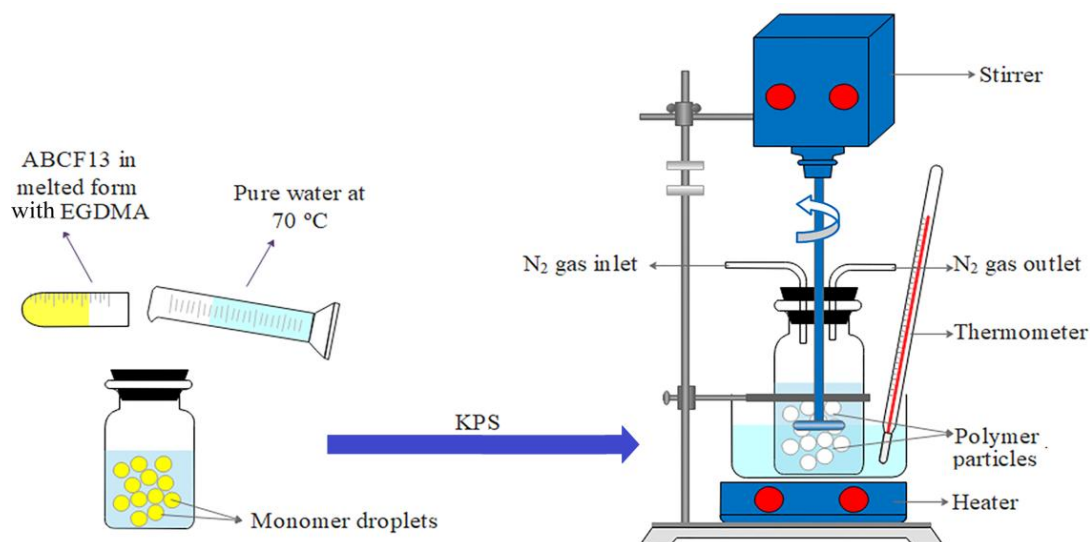


**Figure 5.8.** Reaction stages for the preparation of crosslinked ABCF13 microspheres.

### 5.5    Preparation of Crosslinked poly(ABCF13) Blends with HDPE

The blends of HDPE with crosslinked poly(ABCF13) microspheres at different compositions (1, 3, 5, 7 and 10% of the mixture) were prepared by directly mixing of  the components. In order to achieve good homogeneity in the blends, HDPE in powder form and the microspheres were mixed by grinding for an hour in mortar with pestle.

### 5.6    Characterization Techniques

#### 5.6.1    FTIR Measurements

FTIR analyses of the obtained products were carried out by a Shimadzu 8400 S FTIR spectrophotometer in the region  ranging form 400 to 4000 cm$^{-1}$. KBr pellets containing roughly 3 mg of sample in 100 mg spectroscopic grade KBr were prepared for obtaining FTIR spectra.

#### 5.6.2    $^{1}$H-NMR Measurements

$^{1}$H-NMR spectra of the synthesized ABCF13 monomer was recorded in deuterated chloroform (CDCl$_3$)  with a frequency of 400 MHz. The chemical shifts are reported in ppm (parts per million) by using tetramethylsilane (TMS) as an internal reference.

#### 5.6.3    Differential Scanning Calorimeter (DSC) Analyses

The thermal analysis of the products obtained was carried out by Shimadzu TA-60 WS Differential Scanning Calorimeter under nitrogen atmosphere with a heating rate of 10°C/min and the amount of sample changed between 5-15 mg.

### 5.6.4  TG/IR Analyses

The TG/IR analyses of poly(ABCF13) and samples containing 9.15 and 39.18% poly(ABCF13) were conducted by means of a TGA/FTIR combined system consisting of Exstar SII TG/DTA6300 Thermogravimetric Analyzer and Perkin Elmer Spectrum 400  FTIR Spectrometer (USKIM, KSU). Roundly, 10 mg of samples were pyrolysed with TGA analyzer, the gases evolved from analyzer were directly transmitted to Perkin Elmer Spectrum 400  FTIR Spectrometer via the connected gas line and FTIR spectra were obtained in certain times. The thermogravimetry tests were carried out in not only air but also nitrogen atmosphere in the temperature ranging from 25 to around 600°C with 10°C/min rate of the heating.

### 5.6.5  X-Ray Diffraction (XRD) Analyses

Investigation of crystal structures of the samples were done with Rigaku Multiflex powder X-ray diffractometer system with CuKα target giving a monochromatic beam (λ=1.54°) in the range 2θ=10-60°. The measurements were also conducted at 5°/min scan speed with  0.02° step increment at the room temperature. The intensities of the products having same weights to compare were estimated from XRD patterns.  Moreover, the XRD patterns enabled us to determine the lattice constants (*a*, *b* and *c*) and grain size parameters as a result of the broadening of XRD pattern (Baker and Windle, 2001a and b).

### 5.6.6  Mechanical Test Measurements

The dogbone samples of the graft products (with the thickness of 3 mm, width of 7 mm and gauge length of 62 mm) were prepared at 220°C by using DACA Instruments Microinjector. The crosslinked poly(ABCF13)- HDPE blends dogbone test samples were also prepared at 220°C by using Xplore IM 12 micro-injection molder. LLYOD LR5K Mechanical Tester was utilized to examine tensile properties of dogbone samples of PE and the obtained products with 5 cm/min crosshead speed in testings. The stress strain curve obtained from the software of the instrument give

directly the tensile strengths and moduli. The minimum four samples were analyzed for each composition. The impact strengths of the samples with the thickness of 3 mm and the width 7cm were carried out by Coesfeld Material Test Pendulum Impact Tester at room temperature by Izod method. The computation of the stress-strain values was carried out by means of the load (F)- elongation data during tests as given following equations:

$$\sigma = \frac{F}{A_0} \tag{5.1}$$

$$\varepsilon = \frac{\Delta L}{L_0} \tag{5.2}$$

$$E = \frac{\sigma}{\varepsilon} \tag{5.3}$$

where, $\sigma$ (Mpa), F and $A_o$ imply the tensile stress, applied load (tensile force) and undeformed cross-sectional area of the prepared specimens, respectively. Strain is defined as $\varepsilon$ and also $L_o$ and $\Delta L$ are the initial gauge length and change in the gauge length because of deformation. The Young's Modulus (E) calculated from the Eq. (5.3) is defined as the initial slope of the stress-strain curve.

### 5.6.7 Scanning Electron Microscopy (SEM) Study

The examination of morphologies of tensile and impact fractured surfaces of the graft coproducts and the analysis of the fabricated microspheres and their particle size were conducted with the JEOL 6390-LV scanning electron microscope operated at 20 kV with a resolution power of 3 nm. The analyses of the tensile fractured surfaces of the blends prepared with crossliked poly(ABCF13) and HDPE were carried out by using Quanta FEG 250-FEI scanning electron microscopes worked at 10 kV with the 1 nm resolution power.

### 5.6.8   Positron Annihilation Lifetime Spectroscopy (PALS) Analysis

The free volume characteristics of neat HDPE and coproducts containing various amount of ABCF13 ( 5, 10, 15, 20, 30, 40%) were investigated by means of PALS experiments carried out in Marmara Positron/Positronium Laboratory (MARPOS) in Physics Department at Marmara University. Fast-fast conventional coincidence system was utilized in order to measure the time elapsed between emissions belonging to the $\beta^+$ generated from $^{22}$Na (known as the birth signal of positron with 1.274 MeV photon energy) and gamma annihilation (known as the dead signal with 0.511 MeV photon energy). The $^{22}$Na source was made ready with deposition and evaporation of the 25μCi of $^{22}$NaCI aqueous solution on a thin aluminum foil (5 μm thick)  inserted between two pieces whose surface areas were 0.5x0.5 cm$^2$ and whose thicknesses were 1 mm. The lifetime spectra of the all samples were resolved by means of RESOLUTION and PATHFIT programs to obtain intensities and lifetime and The spectroscopic data yielded from MCA were analyzed by using the code of LT_92_3 (Kirkegaard et al., 1981). The plastic scintillators adhered to Hamamatsu 2059 photomultiplier tubes (PMTs) based by 265 Ortec operated at negative 2000 Volts has been employed for γ ray detection. For windows settings of 1274 keV and 522 keV, and timing signals, two constant fraction differential discriminators (Ortec CFDD 583B) were used. A time to Amplitude Converter, TAC, was used to convert pulses of different heights to a time-to-pulse-height signal. The converted signals were fed to a multichannel analyzer (Ortec Model 919E Ethernim MCA). The system used for the measurements possessed roundly 400 ps (FWHM) resolution and a million counts were detected for each lifetime spectrum of the samples.  The PALS analysis of the sample was conducted at room temperature. The lifetimes of the positron for all samples were obtained and the lifetime spectra were characterized from the viewpoint of three lifetime components. Firstly, the shortest-lived component derived from para-positronium was recorded as $\tau_1$ and $I_1$, secondly the intermediate-lived component caused from positron direct annihilation was recorded as $\tau_2$ and $I_2$  and finally, the longest-lived component originated from ortho-positronium was recorded  as $\tau_3$ and $I_3$. These calculated values were obtained from $\tau_1$ with fixing at 125 ps by presuming that it was independent of free volume.

# 6. RESULTS AND DISCUSSIONS

## 6.1    Characterizations

### 6.1.1    Characterization of HDPE

FTIR spectrum belonging to high density polyethylene (HDPE) used throughout the graft copolymerization experiments is depicted in Figure 6.1. The absorption bands of stretching vibrations of $-CH_2$ group were observed at 2918 and 2848 $cm^{-1}$. The IR bands identified at 1558, 1471 and 1462 $cm^{-1}$ are assigned to bending vibrations of $-CH_2$ groups. The absorption bands observed at 729 and 717 $cm^{-1}$ are ascribed to C-C bending vibrations.

DSC melting point of HDPE annealed at 140°C and of that processed with 2% BPO 140°C in vacuum were found as 130.80 and 131.45°C, respectively, with the heating rate of 10°C/min in $N_2$ atmosphere. The thermograms are depicted in Figure 6.2.
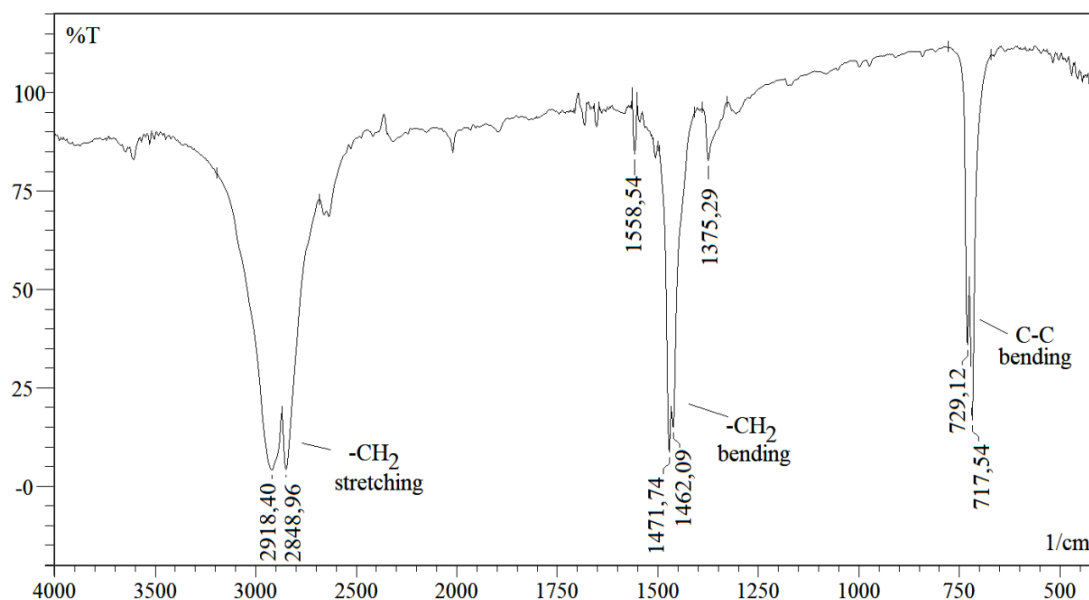


**Figure 6.1.** FTIR spectrum of the neat HDPE.
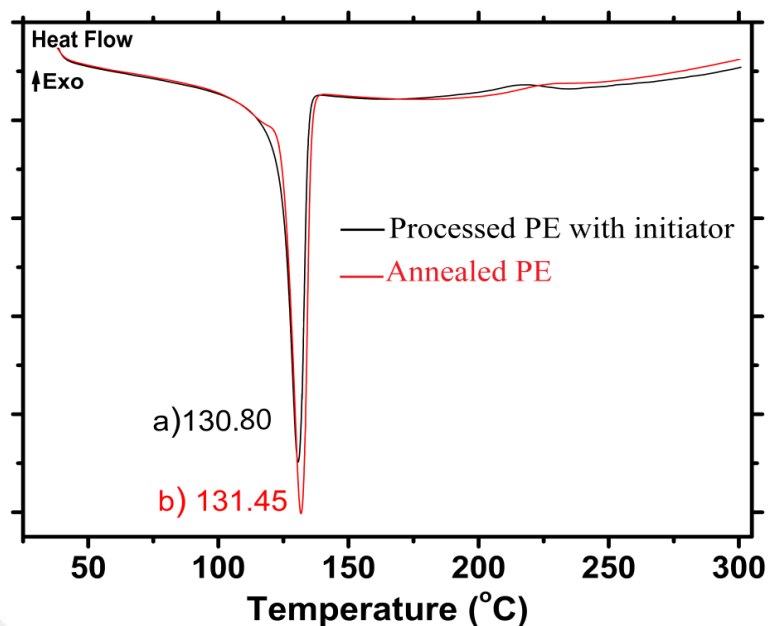
**Figure 6.2.** DSC thermogram of HDPE a) processed with BPO, and b) annealed (Soykan and Cetin, 2015).

### 6.1.2 Characterization of ABCF13

FTIR spectrum of the ABCF13 is illustrated in Figure 6.3. The moderate absorption peaks observed at 3109 and 3070 $cm^{-1}$ are due to aromatic stretching vibrations of C-H bond in the phenyl group of the structure. The moderate IR bands designated at about 2976 and 2926 $cm^{-1}$ are assigned to the stretching vibrations of $CH_2$ groups. The strong band at 1739 and 1716 $cm^{-1}$ are attributed to the C=O stretching vibrations of the ester groups in the molecule. The bands detected at 1635 and 1602 $cm^{-1}$ are due to the stretching vibrations of C=C bonds in the vinyl and phenyl groups, respectively. Also the strong bands observed at about 1205 $cm^{-1}$ is corresponding to C-O stretching vibrations. The absorption bands assigned to stretching vibrations of C-F bonds are observed in the range of 1122-1284 $cm^{-1}$. The moderate bands appearing between 802 and 1089 $cm^{-1}$ represent the vinylic C-H out-of-plane bending vibrations.

Figure 6.4. shows ^{1}H-NMR spectra of the ABCF13 molecule. It can be deduced from the figure that a multiplets at about δ 6.06 and 6.6 are corresponding to Hb and Ha protons of vinylic groups, respectively. The another two doublets observed at δ 6.31 and 6.34 is attributed to Ha-Hc and Hb-Hc trans coupling of vinylic groups, respectively. He and Hd protons which is corresponding to single O-coupling of the -C$_6$H$_4$ groups in the molecule depict two multiplet peaks at δ 7.2 and 8.1, respectively. In addition, the triplet observed at about δ 4.6 is assigned to Hf protons of -CH$_2$ groups found in alfa position of oxygen atom. The broad multiplet detected at δ 3.6 is clearly corresponding to Hg protons of another -CH$_2$ groups located near perfluorinated segment in the molecule.

The results obtained from DSC measurements demonstrated the melting point of ABCF13 at 44.89°C under N$_2$ atmosphere with heating rate of 10°C /min. The thermogram was presented in Figure 6.5. The endotherms at about 197, 203 and 210°C may be attributed to the temperature at which the molecule started to decompose.
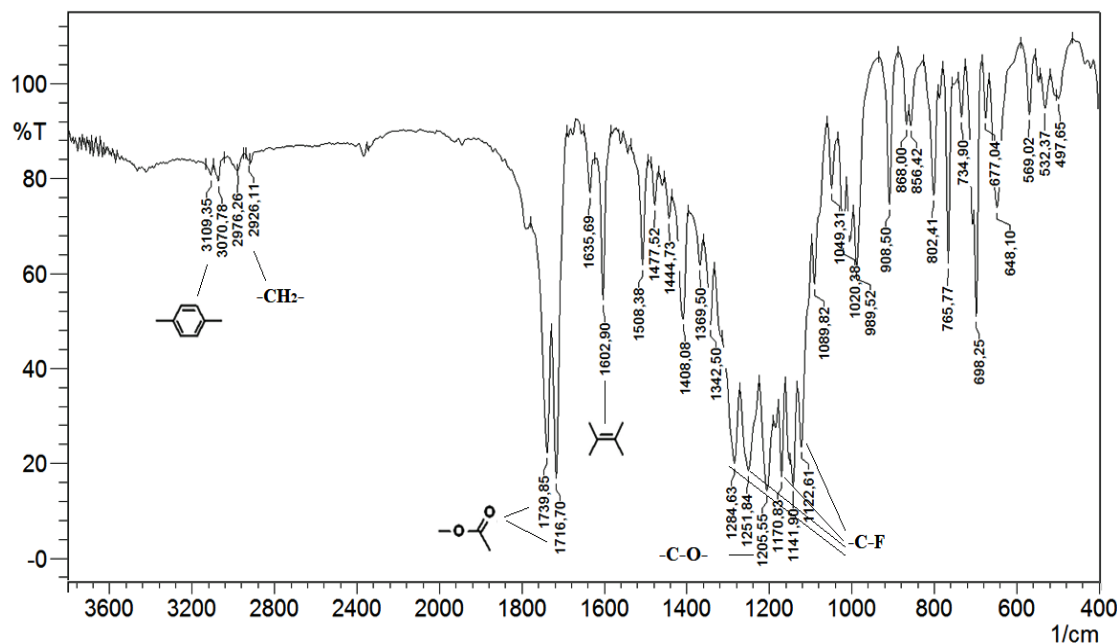


**Figure 6.3.** FTIR spectrum of the ABCF13.
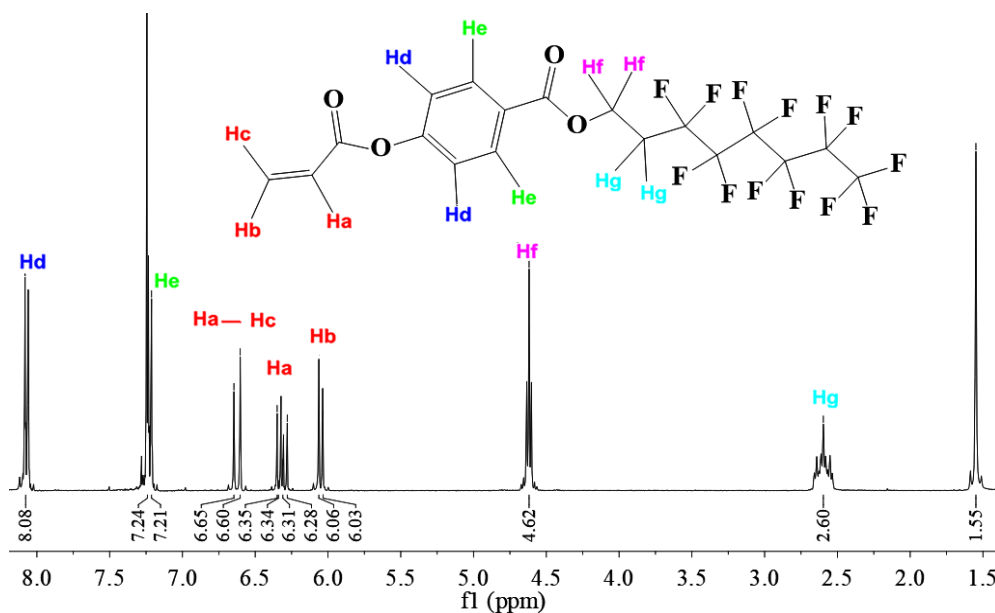
**Figure 6.4.** The $^1$H-NMR spectrum of ABCF13
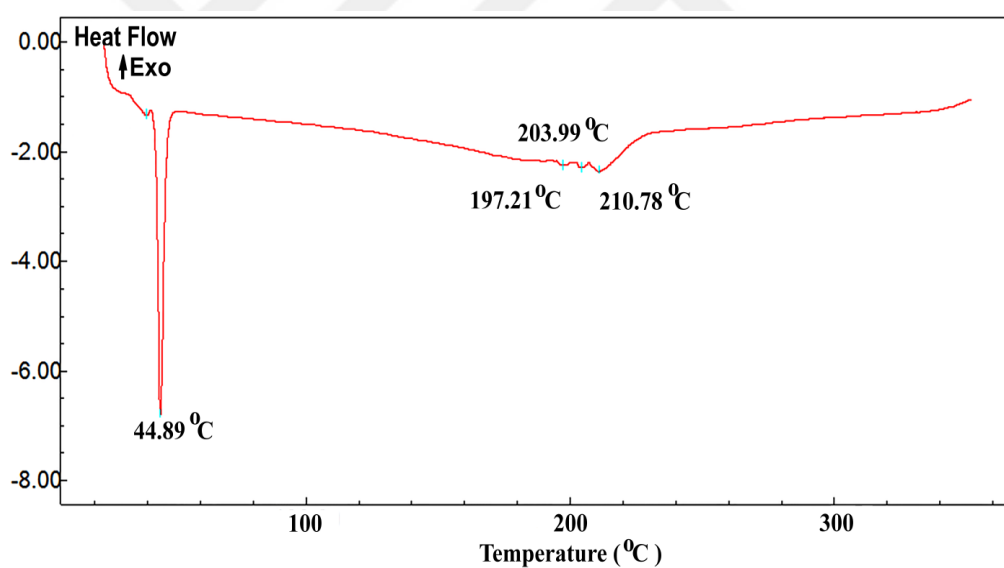


**Figure 6.5.** DSC thermogram of ABCF13.

### 6.1.3 Characterization of poly(ABCF13)

FTIR spectrum of poly(ABCF13) is depicted in Figure 6.6. The moderate IR bands detected at 3128 and 3078 cm$^{-1}$ are corresponding to C-H stretching vibrations of aromatic phenyl group. The other moderate absorption peaks observed at 2966 and 2931 cm$^{-1}$ are due to the stretching vibrations of -CH$_2$ groups in the structure. The

49

strong bands designated at about 1759 and 1728 cm$^{-1}$ are assigned to the stretching vibrations of C=O bonds in ester groups. It is visible that the disappearing of the absorption bands at 1635 cm$^{-1}$ is due to the polymerization reaction progressing through C=C bonds. The absorption band detected at 1608 cm$^{-1}$ is directly related to the stretching vibrations of C=C bonds in phenyl groups. Moreover, the strong absorption band observed at about 1207 cm$^{-1}$ is due to C-O stretching vibrations. The broad and strong bands observed in the range of 1118-1280 cm$^{-1}$ are corresponding to the stretching vibrations of C-F bonds.

Figure 6.7 describes the thermal behavior of poly(ABCF13) in DSC measurement carried out under N$_2$ atmosphere with a heating rate of 10°C/min. Although small endotherm observed at 334.7°C might be attributed to the melting of small crystalline domains, amorphous character is dominant in the thermal behavior of poly(ABCF13). Irregular endothermic behavior seen at higher temperatures, around 340°C and 350°C, presumably shows the decomposition of the homopolymer.
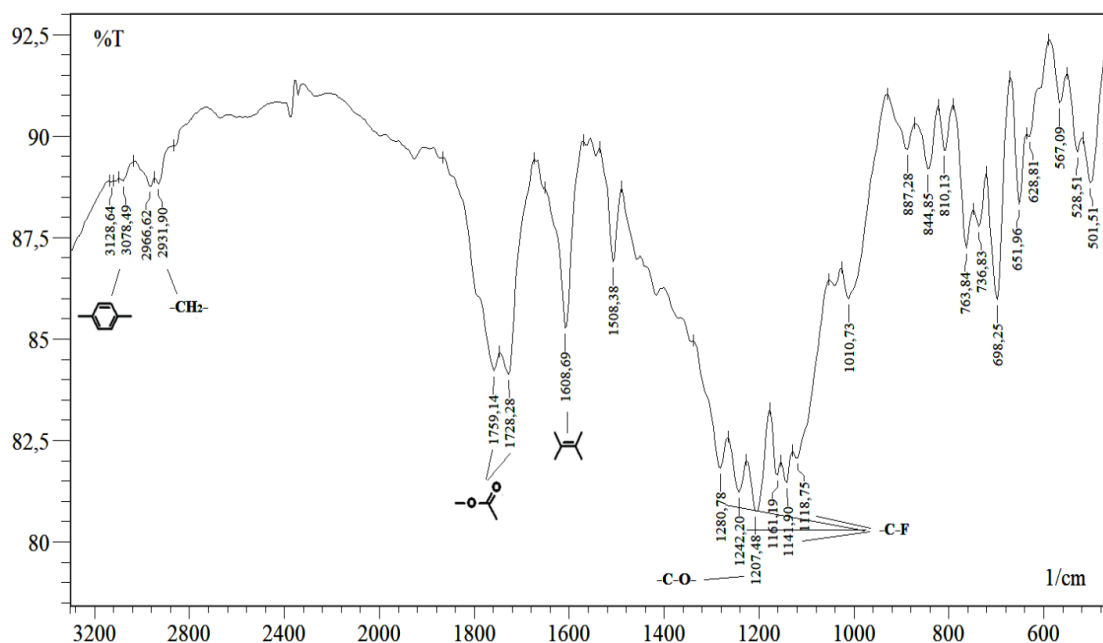


**Figure 6.6.** FTIR spectrum of the poly(ABCF13).
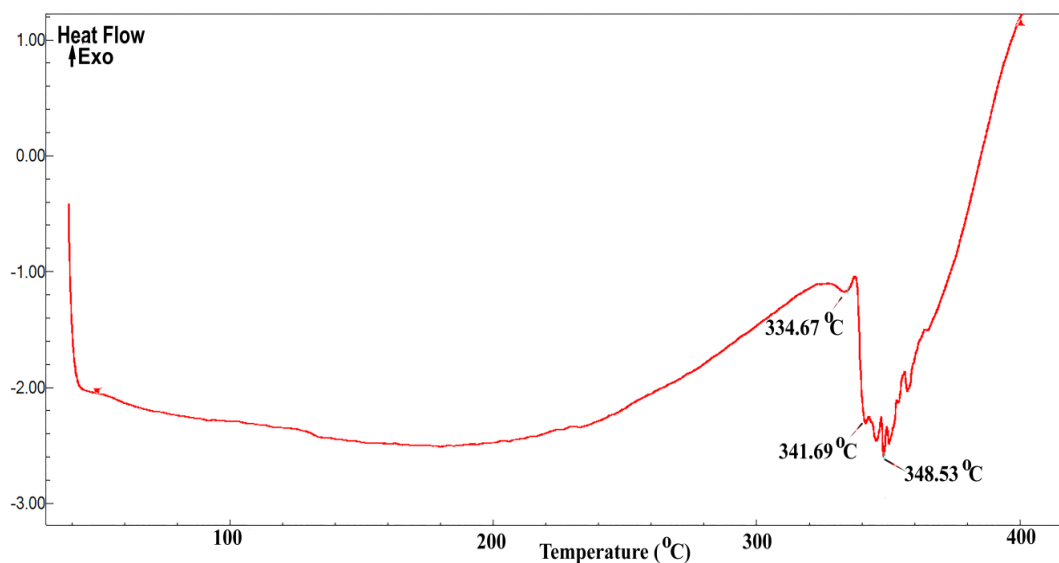
**Figure 6.7.** DSC thermogram of the poly(ABCF13).

### 6.1.4   Graft Copolymerization of ABCF13 onto HDPE

Graft copolymerization of ABCF13 onto HDPE was carried out with the use of BPO initiator at 140°C, the temperature above the melting point of both HDPE (131°C) and ABCF13 (44°C). The grafting was studied in detail with the reaction mixtures prepared at six different percentages of ABCF13 in the medium. Since poly(ABCF13) was not soluble in any conventional, strong solvents such as DMF, DMSO, NMP, acetonitrile and dioxane, the percent grafting could not be determined gravimetrically. Therefore, the findings, the percentage of poly(ABCF13) in the products was reported as the total percentage of poly(ABCF13) involving both the grafted units and ungrafted poly(ABCF13) homopolymer molecules, as presented in Table 6.1. The results showed that the content of poly(ABCF13) in the products continuously increased with the increment of ABCF13 percentage in the reaction mixture. That is, percent conversion increased with concentration of the monomer, from 83.4% at 5% ABCF13 to 97.9% at 40% ABCF13, Figure 6.8. This was probably due to the increase of initiator concentration with the raise of monomer percentage in the reaction mixture. Because the amount of initiator in the mixture was 2% of the weight of the monomer.

The variation of poly(BPOCPA) content in the products with the concentration of ABCF13 in the reaction mixtures and percent conversion were calculated by means of the following equations;

$$\% \, \text{Poly(ABCF13)} = \frac{(W_{\text{Product}} - W_{\text{HDPE}})}{W_{\text{Product}}} \times 100 \tag{6.1}$$

$$\% \, \text{Conversion} = \frac{W_{\text{poly(ABCF13)}}}{W_{\text{ABCF13}}} \times 100 \tag{6.2}$$

Where, $W_{\text{Product}}$ is the weight of the product after the washing and drying processes, and $W_{\text{HDPE}}$ is the weight of HDPE present in the reaction mixture. $W_{\text{Poly(ABCF13)}}$ is the weight of poly(ABCF13) in the product and $W_{\text{ABCF13}}$ is the weight of the monomer ABCF13 in the reaction mixture.

**Table 6.1.** The percentage of HDPE and ABCF13 in the reaction mixtures, content of poly(ABCF13) in the products and percent conversion.

| Sample | 1. | 2. | 3. | 4. | 5. | 6. |
|---|---|---|---|---|---|---|
| % HDPE in rxn. mixture | 95 | 90 | 85 | 80 | 70 | 60 |
| % ABCF13 in rxn. mixture | 5 | 10 | 15 | 20 | 30 | 40 |
| % Poly( ABCF13) in the products | 4.17 ±0.44 | 9.15 ±0.39 | 13.96 ±0.10 | 19.18 ±0.03 | 28.89 ±0.14 | 39.18 ±0.53 |
| % Conversion | 83.4 ±8.8 | 91.5 ±3.9 | 93.1 ±0.7 | 95.9 ±0.1 | 96.9 ±0.5 | 97.9 ±1.3 |
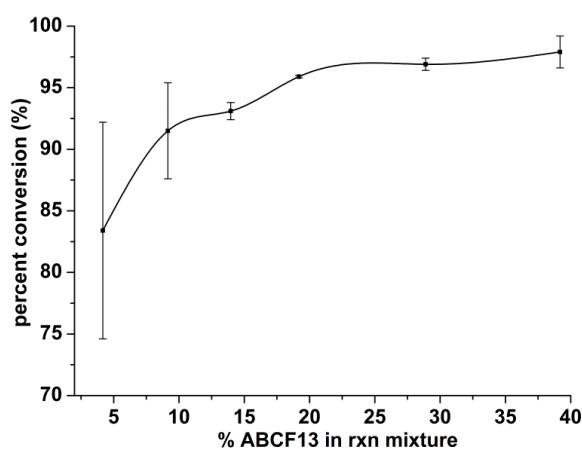


**Figure 6.8.** The variation of percent conversion with poly(BPOCPA) content in the products.

### 6.1.5 FTIR Characterization of Crosslinked poly(ABCF13) Microspheres

The FTIR spectrum of the poly(ABCF13) microspheres obtained with the use of the crosslinking agent EGDMA displaying the characteristic peaks was illustrated in Figure 6.9. The small bands detected at 2970 and 2931 cm$^{-1}$ are corresponding to stretching vibrations of aliphatic -CH$_2$ groups. The strong and broad band detected at 1735 cm$^{-1}$ is due to the stretching vibrations of C=O bonds of ester groups present in the structure of both the monomer and the crosslinking agent. The absorption band detected at 1620 cm$^{-1}$ is corresponding to the stretching vibrations of C=C bonds in phenyl groups. The moderate bands appearing between 1141 and 1280 cm$^{-1}$ represent the stretching vibrations of C-F bonds in structure.
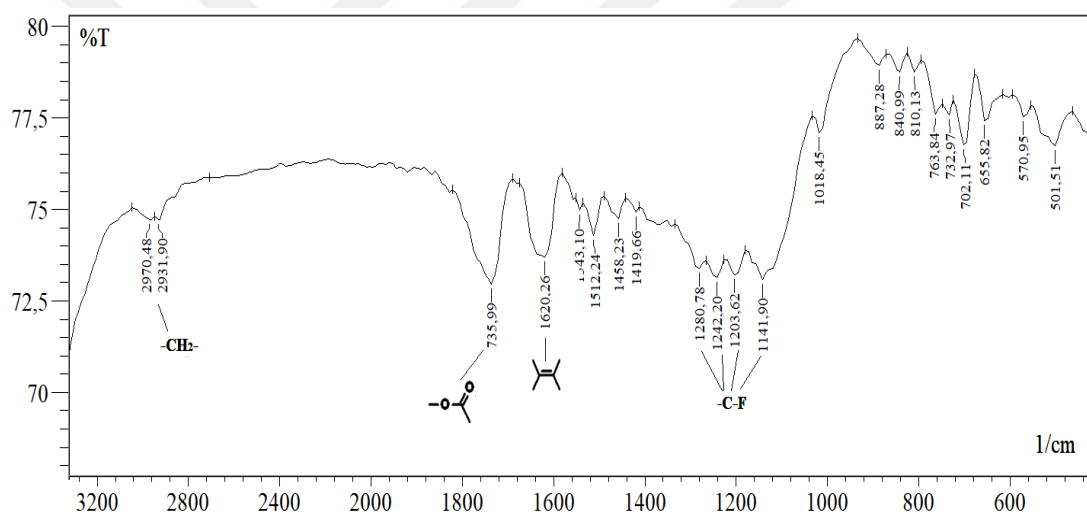


**Figure 6.9.** FTIR spectrum of poly(ABCF13) microspheres.

## 6.2    Thermal Analysis of the Products

### 6.2.1    DSC Analysis of the Products

The effect of the graft copolymerization of ABCF13 onto HDPE on the thermal properties of the coproducts was comprehensively investigated by DSC. The thermograms obtained with heating rate of 10°C/min under $N_2$ atmosphere were presented in Figure 6.10. The endothermic heat flows attributed to the crystalline melting were merely that showing the melting of HDPE crystalline domains, recorded between 130.18°C and 134.21°C. Poly(ABCF13) component of the coproducts exhibited completely amorphous character in the analyses, as was observed in the anaysis of pure Poly(ABCF13). On the other hand, exothermic heat flows observed around 220°C and becoming more prominent with the increase of poly(ABCF13) content up to about 20% presumably arose from some reorganizations in the poly(ABCF13) units.

The dependence of melting temperature of HDPE crystalline domains on poly(ABCF13) content in the products was presented in Table 6.2 and the variation with the content was graphically displayed in Figure 6.11.a. The melting temperature initially increased with the content and reached the the maximum 134.21°C at 13.96% poly(ABCF13) which was followed by a sharp decrease reducing to comparable values with that of pure HDPE, Figure 6.11.a. In general, high melting points are associated with highly regular structures, close packing capability, rigid molecules, strong interchain attraction, or several combination of these factors (Sperling, 2006). Melting temperature is also directly related to crystallization process, affected by nucleation and miscibility of the components in polymer combinations (Chen et al., 2014). The initial increase in melting temperature of HDPE component at relatively lower contents up to 14% poly(ABCF13) are believed to arose from the improvements in the packing order of the chains due to the attractive interactions between the polar groups belonging to graft units. The decrease following the maximum presumably resulted from that the assisting function of the graft units with polar groups in more ordered packing of HDPE chains might be lost with the increase of poly(ABCF13) percentage in the products. Because the graft units with polar groups, while assisting the more ordered packing

54

of HDPE chains at lower percentages might loose their effect as the content is increased due to preferred and advanced interactions between the poly(ABCF13) units.
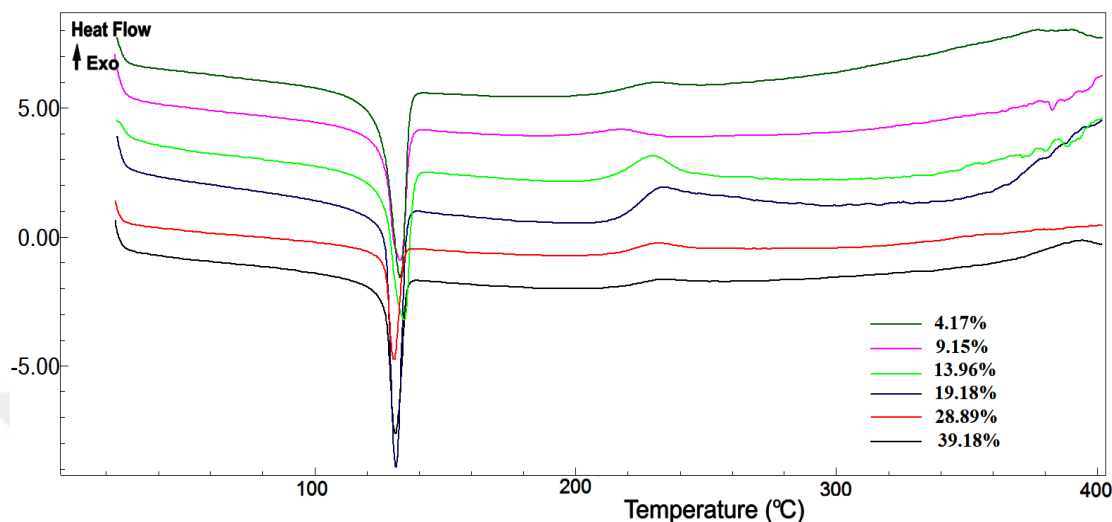


**Figure 6.10.** DSC thermograms of coproducts formed with different ABCF13 contents.

**Table 6.2.** The variation of the melting point (Tm), enthalpy of fusion (ΔHm) and percent crystallinities (Xc, %) of products with poly(ABCF13) percentages.

| Sample | $T_m$ (°C) | $\Delta H_m$ (J/g) | $X_c$ (%) |
|---|---|---|---|
| Neat HDPE | 130.80±0.19 | 118.48±5.02 | 40.86±3.79 |
| 4.17 % poly(ABCF13) | 132.56±0.42 | 162.19±2.94 | 55.93±2.21 |
| 9.15 % poly(ABCF13) | 132.93±1.20 | 190.92±2.16 | 65.83±1.63 |
| 13.96 % poly(ABCF13) | 134.21±0.55 | 178.25±2.47 | 61.47±1.86 |
| 19.18 % poly(ABCF13) | 131.25±1.05 | 172.27±2.98 | 59.40±2.25 |
| 28.89 % poly(ABCF13) | 131.19±0.39 | 183.57±4.11 | 63.30±3.10 |
| 39.18 % poly(ABCF13) | 130.19±0.39 | 202.17±4.64 | 69.71±3.50 |

In addition, the heat of fusion values of HDPE crystalline domains in the coproducts were determined directly by using software of the DSC instrument from the endotherms of the thermograms, and percent crystallinities ($X_c\%$) in HDPE matrices were calculated by using following equation:

$$X_C\% = \frac{\Delta H_f}{\Delta H_f^o} \text{ x } 100 \tag{6.3}$$

Where, $\Delta H_f$ and $\Delta H_f^o$ donate heat of fusion (specific enthalpy of melting) of HDPE crystalline domains in the matrix of the coproducts and heat of fusion of 100% crystalline HDPE (290 J/g) (Alothman, 2012; Fouad, 2010), respectively. The results were given in Table 6.2, and the variation of the percent crystallinity with poly(ABCF13) content in the products were drawn in Figure 6.11.b.

Percent crystallinity properties of the products were considerably affected from poly(ABCF13) content existing in the matrix, as shown in Figure 6.11.b. The results showed that the degree of crystallinities of all products were larger compared to that of neat HDPE. The percent crystallinity of HDPE domain increased initially with the increasing of poly(ABCF13) content and reached to 65.83% at the product containing 9.15% poly(ABCF13), which was followed by decreasing trend until to 19.18% poly(ABCF13) content. This decreasing trend may be derived from the weakening of spatial ordering effects assisted by poly(ABCF13) and increment in defects stemming from regional irregular crystallization at 13.96 and 19.18% poly(ABCF13) products. Up to 20% poly(ABF13), the increasing trend was observed again and the percent crystallinity reached the maximum value, 69.71% with 39.18% poly(ABCF13) product. The larger degree of crystallinity means the existence of higher orderly arranged polymer chains in the crystalline region of solid polymers. That is, at high contents, the poly(ABCF13) bearing rigid and stiff segments in its structure may contribute to the arrangement of the HDPE chains, which ending up larger percent crystallinity of HDPE domains. Moreover, that the increasing of poly(ABCF13) content in polymer matrix may create the additional co-crystallization effects, which resulting in increment in the percent crytallinity at high contents (Shi et al., 2009).
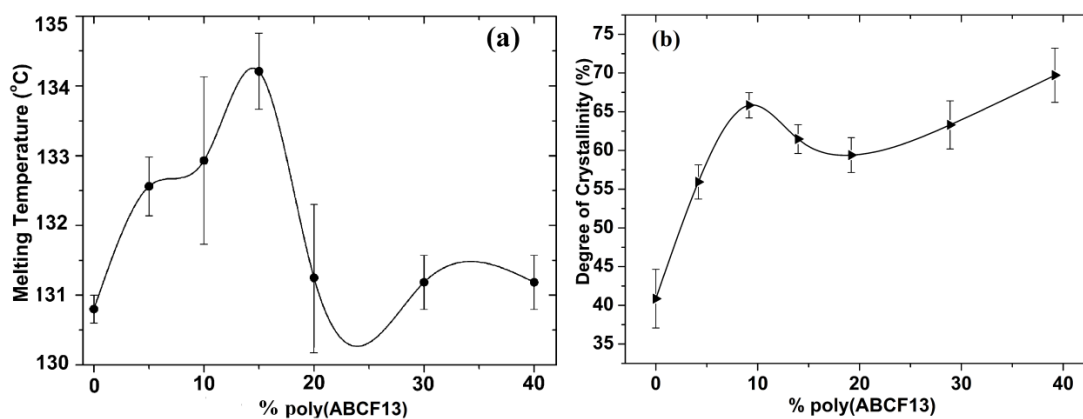
**Figure 6.11.** Dependence of (a) melting temperature and (b) degree of crytallinity on poly(ABCF13) content in products.

### 6.2.2 TG/IR Analysis of the Products

In order to elucidate the thermal properties, the optimum processing temperatures and to determine decomposition products, the TG/IR analyses of the homopolymer, poly(ABCF13) and the products containing 9.15 and 39.18% poly(ABCF13) were conducted in not only air but also $N_2$ atmosphere successfully.

#### 6.2.2.1 TG/IR Analysis of poly(ABCF13)

Thermogravimetric analysis of the poly(ABCF13) was carried out in both air and $N_2$ atmospheres in order to clarify its thermal behavior and decomposition mechanism. The variation of the percentage of weight loss with the raising temperature in both atmospheres was illustrated in Figure 6.12. The results showed that the temperature, which the first weight losses of poly(ABCF13) in air and $N_2$ atmospheres started, was found to be at about 226°C (1.00%). The weight loss trend were nearly similar for both atmospheres, Figure 6.12. However, as the temperature increased, poly(ABCF13) in air atmosphere decomposed at a little lower temperature. Namely, the about 6% weight loss was recorded at 305.8°C and 307.4°C in air and $N_2$, respectively. Hence, the thermal stability of the poly(ABCF13) was a little higher in $N_2$ atmosphere. It may be caused that the functional groups in poly(ABCF13) molecules could react easily with oxygen to give decomposed products, resulted in earlier decomposition. Moreover, slow weight

losses for both atmosphere were observed until about 300°C, but the impressive weight loss commenced at above 300°C and reached the maxima in the region of approximately 320-370°C in both atmospheres, as seen in Figure 6.12. In this temperature range, the percent weight losses for both atmospheres was found as roundly 66% by decreasing approximately from ~89% to ~23%. At 350°C, the homopolymers lost approximately half of the their weight in both air and nitrogen atmospheres during analyses. Furthermore, the decomposition of homopolymer continued to 567°C with 95.1% weight loss in $N_2$ atmosphere and to 572°C with 94.9% weight loss in air atmosphere, Figure 6.12.
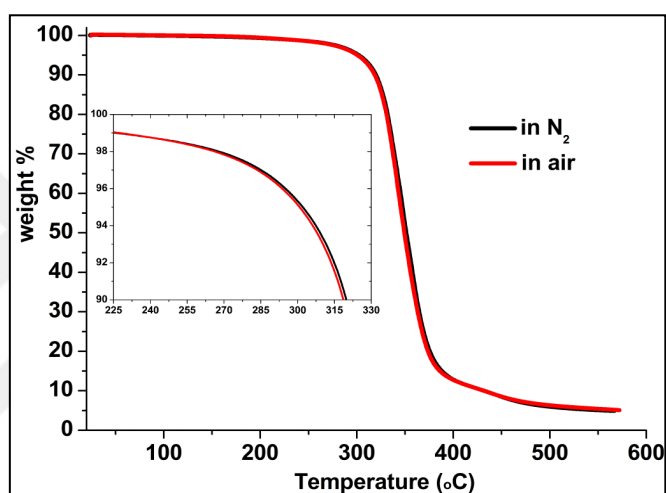


**Figure 6.12.** TGA thermogram of poly(ABCF13) in $N_2$ and air atmospheres.

The determination of the decomposition products of the homopolymer in both $N_2$ and air atmospheres was done by means of FTIR spectrometer combined with TGA. In $N_2$ atmosphere, the findings showed that the observed absorption bands were nearly similar from the beginning to end of the heating and only the intensities of the absorption bands changed in spectra, as depicted in Figure 6.13. It was observed that the carbon dioxide ($CO_2$) formed throughout the heating with varying intensity and the its characteristic absorption bands was detected at around ~2300 cm$^{-1}$, which was attributed to C=O stretching vibrations of $CO_2$. At the beginning of the decomposition (at about ~330°C with 17,6% weight loss), the weak and tentative absorption bands were observed in spectrum, Figure 6.13.a. However, the distinct absorption bands belonging to stretching vibrations of C-F bonds were observed in the range of 1100-1300 cm$^{-1}$ at early stage of decomposition. The apparent and

notable absorption bands were detected by the time the decomposition became fast and all characteristic absorption bands of the decomposition products of poly(ABCF13) in $N_2$ were observed at the spectrum taken at 390°C, Figure 6.13.b. The intensity of the absorption bands due to C-F stretching vibrations reached maximum and become more clear. The bands detected at about 3642 cm$^{-1}$ was presumably due to O-H stretching of the phenolic groups. The more small bands designated at about ~3100 and ~2900 cm$^{-1}$ were assigned to the stretching vibration of aromatic C-H and aliphatic -CH$_2$ bonds, respectively. The bands observed at around 1740 cm$^{-1}$ were due to C=O stretching vibrations of the ester groups. Moreover, the absorption bands seen at about 1500 and 1600 cm$^{-1}$ were probably due to vinylic and aromatic C=C stretching, respectively. The stretching vibrations of C-O bond were detected at seemingly around 1240 cm$^{-1}$. The bands at about ~700 and 840 cm$^{-1}$ may be attributed to out-of-plane bending vibrations of vinylic C-H bonds. The absorption bands became weaker as the temperature increased and some characteristics bands disappeared or weakened after about 420°C as showed in Figure 6.13.c.
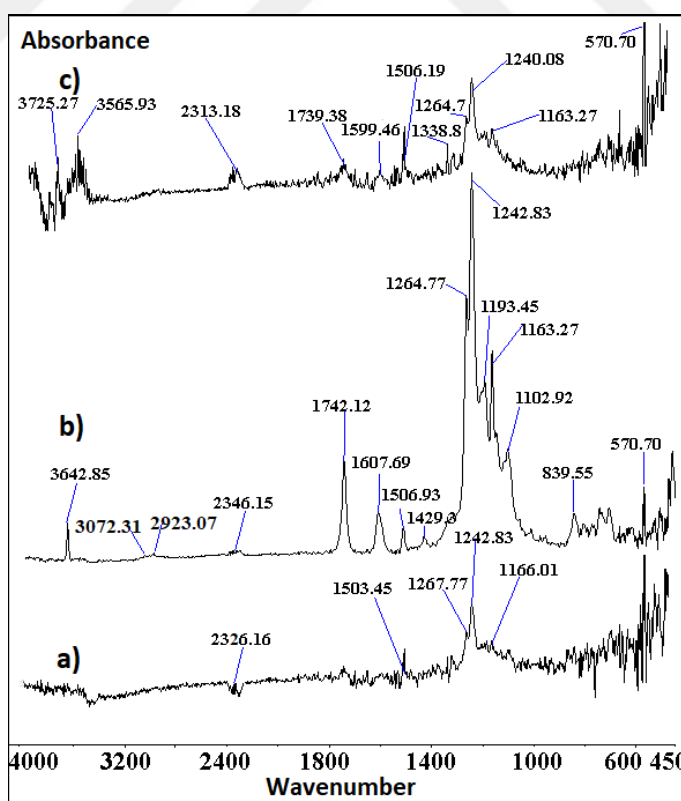


**Figure 6.13.** FTIR spectrum of the decomposition products of poly(ABCF13) formed at a) 330°C, b) 390°C and c) 440°C in nitrogen.

59

In addition, poly(ABCF13) was analyzed in air atmospheres. The FTIR spectra showed that the decomposition mechanism of poly(ABCF13) in air atmosphere resembled to that observed in $N_2$ atmosphere, Figure 6.14. The mostly similar characteristic bands belonging to poly(ABCF13) were observed in spectra taken in air. The stronger absorption bands of the decomposition products, especially due to $CO_2$, were detected at early and further temperatures during analysis. However, several newly peaks formed around the characteristics bands of poly(ABCF13) could not be assigned. Moreover, these formed undefined absorption bands were observed from the beginning to the end of the heating, as seen in Figure 6.14.a, b and c.
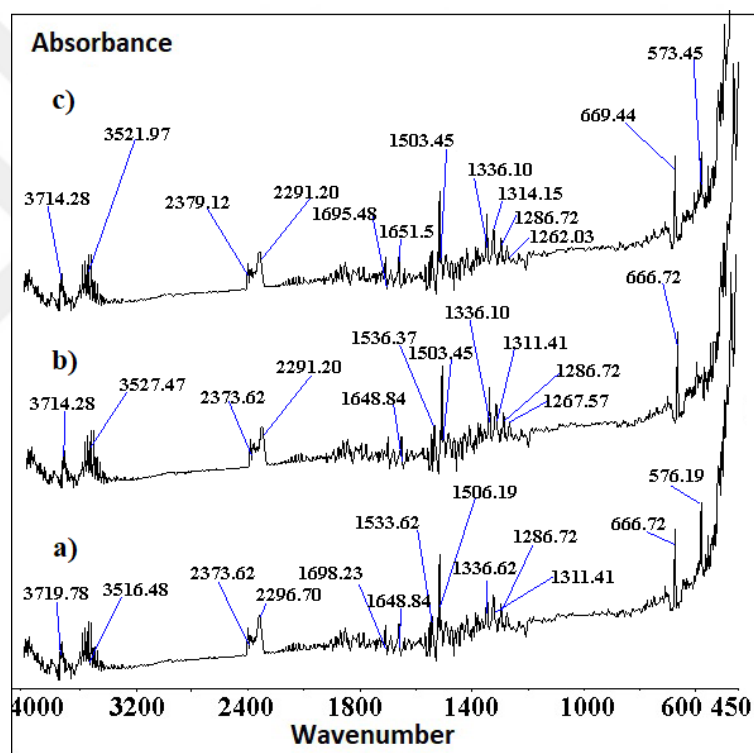


**Figure 6.14.** FTIR spectrum of the decomposition products of poly(ABCF13) formed at a) 320°C, b) 370°C and c) 450°C in air.

### 6.2.2.2 TG/IR Analysis of Graft Products

Initially, thermogravimetric analyses of the products containing 9.15 and 39.18% poly(ABCF13) were conducted in $N_2$ atmosphere. The change of the percentage of weight losses of the mentioned products with temperature was depicted

in Figure 6.15.a and b. At low content, the weight loss trend roundly resembled homopolymer, but, at high content, the products showed different decomposition mechanism with gradual decreasing trend. This segmental behavior may be evidence for the presence of the both homopolymer and grafted units in matrix. The findings also revealed that the first weight losing of 9.15 and 39.18% poly(ABCF13) products commenced at about 299.5°C (0.99%) and 236.2°C (1.2%), respectively. It means that both poly(ABCF13) and HDPE contents effected highly to the weight loss and decomposition mechanism of the products, Figure 6.15. Namely, the increasing of percentage of poly(ABCF13) in the matrix (meaning the decrease in PE percentage) led to the easier and earlier decomposition of the products. This may be attributed to the weakening of retardation effect of PE during heating. Accordingly, when the products were compared to homopolymer in terms of the thermal stability, the retardation effect of PE in the 9.15% poly(ABCF13) product could be seen in Figure 6.15.a. Moreover, at a certain temperature, the percent weight losses of the products at high poly(ABCF13) content was larger than that observing at low poly(ABCF13) content, Figure 6.15.a and b. When the heating temperature reached to about 350°C during analysis, the weight losses of the 9.15 and 39.18% poly(ABCF13) products were found as 5.6% and 16.5%, respectively. The immense weight losses for the products were observed in the region of about 420-490°C and the 99% weight loss was reached at about 484°C for the products, as seen in Figure 6.15.a and b.
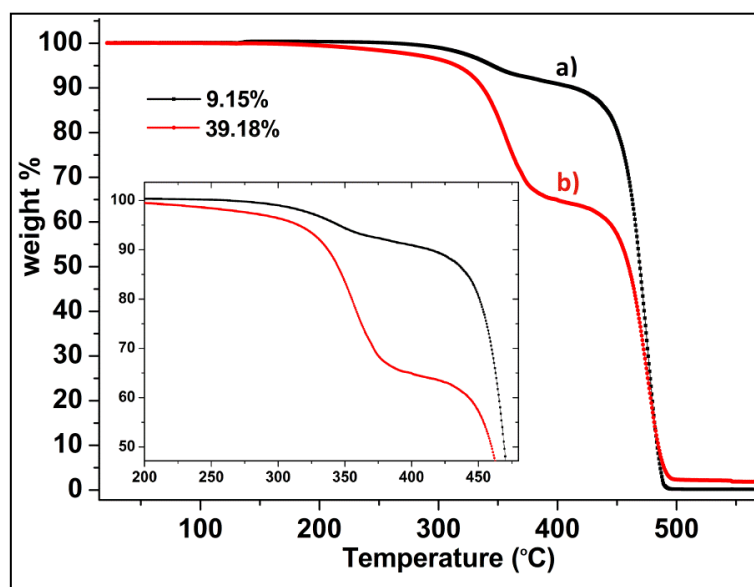


**Figure 6.15.** TGA thermogram of the products with a) 9.15% and b) 39.18% poly(ABCF13) taken in nitrogen.

FTIR spectra taken in $N_2$ atmosphere revealed that the products containing 9.15% and 39.18% poly(ABCF13) had nearly similar characteristic absorption bands with corresponding to that seen in homopolymer, Figure 6.16. and 6.17, respectively. However, the absorption bands at about 2920, 2860 and 760 $cm^{-1}$ were not observed in the spectra of homopolymer since they were the characteristic bands of PE. The bands detected at about 2920 and 2860 $cm^{-1}$ were assigned to stretching vibrations of -$CH_2$ groups of PE and these bands became more massive and apparent at further temperature (especially above 440°C), Figure 6.16.c. The bands observed at about 760 $cm^{-1}$ were ascribed to C-C bending vibrations of PE, Figure 6.16.b and c, also Figure 6.17.c. These peaks were also not observed at early stages of decomposition of 9.15% and 39.18% poly(ABCF13) products, Figure 6.16.a, Figure 6.17.a and b. The characteristic absorption bands of the decomposition products of poly(ABCF13) were more dominant and distinct in spectra belonging to 39.18% poly(ABCF13) due to containing relatively much more poly(ABCF13). Herein, it might be said that the homopolymers existing in polymer matrix firstly decomposed with a massive weight loss at about 350°C and then the grafted units in matrix decomposed largely at about 450°C. Accordingly, the segmental behaviours of products, Figure 6.15 were derived from the difference in decomposition mechanisms of the homopolymers and grafted units in the polymer matrix. Moreover, the absorption bands at about 2300 $cm^{-1}$ belonging to $CO_2$ were almost detected throughout the heating for the both products, but, at the 9.15% poly(ABCF13) product, the bands were more visible and detectable, Figure 6.16.b. Accordingly, the characteristic absorption band due to C-F bonds were observed at about 1260 $cm^{-1}$ throughout heating for both products, Figure 6.16 and 6.17. The spectra of the products including 19.18 and 39.18% poly(ABCF13) also contained undefined newly forming absorption bands.
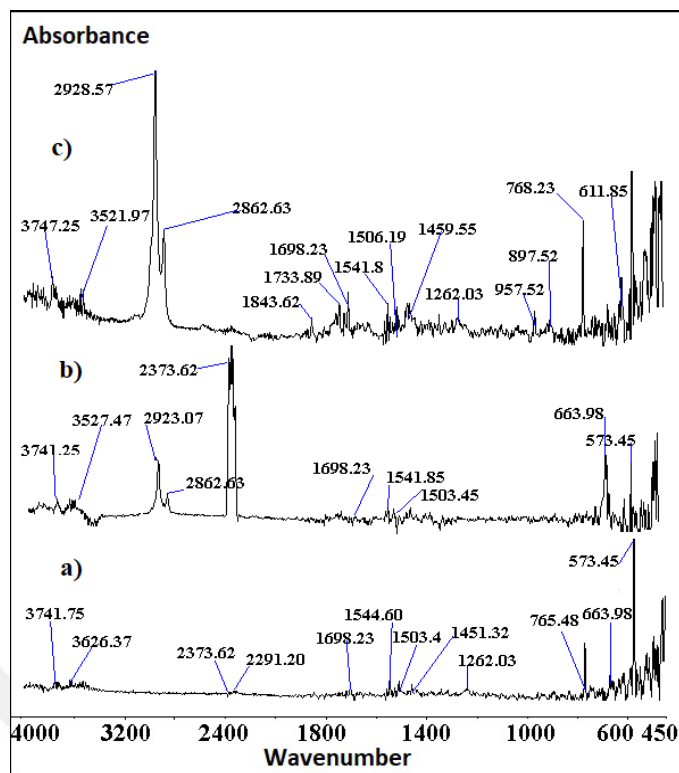
**Figure 6.16.** FTIR spectrum of the decomposed products formed at a)360°C b)480°C and c)510°C during the heating of the product containing 9.15% poly(ABCF13) in nitrogen.
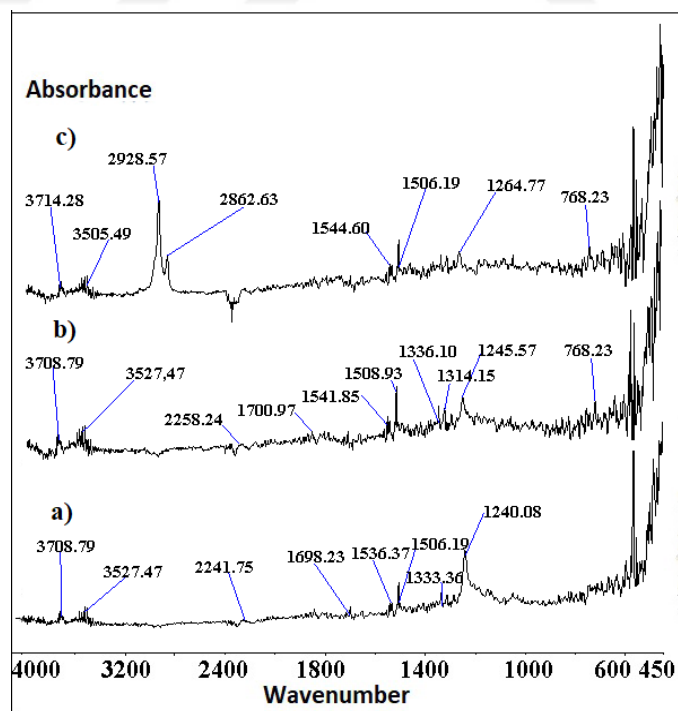


**Figure 6.17.** FTIR spectrum of the decomposed products formed at a)380°C, b)430°C and c)500°C during the heating of the product containing 39.18% poly(ABF13) in nitrogen.

In addition to TG/IR analysis in $N_2$ atmosphere, the analyses were also carried out in air for the same products. The thermograms of the products with 9.15% and 39.18% poly(ABCF13) were given in Figure 6.18.a and b. The results depicted that the decomposition of products took place nearly with similar mechanism with respect to that seen in $N_2$ atmosphere. The first weight losing temperatures for 9.15 and 39.18% poly(ABCF13) products were recorded at about 274.2°C (0.99%) and 235.2°C (0.99%), respectively. Herein, it may be said that the temperatures at which first weight losses were observed in air were a little lower than that being in $N_2$ when comparing to relative contents. When the heating temperature reached to about 350°C during analyses, the weight losses of the 9.15% and 39.18% poly(ABCF13) products in air were found as 13.5% (5.6% in $N_2$) and 19.7% (16.5% in $N_2$,) respectively. The results showed that the products in air lost more weight at relatively certain heating temperature in comparison with products in $N_2$ and the thermal stability of the products in air was lower than in $N_2$. Moreover, the massive weight losses with sharply decrease were observed in the range from about 380 to 470°C, Figure 6.18.a and b.

In addition, in all FTIR spectra, taken in air atmosphere, of the mentioned products, the nearly same characteristic absorption bands were observed due to the similar decomposition mechanism, as illustrated in Figure 6.19.
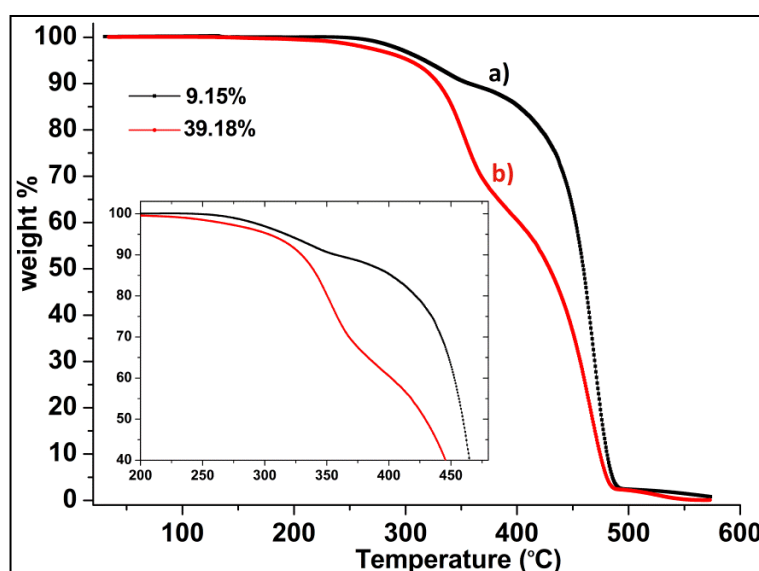


**Figure 6.18.** TGA thermogram of the products with a) 9.15% and b) 39.18% poly(ABCF13) taken in air.
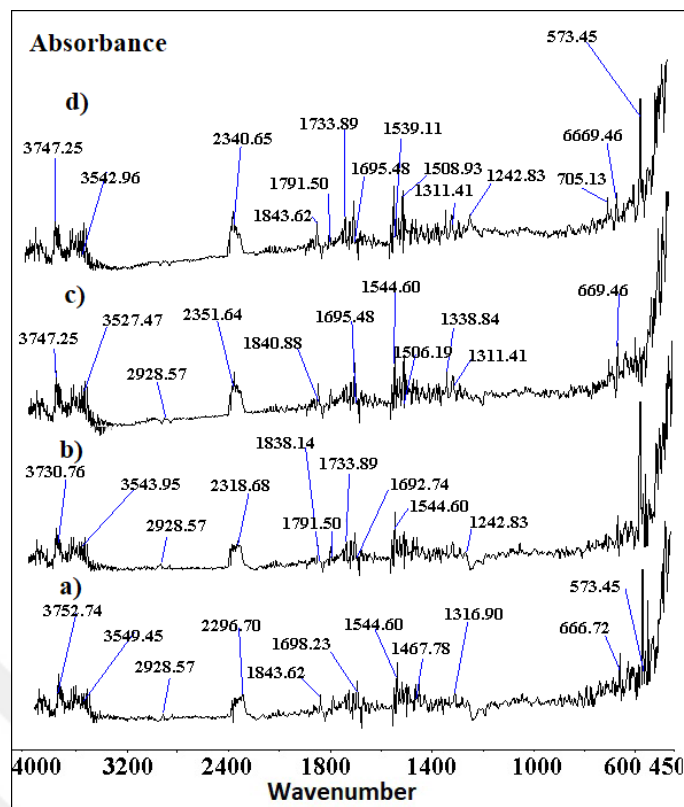
**Figure 6.19.** FTIR spectrum of the decomposed products formed at a)340°C, b)530°C for 9.15% poly(ABCF13) products and c)330°C, d)400°C for 39.18% poly(ABCF13) products during the heating.

## 6.3    XRD Analysis of the Graft Coproducts

The products were also analyzed by XRD in order to unfold the effect of the graft copolymerization of ABCF13 onto HDPE on the microstructural properties of the products. The crystal parameters were estimated from the XRD patterns by means of the least square method using Miller indices (*h k l*) and *d* values. The unit cell size of crystal domains of the products was calculated from the patterns by using the formula;

$$d = \frac{0.941\,\lambda}{B\,\cos\theta_B} \tag{6.4}$$

where *d* represents the thickness of the crystal, λ is the wavelength of the XRD source, B donates the full width at half maximum (FWHM) of the Bragg peak and θ denotes the Bragg angle. *B* value is calculated from;

65

$$B^2 = B_m^2 - B_s^2 \tag{6.5}$$

where $B_s$ exhibits the half-width of the standard material in radians and $B_m$ depicts the difference between the angles at FWHM of the corresponding peak.

Since the polymer poly(ABCF13) was completely amorphous in both homopolymer and grafted form, revealed in DSC analyses, the diffraction patterns of the products with Braggle's angle (2θ) varying from 10º to 60º displayed the reflections corresponding merely to HDPE crystalline characteristics. The patterns revealed the peaks corresponding to the crystallographic planes belonging to the orthorhombic form of HDPE, Figure 6.20. That is, the microstructure of HDPE, the crystalline packing of the chains in orthorhombic system has been preserved throughout the graft copolymerizations. The lateral dimensions of orthorhombic unit cell, on the other hand, were recorded to be considerably affected by poly(ABCF13) content in the products. At relatively lower percentages significant expansions and at higher contents remarkable contractions in the unit cell parameters were recorded. The expansions and contractions were also evidently revealed by shifts of the reflections in the patterns to the left and right, respectively.
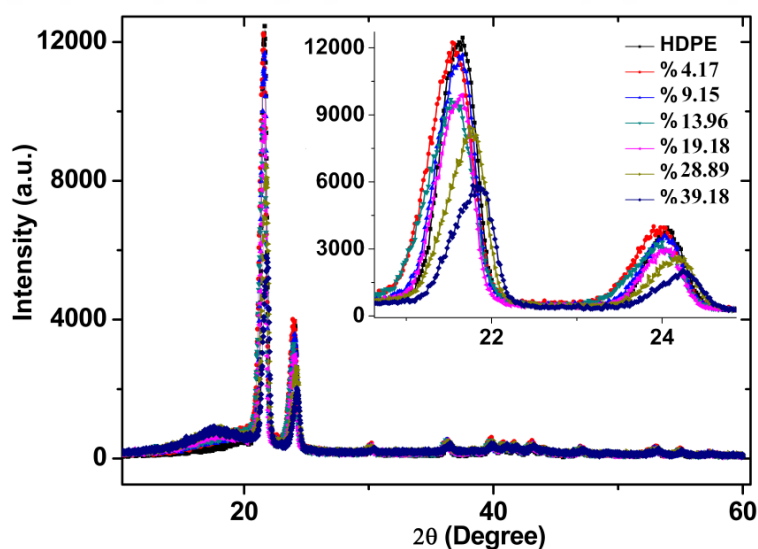


**Figure 6.20.** The XRD patterns of HDPE and the products with varying compositions of poly(ABCF13).

The dependence of the unit cell dimensions (*a*, *b* and *c* parameters) and *ab* basal area of the unit cells on the percentage of poly(ABCF13) in the products were presented in Table 6.3 in detail, and their variations were drawn in Figure 6.21.a, b, c

and d. Both parameters a and b increased initially with the content. The maxima, 7.420 Å in the parameter *a* (0.84% increase) and 4,957 Å in the parameter *b* (0.98% increase) were recorded with the product involving 13.96% poly(ABCF13). The maxima were then followed by contractions. The minimum 7.329 Å in the parameter *a* (0.39% decrease) and 4,897 Å in *b* (0.24% decrease) were measured at 39.18% poly(ABCF13).

In the literature, the lateral enlargements in the unit cell dimensions of oriented and branched polyethylene were explained in terms of the type, distribution and content of the branches (Howard and Crist, 1989; Baker and Windle, 2001a and b). The branches existing in the crystalline regions were reported to compel the chains laterally to expanded dimensions of the unit cells. Additionally, branch rejection was also announced to have possible contribution to the structural changes (Baker and Windle, 2001b). Accordingly, at relatively lower contents in the coproducts, up to about 14% poly(ABCF13), the grafted polar units probably forced the HDPE chains apart laterally to expanded lateral dimensions, and thus led to the enlarged *ab* basal area. The contraction trends in the dimensions after the maxima, on the other hand, probably arose from the compressing effect of the graft units. That is, at further percentages beyond about 14% poly(ABCF13), the accumulation of the graft units with the interactions between the polar groups might have created a squeezing effect on the packing of HDPE chains in the crystalline ordering and arrangements. This effect accordingly resulted in packing of the HDPE chains in the unit cells with relatively smaller dimensions and smaller *ab* basal area. In the coproduct involving 39.18% poly(ABCF13) the consequence was perceived as 0.39% decrease in the parameter *a* and 0.24% decrease in *b*, comparing to the dimensions of virgin HDPE. In addition, due to reductions in van der Waals and steric repulsions, obtained by twisting of each $CF_2$-$CF_2$ bond, helical conformation is thermodynamically favored in perfluoroalkanes. Therefore, perfluoroalkanes are expected to have rigid, rod-like conformation, imparting liquid crystalline properties to these molecules (Krishnan et al., 2004). Thus, the probable rigid, rod-like characteristics of the fluorinated segments of the grafted poly(ABCF13) units in the coproducts might have also additionally contributed to the functions of the units mentioned above on the microstructural changes, that is, on the enlargements at lower percentages and on the contractions at higher contents. On the other hand, the

dimension of the unit cells parallel with the axis of HDPE chains, that is, the parameter c was found to be slightly affected by the graft copolymerization, comparing to the other parameters. The maximum 2.548 Å (0.24% increase) was recorded with the product involving 9.15% poly(ABCF13), Table 6.3 and Figure 6.21.c. In the other coproducts, the parameter remained either slightly smaller or comparable.

**Table 6.3.** The dependence of the unit cell dimensions (*a*, *b* and *c* parameters) and ***ab*** basal area of the unit cells on the percentage of poly(ABCF13) in the products

| % poly(ABCF13) | a (Å) | b (Å) | c (Å) | Basal area (nm) |
|---|---|---|---|---|
| 0 | 7.358±0.008 | 4,909±0.009 | 2,542±0.002 | 36.120 |
| 4.17 | 7.401±0.004 | 4,934±0.007 | 2,545±0.001 | 36.517 |
| 9.15 | 7.400±0,010 | 4,936±0.006 | 2,548±0.002 | 36.526 |
| 13.96 | 7.420±0.009 | 4,957±0.007 | 2,545±0.002 | 36.781 |
| 19.18 | 7.388±0.006 | 4,941±0.005 | 2,546±0.001 | 36.504 |
| 28.89 | 7.337±0.007 | 4,910±0.008 | 2,543±0.002 | 36.025 |
| 39.18 | 7.329±0.009 | 4,897±0.008 | 2,547±0.002 | 35.890 |
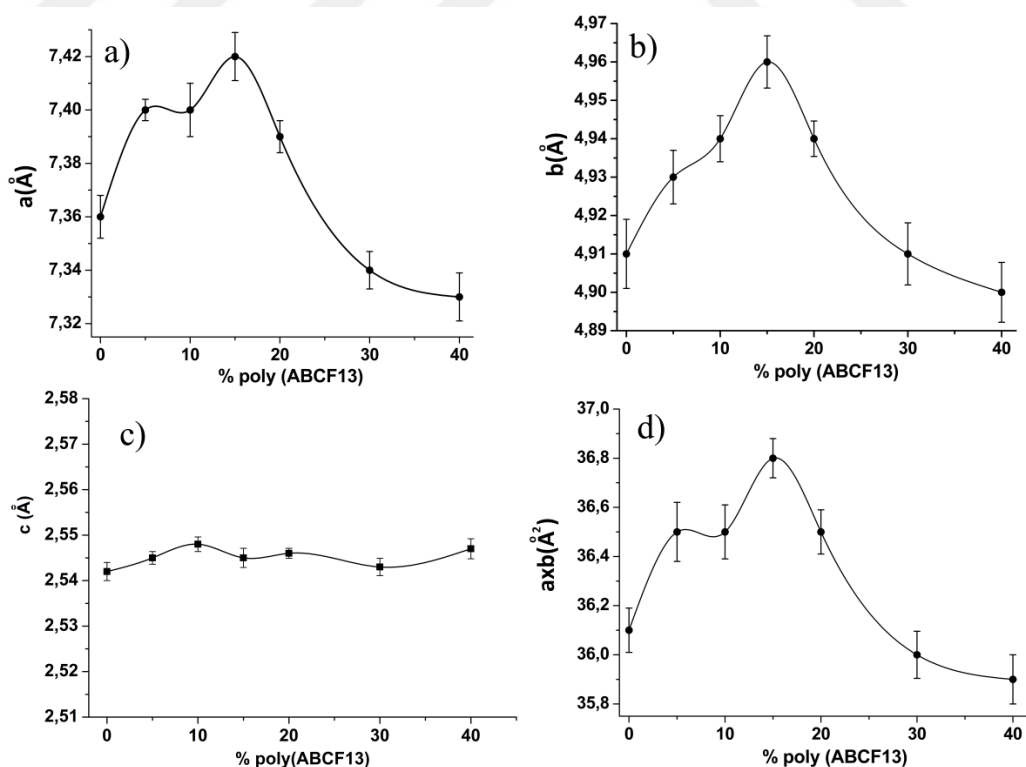


**Figure 6.21.** The dependence of cell parameters a) a, b) b, c) c and d) unit cell basal area *ab* on the poly(ABCF13) percentage in products.

68

In addition to the dimensional variations in the unit cell with the content, the change in grain size, that is, the variation of size of the HDPE crystals with the percentage of poly(ABCF13) in the products was also studied by XRD measurements. The dependence of the size on the poly(ABCF13) content was presented in Table 6.4, and its variation was drawn in Figure 6.22. The trend in the grain size of the products was dissimilar from that seen in a, b and c cell parameters. The size increased initially with the percentage, and reached the maximum value, 19.42 nm (18.3% increase comparing to virgin HDPE), in the sample involving 9.15% poly(ABCF13). The maximum was then followed by a consistent shrinkage with the increase in the content. The minimum size, 14.25 nm (13.2% decrease) was recorded with the sample involving 39.18% poly(ABCF13). The initial rise in the size could be explained by contribution of two factors; The initial increase in the conformational freedom of HDPE chains arising from the increase in the free volume (Section 6.4) and the enlargement in the basal area of the unit cells. The initial increase in the conformational freedom probably conduced to the packing of the chains to relatively larger sized crystals in their growth. The enlargements in the basal area of the unit cells might have additionally resulted in the growth of the crystals to larger sizes. The similar increase and decrease trends in the basal area and the size of the grains evidently support the contribution of the basal area. In fact, a larger size might be normally expected when the crystals grow on the unit cells with larger basal area. The decrease trend in the size after the maximum, on the other hand, might have arisen from the decrease in the free volume fraction and, with the same line of reasoning, the decrease in the basal area of the unit cells. The accumulation of the graft units with the presumable rigid, rod-like characteristics of the fluorinated segments, besides leading to consistent decrease in the free volume fraction, might have had a blocking role on the growth of the crystals to larger sizes.

**Table 6.4.** The dependence of grain size (crystal size) on the percentage of poly(ABCF13) in the products.

| % poly(ABCF13) | 0 | 4.17 | 9.15 | 13.96 | 19.18 | 28.89 | 39.18 |
|---|---|---|---|---|---|---|---|
| Crystal size (nm) | 16.42 ±0.18 | 16.74 ±0.28 | 19.42 ±0.50 | 17.59 ±0.26 | 15.93 ±0.74 | 15.59 ±0,73 | 14.25 ±0.29 |
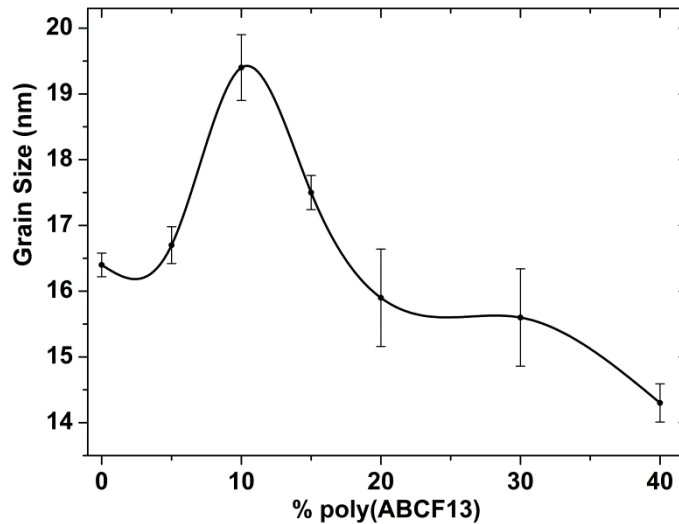
**Figure 6.22.** The variation of grain size (crystal size) with the percentage of poly(ABCF13) in the products.

## 6.4 PALS Analysis of the Products

Many material properties such as structure relaxation, mobility, permeability, viscosity, molecular transport and physical aging etc are all free volume dependent (Yang Y, 2011; Yahsi et al., 2015; Sahin et al., 2015; Akdeniz et al., 2010; Dinc et al., 2014; Yahsi et al., 2008; Yahsi and Sahin, 2004; Sahin et al., 2006; Yahsi et al., 2018). Therefore, both HDPE and the coproducts were meticulously analyzed by Positron Annihilation Lifetime Spectroscopy, PALS, so as to unfold the influence of the graft copolymerization of ABCF13 on the free volume characteristics of the material.

The lifetime spectra obtained by measurement of lifetimes of positrons in the analysis of the products and virgin HDPE were analyzed into components; $\tau_1$, the shortest-lived component with an intensity $I_1$, $\tau_2$, the intermediate-lived component with an intensity $I_2$, and $\tau_3$, the longest-lived component with an intensity $I_3$. $\tau_1$ and $I_1$ are associated with the annihilation of *para-positronium* (*p-Ps*), $\tau_2$ and $I_2$ are allied with direct annihilation of positrons, and $\tau_3$ and $I_3$ are associated with pick off annihilation of *ortho-positronium* (*o-Ps*). In calculation of the parameters analyzed, $\tau_1$ was assumed as independent of free volume and used as fixed at 125 ps.

Ortho-positronium lifetime, $\tau_3$ is sensitive to free volume hole size and the intensity, $I_3$ has straight correlation with the number of free holes in the materials. Accordingly, $\tau_3$ increases with increase in the size of the free volume, and a rise in the number of free volumes is accompanied with an intensification in $I_3$ ( Mostafa et al., 2009). The relation between the radius of free volume hole (R) and pick-off annihilation lifetime proposed by Tao (Tao SJ, 1972) was modified by Eldrup et al. (Eldrup et al., 1981) and then by Naganishi et al. (Nakanishi et al., 1988). In the model, called Tao-Eldrup Model, the radius was related with the lifetime $\tau_3$ by the equation;

$$\tau_3(ns) = \frac{1}{2}\left(1 - \frac{R}{R_0} + \frac{1}{2\pi}\sin\frac{2\pi R}{R_0}\right)^{-1}$$ (6.6)

where $R_0 = R + \delta R$ with $\delta R = 0.1656\,nm$ as an adjustable parameter for a measure of electron layer inside the spherical potential well. By assuming spherical free volume, the size of free volume holes ($V_f$) is then calculated by using the equation;

$$V_f = \frac{4}{3}\pi R^3$$ (6.7)

The free volume fraction (*f*) was proposed by Kobayashi et al. (Kobayashi Y et al., 1989) and stated as;

$$f_v = AI_3V_f(\tau_3)$$ (6.8

**Table 6.5.** The dependence of the lifetimes of the positrons, the intensities, the radii of the free volume holes, the free volume hole sizes and the free volume fractions on poly(ABCF13) content in the coproducts.

| wt. (%) | $\tau_2$(ns) (±0.001) | $\tau_3$(ns) (±0.01) | $I_2$ (%) (±0.2) | $I_3$ (%) (±0.1) | R(Å) (±0.01) | $f_v$(%) (±0.06) | $\upsilon_{f3}(Å^3)$ |
|---|---|---|---|---|---|---|---|
| 0 | 0.37 | 2.30 | 48.5 | 19.8 | 3.11 | 4.47 | 125.7±0.8 |
| 4.17 | 0.34 | 2.36 | 62.1 | 15.1 | 3.16 | 3.58 | 132.0±1.0 |
| 9.15 | 0.35 | 2.43 | 56.8 | 18.3 | 3.21 | 4.58 | 138.6±0.9 |
| 13.96 | 0.37 | 2.46 | 59.6 | 16.1 | 3.24 | 4.12 | 142.0±1.1 |
| 19.18 | 0.36 | 2.53 | 62.3 | 15.8 | 3.29 | 4.24 | 149.1±0.9 |
| 28.89 | 0.37 | 2.69 | 61.2 | 15.7 | 3.41 | 4.69 | 166.1±1.0 |
| 39.18 | 0.36 | 2.80 | 64.5 | 14.4 | 3.49 | 4.62 | 178.2±1.1 |

The variation of the direct annihilation lifetime ($\tau_2$) and ortho-positronium lifetime ($\tau_3$) with poly(ABCF13) content in the samples were illustrated in Figure 6.23. There existed no considerable change in the direct annihilation lifetime values of all the products. In spite of some small decreases in the $\tau_2$ values, as 0.34 ns was recorded in the sample involving 4.17% poly(ABCF13), either comparably lower or the same lifetime that virgin HDPE had (0.37 ns) were measured. In contrast to $\tau_2$, the significant and remarkable changes were recorded in the ortho-positronium lifetime. The lifetime $\tau_3$ was found to be highly dependent on poly(ABCF13) content in the samples. It increased almost linearly with the content as shown in Figure 6.23. The highest $\tau_3$ value was recorded as 2.80 ns with the product containing 39.18% poly(ABCF13), which was 22.4% larger than that neat HDPE had (2.30 ns).

The lifetime $\tau_3$ is proportional to size of free volumes in the materials (Mostafa et al., 2009). The dependence of the free volume size calculated by using the free volume model on poly(ABCF13) content in the products was drawn in Figure 6.24. The size increased almost in consistence with the percentage of poly(ABCF13). It reached the maximum $178.2\pm1.1$ Å$^3$ (42% raise comparing to virgin HDPE) with the sample involving 39.18% poly(ABCF13). It can be concluded that the poly(ABCF13) units with voluminous side groups bearing rigid, rod-like fluorinated segments presumably led to the formation of larger holes, cavities or openings in the material. The size of the free holes thus got larger as the content increased. In addition, since the free volume is higher in glassy and amorphous polymers with local kinks (Bilchak et al., 2017), the ungrafted homopolymer molecules might have played a hindering role in compact packing of the polymer chains in the matrix, which resulted in larger free volumes with the increment in the poly(ABCF13) content. Furthermore, the weak secondary molecular interactions between polar groups of poly(ABCF13) units and nonpolar HDPE chains might have additionally contributed to the reduction in close packing of the chains in the matrix, and thus to larger free volumes.
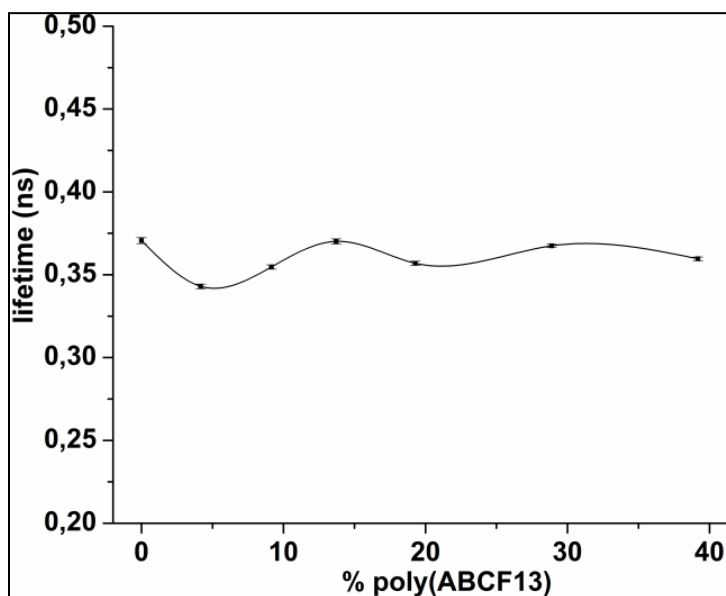
**Figure 6.23.** The variation of intermediate-lived component ($\tau_2$) with poly(ABCF13) content in the product.
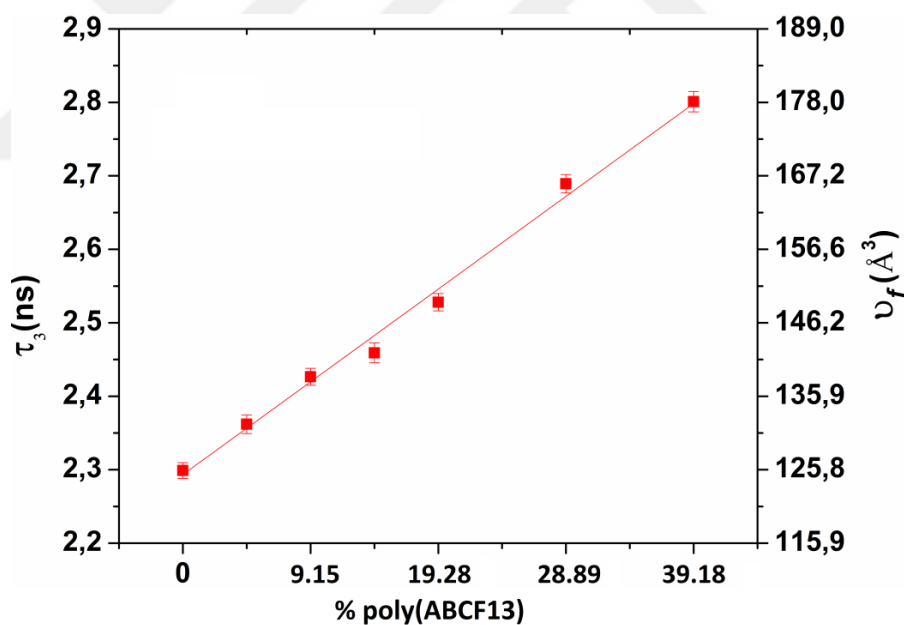


**Figure 6.24.** The dependence of free volume hole sizes ($A^3$) and ortho-positronium lifetime ($\tau_3$) on poly(ABCF13) content in the products.

In the free volume model, the o-Ps intensity ($I_3$) was defined as a measure of the number of free volume holes. Figure 6.25 graphically display how the o-Ps intensity ($I_3$) changed with poly(ABCF13) content in the products. The intensity $I_3$ decreased rapidly with a 23.7% reduction in the sample with relatively low content (4.17%) of poly(ABCF13). After this percentage, the increase in the content caused an increase in the intensity, and maximum intensity, 18.3, was observed at 9.15%. The maximum, which is still lower than that observed in pure HDPE (19.8), was followed by a decrease trend with the increase in the content of poly(ABCF13), and reduced to the minimum at the percentage of 39.18%. The dramatic decrement at 4.17% poly(ABCF13) and the decrease trend in the intensity after the percentage of 9.15% might have arisen from the formation of the bigger and larger holes due to the coalescence of the holes in the matrix, resulting in the decrease in the number of the holes and thus the decrease in the intensity. The increase in the size of free volume, as mentioned above, and the decrease in the intensity evidently support this commentary. Moreover, occupation and filling of free volume holes by the graft units thus reducing the number might have played an additional role in decreasing the intensity values. At the percentage of 9.15%, on the other hand, the graft units in the material probably led to formation of additional free volume holes, which gave rise to the observed increase in the intensity $I_3$.
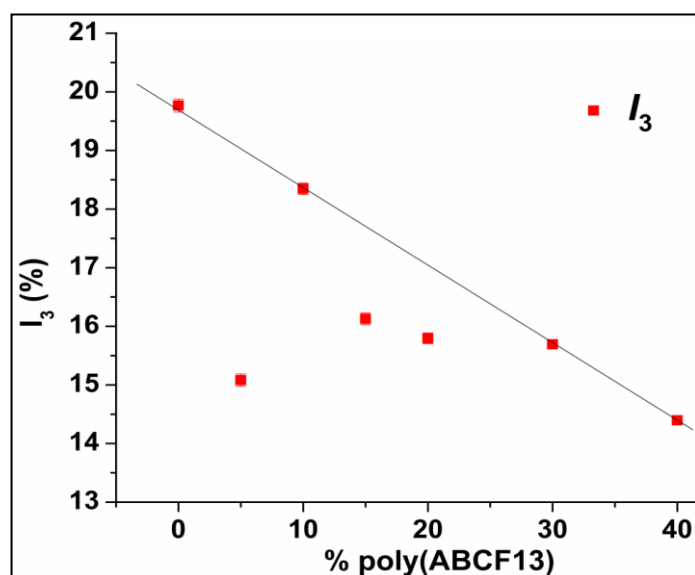


**Figure 6.25.** The variation of the o-Ps intensity ($I_3$) with poly(ABCF13) contents in the products.

The free volume fractions ($f_v$) of the products were determined by means of the equation 6.6 suggested by Kobayashi et al. (Kobayahsi et al., 1989). The dependence of the free volume fractions ($f_v$) on poly(ABCF13) content were given in Table 6.5, and drawn in Figure 6.26. Free volume fraction decreased rapidly with a decrease of 19.91% at the initial concentration of grafting, 4.17%. The fraction then exhibited an increase trend with the content. 4.58% fraction was recorded at 9.15% poly(ABCF13) (2.47% greater than that of virgin HDPE), which was followed by a relatively slower decrease and then a relatively slower increase. The reduction in the fraction at 4.17% poly(ABCF13) was probably due to the fact that the graft units occupied the free volume holes between the HDPE chains rather than creating new gaps and holes between them. The potential weak interactions between the polar groups of the graft units and the nonpolar HDPE chains may have played a role in filling these holes. At the grafting content of 9.15%, however, the voluminous side groups of the graft units gave rise to enlargements in both size and number of the free volumes, and thus resulting in a sharp increase in the fraction. The voluminous side groups presumably preventing the close packing of the chains in the material might have played an efficient role in the increase of the fraction at that percentage. Relatively slower decrease in the fraction after that content, at 13.71% poly(ABCF13), probably resulted again from the occupation of the holes by the newly added graft units. Further increases of poly(ABCF13) in the products seemingly led to rises in the fraction.
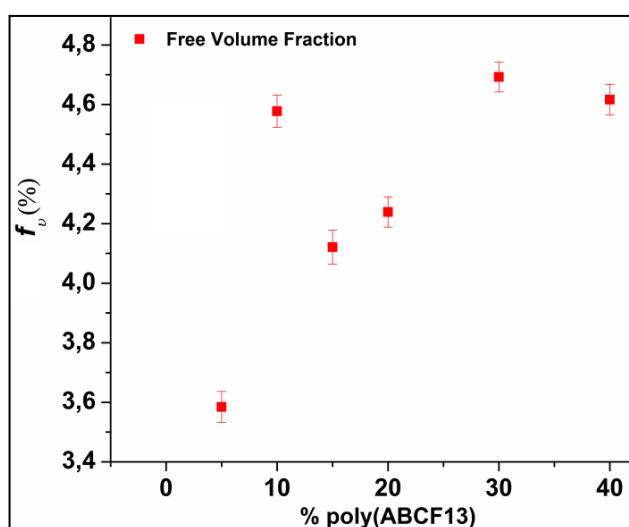


**Figure 6.26.** The variation of the free volume fraction with poly(ABCF13) content in the products.

## 6.5    Mechanical Characteristics of the Graft Coproducts

The effect of graft copolymerized poly(ABCF13) existing as both grafted units and homopolymer molecules in the matrix on the mechanical performance of the products was examined in-depthly by focusing on their tensile and impact behaviors. In order to prepare test samples, the products were molded into dog-bone shape by means of micro injection molding at 200°C. Because of the difficulties encountered in molding the products due to high viscosity at lower temperatures and of the onset of degradation at higher temperatures, revealed in TG-IR analyses (section 6.2.2), 200°C was determined as the optimum processing temperature. Very important and significant improvements were observed in the mechanical properties of the material, especially in tensile and impact strength. On the other hand, yield stress and percent elongation decreased with the increasing of the poly(ABCF13) content, and at high contents, brittle nature became dominant in the mechanical behavior of the products.

The stress strain curves of both virgin HDPE and the products, determined by 5 cm.min$^{-1}$ elongation speed, were presented in Figure 6.27. While great extension and orientation were recorded in virgin HDPE during cold drawing, the tests of the products exhibited increasing brittleness in the characters, Figure 6.27. Up to 20% content, the products failed in the region close to the yield point or at the beginning of strain softening, that is, before or at the beginning of neck formation. At higher concentrations, failure of the samples were recorded at the onset of plastic deformation, which indicated the increase of brittleness in the characters. The presence of poly(ABCF13) units in the products thus imparted rigidity to the material. The brittleness was also perceived in the SEM images of the fractured surfaces of the samples.

76
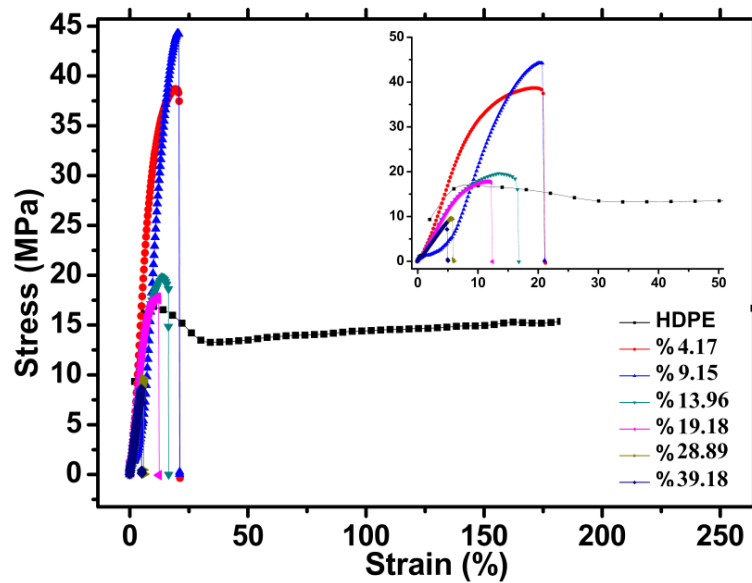
**Figure 6.27.** The stress-strain curve of HDPE and products with 4.17, 9.15, 13.96, 19.18, 28.89 and 39.18% poly(ABCF13) contents.

The experimental findings obtained from the mechanical measurements of the products and neat HDPE were numerically tabulated in Table 6.6 and graphically displayed in Figure 6.28. Tensile strength of the products increased initially with the content, and reached the maximum 43.75 MPa (133% improvement comparing to virgin HDPE) at 9.15% poly(ABCF13). The maximum was followed by a sharp decline as the grafting percentage increased further. 19.17 MPa and 17.69 MPa strengths, comparable with that of virgin HDPE, 18.78 MPa, were recorded with the products involving 13.96% and 19.18% poly(ABCF13), respectively. The strength then continued to decrease with the percentage and reduced to 8.86 MPa at 39.18% poly(ABCF13). A similar behavior was also recorded in Young's modulus of the products except for that the initial increase was not so great as was noted in the tensile strength. The maximum 393 MPa (8.6% improvement comparing to virgin HDPE), achieved with the sample again involving 9.15% poly(ABCF13) was followed by a sharp decline as the content increased further.

**Table 6.6.** The mechanical properties of PE and graft coproducts with the content of 5, 10, 15, 20, 30 and 40% of ABCF13.

| Coproducts | Ultimate Strenght (MPa) | Young's Modulus (MPa) | Absorbed Energy in Impact Strenght (kj/m$^2$) |
|---|---|---|---|
| Virgin HDPE | 18.78±3.15 | 362.16±15.12 | 19.30±2.64 (NB) |
| 4.17% poly(ABCF13) | 34.40±2.08 | 381.82±13.22 | 32.23±2.55 (NB) |
| 9.15% poly(ABCF13) | 43.75±0.75 | 393.15±16.72 | 38.72±2.90 (NB) |
| 13.96% poly(ABCF13) | 19.17±1.19 | 280.32±14.86 | 33.19±3.00 (NB) |
| 19.18% poly(ABCF13) | 17.69±0.30 | 272.18±9.28 | 20.99±4.17 (NB) |
| 28.89% poly(ABCF13) | 9.84±0.69 | 253.63±3.71 | 10.23±0.42 (B) |
| 39.18% poly(ABCF13) | 8.86±0.38 | 237.58±3.43 | 3.09±0.69 (B) |

NB: Not Broken          B: Broken
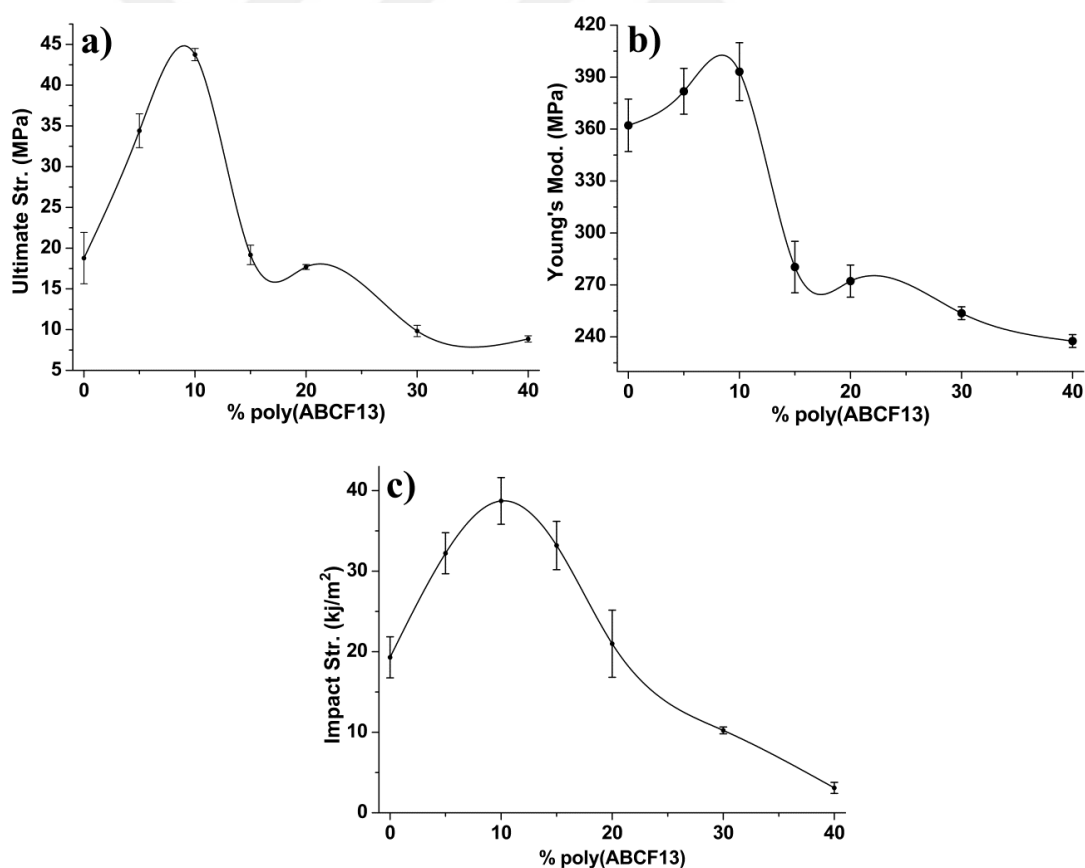


**Figure 6.28.** The variation of the a) ultimate strength, b) Young's Modulus, c) absorbed energy in the impact test, of the samples with percentage of poly(ABCF13) in the products.

The improvements in the tensile properties at lower percentages of poly(ABCF13), that are at 4.17% and 9.15%, could be explained by that the first enlargements in the free volume (Section 6.4) probably gave rise to increase in the conformational freedom of the chains in the material, conducing to a significant alignment and orientation of the chains in the draw direction and thus resulting in increase in the tensile behaviors. The extensive fibrillation at those graft contents verified by the SEM analyses of the fractured surfaces (Section 6.6) evidently support this commentary. On the other hand, the SEM analyses of the samples also displayed that, the high level of fibrillation recorded in the samples containing 4.17% and 9.15% poly(ABCF13) were gradually lost with the increase of graft content and disappeared at higher percentages. The loss of fibrillation in the products was also accompanied with reduction in the tensile properties in spite of the increases in the free volume. It is noteworthy that poly(ABCF13) chains are composed of voluminous side groups bearing rigid, rod-like fluorine segments. The presence of such voluminous side groups comprising such rigid segments might play a role in preventing the orientation and alignment of the chains in the draw direction. Thus, the poly(ABCF13) molecules in the HDPE matrix, after a certain concentration (after 10% in these graft copolymers), presumably played such role in limiting the orientation of HDPE chains in the tests, the effect of which probably became more dominant as the graft content increased. Therefore, fibrillation decreased after 10% poly(ABCF13) and were completely lost at higher contents despite the free volume gradually enlarged with the content. The fact that the chains are not oriented and aligned in the draw direction causes the material to exhibit low tensile behavior. Accordingly, the increase in graft concentration resulted in low tensile strength and caused the samples to exhibit lower strain. In addition, the poly(ABCF13) chains with so voluminous side groups comprising rigid, rod-like segments are difficult to exhibit an appreciable load capacity in tensile tests, comparing to pure HDPE which is composed of linear chains. Accordingly, this might have made the products less withstanding in the tensile tests at high contents. Therefore, the probable lower load capacity of the graft units might have also had considerable contribution to the weakenings and worsenings in the tensile properties at higher contents than 10%. On the other hand, in the studies on the relation between mechanical properties and free volume characteristics of polymer composites and blends, tensile strength and modulus were reported to have anti-correlation with free volume and free volume

fraction (Ponnamma et al., 2015; El-Nashar et al., 2009; Gomaa et al., 2003). In fact, except for the initial increases, the strength and modulus of the products exhibited a trend in accordance with the reported behavior. Both property got worse with the increase of the free volume in the products with the content beyond about 10% poly(ABCF13). For the initial improvements in the tensile properties, besides the probable alignment and orientation of the chains in the draw direction, conduced by the initial enlargements in the free volume, it can also be hypothesized that the grafted units with so voluminous side groups bearing rigid, rod-like fluorine segments probably restricted extensive flow of HDPE in the draw direction, giving rise to a striking improvement in the tensile strength (133%) at 9.15% poly(ABCF13). Furthermore, at low graft contents, the grafted units with such rigid, rod-like side groups might have contributed to the achieved improvements by a presumable fiber reinforcement effect in the orientation of the chains and thus to the mentioned results. Moreover, the sample (with 9.5% poly(ABCF13)) having the largest grain size (crystal size) showed the maximum tensile strength and elastic modulus among the products. The crystals with larger sizes might have additionally contributed to the achieved enhancements in the strength by behaving as cross-link centers between the chains in the amorphous domains. Additionally, the mechanical properties of polymer blends may be strongly influenced by the compatibility of components in the polymer combinations (Hamad et al., 2016). Perfect interfacial adhesion, lower interfacial tension and the higher stress transfer in the products may give rise to impressive mechanical performance (Chen and White, 1993). The poly(ABCF13)-g-HDPE units in the products might have acted as a compatibilizing agent between the components (poly(ABCF13) and HDPE) hence providing a better interfacial adhesion and lower interfacial tension. This might have also contributed to the observed advances. On the other hand, the uncomparable increase in elastic modulus comparing to the improvement in tensile strength, that is, 8.6% increase comparing to 133% improvement in the strength could be explained by easier flow of the chains in the material comprising larger free volume accompanied with an increase in conformational freedom of the molecules and thus relatively low resistance of the material to plastic deformation.

Impact resistance of the products was examined by Izod impact test. The impact energy is defined as the absorbed energy loaded on the certain area in a short time during the impact fracture of the sample in the test. In the tests, while the samples involving 28.89% and 39.18% poly(ABCF13) failed, virgin HDPE and the products with 4.17%, 9.15%, 13.96% and 19.18% poly(ABCF13) were not broken. Therefore, for those unbroken samples, only the absorbed energies in the tests could be measured. The dependence of the absorbed energies on the content of poly(ABCF13) was graphically displayed in Figure 6.28.c. The graph revealed a good correlation between the absorbed energies and the tensile strength, modulus and grain size of the products. The absorbed energy increased initially with the content and reached maximum value 38.72 kJ/m$^2$ (100% larger compared to 19.30 kJ/m$^2$, the energy absorbed by virgin HDPE) in the product containing 9.15% poly(ABCF13). The energy then exhibited a decrease trend as the content increased further, and reduced to 3.09 kJ/m$^2$ at 39.18% poly(ABCF13), displaying rise of brittleness in the character. The initial increase in the absorbed energy might be explained by the increase in the free volume. The increased conformational freedom and mobility of the chains accompanied with the enlargements in the free volume probably resulted in the more absorbed energy because of more effective delocalization of the loaded energy on the material in the test. In addition, advances in the order of packing and in regularity in the organization of HDPE chains due to the grafted poly(ABCF13) units in the matrix might have contributed to the withstanding against the loaded energy in the tests thus to the higher absorbed energy. On the other hand, the increasing brittleness, that is, the decreases in the absorbed energy and failure of the samples at high contents of poly(ABCF13) (at 28.89% and 39.18%) could be explained by the decreases in the chain mobility in the products. The voluminous side groups of poly(ABCF13) units bearing rigid, rod-like fluorine segments probably gave rise to decreases in the mobility of the chains at relatively higher percentages despite of the increases in the free volume. The losses in the mobility probably caused restrictions in the delocalization of the impact energy thus resulting in the increase of brittleness in the products.

## 6.6    Morphological Properties of the Graft Coproducts

The mechanical properties of polymer composites and blends are highly dependent on size and size distribution of reinforcing component and degree of interfacial adhesion between components in matrix. Therefore, the fractured surfaces (obtained from tensile and impact tests) of the products were analyzed by using SEM in order to examine the morphological characteristics in details. It is visible from SEM images that there existed no phase separation in all products, and the samples had completely homogeneous structure although HDPE with nonpolar structure has a different nature from poly(ABCF13) comprising polar groups. Thus, the findings depicted the formation of chemical bonds between HDPE chains and poly(ABCF13) units. It was also revealed by the images that poly(ABCF13)-g-HDPE units acted as compatibilizing agent giving rise to good interfacial adhesion between ungrafted poly(ABCF13) and HDPE matrix. On the other hand, the fractographs displayed that the morphological properties of fractured surfaces changed highly with the content of poly(ABCF13). At low contents, the products exhibited ductile behavior with the formation of large, thick and long fibrillar structures formed probably as a consequence of the orientations and alignments of the chains of the matrix, Figure 6.29 and 30. Hence, these images might be evaluated as the empirical evidence for how the products withstood against the applied force during mechanical tests. However, the images also displayed that the ductile elongations decreased with the increase of poly(ABCF13) percentage. At relatively high percentages, the thick and long extensions were replaced by shorter and thin fibrillar structures, Figure 6.31-34. In addition, as the content increased further, layered structures with holes, openings and microcracks began to appear. The microstructural defects with rarely seen small extensions were found to be high in the products especially containing 28.89% and 39.18% poly(ABCF13), which were in substantially brittle nature, Figure 6.33 and 6.34. Thus, these changes in morphology present significant visible evidence for why the tensile strengths of the products decreased with the increase of poly(ABCF13) content in the products.
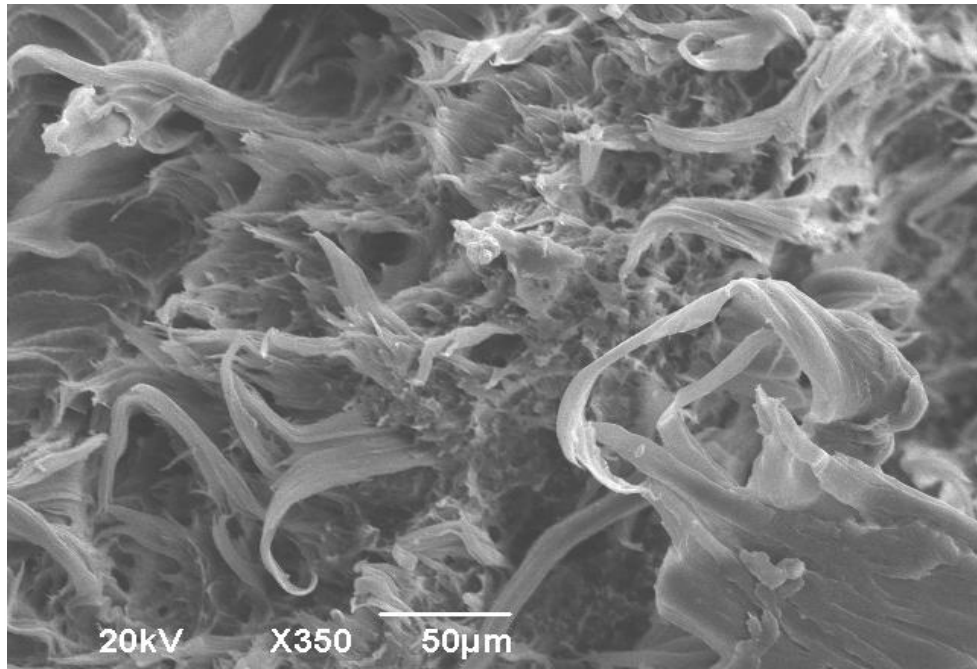
**Figure 6.29**. SEM micrographs of the product with 4.17% poly(ABCF13), Tensile Tests.
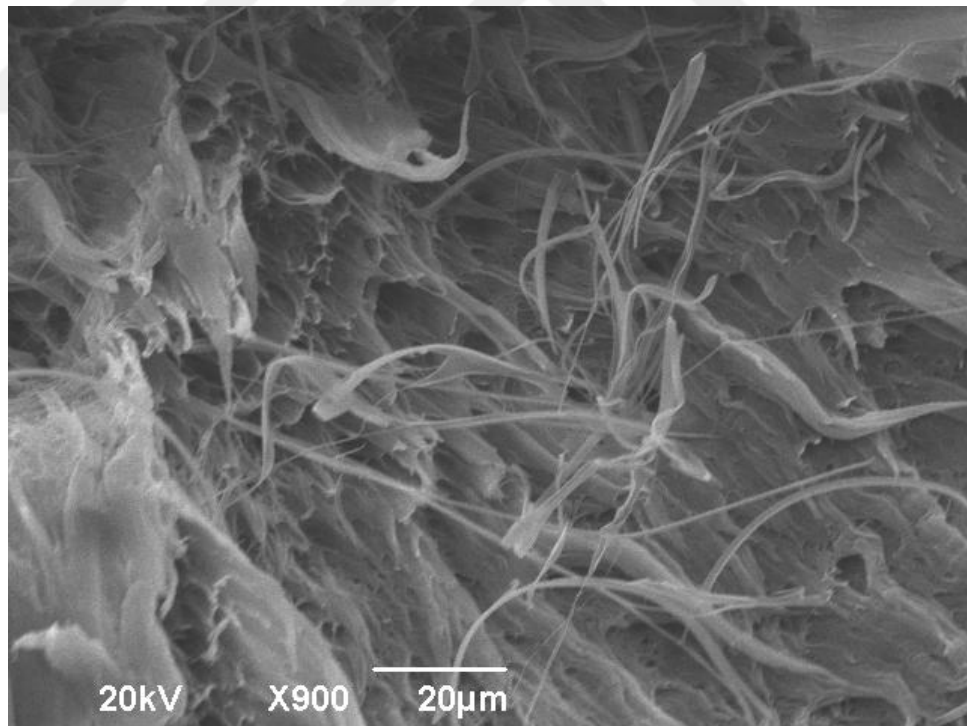


**Figure 6.30.** SEM micrographs of the product with 9.15% poly(ABCF13), Tensile Tests.
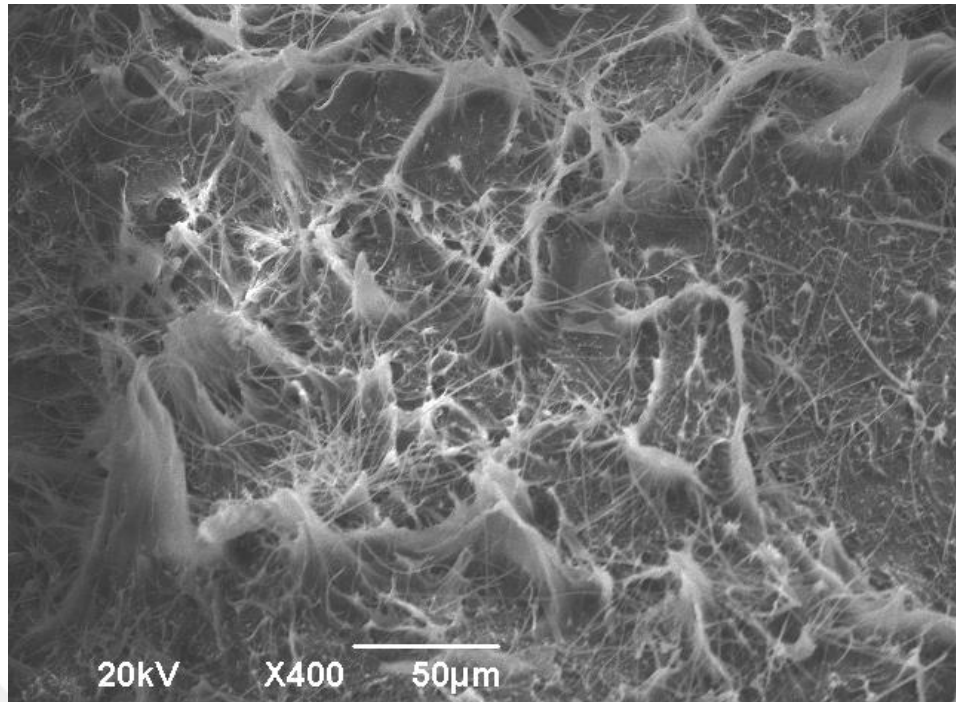
**Figure 6.31.** SEM micrographs of the product with 13.71%poly(ABCF13), Tensile Tests.
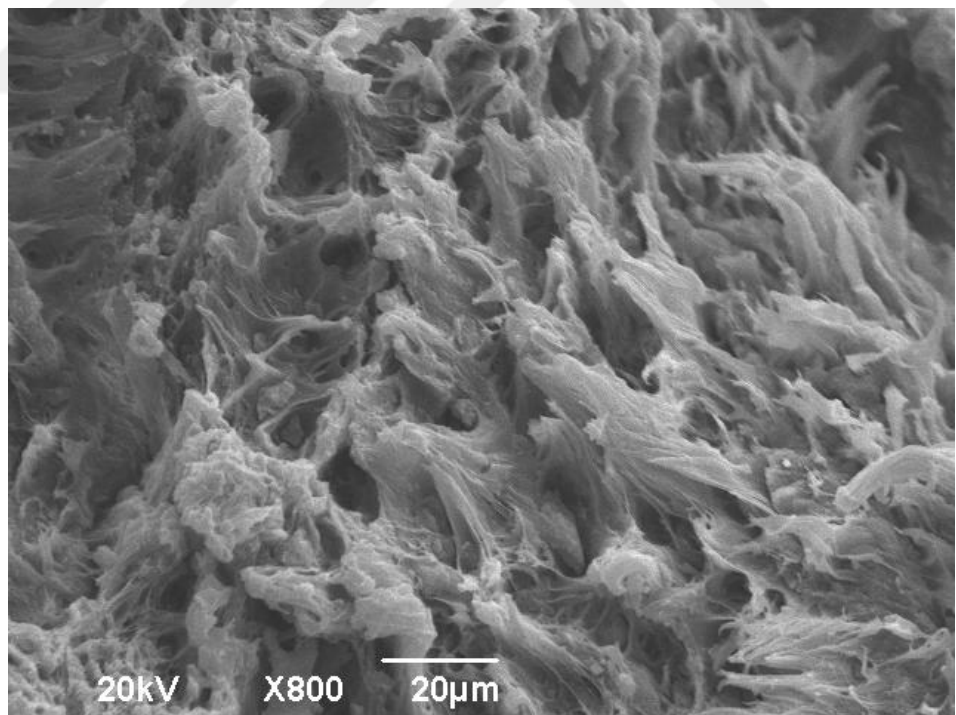


**Figure 6.32.** SEM micrographs of the product with 19.18% poly(ABCF13), Tensile Tests.
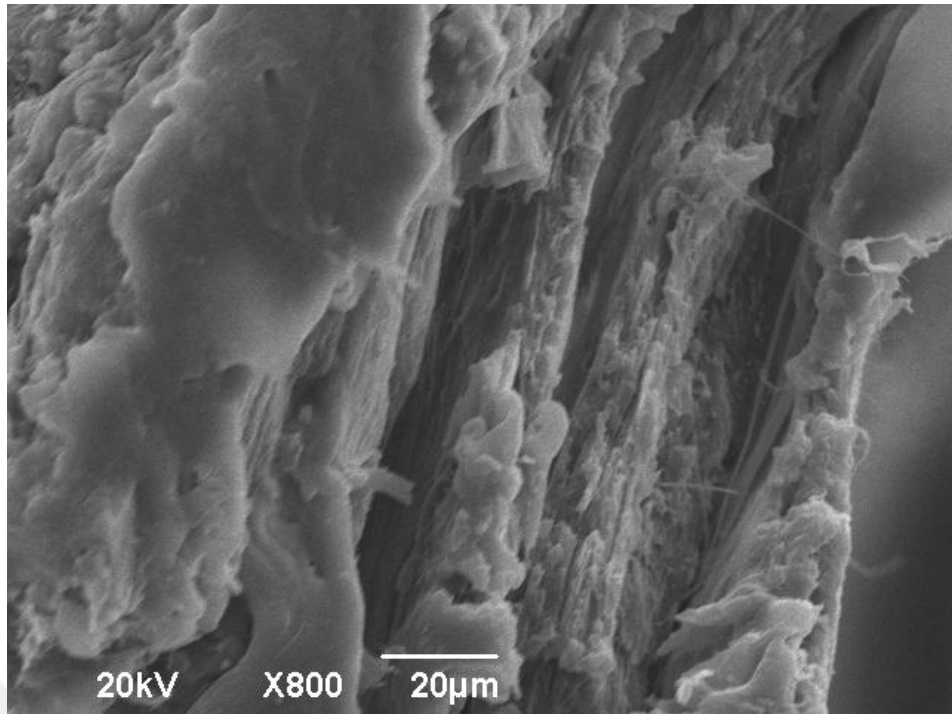
**Figure 6.33.** SEM micrographs of the product with 28.89% poly(ABCF13), Tensile Tests.
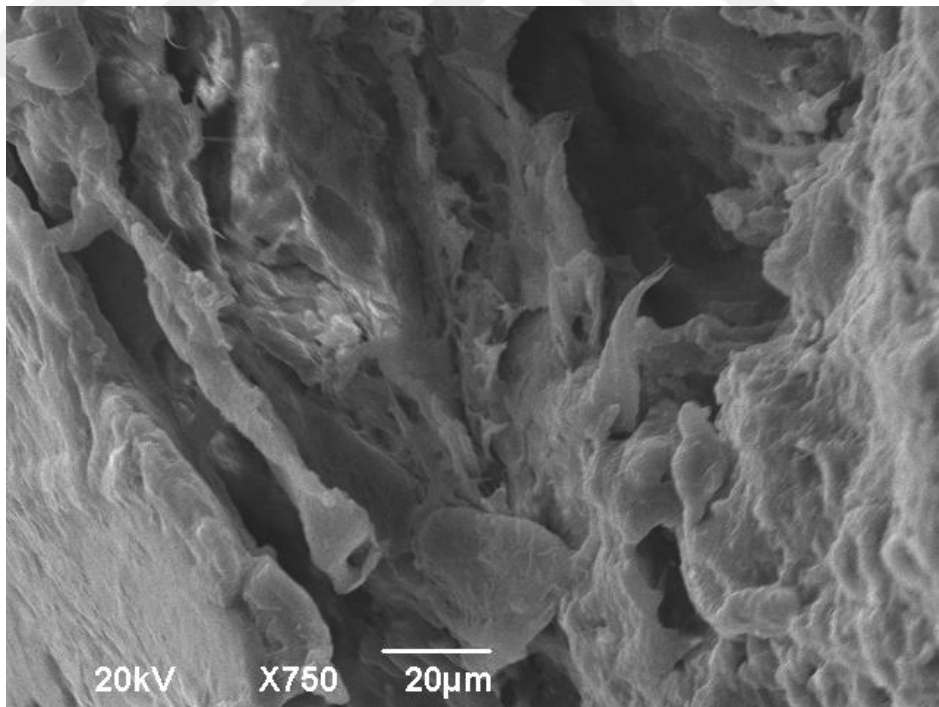


**Figure 6.34.** SEM micrographs of the product with 39.19% poly(ABCF13), Tensile Tests.

In addition to the analyses of the tensile fractured surfaces, the impact fractured surfaces of the products including 28.89 and 39.18% poly(ABCF13) were also analyzed in-depthly by SEM. The images were depicted through Figure 6.35-38. While the products with lower contents were not broken, the samples containing 28.89 and 39.18% poly(ABCF13) failed during the tests. The fractographs of the the broken samples revealed that the fractures are brittle, and the brittleness increased monotonously with the increment of poly(ABCF13) content. Almost no fibrillation was observed except for rarely detected and very thin microextensions. This was attributed to the increase of the restrictions in orientations at molecular level. Namely, absorption and effective delocalization of impact energy loaded during the tests are inhibited due to the restrictions in the orientations of the chains. Therefore, the energy is localized in relatively weak regions to form cracks and holes and thus resulting in the failure of the material. Figure 6.35, 6.36 and 6.38 clearly display crack formation with voids, openings and holes.  But, all the graft coproducts are completely homogeneous.
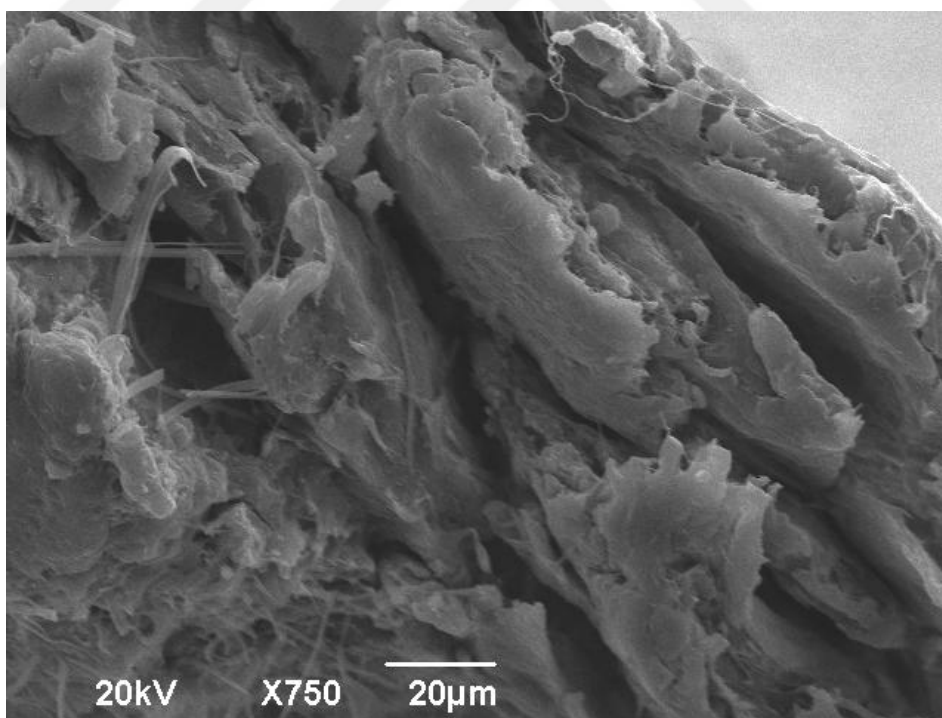


**Figure 6.35.** SEM photograph of the product with 28.89% poly(BPOCPA), after obtained from impact test.
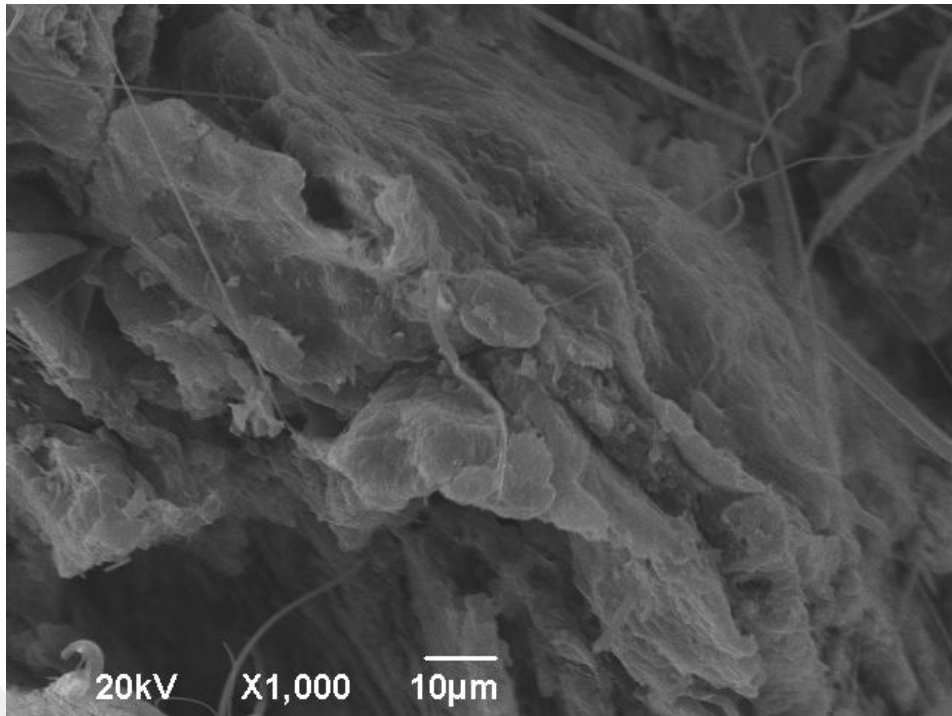
**Figure 6.36.** SEM photograph of the product with 28.89% poly(BPOCPA), after obtained from impact test.
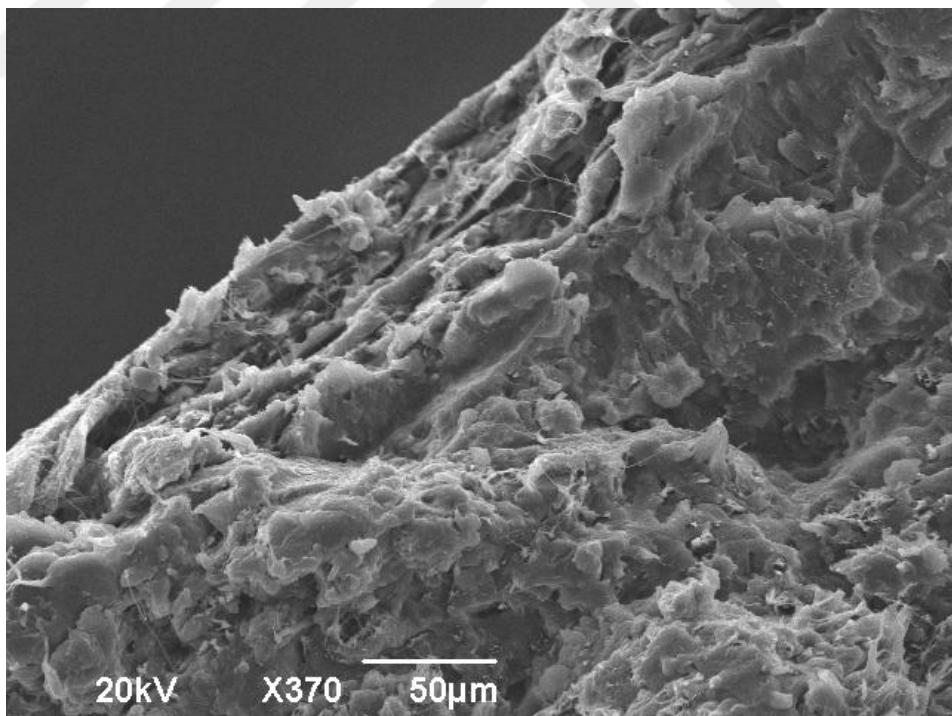


**Figure 6.37.** SEM photograph of the product with 39.18% poly(BPOCPA), after obtained from impact test.
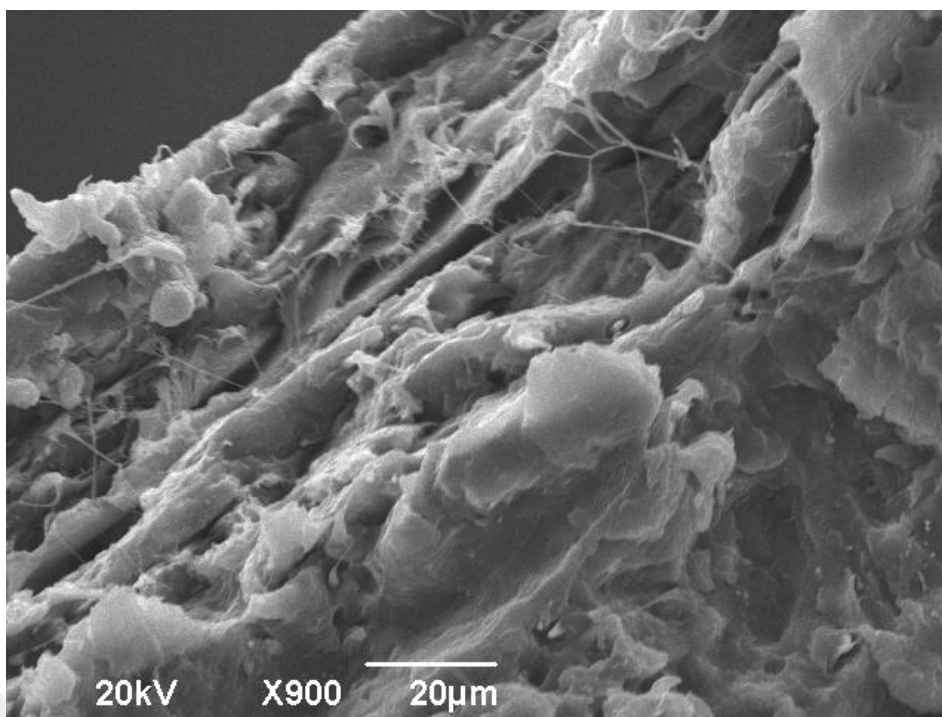
**Figure 6.38.** SEM photograph of the product with 39.18% poly(BPOCPA), after obtained from impact test.

## 6.7 Preparation of Crosslinked Poly(ABCF13) Microspheres

The well-defined crosslinked poly(ABCF13) microspheres were successfully prepared by suspension polymerization method. In the syntheses, ABCF13 melt was employed as dispersed phase, water as continuous phase, ethylene glycol dimethacrylate (EGDMA) as a crosslinking agent and potassium persulfate (KPS) as a water soluble initiator. The synthesis was precedingly attempted several times by using benzoyl peroxide initiator. However, the initiator was not soluble in ABCF13 melt and the polymerization was not successful. In the studies, the dependence of the microsphere structure and morphology on many parameters such as the crosslinking agent, the monomer and the initiator concentration as well as stirring rate were investigated in depth. The morphology of the products and its changes with synthesis conditions were probed and monitored by SEM analyses.

### 6.7.1 Optimization of Synthesis Conditions

### 6.7.1.1 Effect of Crosslinking Agent Concentration on Poly(ABCF13) Microsphere Formation

Use of crosslinking agents at relatively high proportions in the microsphere preparation reactions gives rise to rapid hardening of the particles due to partially more effective polymerizations in the drops and to decrease of the coalescence of the dispersed particles in the medium (Kurt, 2010). High concentration of crosslinking agents or well-suited crosslinkers are essentially important in order to obtain more stable and well-shaped microspheres, (Park et al., 2006). The insufficient crosslinking agent concentration in polymerization medium results in the distortion of the droplets and deterioration of the spherical shape (Margel et al., 1991). On the other hand, agglomeration of the drops due to the formation of sticky state might be seen during the reactions when there existed high molecular interactions between drops containing both monomers and crosslinking agents. For these reasons, the concentration and nature of the crosslinking agent in the drops play an important role in binding or fixation of the microspheres in the medium. Therefore, the effect of the crosslinking agent, EGDMA, concentration on the formation of crosslinked poly(ABCF13) microspheres was studied meticulously by employing it at the percentages of 0.5, 1.0, 1.5, 2.0, 5.0 and 10% with respect to monomer (0.2 g) in 150 mL of water. The reactions were carried out at 70°C with the stirring rate of 500 rpm. The SEM analyses displayed that the variations in EGDMA concentration considerably affected the microstructural characteristics of the products, Figure 6.39-49. It is notable that, at all EGDMA percentages employed, the formations of non-spherical particles in distorted shapes and in sizes ranging from 1 to 20 μm were encountered in the products, Figure 6.39-49. At the lowest concentration of EGDMA (0.5%), formation of odd-shaped, bulky, accumulated and adhered particles were observed, Figure 6.39 and 6.40. When EGDMA concentration was increased to 1%, the particles more stable and nearly spherical were obtained with significantly lower aggregation, Figure 6.41 and 6.42. Nevertheless, coalescences, aggregations, coagulations and bulky structures started to appear when the concentration was raised further, Figure 6.43-45, but, still there existed well-shaped microparticles,

Figure 6.45. As the concentration is increased more, at 5 and 10% percentages, the stability in the shapes of the particles was almost completely lost, and substantial deformations and considerable distortions were observed in the shapes, Figure 6.46-49. The crosslinking agents in droplets may enhance the co-stabilizing effect of monomers in order to obtain primarily stable particles forming fast (Park et al., 2006). Seemingly, the optimum co-stabilization in droplets probably due to the interactions between the polar groups of both ABCF13 and EGDMA and the hydrophobic property of the dispersed phase was achieved with 1% EGDMA, which resulted in forming more stable particles at this concentration. EGDMA was miscible with ABCF13 melt but not with the aqueous phase. This property might have provided a contribution to the good dispersion of the droplets, even at the initial stages of the reactions. On the other hand, at the concentrations higher than 1%, the relative loss of the stability, that is, appearance of the coalescence and bulky structures was probably arisen from the interactions between polar groups of the molecules present in neighboring droplets. In addition, the increase in EGDMA concentration in the droplets giving rise to formation of relatively more reactive sites probably resulted in the increase of the possibility of agglomeration of the primarily formed particles by binding the droplets to each other.
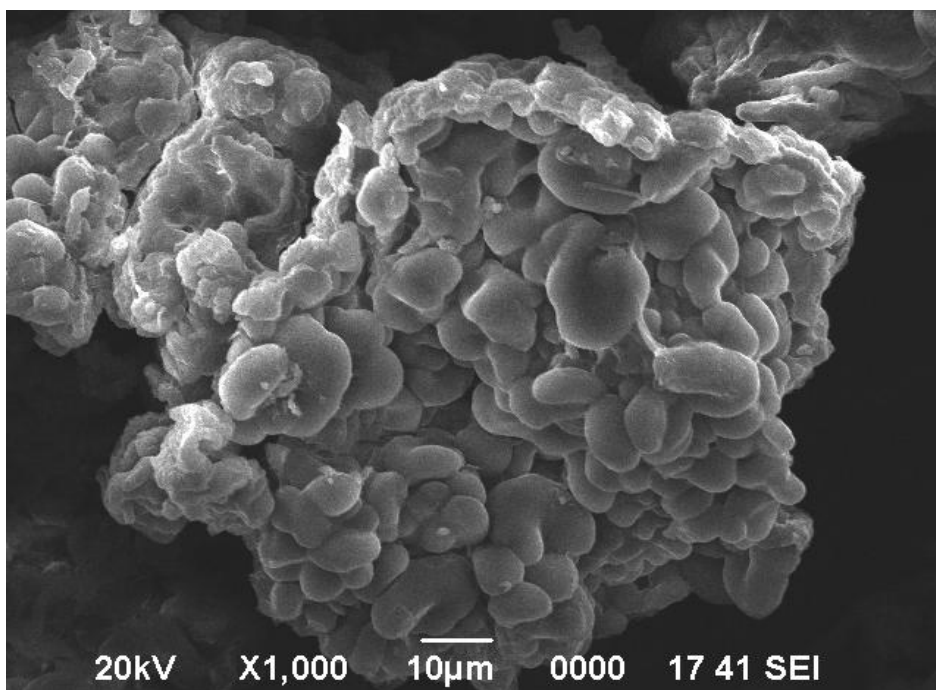


**Figure 6.39.** The micrograph of crosslinked poly(ABCF13) microparticles formed with 0.5% EGDMA content.
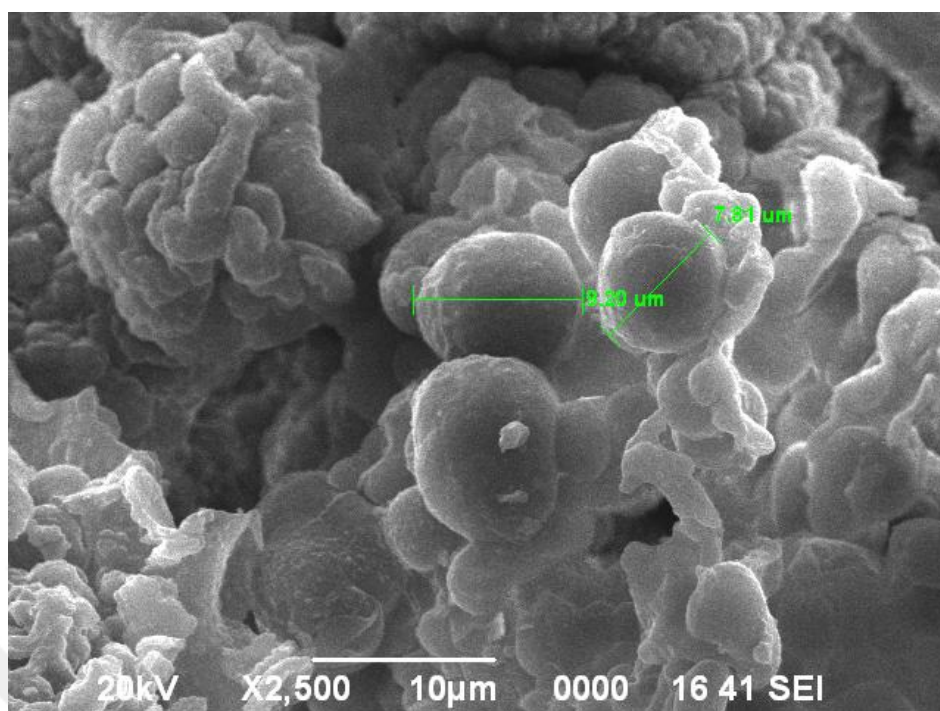
**Figure 6.40.** The micrograph of crosslinked poly(ABCF13) microparticles formed with 0.5% EGDMA.
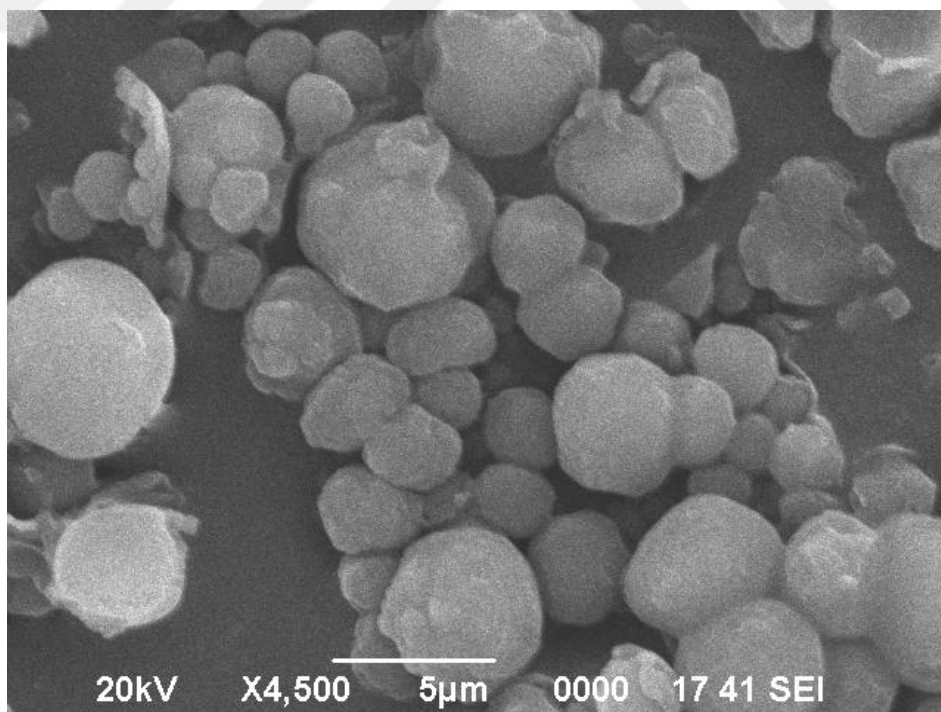


**Figure 6.41.** The micrograph of crosslinked poly(ABCF13) microparticles formed with 1.0% EGDMA.
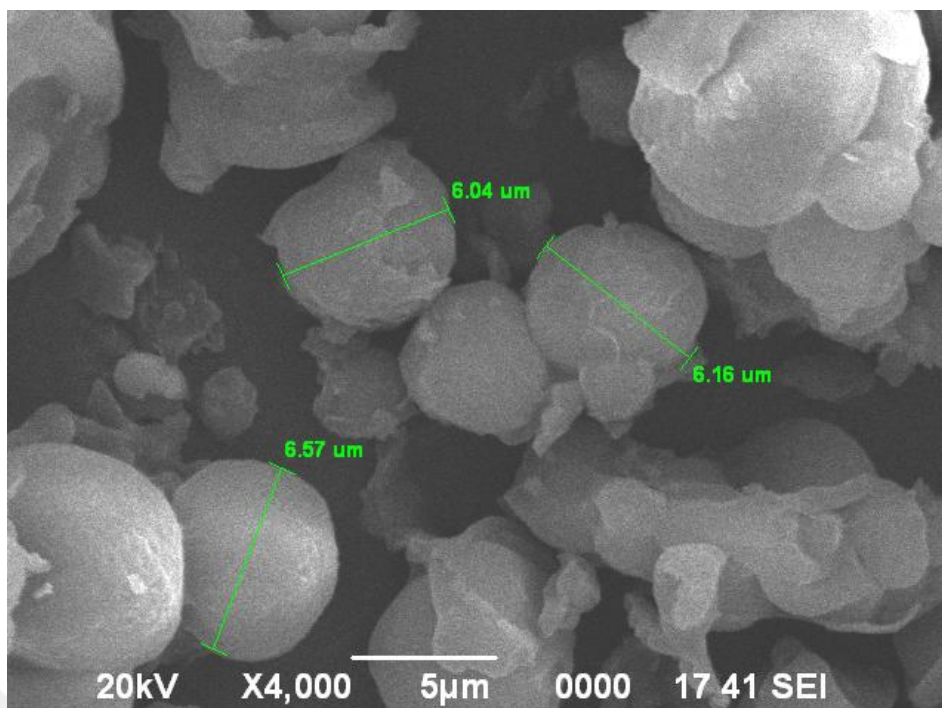
**Figure 6.42.** The micrograph of crosslinked poly(ABCF13) microparticles formed with 1.0% EGDMA.
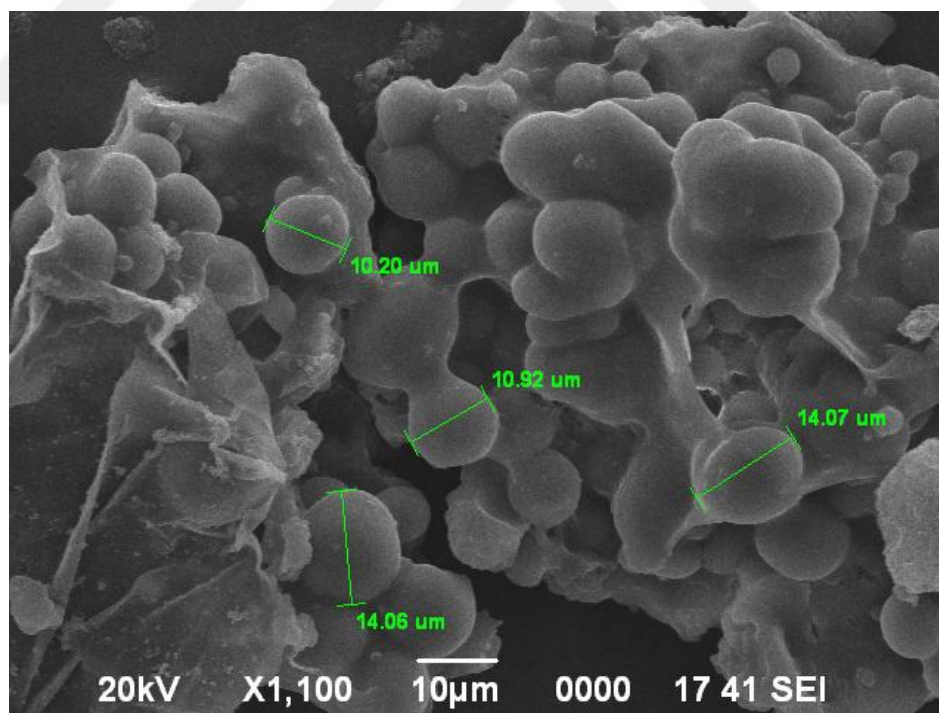


**Figure 6.43**. The micrograph of crosslinked poly(ABCF13) microparticles formed with 1.5% EGDMA.
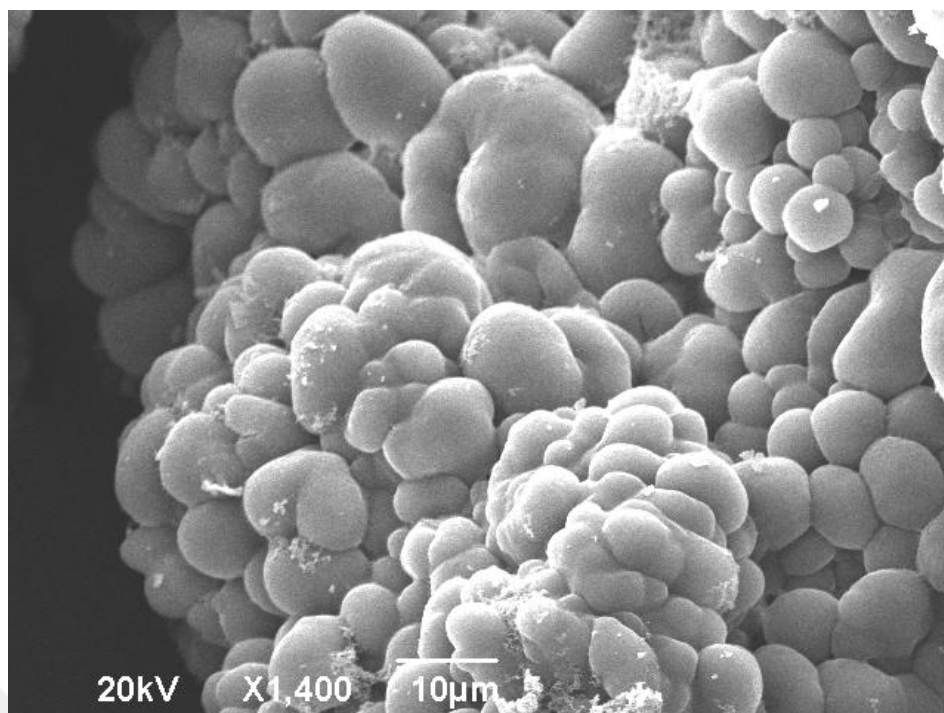
**Figure 6.44.** The micrograph of crosslinked poly(ABCF13) microparticles formed with 2.0% EGDMA.
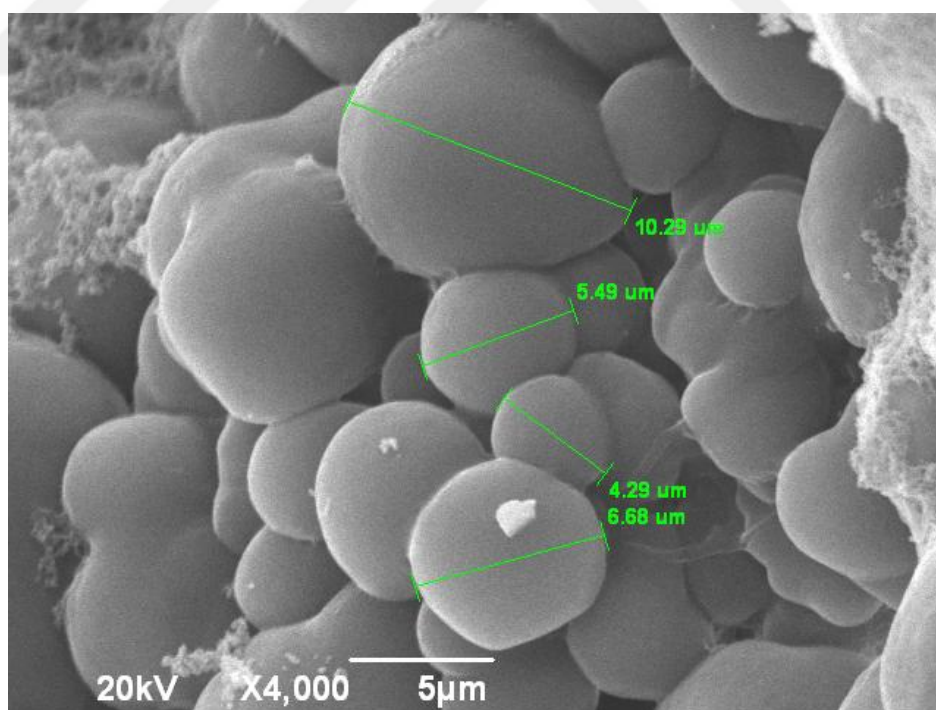


**Figure 6. 45**. The micrograph of crosslinked poly(ABCF13) microparticles formed with 2.0% EGDMA.
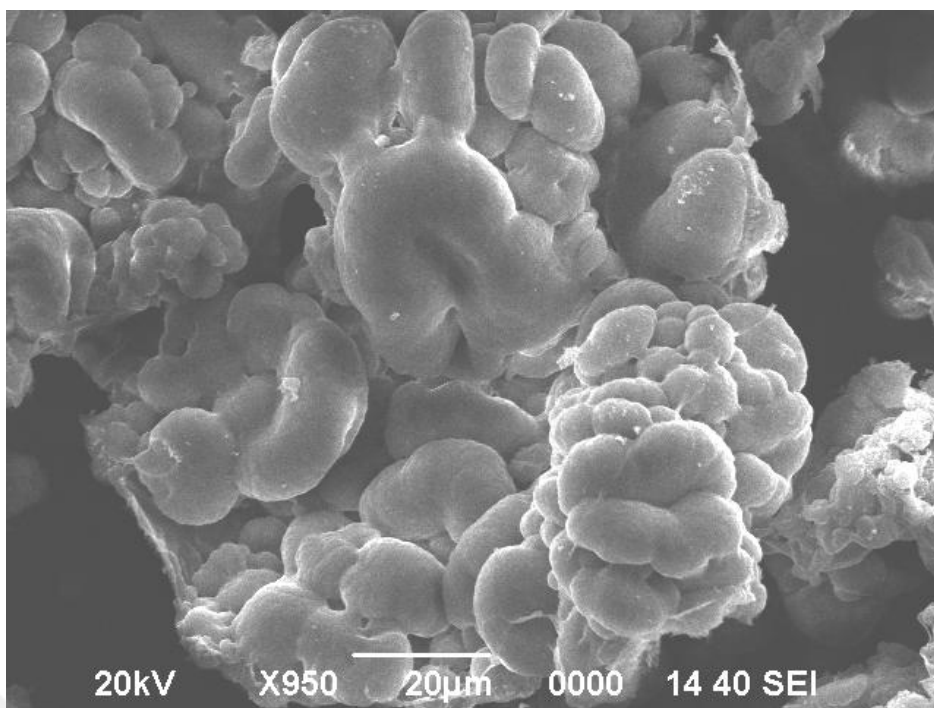
**Figure 6.46**. The micrograph of crosslinked poly(ABCF13) microparticles formed with 5.0% EGDMA.
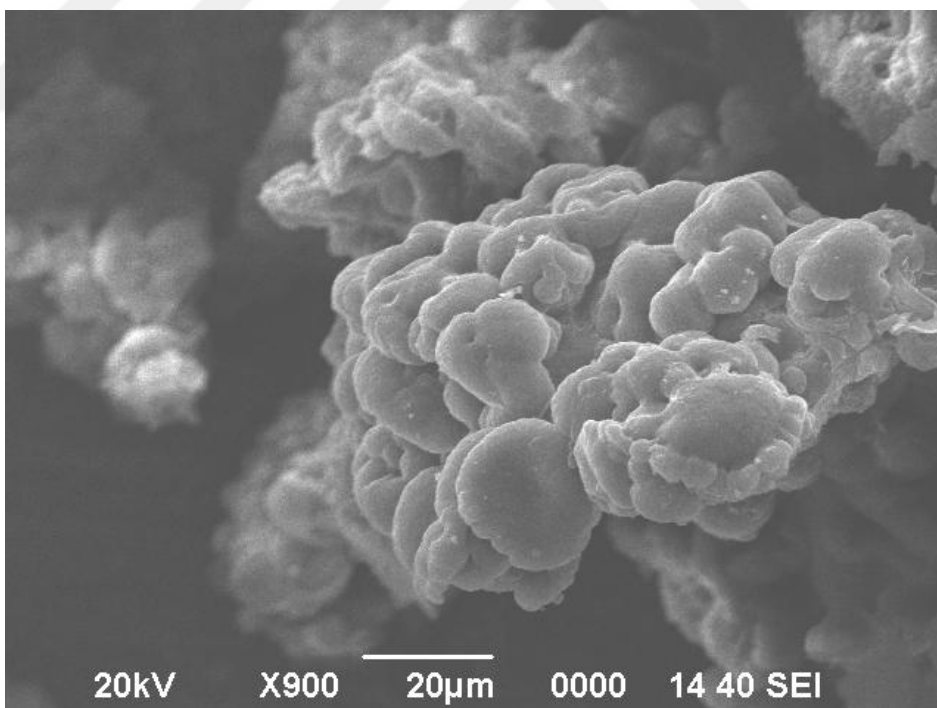


**Figure 6.47**. The micrograph of crosslinked poly(ABCF13) microparticles formed with 5.0% EGDMA.

94
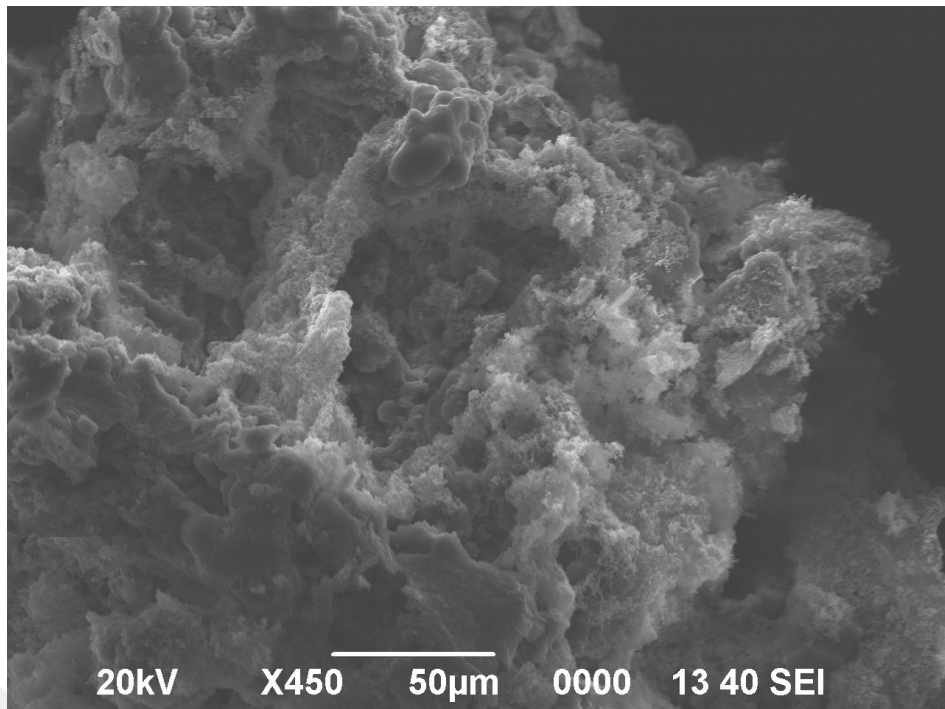
**Figure 6.48.** The micrograph of crosslinked poly(ABCF13) microparticles formed with 10.0% EGDMA.
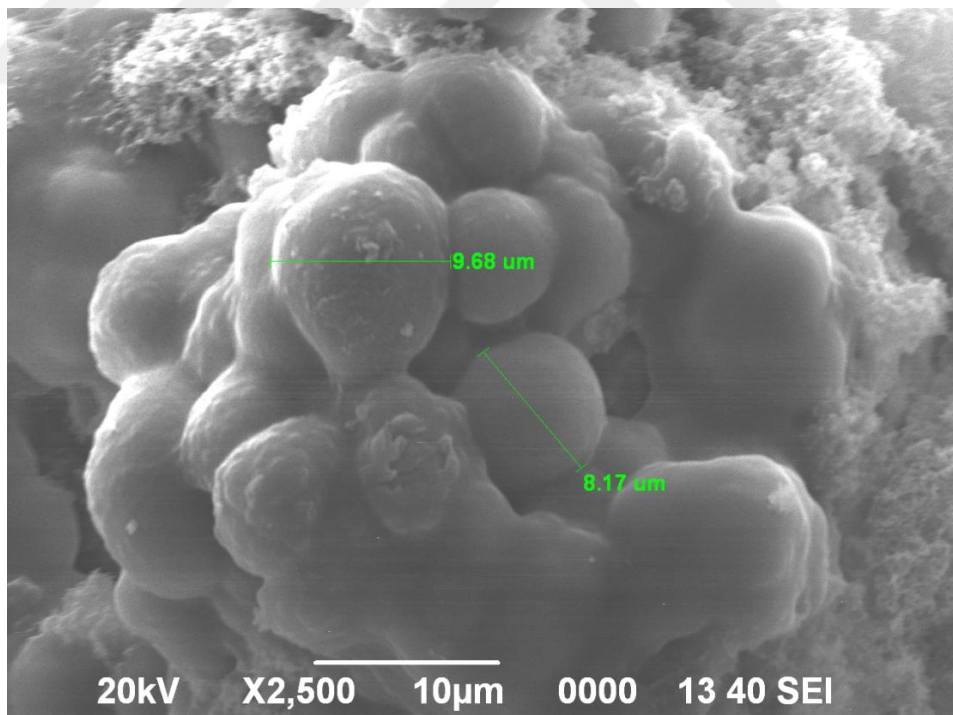


**Figure 6.49.** The micrograph of crosslinked poly(ABCF13) microparticles formed with 10.0% EGDMA.

Additionally, so as to find out how the much higher content of the crosslinking agents affected the properties of microspheres and to obtain highly crosslinked poly(ABCF13) microspheres, reaction mixture involving 200% of EGDMA (0.5 g of melt ABCF13 was mixed with about 0.95 mL of EGDMA) was also examined. The SEM analyses showed that the sizes of the formed particles ranged from approximately 1µm to 30 µm. It was also seen that the prepared microspheres possessed distorted, wrinkled and collapsed morphologies like a deflated soccer ball appearance, Figure 6.50-52. The nature, content and feeding times of the crosslinking agents (Dullens et al., 2004), polymer molecular weight in the droplets (Peng et all, 2014), the molecular interactions between the droplets (Badaire et all., 2008), chemical reactions on the surfaces of the microspheres (Yin et al., 2014) and the solvents used in medium (Peng and Imhof, 2015) have considerable effect on the surface modification of the microspheres. Moreover, excessive presence of the crosslinking agent, EGDMA in the dispersed phase was reported lead to more rapid polymerization reaction due to bifunctional property of EGDMA consumed faster than mono functional monomers (Dullens et al., 2004). Therefore, the crosslinking agents may cause flocculation and deformation by interfering with the nucleation stages of the particles in drops, which allows the possibility of controlling the particle shapes and growth stage (Peng and Imhof, 2015). Accordingly, microspheres possessed distorted, wrinkled and collapsed morphologies like a deflated soccer ball appearance, and as a result, the microspheres without good roundness with the formation of depressed pits were observed due to heterogeneous shrinkage in the drops. Additionally, at excessive content, the stronger binding of molecules due to relatively high degree of crosslinking gave rise to decrement in the intermolecular distance (Broer et al., 2011). As a results of that, the sunken holes on the surfaces of the microspheres due to the mentioned above probable reasons were observed in SEM images, Figure 6.50-52.
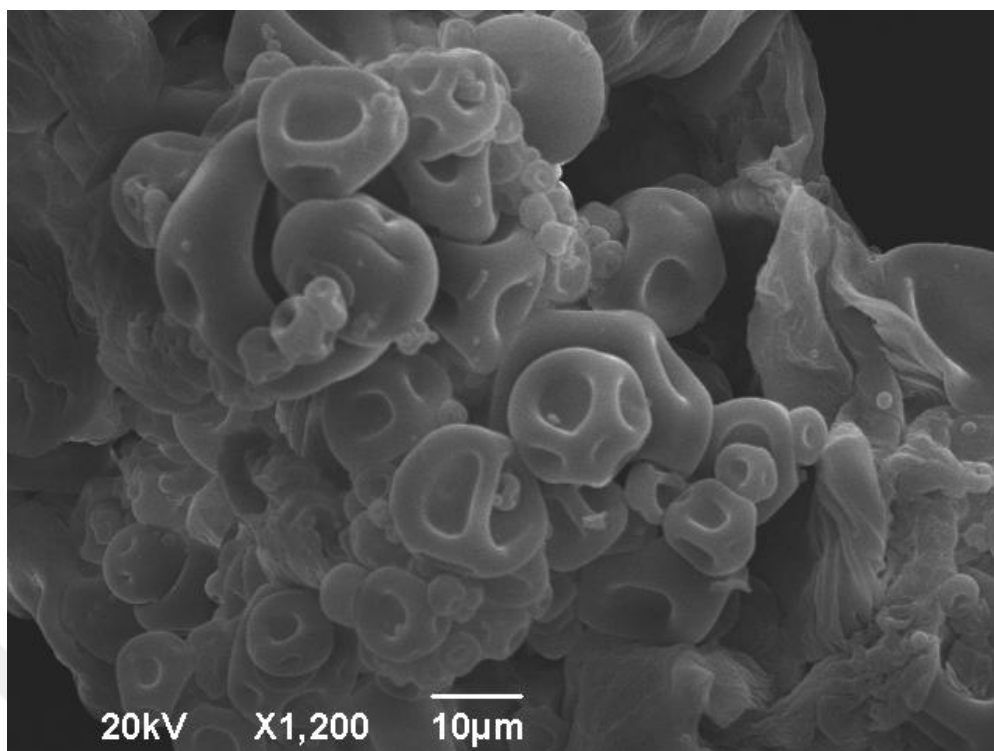
**Figure 6.50.** SEM images of the crosslinked poly(ABCF13) microparticles prepared with 200.0% EGDMA.
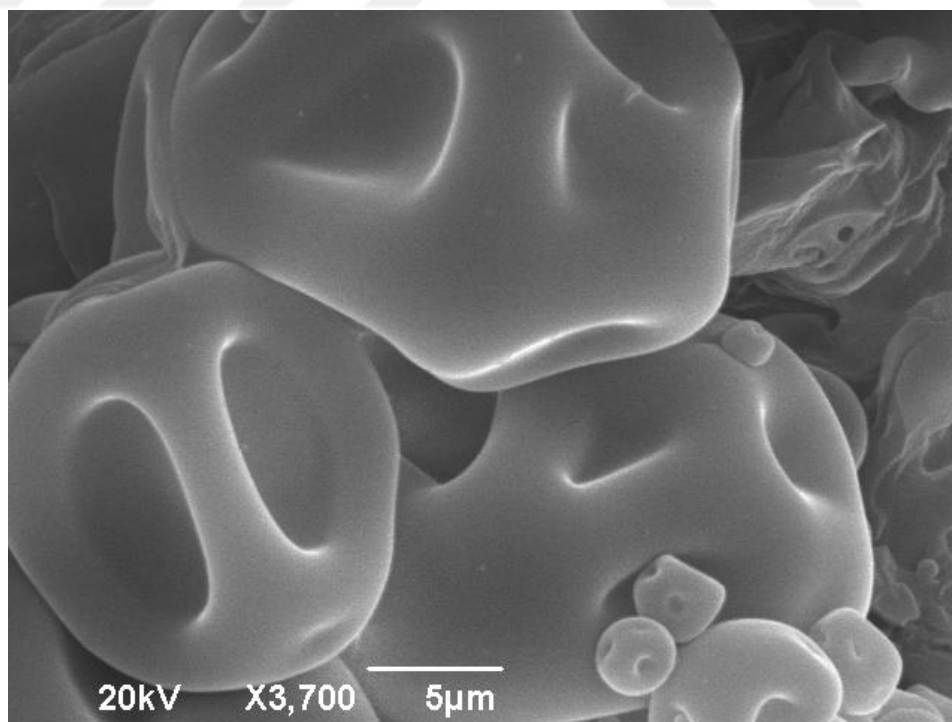


**Figure 6.51.** SEM images of the crosslinked poly(ABCF13) microparticles prepared with 200.0% EGDMA.
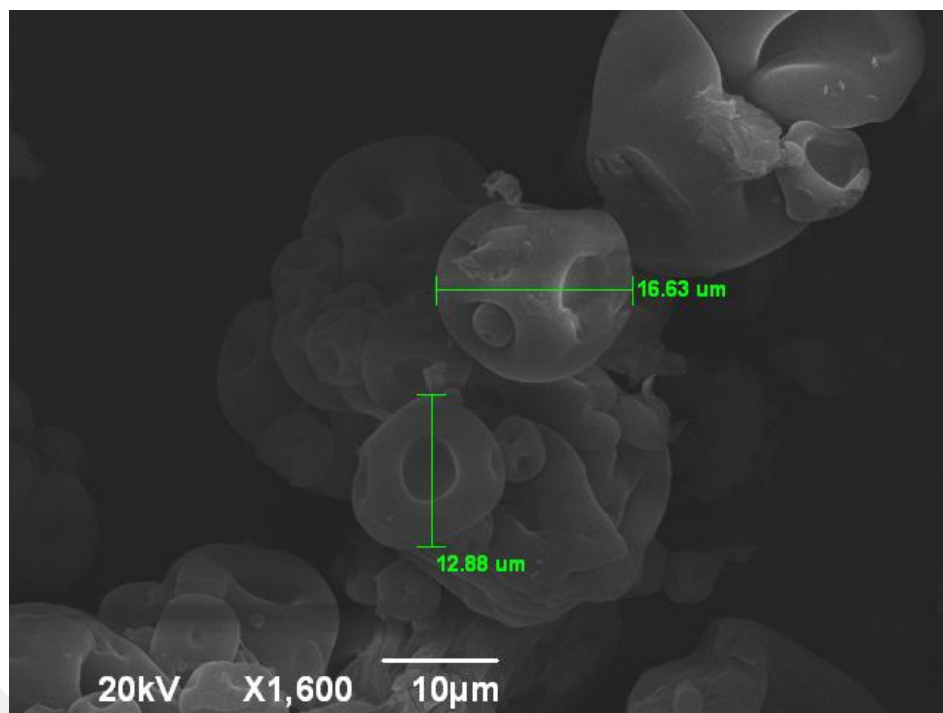
**Figure 6.52.** SEM images of the crosslinked poly(ABCF13) microparticles prepared with 200.0% EGDMA.

## 6.7.1.2 Effects of ABCF13 Concentration on Microsphere Formation

The effect of the monomer concentration (the ratio of dispersed phase to water phase) on microsphere structure and morphology, monitered by SEM analyses, was also investigated in depth. The productions were carried out at varying amount of monomer (0.05, 0.1, 0.2, 0.3, and 0.4 g in 150 mL of water) and at constant amount of the crosslinking agent (at the optimum percentage, 1%) and the initiator (1% with respect to the monomer) for 24 hours reaction time. Throughout the syntheses the reaction temperature was kept constant at 70°C and the stirring rate at 500 rpm. The SEM analyses exhibited that the amount of the monomer in reaction medium had no appreciable influence on the morphology of the particles under the prevailing production conditions. Almost at all concentrations, bulk products, particles accumulated in bulk, agglomerated microspherical particles but with deformed and distorted shape were observed, Figure 6.53-58. But, among the samples, the products obtained with 0.2 ABCF13 have relatively better morphology from the viewpoint of microspherical structure, in spite of the aggregations, Figure 6.55 and 6.56. Relatively lower deformity and lower adhesion of the particles were

detected at this concentration. Thus, 0.2 g ABCF13 in 150 mL of water was evaluated as the most promising concentration to achieve the desired morphology in the production of the microparticles by adjustment of the reaction conditions. This is attributed to establishment of relative co-stabilization balance between dispersed and continuous phases at this concentration, which highly depends on stability and viscosity of the monomer droplets (Arshady, 1992). The insufficient separation of the droplets, on the other hand, presumably caused the droplets to accumulate together during reaction, and consequently, relatively large agglomerations were observed in the products, Figure 6.57. Moreover, monomer droplets in the dispersed phases might be repelled toward each other by water molecules due to the hydrophobic effect, potentially resulting in binding and adhesion of the drops with sticking tendency. The size range of agglomerations formed by the combination of the smaller particles was found as about 100-200 μm, Figure 6.57.



**Figure 6.53.** The SEM image of crosslinked poly(ABCF13) microparticles containing 0.05 g of ABCF13.

**Figure 6.54.** The SEM image of crosslinked poly(ABCF13) microparticles containing 0.1 g of ABCF13.



**Figure 6.55.** The SEM image of crosslinked poly(ABCF13) microparticles containing 0.2 g of ABCF13.

**Figure 6.56.** The SEM image of crosslinked poly(ABCF13) microparticles containing 0.2 g of ABCF13.



**Figure 6.57.** The SEM image of crosslinked poly(ABCF13) microparticles containing 0.3 g of ABCF13.
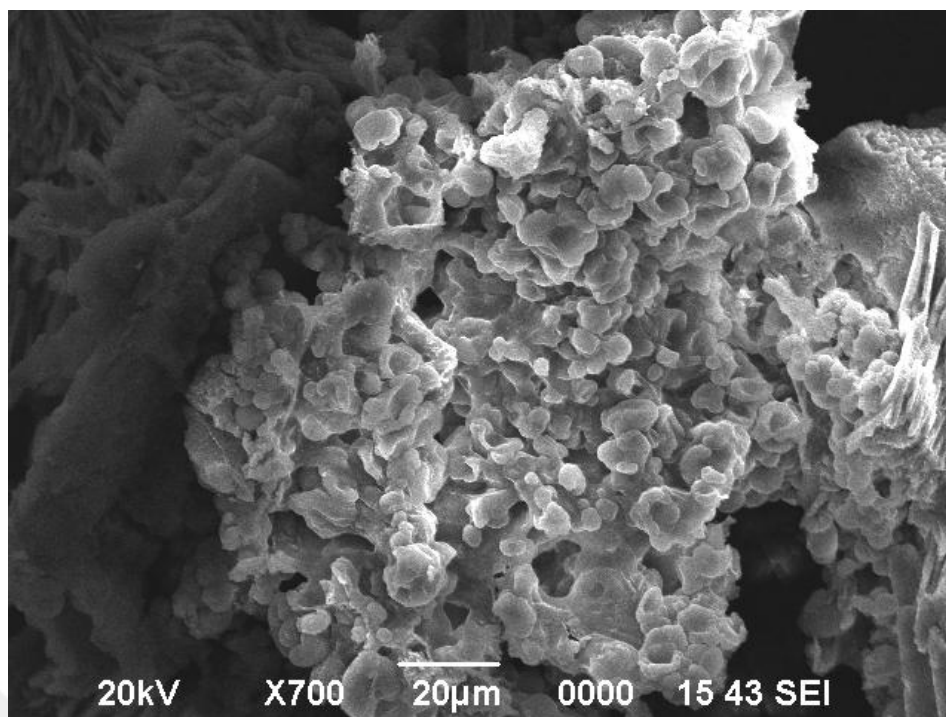
**Figure 6.58.** The SEM image of crosslinked poly(ABCF13) microparticles containing 0.4 g of ABCF13.

**6.7.1.3 Effects of Initiator Content on Microsphere Formation**

The dependence of microsphere formation and morphology on concentration of the initiator, KPS was investigated by employing the initiator at the percentages of 0.1, 0.3, 0.5, 0.8, 1.0 and 1.3% (with respect to weight of the monomer). The syntheses were carried out at 70°C for 24 hours with the reaction mixtures composed of 0.2 g ABCF13, 1% crosslinking agent, EGDMA, 150 mL of water, the initiator at predetermined percentage and with the stirring rate of 500 rpm. The SEM images of the products were presented in Figure 6.59-66. The analyses revealed that almost no microspherical structure was recorded at low percentages of KPS, up to 0.5%, Figure 6.59-61. As the concentration of KPS was increased further, the formation of microspherical particles started to appear, but, in agglomerated form, Figure 6.62 and 63. Relatively well-shaped microspheres were obtained with the use of 1.3% KPS, Figure 6.64-66. Thus, 1.3% KPS was determined as the optimal and favorable concentration for the preparation of the stable microspherical particles with the desired morphology and good roundness. Accordingly, the products with negligible agglomeration, coagulum or coalescence were achieved at this concentration, and the

microspheres had smooth and plain surfaces with sizes ranged roughly from 1µm to 25 µm, as shown in Figure 6.65. Presumably, in continuous phase of the system since the radicals formed with relatively higher amounts in relatively shorter time periods, the encountering (collision) probability of radicals with monomer droplets is at optimum with this concentration of the initiator, which resulted in the formation of the primary stable and permanent microspheres with no deformation. Conversely, it is visible that 0.1, 0.3, 0.5 and 0.8% of KPS were unfit to prepare the microspheres, and there existed bulky structures, agglomerations and oddly-shaped particles without any microspherical formations, Figure 6.59-62. This probably arose from the decomposition mechanism nature of KPS in water. That is, both sulfate ion radicals and OH radicals are produced from the decomposition of KPS in water. But, the polymerization reaction of the monomers in droplets takes place via the former rather than OH radicals. However, when the sulfate ion radicals are not captured by monomer droplets in a certain time interval, they react with water instead of the monomers. This potentially results in the depletion of the activities of the formed radicals with time (Henton et al., 1996). Accordingly, at low percentages of KPS, the cooperation of monomers with sulfate ion radicals in water become more difficult when the radicals are produced at relatively lower amounts, and the polymerization reactions are affected negatively, resulting in the accumulations of the particles and the formation of bulky structures. Additionally, slow increase of viscosity in the droplets due to partial polymerization (arisen from the presence of lower amount of radicals in the medium) probably brought about tendency to form coalescence and sedimentation, as was reported by Kurt (Kurt, 2010). Therefore, at low KPS concentrations, the bulky structures and accumulations might be stated to arise primarily from the sticking of the forming particles. Conversely, with the increase in the concentration of the initiator, the droplets presumably become gradually more stable and permanent due to relatively more effective polymerization.
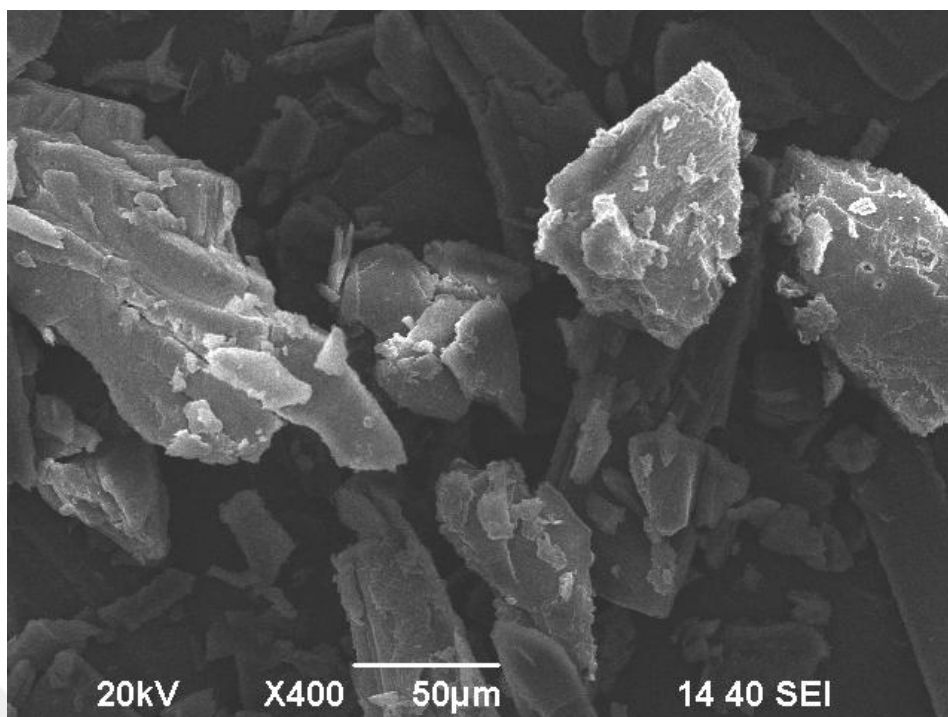
**Figure 6.59.** The SEM image of crosslinked poly(ABCF13) products containing 0.1% KPS.
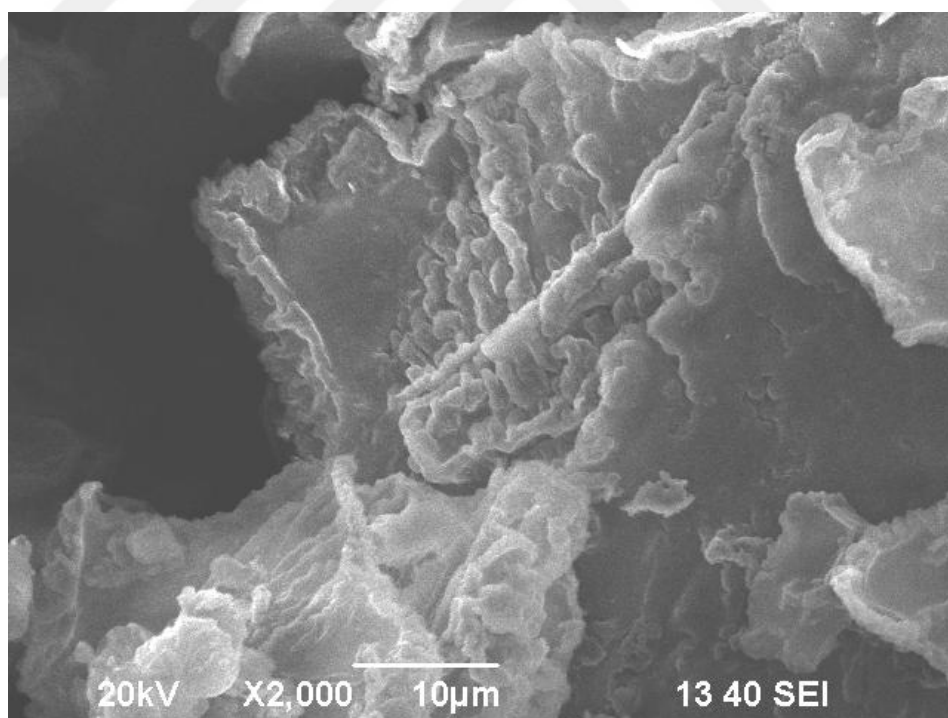


**Figure 6.60.** The SEM image of crosslinked poly(ABCF13) products containing 0.3% KPS.
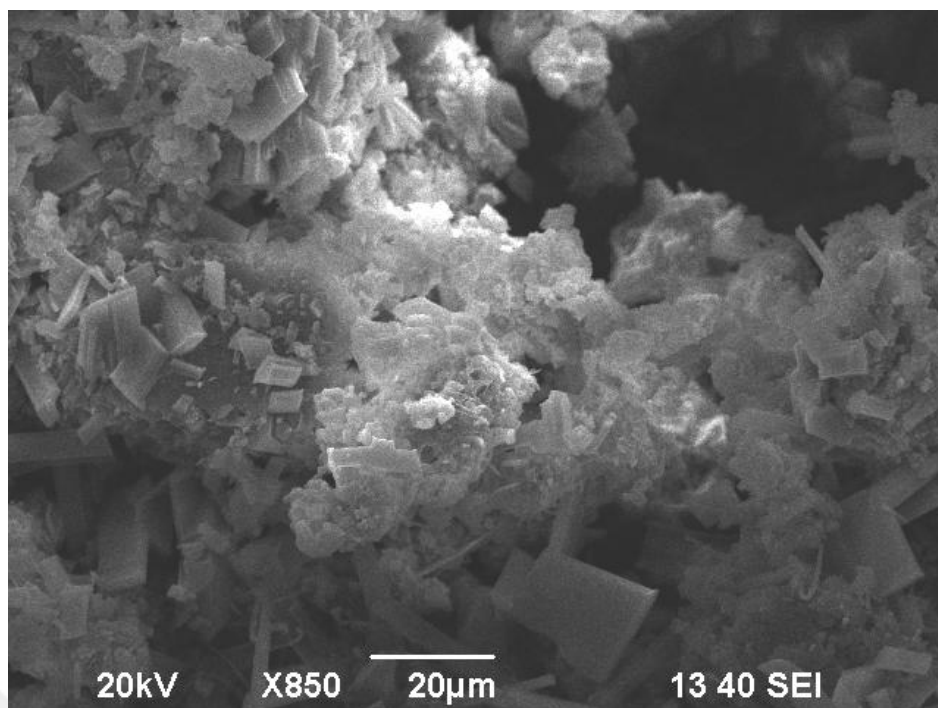
**Figure 6.61.** The SEM image of crosslinked poly(ABCF13) products containing 0.5% KPS.
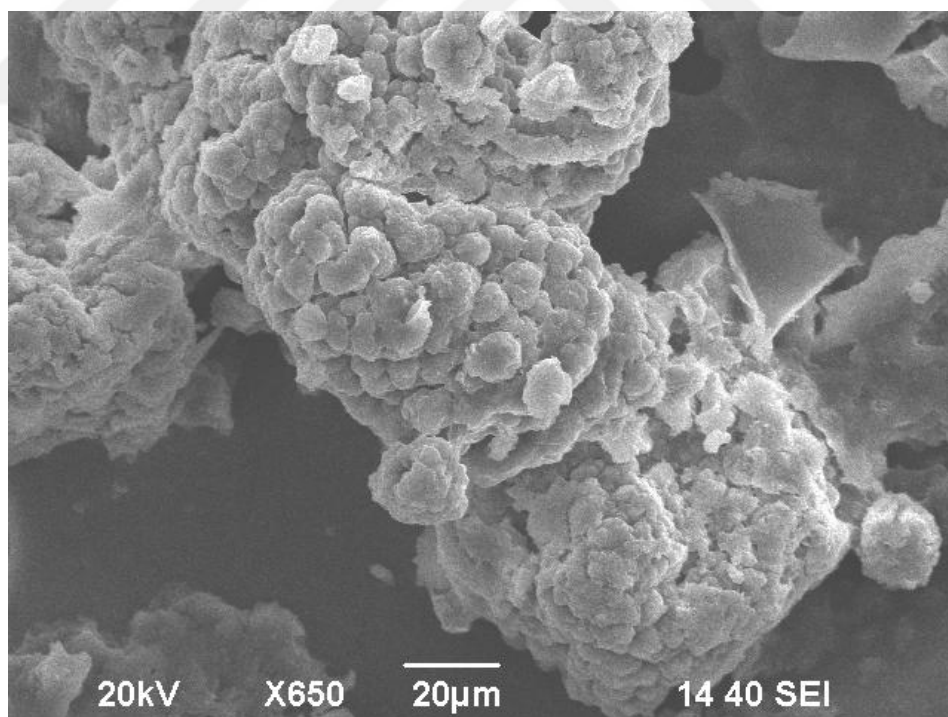


**Figure 6.62.** The SEM image of crosslinked poly(ABCF13) products containing 0.8% KPS.
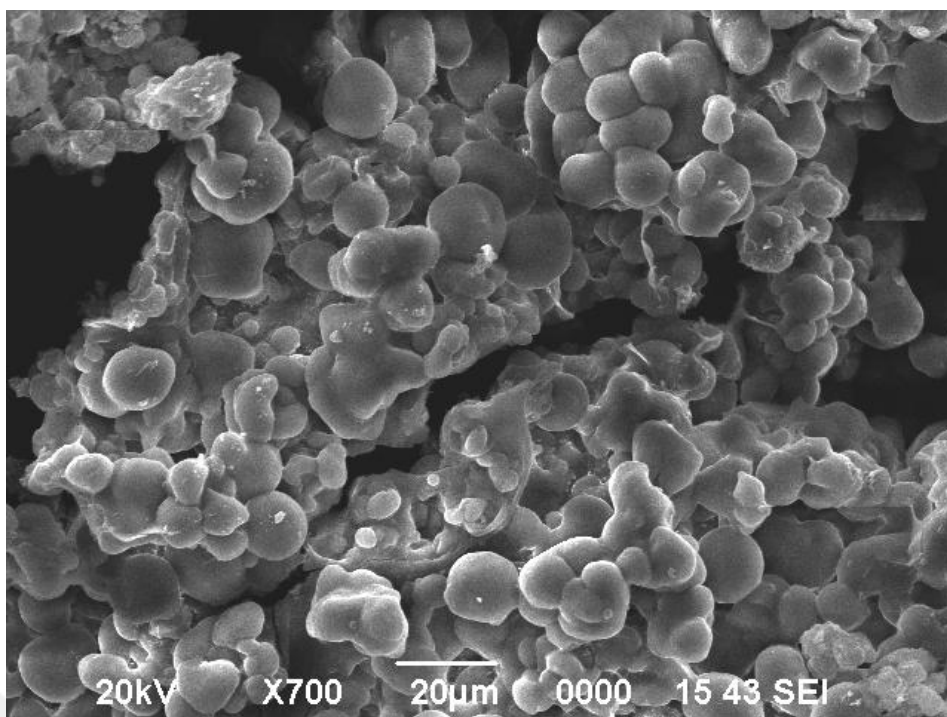
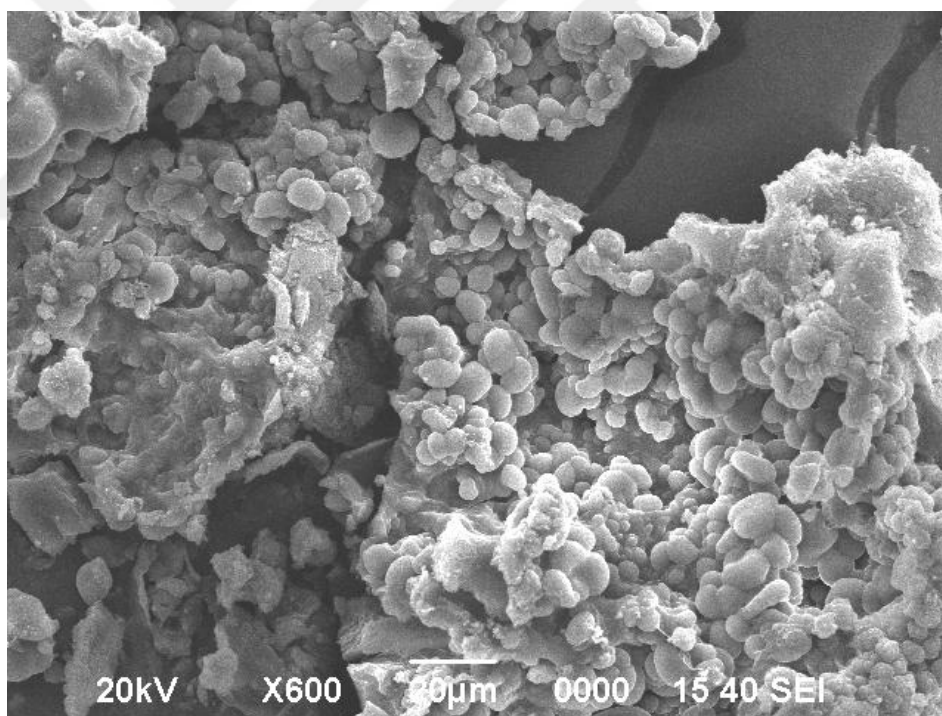**Figure 6.63.** The SEM image of crosslinked poly(ABCF13) products containing 1.0% KPS.
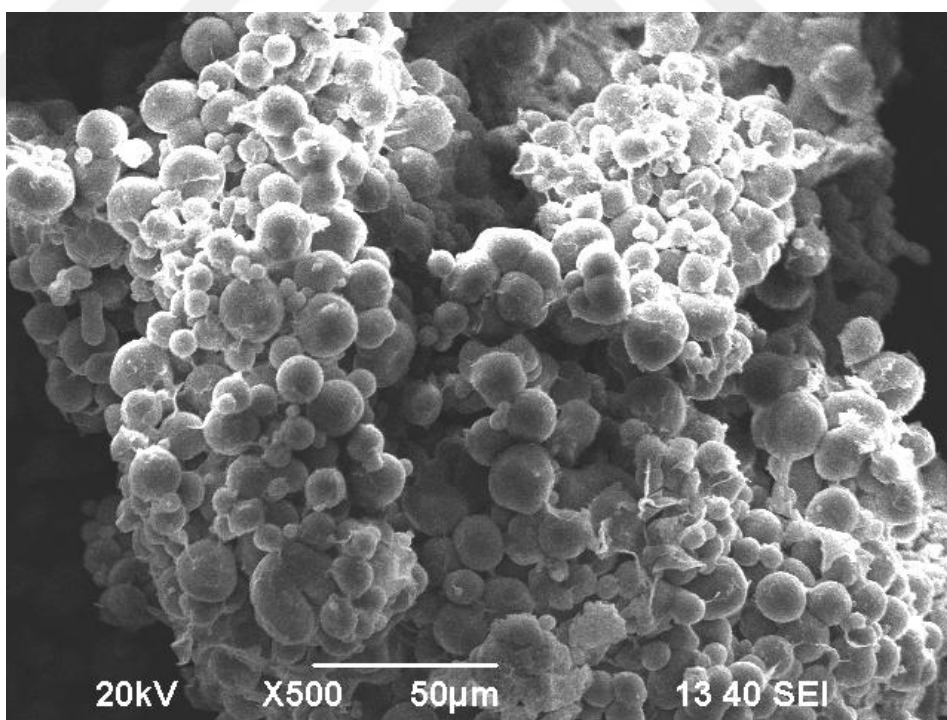


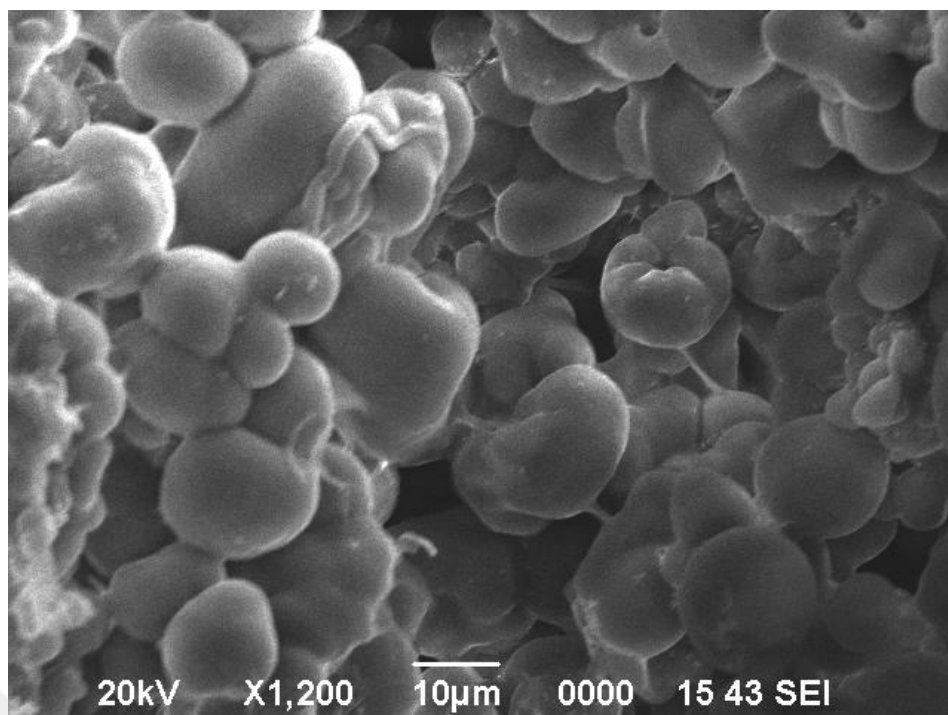**Figure 6.64.** The SEM image of crosslinked poly(ABCF13) microspheres containing 1.3% KPS.

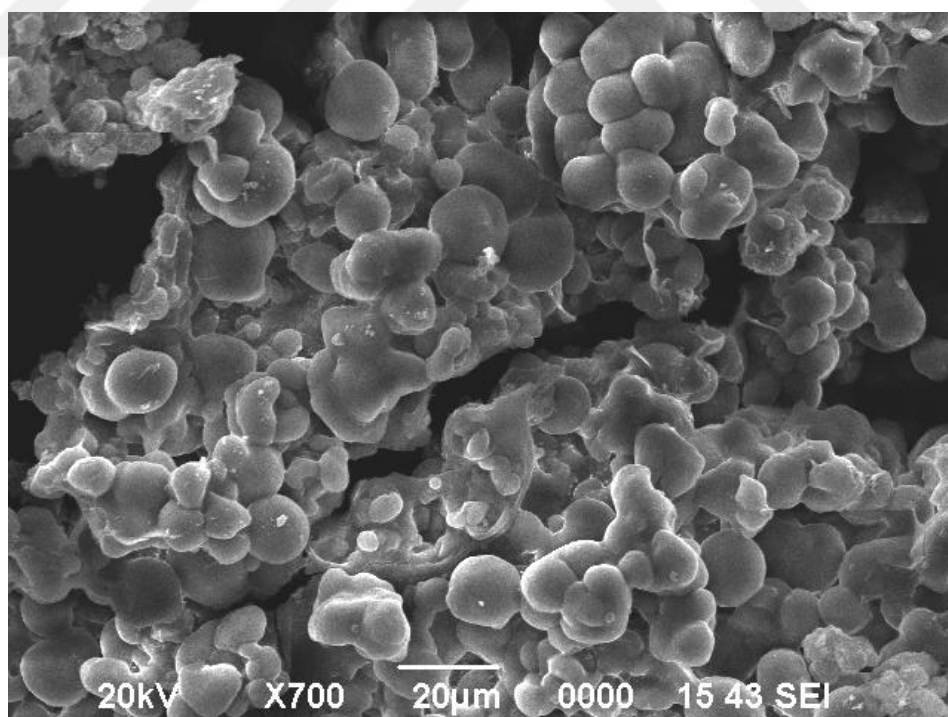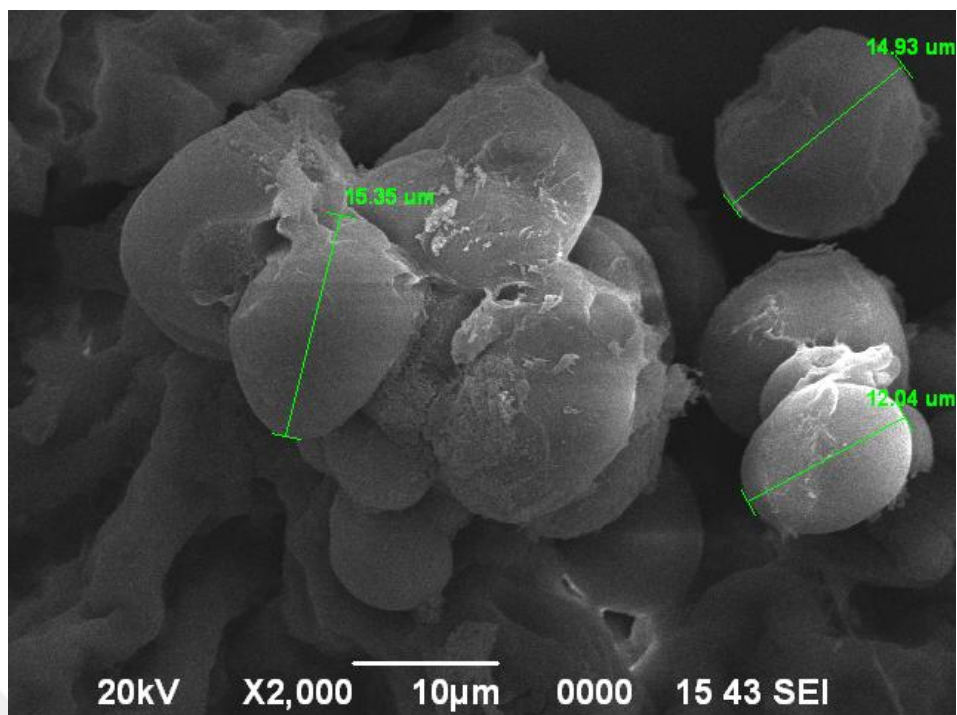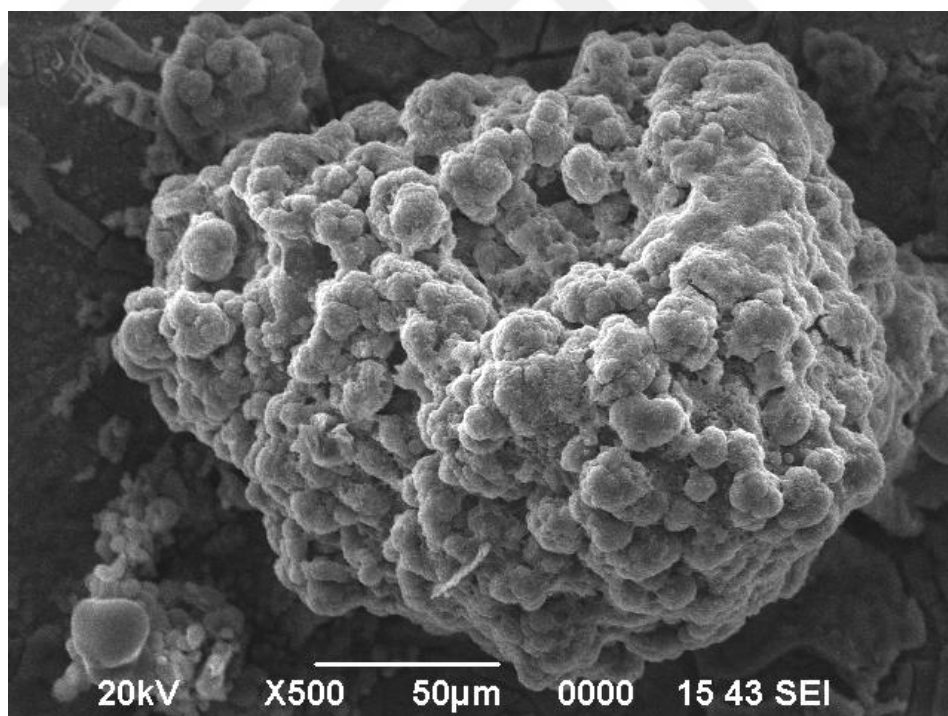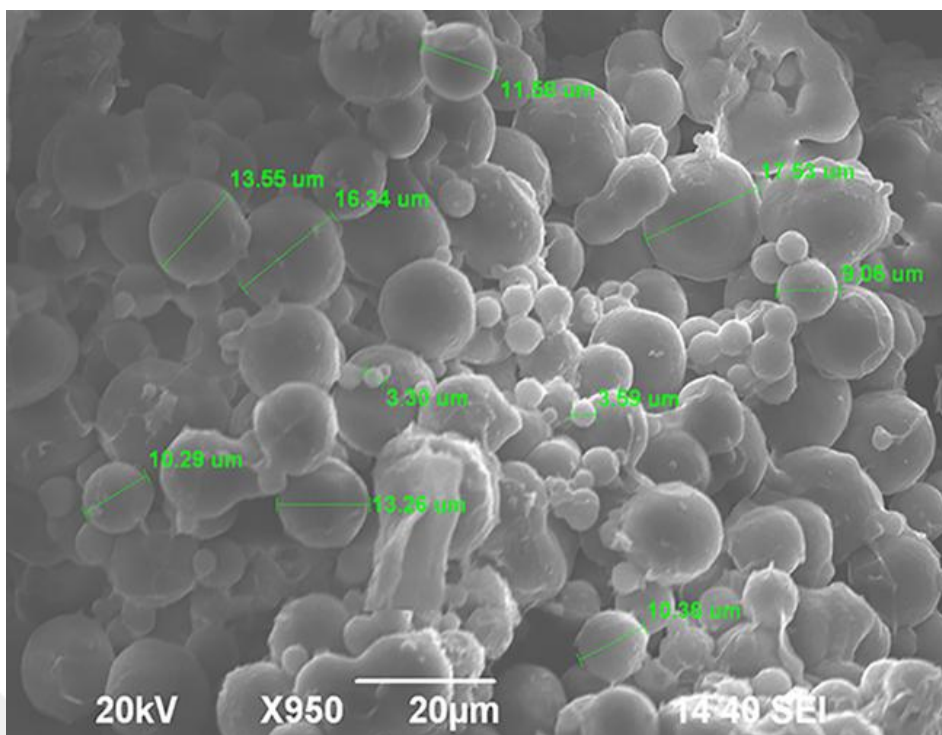**Figure 6.65.** The SEM image of crosslinked poly(ABCF13) microspheres containing 1.3% KPS.
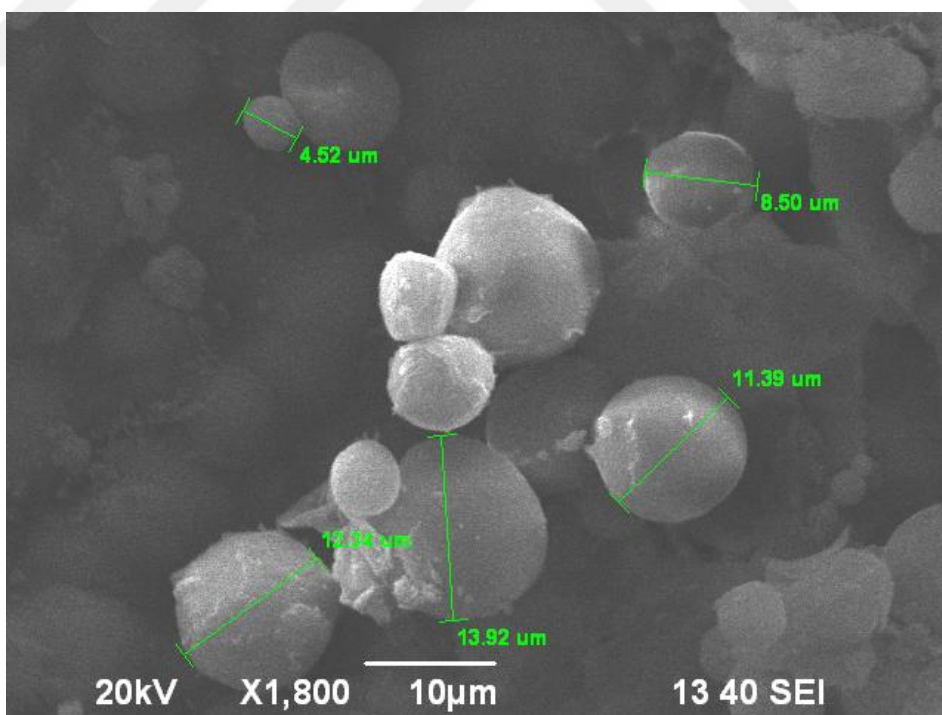


**Figure 6.66**. The SEM image of crosslinked poly(ABCF13) microspheres containing 1.3% KPS.

### 6.7.1.4 Effects of Stirring Rates on Microsphere Formation

The influence of stirring rate on the production and morphology of the microspheres was studied meticulously by conducting the polymerizations at stirring rates of 300, 500, 700, 900 and 1100 rpm. The polymerizations were carried out at 70°C for 24 hours with the reaction mixtures composed of 0.2 g ABCF13, 1% EGDMA, and 1.3% KPS in 150 mL of water. The variations of the morphology of the products with stirring rate were depicted in the SEM images through Figure 6.67-73. The images displayed that stirring rate directly affected the characteristics of produced microspheres, especially size of the particles. The stirring rate, defined as provided the energy for dispersion of the droplets in continuous medium, is inversely proportional to the size of the microspheres. In other words, the increment in the stirring rate results in the decrement in the size of the microspheres since the higher input stirring power separates the larger droplets into smaller ones (Yang et al., 2001; Ravi et al., 2008; Yang et al., 2008; Dinarvand et al., 2003; Arshady, 1992). Accordingly, at 300 rpm, a product involving odd-shaped and bulky particles and with broad particle size distribution was obtained. The particles were not in a spherical formation. Seemingly, the lower stirring speed with inadequate input energy to break up the droplets gave rise to insufficient and ineffective dispersion of the droplets, and thus resulted in the undesired morphology in the product, Figure 6.67. Among the products, largest particles with size of about 90 μm were achieved with 300 rpm stirring rate. The optimum agitation rate for the preparation of well-shaped, smooth and spherical microparticles, on the other hand, was found to be 500 rpm, revealed by the SEM analyses, Figure 6.68 and 6.69. As the speed was increased further, deteriorations started to appear in the shape of microspheres, Figure 6.70-73. Furthermore, the sizes of microspheres produced at 500 rpm was roughly higher than those formed at 700 rpm. These results showed good agreement with the literature (Lin et al., 2015). However, at excessively high stirring speeds, especially at 900 and 1100 rpm, the formation of bulky structures, aggregations and coagulum were observed due to the sticking of the primarily formed microparticles to one another, Figure 6.72 and 6.73. It can be stated that the droplets in dispersed phase have a tendency to stick to each other when the drops reach a certain viscosity degree during polymerization. Seemingly, inadequately high input energy, instead of breaking up the droplets into smaller ones, serves to stick the droplets to the others.

Consequently, the coupling, accumulating, coalescence or sticking of the primarily formed particles became inevitable to form oddly-shaped bulky structures when the stirring rates was too high (Kurt, 2010).
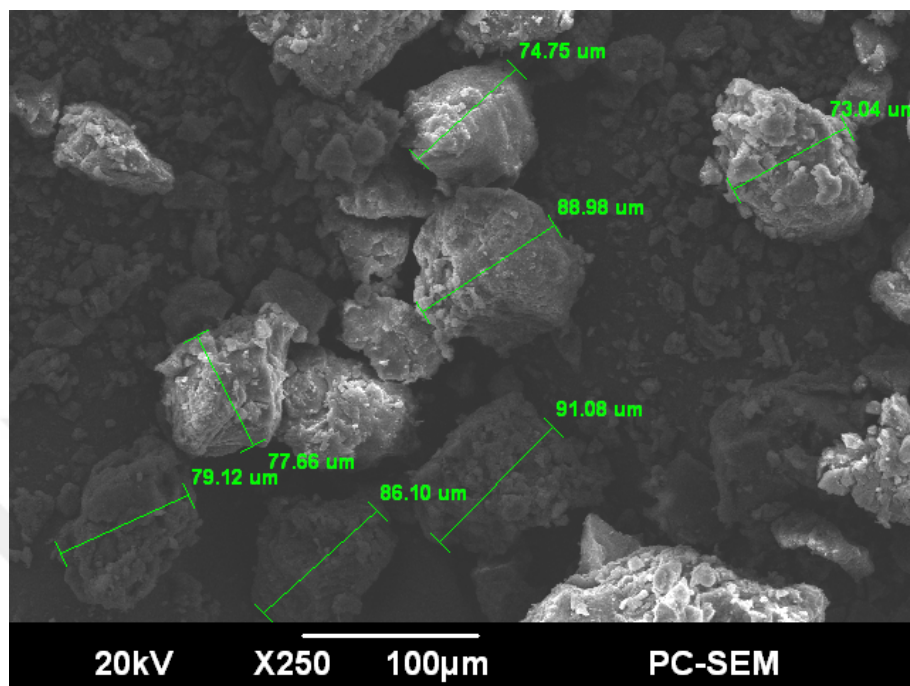


**Figure 6.67.** The SEM image of crosslinked poly(ABCF13) particles produced with 300 rpm stirring rate.
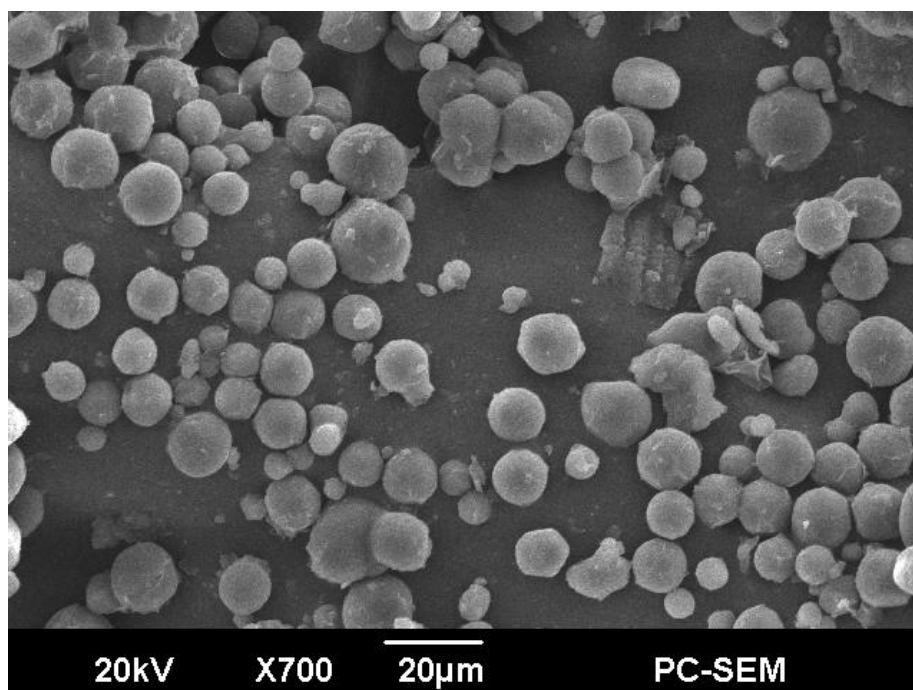


**Figure 6.68.** The SEM image of crosslinked poly(ABCF13) microspheres produced with 500 rpm stirring rate.
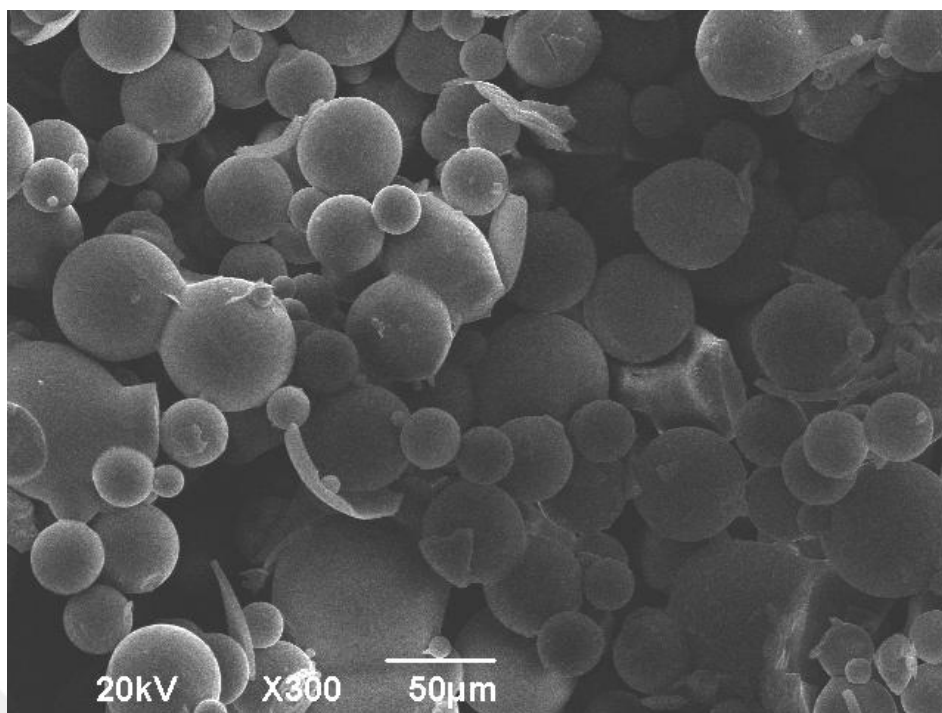
**Figure 6.69.** The SEM image of crosslinked poly(ABCF13) microspheres produced with 500 rpm stirring rate.
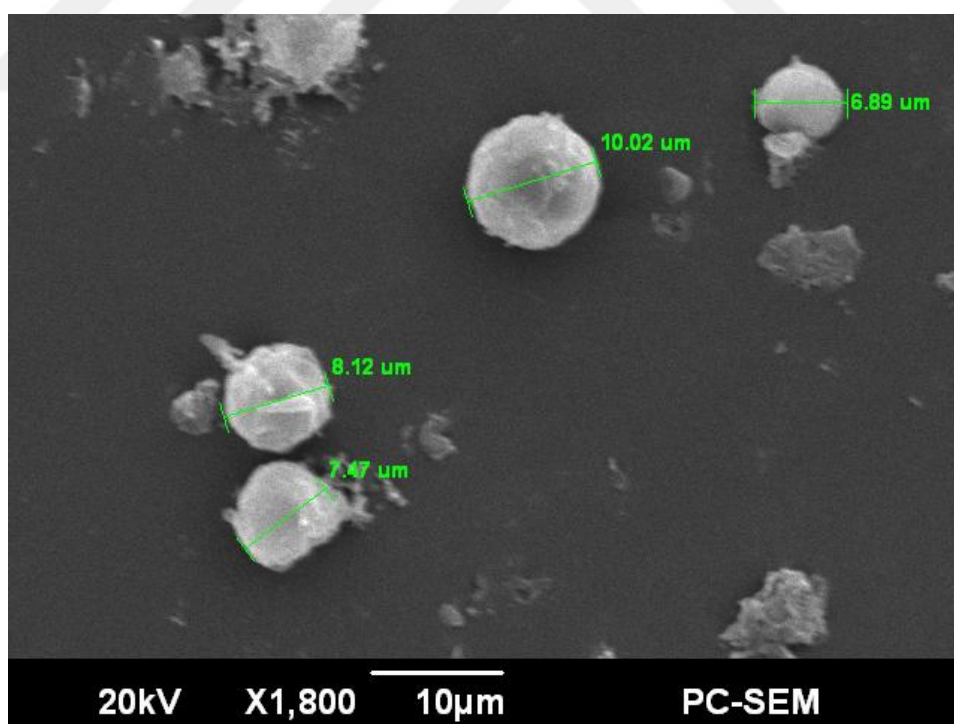


**Figure 6.70.** The SEM image of crosslinked poly(ABCF13) microparticles produced with 700 rpm stirring rate.
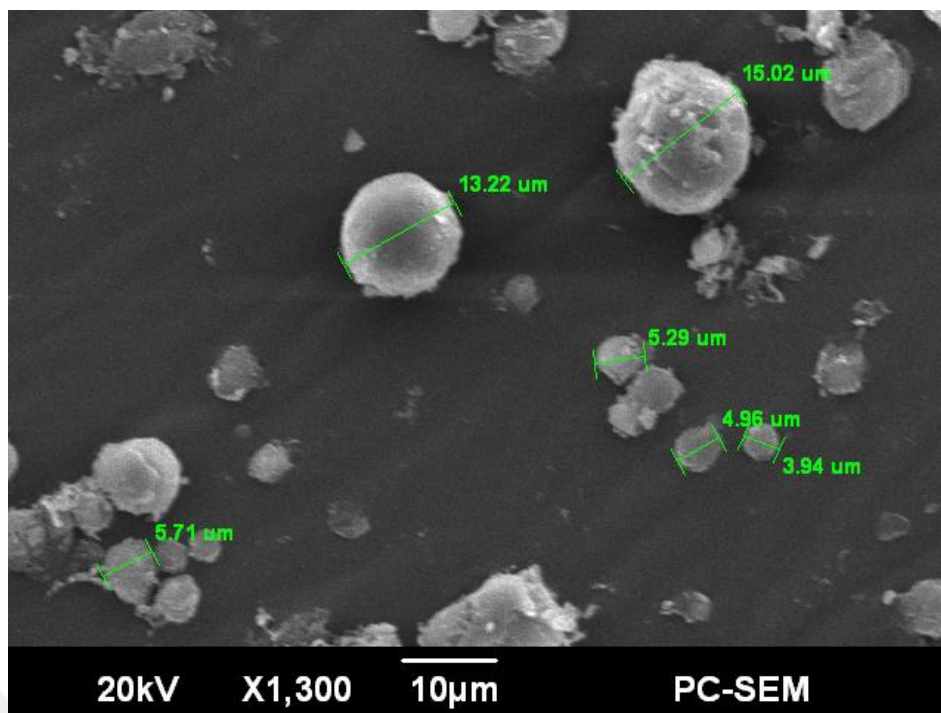
**Figure 6.71.** The SEM image of crosslinked poly(ABCF13) microparticles produced with 700 rpm stirring rate.
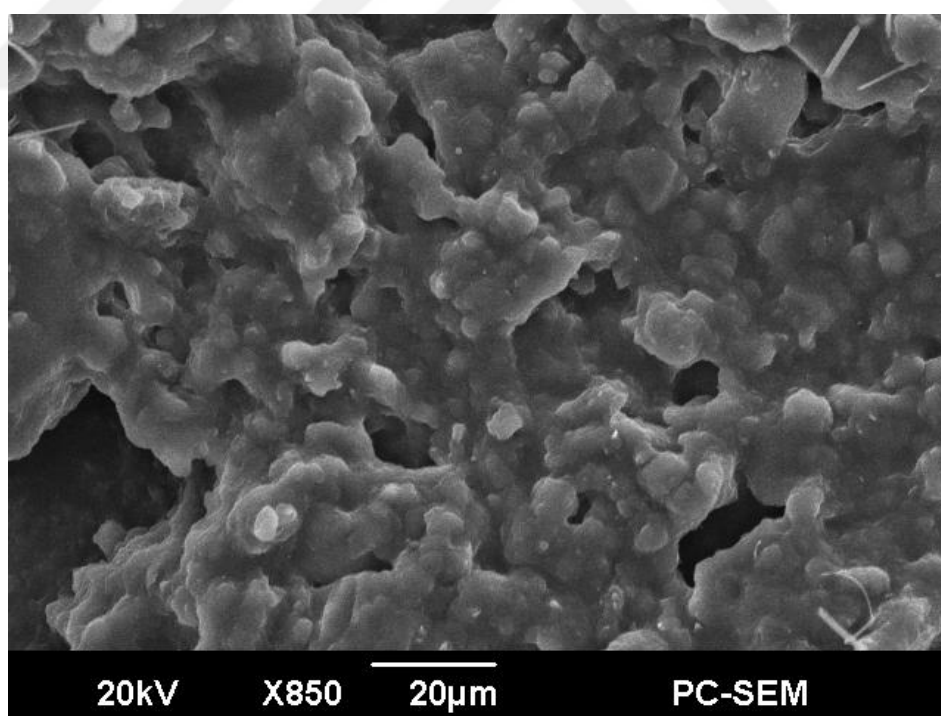


**Figure 6.72.** The SEM image of crosslinked poly(ABCF13) particles produced with 900 rpm stirring rate.
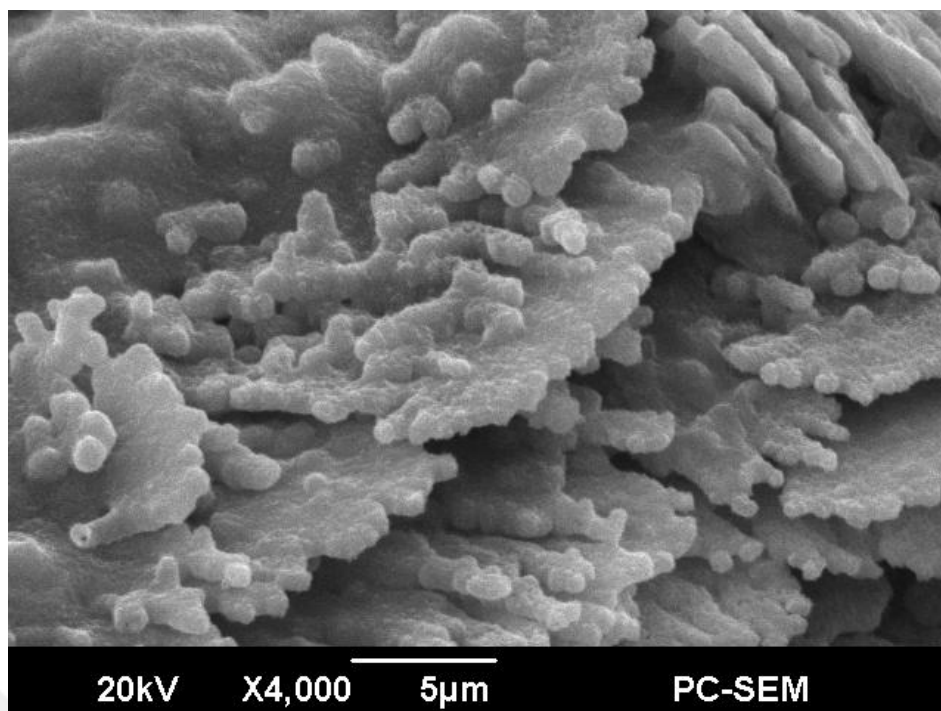
**Figure 6.73.** The SEM image of crosslinked poly(ABCF13)   particles produced with 1100 rpm  stirring rate.

After the optimization studies, the dependence of the microsphere morphology on the crosslinking agent EGDMA, the monomer ABCF13, the initiator KPS concentration and stirring rate was clarified by means of SEM analyses. The size of the fabricated microspheres at the optimized conditions ranged approximately from 10 µm to 100 µm, Figure 6.74. The magnified images of the perfect, well-defined, desired and well-shaped microspheres with smooth surfaces and good roundness were illustrated in Figure 6.75-6.77. The optimum parameters in order to prepare well-defined crosslinked poly(ABCF13) microspheres were stated as the followings;

- ✓ 0.2 g of melted ABCF13 monomer as  dispersed phase,
- ✓ 1% of crosslinking agent (EGDMA) with respect to weight of monomer,
- ✓  1.3% of water soluble initiator (KPS) with respect to weight of monomer,
- ✓ 150 mL of pure water as the continuous phase,
- ✓ 70°C reaction temperature,
- ✓ 500 rpm agitation rate,
- ✓ 24 hours reaction time.
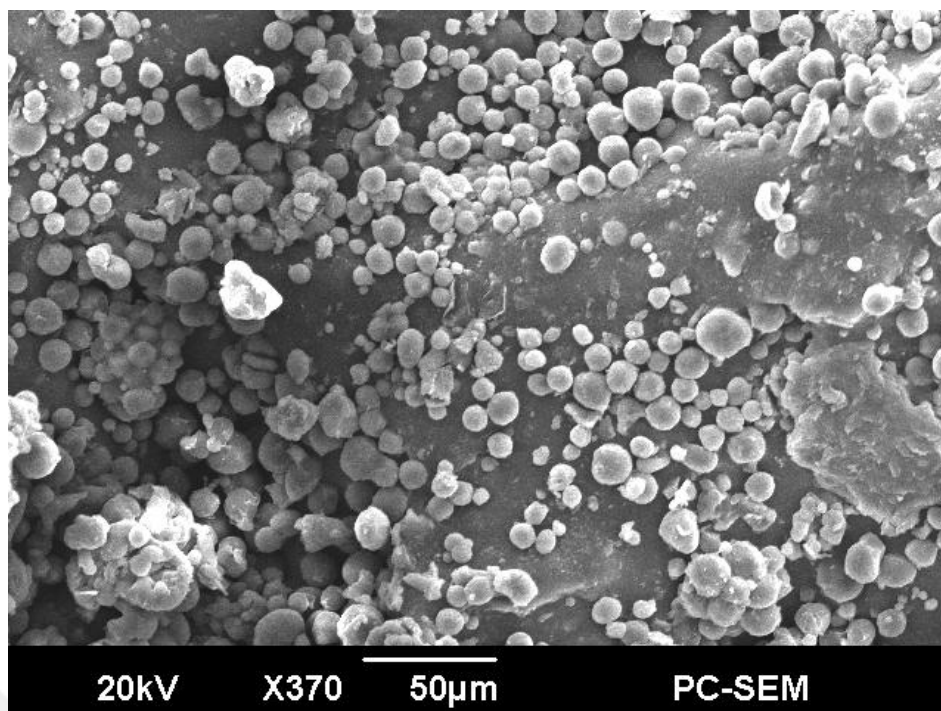
**Figure 6.74.** The clear SEM image of the crosslinked poly(ABCF13) microspheres after optimization.
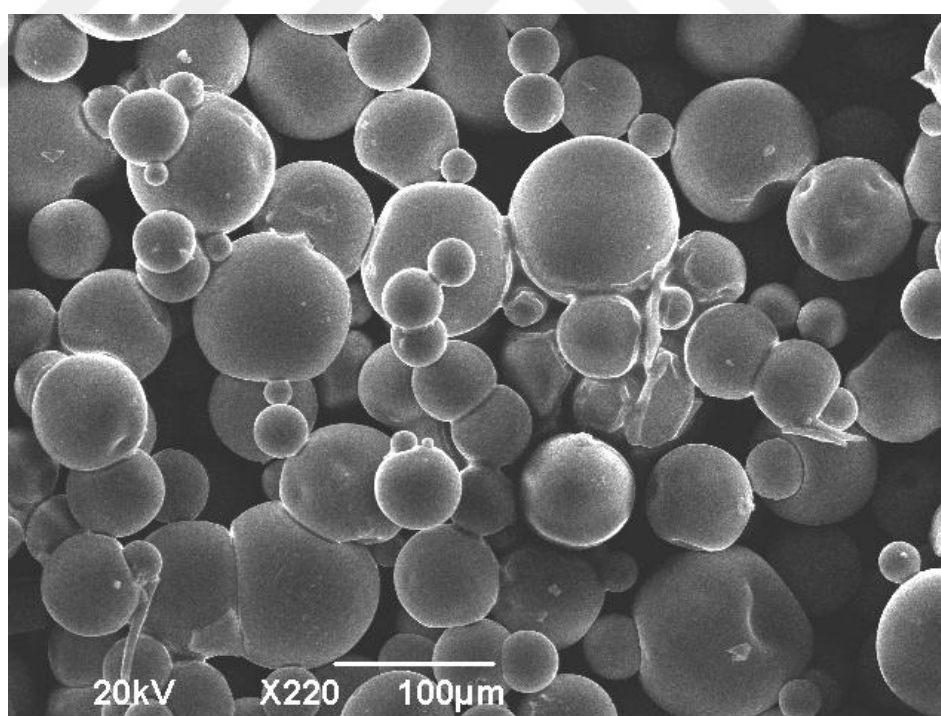


**Figure 6.75.** The clear SEM image of the crosslinked poly(ABCF13) microspheres after optimization.

113
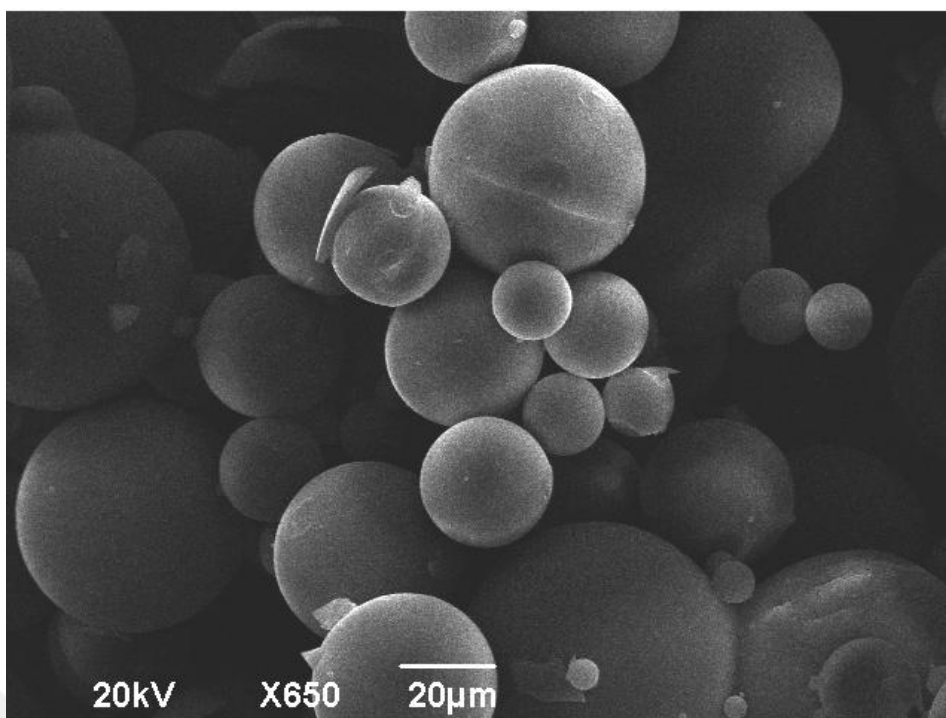
**Figure 6.76.** The clear SEM image of the crosslinked poly(ABCF13) microspheres after optimization.
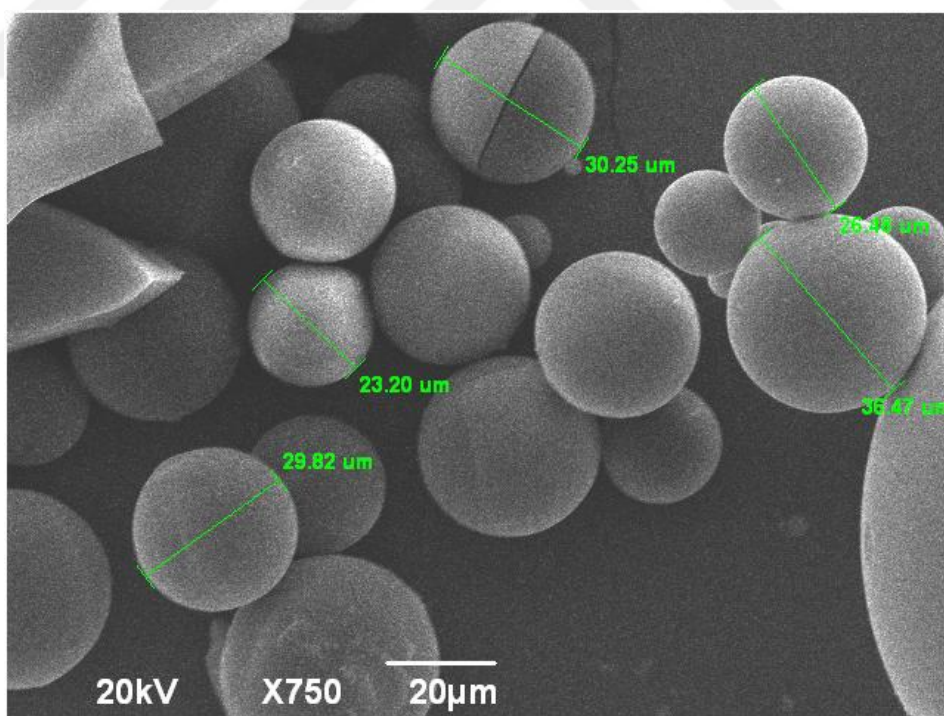


**Figure 6.77.** The clear SEM images of the crosslinked poly(ABCF13) microspheres after optimization.

114

## 6.8    HDPE/Croslinked poly(ABCF13) Microsphere Blends

In order to find out the effect of crosslinked poly(ABCF13) microspheres on the thermal, mechanical, microstructural and morphological properties of HDPE, the blends of HDPE with the microspheres at varying percentages (1, 3, 5, 7 and 10% of the mixture) were prepared by direct mixing of the components. After processing with microinjection molding at 220°C, the blends were analyzed by XRD, DSC, SEM tensile and impact test.


### 6.8.1   XRD Analysis of the Blends

In this section of the thesis, the influence of the blending of HDPE with crosslinked poly(ABCF13) microspheres on the microstructural characteristics of HDPE matrix was investigated. The unit cell parameters and grain sizes in the crystalline domains of the blends were determined by the previously used method in section 6.3, by means of the least square method with Miller indices (*h k l;* 110, 200 and 211) and *d* values. The X-ray diffraction patterns of HDPE and the products, ranging from 10° to 60°, were presented in Figure 6.78. The patterns displayed only the reflections from crystalline domains of HDPE matrix since the crosslinked poly(ABCF13) microspheres were in amorphous character. The patterns also revealed that the orthorhombic arrangement has been maintained in the crystalline domains. On the other hand, the orthorhombic unit cell parameters of the crystals, that is, the unit cell dimensions, were found to be markedly influenced by the increasing microsphere content in the matrix. This was also evidently supported by the shifts of the reflections to the right and left in the patterns besides the broadenings and sharpenings. Because a shift in the pattern is directly related to changing of the distances of crystallographic lattice planes. The changes in the unit cell dimensions thus the shifts in the reflections were attributed to the formation of lattice distortions, generation of microstructural disorders and the defects in the crystal structures of the crystalline domains of HDPE matrix due to the processing with the microspheres. Moly, in the studies of LLDPE/EVA blends, announced the shifts of the diffraction peaks towards a lower angle to be caused from the increasing in the crystallographic unit cells (Moly et al., 2005). Similarly, the diffraction peak of

115

the sample containing 5% poly(ABCF13) microsphere shifted significantly to lower angle in the pattern, comparing to unprocessed HDPE. Accordingly, the findings obtained fron XRD calculations showed that the maximum crystal unit cell dimensions were recorded in this product.
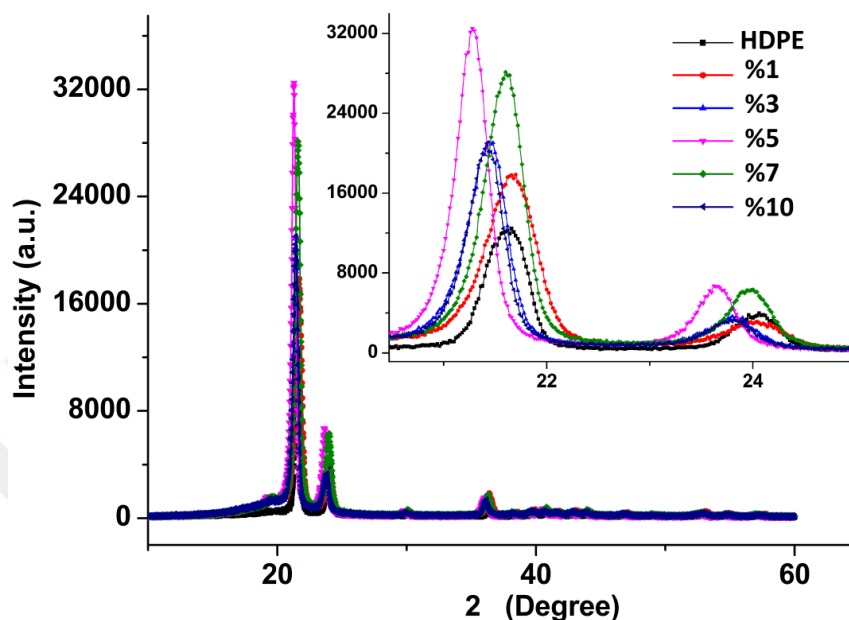


**Figure 6.78.** The XRD patterns of HDPE and the blends containing crosslinked poly(ABCF13) microspheres at varying content.

The effect of the poly(ABCF13) microsphere content in the blends on the orthorhombic unit cell dimensions (*a,b,c*) and unit cell basal areas (*ab*) were investigated via the calculations made by using X-ray diffraction patterns (by using the reflections 110, 200 and 211). The findings were tabulated in Table 6.7 and the dependence of cell parameters (*a,b,c*) and unit cell basal area (*ab)* on the percentage of the microsphere was drawn in Figure 6.79. The results revealed that the unit cell dimensions of the orthorhombic system were highly dependent on the microsphere content in the blends. The lateral dimensions, the *a* and *b* parameters of the unit cells of HDPE crystals (7.391 Å and 4.927 Å, respectively, in unprocessed HDPE) increased initially with the same trend and reached to maximum values (7.514 Å and 5,016 Å, respectively) with the sample including 5% microsphere, Figure 6.79.a and b. These expansions (1.66% in the parameter a and 1.82% in b) could be attributed to free volume increase due to the presence of the microspheres in the matrix. The initial additions of poly(ABCF13) microparticles to the HDPE matrix probably led to

the increases in the free volumes in the matrix, and this presumably brought about the increase in the mobility and conformational freedom of the chains, which were potentially accompanied with the lateral expansions in the unit cells. Moreover, the miniature ball bearing behaviour of the crosslinked poly(ABCF13) microspheres in matrix presumably affected the organization of HDPE crystals. That is, due to the difference in chemical nature between the poly(ABCF13) particles with relatively polar character and HDPE with nonpolar nature, the poly(ABCF13) microspheres might have compelled the neighbouring folded HDPE chains in crystalline regions, which resulted in the expanded unit cells, Figure 6.79.d and the formation of larger lamellar stacks in HDPE spherulites. After the maxima, both cell parameters, (*a* and *b*) illustrated decrease trend with increasing microsphere content and almost reduced to the values comparable with those of HDPE, Figure 6.79.a and b. Thus, while the initial additions of the microspheres resulted in the lateral enlargements due to the probable increases in the free volume, the latter additions gave rise to contractions in the dimensions to almost original parameters of HDPE, presumably due to the losses of the initial effects. That is, at the concentrations of the microspheres higher than 5% the increased mobility and conformational freedom were probably lost which resulted in the decreases of the parameters. On the other hand, there existed no considerable effect of the poly(ABCF13) microsphere content on c unit cell parameter. It remained relatively unchanged at all contents. That is, the unit cell dimension parallel with HDPE chain axis (Peacock, 2000) was not affected appreciably by the presence of the microspheres and the variation in the concentration.

**Table 6.7.** The effect of crosslinked poly(ABCF13) microshere content in the blends on the unit cell parameters (*a,b* and *c)* and crystal sizes.

| % poly(ABCF13) microsphere | *a* (Å) | *b* (Å) | *c* (Å) | Crystal size (nm) |
|---|---|---|---|---|
| 0 | 7.391±0.010 | 4,927±0.008 | 2,5387±0.0008 | 16.42±0.21 |
| 1 | 7.410±0.011 | 4,931±0.005 | 2,5379±0.0005 | 17.67±0.48 |
| 3 | 7.458±0,008 | 4,979±0.004 | 2,5317±0.0004 | 19.90±0.88 |
| 5 | 7.514±0.009 | 5,016±0.009 | 2,5347±0.0009 | 24.42±0.59 |
| 7 | 7.416±0.012 | 4,932±0.009 | 2,5408±0.0009 | 22.26±0.67 |
| 10 | 7.398±0.013 | 4,931±0.009 | 2,5386±0.0009 | 20.40±0,75 |
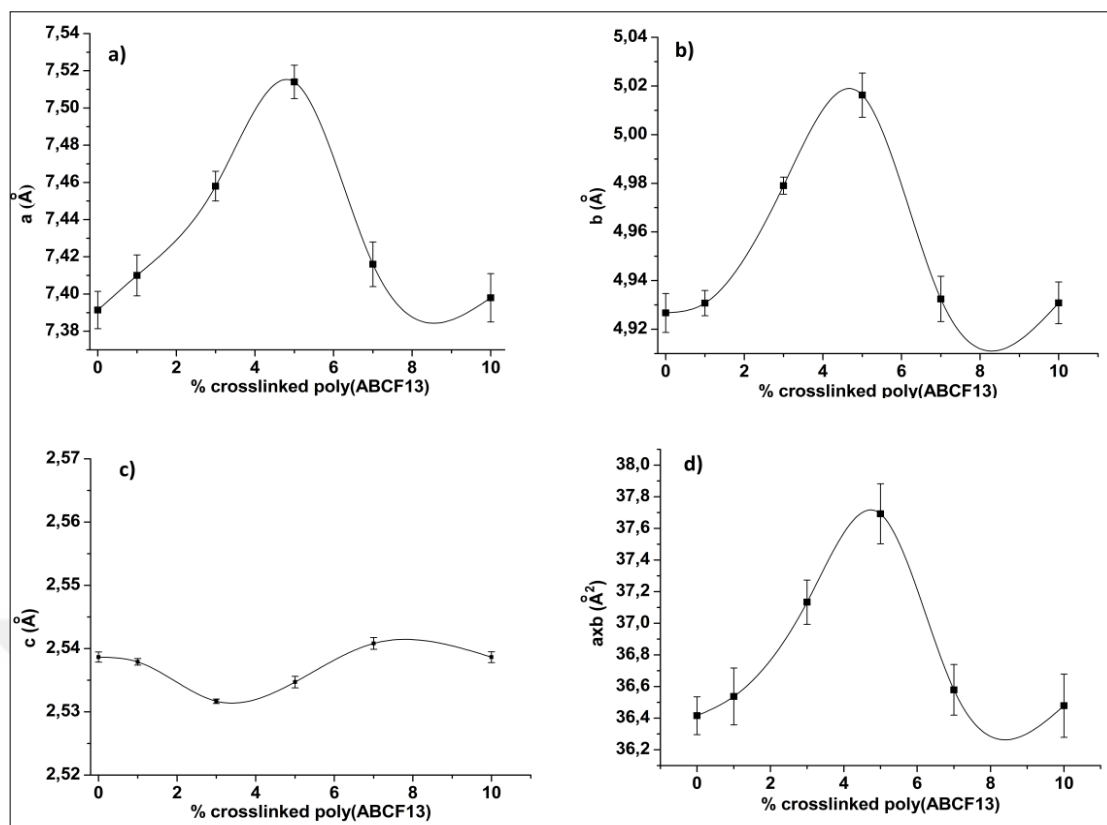
**Figure 6.79.** The dependence of orthorhombic unit cell parameters a) *a*, b) *b*, c) *c* and d) unit cell basal area on poly(ABCF13) microsphere content in the blends.

Based on the XRD findings, the relationship between crystal size in the HDPE crystalline domains and the poly(ABCF13) microsphere content was also investigated. A similar behaviour as recorded in the unit cell dimensions *a* and *b* was observed in crystal size (grain size), Figure 6.80. Namely, the grain size in the HDPE crystalline domains increased initially with the addition of the microsphere, and after reaching maximum at 5% microsphere, decreased significantly with further additions. On the other hand, the crystal size (grain size) in all prepared blends was larger than that of unprocessed HDPE. The maximum and notable increment, from 16.42 to 24.42 nm (48.72% increase) was recorded with the blend containing 5% microsphere. It seems that the variation in the crystal size was largely affected by the unit cell basal area, which was evidently supported by the similar trends in them. That is, larger crystals formed when they grew on the unit cells with larger basal area. Moreover, the presence of the crosslinked poly(ABCF13) microspheres causing the free volume increase in the matrix might impart the optimum conformational freedom to HDPE chains, which led to growth of the HDPE crystals.
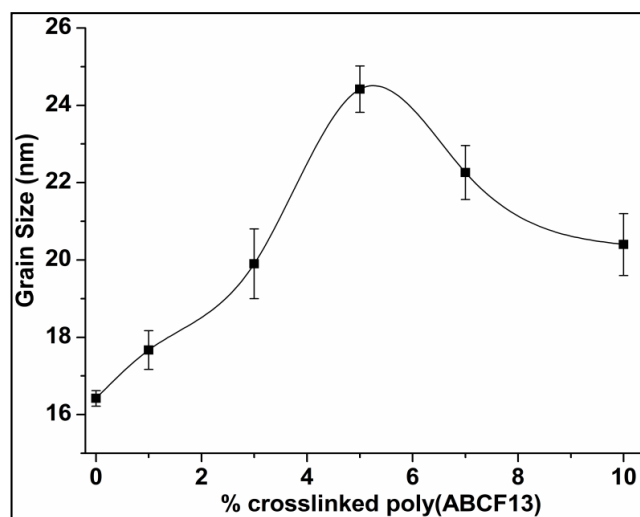
**Figure 6.80.** The variation of the crystal size (grain size) with the poly(ABCF13) microsphere content.

### 6.8.2 Thermal Analysis of the Blends

The effect of the crosslinked poly(ABCF13) microspheres existing in HDPE matrix on the melting temperature of the material was studied in the temperature range of 25-400°C by the means of DSC analyses. The thermograms of the blends processed with microinjection molding at 220°C were presented in Figure 6.81. The dependence of melting temperature of HDPE crystalline domains on the content of microsphere was tabulated in Table 6.8 and graphically displayed in Figure 6.82. The melting temperature gradually decreased (from 130.8°C, the melting point of powdered HDPE) in consistence with the increase of the microsphere content, and reduced to 129.0°C at 10% microsphere, Figure 6.82. Although the falls can be regarded as not so great, the maximum decrease, about 1°C, was achieved with the first addition of microsphere, 1%. The decrease then slowed down with further additions of the microsphere. The melting point then might be stated to stay at a plateau value of about 129°C, without a significant change, Figure 6.82. It seems that the processing with the crosslinked poly(ABCF13) microspheres influenced the nucleation of the crystals during the formation of HDPE crystalline domains in the matrix. The decreases in the crystallinity, determined by the DSC analyses, Figure 6.82, and the changes in the orthorhombic unit cell dimensions, determined by XRD studies (Section 6.8.1), evidently support the effect of the processing on the crystallization behaviour of HDPE. The decreases in the melting temperature thus

119

might be attributed to the formation of lattice distortions, generation of microstructural disorders and the defects in the crystal structures of the crystalline domains of HDPE matrix due to the processing with the microspheres.

The crystallinities in the HDPE matrices of the blends were determined by using the thermograms and the Equation 6.3 previously used. It was seen that the crystallinity was highly dependent on the microsphere content in the matrix. It increased initially with the increase of the content and reached the maximum value, 60.13% (50.3% larger than that of powdered HDPE) with the product containing 5% microsphere, Figure 6.82.b. The presence of fillers in polymer matrix could markedly influence the crystallization behaviour of HDPE with the formation of a new fraction of crystallites (Bartczak et al., 1999; Wunderlich, 2005). It was hypothesized that the initial additions of the microsphere probably gave rise to enlargements in the free volumes. Thus, the increased conformational freedom and chain mobility accompanying the enlargements in the free volumes presumably led to the increases in the crystallinities. Because the HDPE chains with greater conformational freedom and mobility could be expected to have a greater potential to take place and organize in the crystalline arrangements. On the other hands, after the maximum, the further addition of the microspheres to the blends resulted in the worse crystallinity in the HDPE matrix, and caused amorphous character to increase. At 10% content, the crystallinity reduced to the minimum value, 30.57% which was 23.1% lower than that of pure HDPE. It was reported that the excessive number of particles dispersed in polymer could limit or hinder growth and progression of polymer crystals (Tjong, 2006; Piorkowska and Rutledge, 2013). Also, the crystallization of polymers is negatively affected from the restrictions in the mobility of polymer chain segments and heterogeneous nucleation (Akhtar et al., 2008). Accordingly, the presence of the microspheres at high concentrations have negatively affected the crystallization in HDPE matrix. This was probably arisen from the decreases in the conformational freedom and chain mobility due to the excessive amount of the microspheres.
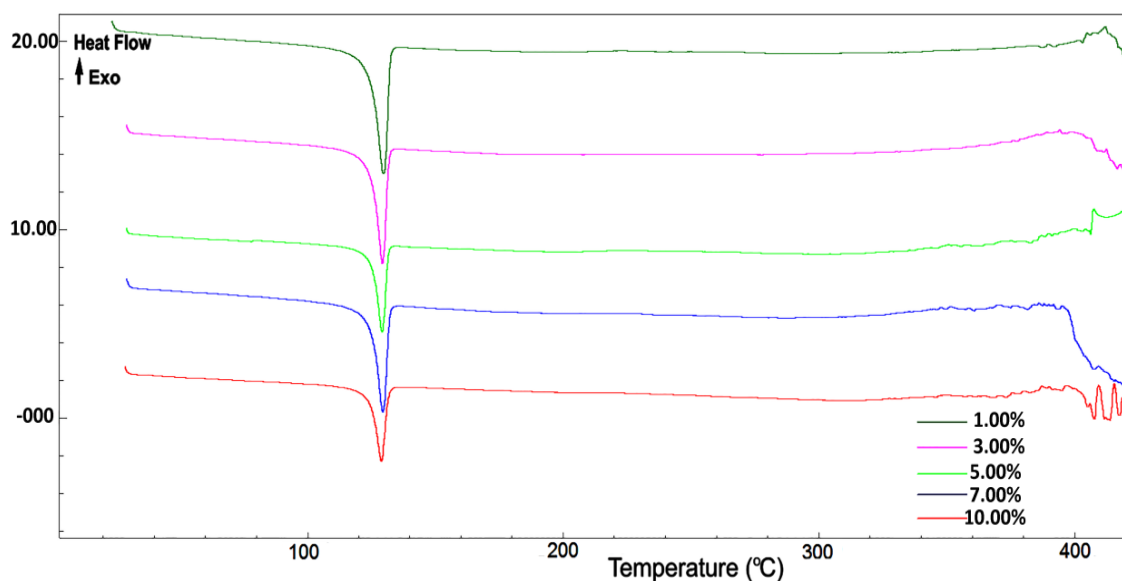
**Figure 6.81.** DSC thermograms of HDPE blends formed with different crosslinked poly(ABCF13) contents.

**Table 6.8.** The variation of the melting point (Tm), enthalpy of fusion (ΔHm) and percent crystallinity ($X_c$, %) of the products with percentage of poly(ABCF13) microsphere.

| Sample | $T_m$ (°C) | $\Delta H_m$ (J/g) | $X_c$ (%) |
|---|---|---|---|
| Pure HDPE | 130.80 | 118.48 | 40.86 |
| 1% microsphere | 129.84 | 156.95 | 54.12 |
| 3% microsphere | 129.43 | 179.77 | 61.99 |
| 5% microsphere | 129.29 | 156.58 | 53.99 |
| 7% microsphere | 129.11 | 150.98 | 52.06 |
| 10% microsphere | 129.03 | 98.51 | 33.97 |
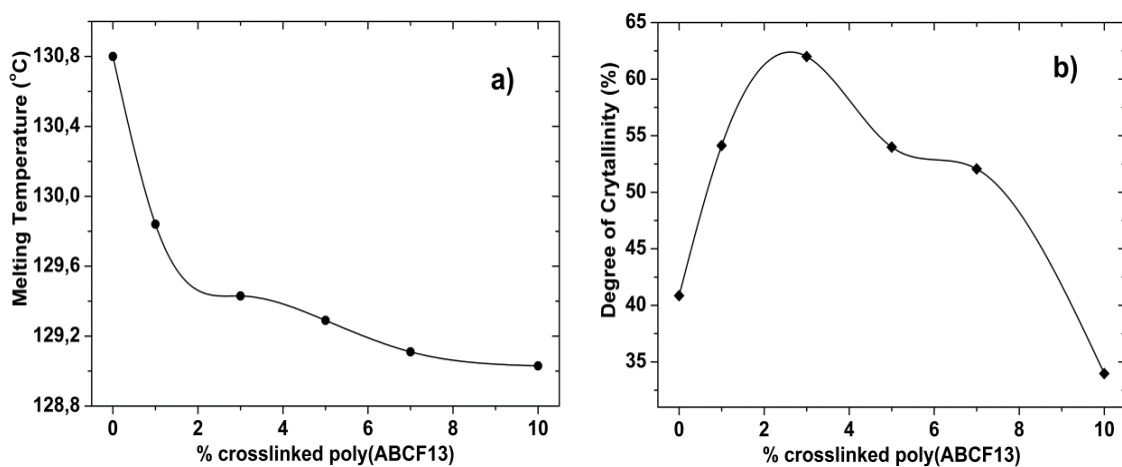


**Figure 6.82.** Variation of the melting point (a) and degree of crystallinity (b) with content of the poly(ABCF13) microsphere in the blend.

121

### 6.8.3   Mechanical Properties of Blends

The mechanical properties of the blends were studied so as to figure out the effect of the poly(ABCF13) microspheres on the mechanical characteristics of HDPE. For the tensile and impact tests, the samples in dogbone shape were prepared at 220°C by using micro injection moulding machine with 8 bar injecting pressure. Although the molding temperature 220°C was considerably higher than the melting point HDPE, 131°C, it was highly compelling to process the blends at that temperature because of the difficulties in the flow of the melts at lower temperatures. The difficulties encountered during molding at lower temperatures probably caused from the limitations and restrictions in the slip and flow of HDPE chains over each other due to crosslinked poly(ABCF13) microspheres that have stiff and rigid natures. On the other hand, the significant improvements in ultimate tensile strength, Young's Modulus and impact strength were recorded with the initial addition of the microspheres into the blends. Almost all the samples exhibited ductile behaviour. Gradual loss in percent elongation and fractures at neck formation were observed, however, with the increase of the content. At higher percentages of the microsphere studied, the brittle nature started to be seen in the behaviour.

The tensile tests of all the specimens were carried out at room temperature with 5 kN cell load and 5 cm/min deformation speed. The nominal stress-strain curves of the blends with varying percentage of the poly(ABCF13) microspheres were depicted in Figure 6.83. While great extension of cold drawing was observed in the pure HDPE, the failures were recorded at strain softening region almost in all the products. The elongations during the strain softenings were highly dependent on the microsphere content, and gradually decreased with the percentage. The maximum and minimum elongations, 60% and 18%, were achieved with the samples involving 1% and 10% microsphere, respectively. These results revealed that the products gradually gained brittle nature with the content in the matrix. This may be attributed to that the rigid and stiff character of the poly(ABCF13) microspheres dispersed in the matrix probably restrict the mobility of HDPE chains and hinder the chains from slipping over each other, which resulted in reduction in the percent elongations of the products. Furthermore, partial interfacial adhesion between the microspheres and HDPE, resulting in the increase of molecular level frictions, might prevent the easy

sliding of the HDPE chains, and thus led to the shorter elongations. Accordingly, the products with 7 and 10% microsphere failed at about the yield point without showing extensive elongation. On the other hand, the increases of the microsphere content in the matrix brought about the significant improvements in the yield stress of the products.
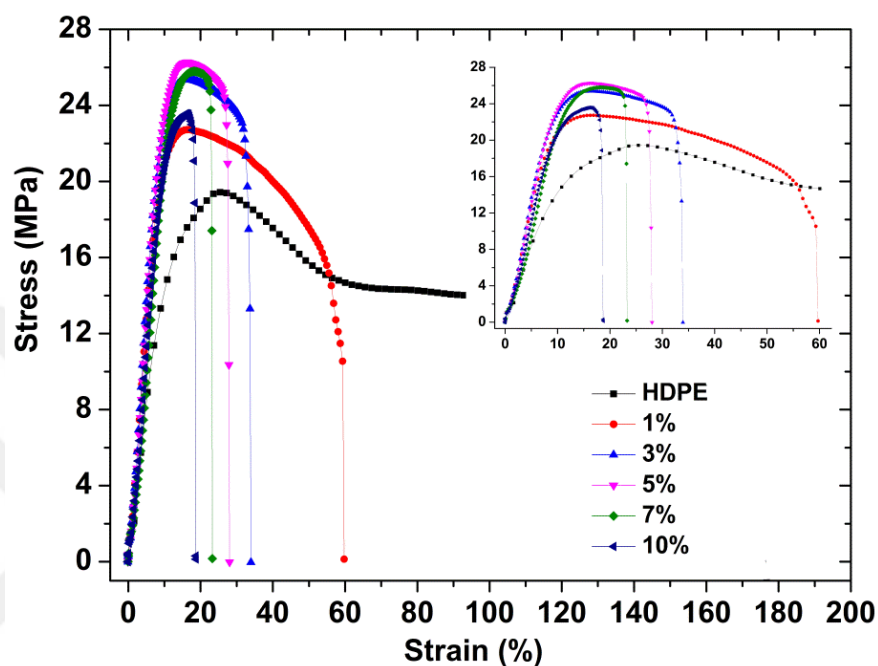


**Figure 6.83.** Stress-strain curves of pure HDPE and blends including 1, 3, 5, 7 and 10% poly(ABCF13) microspheres.

The findings obtained from mechanical measurements of the products and pure HDPE were presented in the Table 6.9, and the variations of the tensile and impact properties with microsphere content were drawn in the Figure 6.84. The results showed that mechanical characteristics of the products were significantly affected by fraction of the microsphere in the matrix. Both the ultimate tensile strength and elastic modulus of the products increased initially with the increase of the concentration of the microsphere, and reached the maxima, 25.66 MPa and 499.30 MPa at 5% content (29.3% and 42% improvement, respectively, with respect to virgin HDPE). The blends then had a decrease trend in the properties as the percentage of the microsphere was increased further. Murphy announced that the microspheres by acting as miniature balls imparted remarkable dimensional stability into the matrix by improving flatness and stress distribution (Murphy, 2001).

Accordingly, the initial improvements were attributed to that the crosslinked microspheres presumably led to the dimensional orientations and alignments of the HDPE chains by acting as ball bearing during the processing. The orientations and alignments thus probably resulted in the greater load capacity, that is, in the greater tensile strength. In addition, the same developments probably also gave rise to resistance of the HDPE chains to flow in the draw direction thus resulted in the initial advances in the modulus. Moreover, the crystals with larger sizes might have additionally contributed to the advances in the tensile properties by behaving as cross-link centers between the chains in the amorphous domains. The similarity between the variation of crystal size and the tensile properties with the content evidently support this function of the crystals. After the maxima, the gradual decreases in both tensile properties could be explained by negative affects arisen from the restrictions in the mobility of HDPE chains and thus decreases in conformational freedom due to the increase of microsphere content. The losses in elongations with the increase of the content evidently support this effect. But it is noteworthy that all the tensile values of the products were still higher than that of pure HDPE, in spite of the decreases, Figure 6.84.a and b. The minimum values of tensile strength and Young's modulus were recorded as 22.58 MPa and 391.0 MPa, respectively (12.1% and 11.4% larger compared to pure HDPE) at the product containing 10% microsphere among the products.

In order to unfold the dependence of the impact strength of the blends on the microsphere content, Izod impact tests were carried out at room temperature. The findings in the tests were tabulated in Table 6.9, the variation with the percentage was drawn in the Figure 6.84.c. As all the samples exhibited the ductile behaviour in the tensile tests, breaking of any sample was not observed in the course of the impact tests. Thus the results were recorded as the absorbed energy by the products during the tests. The absorbed energy increased initially with the content and after reaching the maximum value, 26.84 MPa (41% advance with respect to pure HDPE) at 5% microsphere, exhibited a decreasing trend. The initial advances in the absorbed energy were attributed to increase of the conformational freedom and chain mobility arising from the probable enlargements in the free volumes. That is, the initial additions of the microsphere probably gave rise to enlargements in the free volumes. Thus, the increased conformational freedom and chain mobility resulted in the

increases in the absorbed energies loaded during the tests. After the maximum, the decreasing trend was explained by the losses in the conformational freedom and chain mobility due to probable contractions in the free volumes. The higher contents of the microsphere than 5% probably led to the reductions in the free hole size or in its fraction thus in the restrictions in chain mobility, which resulted in the decrease in the absorbed energy. The minimum value was recorded as 9.97 kJ/m$^2$ (48% smaller than that virgin HDPE had) with the product including 10% microsphere. Moreover, due to partial interface adhesions between the components, the crosslinked poly(ABCF13) microspheres may act as a blocking or pinning centres in the matrix at high contents. Thus, the mobility of HDPE chains was probably restricted and therefore the amount of energy absorbed by the products decreased. In other words, the products absorbed relatively lower energy since the energy loaded in a small time scale in the test was not effectively delocalized in the matrix.

**Table 6.9.** Ultimate tensile strength, Young's modulus and impact strenght of the pure HDPE and the blends at different poly(ABCF13) microsphere contents.

| Specimen | Ultimate Strenght(MPa) | Young's Modulus(MPa) | Impact Strenght (kj/m$^2$) |
|---|---|---|---|
| Pure HDPE | 19.85±0.99 | 350.95±6.18 | 19.01±1.65 (**NB**) |
| 1% microsphere poly(ABCF13) | 23.90±0.52 | 449.59±3.61 | 21.35±0.72 (**NB**) |
| 3% microsphere poly(ABCF13) | 25.30±0.16 | 464.77±5.47 | 23.56±1.39 (**NB**) |
| 5% microsphere poly(ABCF13) | 25.66±0.68 | 499.30±10.48 | 26.84±1.75 (**NB**) |
| 7% microsphere poly(ABCF13) | 23.03±0.32 | 414.46±6.14 | 15.71±1.67 (**NB**) |
| 10% microsphere poly(ABCF13) | 22.58±0.53 | 391.05±4.52 | 9.97±1.23 (**NB**) |

**NB**: Not Broken
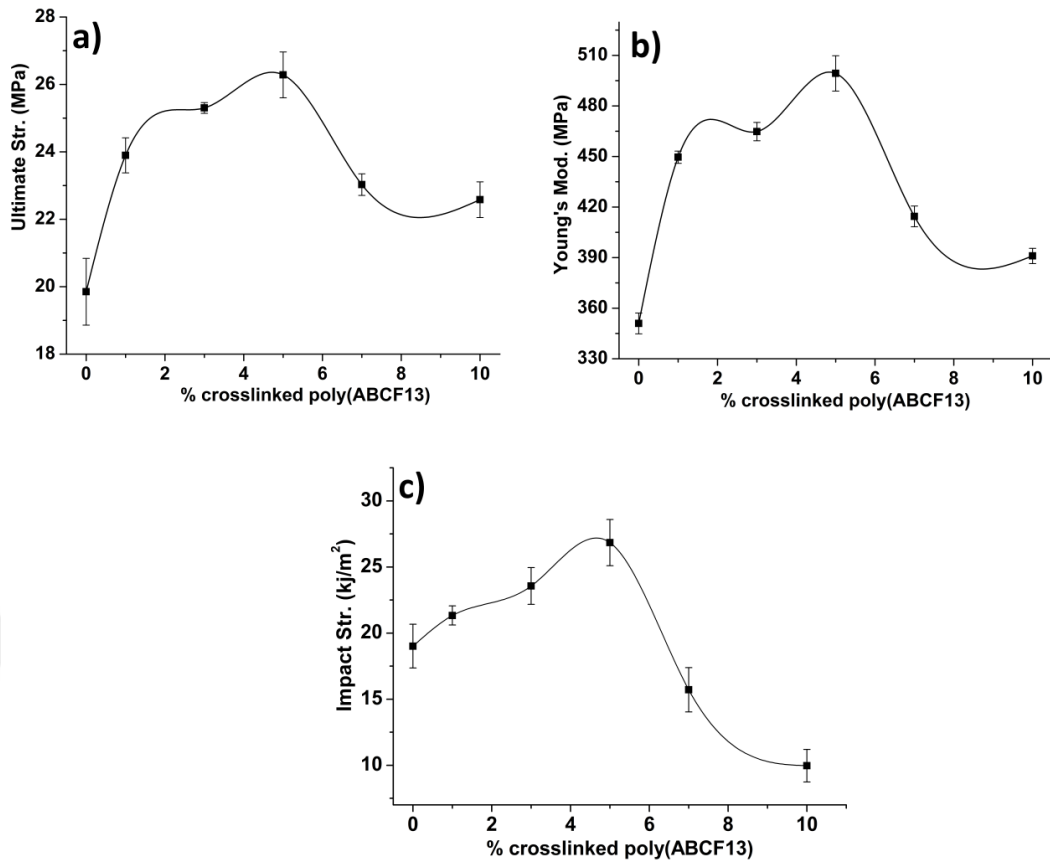
**Figure 6.84.** The variation of a) ultimate tensile strength, b) Young's modulus and c) absorbed energy in the impact test with poly(ABCF13) microsphere content in the blends.

### 6.8.4 Morphological Properties of Blends

In order to find out the effect of blending HDPE with the poly(ABCF13) microspheres on the morphological characteristics of the material, the fractured surfaces of the samples obtained from the tensile tests were investigated meticulously by SEM. Since there is not any impact fractured sample, (the samples were not broken during the impact tests), merely the tensile fractured samples were analyzed. In all the blends the microspheres were perceived as a separate phase, more distinguishably at high contents. The poly(ABCF13) microspheres have a chemically different nature with polar groups from HDPE, leading to the phase separation, Figure 6.85-92. On the other hand, fibrillar extensions broken in ductile were observed almost at all contents in the blends, but the extension shortened as the content of the microsphere increased in the matrix. The extensions were long and

bulky at relatively lower contents as shown in Figure 6.86-90. Shorter and thinner fibrillar structures denoting the decrease in ductile property were detected at relatively higher contents, Figure 6.91 and 92. This behaviour probably was caused from the decreases in the orientations and alignments of HDPE chains in the matrix presumably due to the restrictions and limitations in the mobility and conformational freedom of the chains. Furthermore, at higher percentages of the microspheres, the brittle nature started to appear in the products and, as depending on that, the holes, openings, cracks and cavities in the matrix were observed in the tensile fractographs, Figure 6.91 and 92. These changes in the morphology were found as visible evidences for why the energy absorbed in the impact tests and the tensile strengths have a decreasing trend after the maxima, and the minima were observed with the blend 10% microsphere.
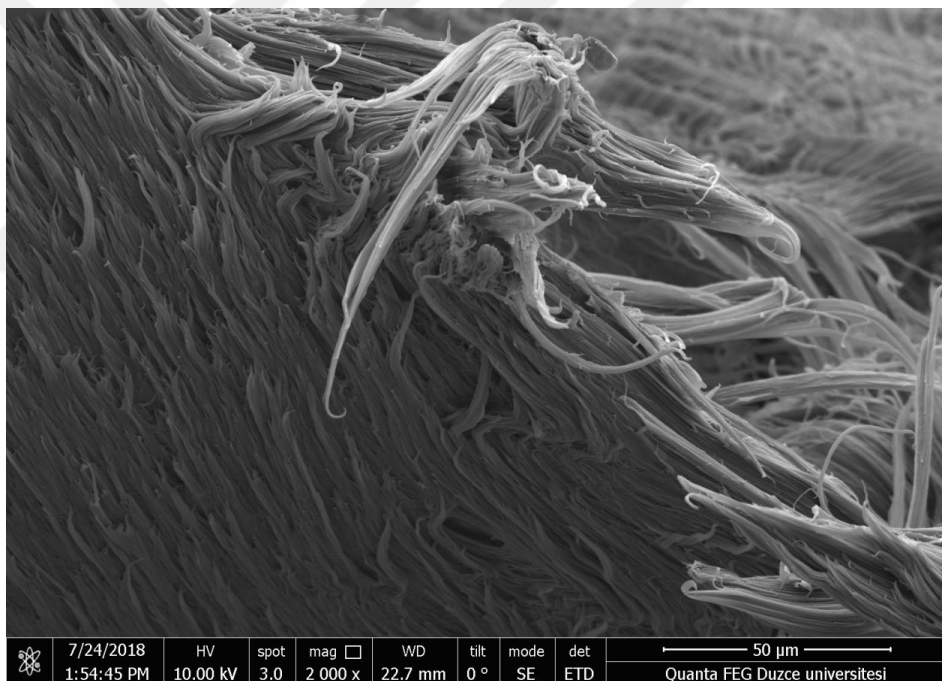


**Figure 6.85.** SEM micrograph of the fractured surface of pure HDPE, Tensile Test.
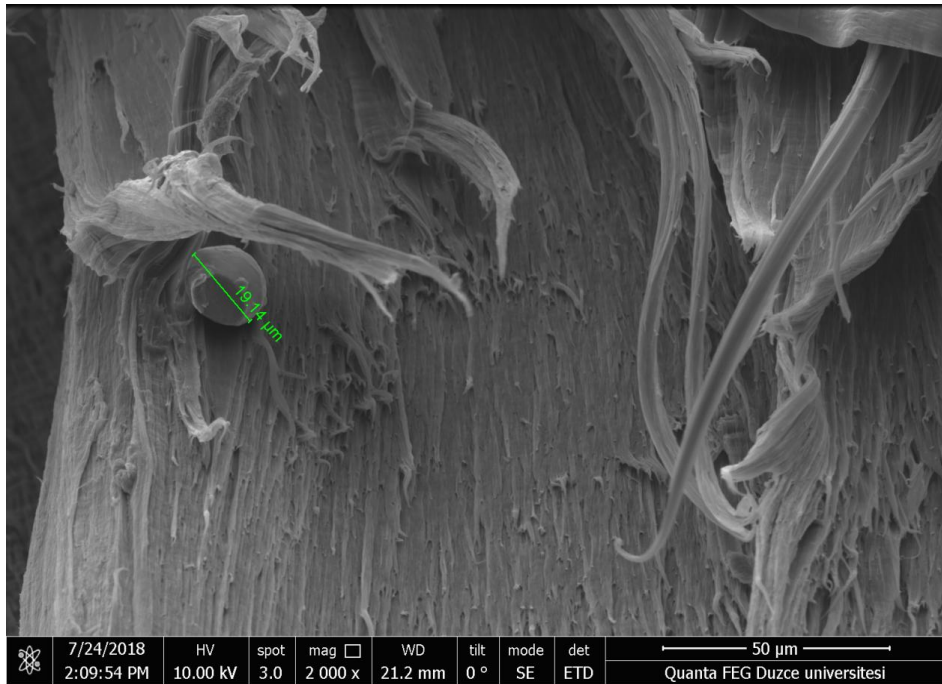
**Figure 6.86.** SEM micrograph of the blend containing 1% crosslinked poly(ABCF13) microsphere, Tensile Test.
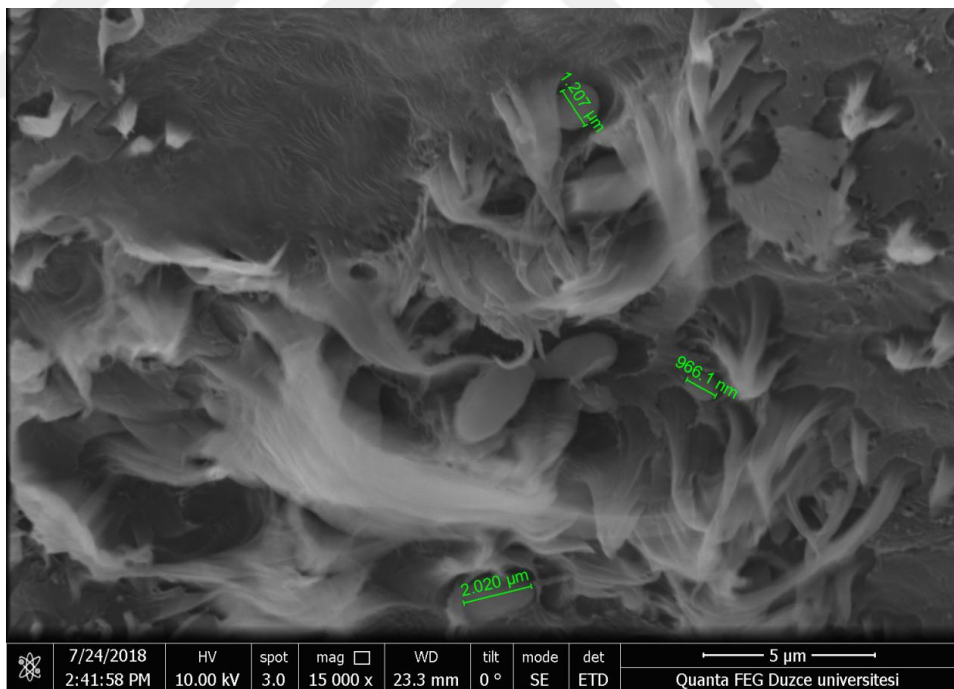


**Figure 6.87.** SEM micrograph of the blend containing 3% crosslinked poly(ABCF13) microsphere, Tensile Test.
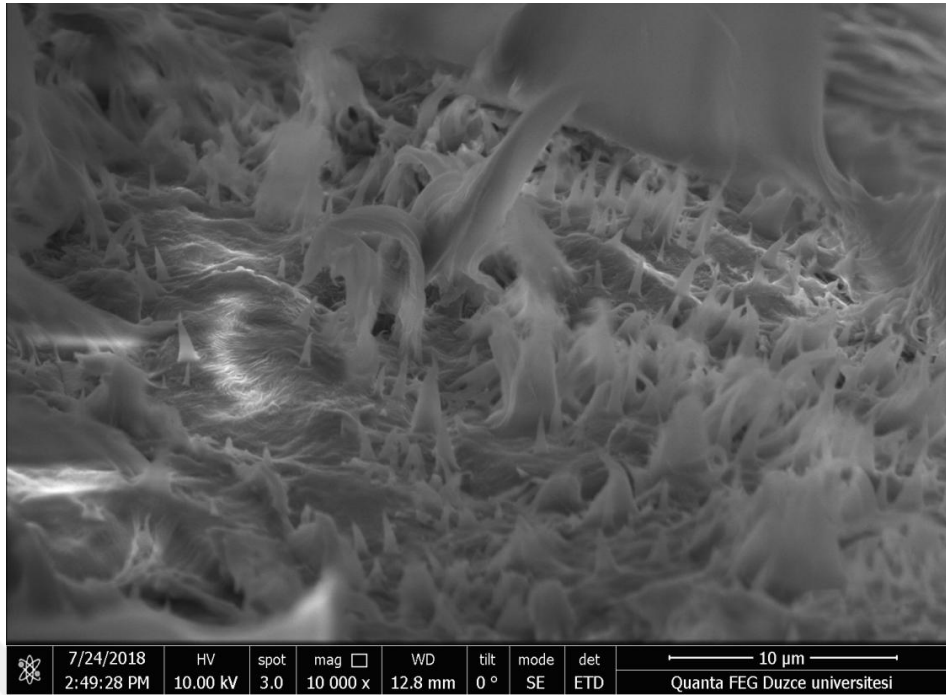
**Figure 6.88.** SEM micrograph of the blend containing 3% crosslinked poly(ABCF13) microsphere, Tensile Test.
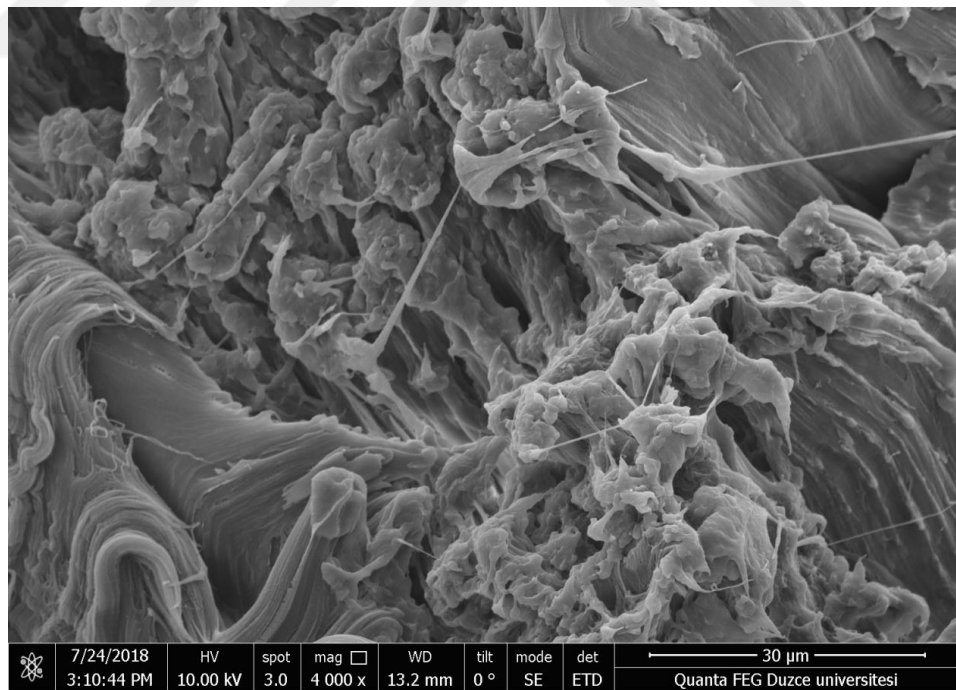


**Figure 6.89.** SEM micrograph of the blend containing 5% crosslinked poly(ABCF13) microsphere, Tensile Test.
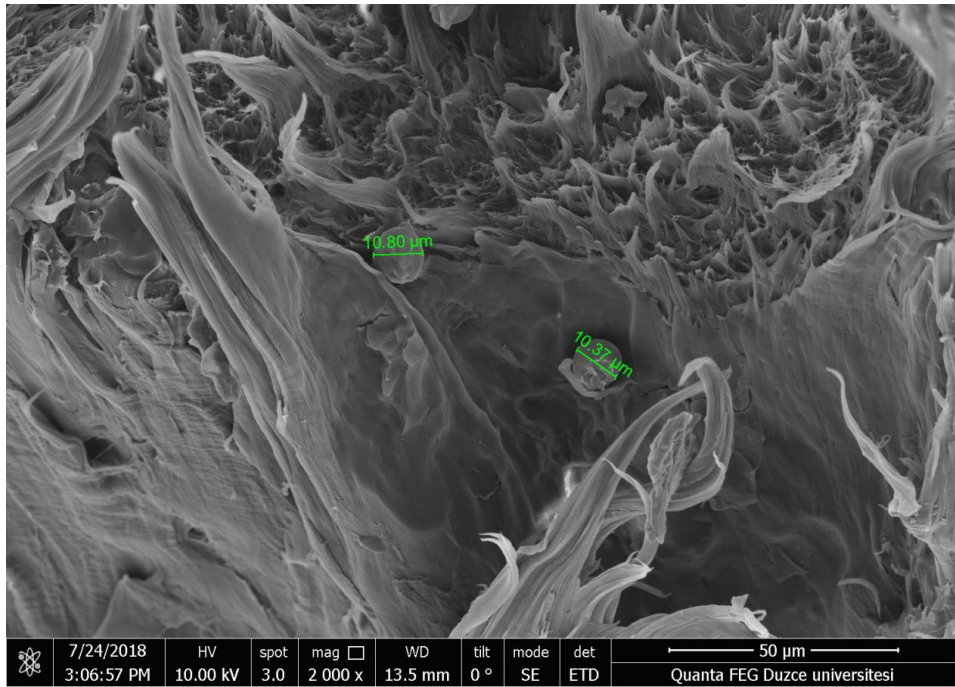
**Figure 6.90.** SEM micrograph of the blend containing 5% crosslinked poly(ABCF13) microsphere, Tensile Test.
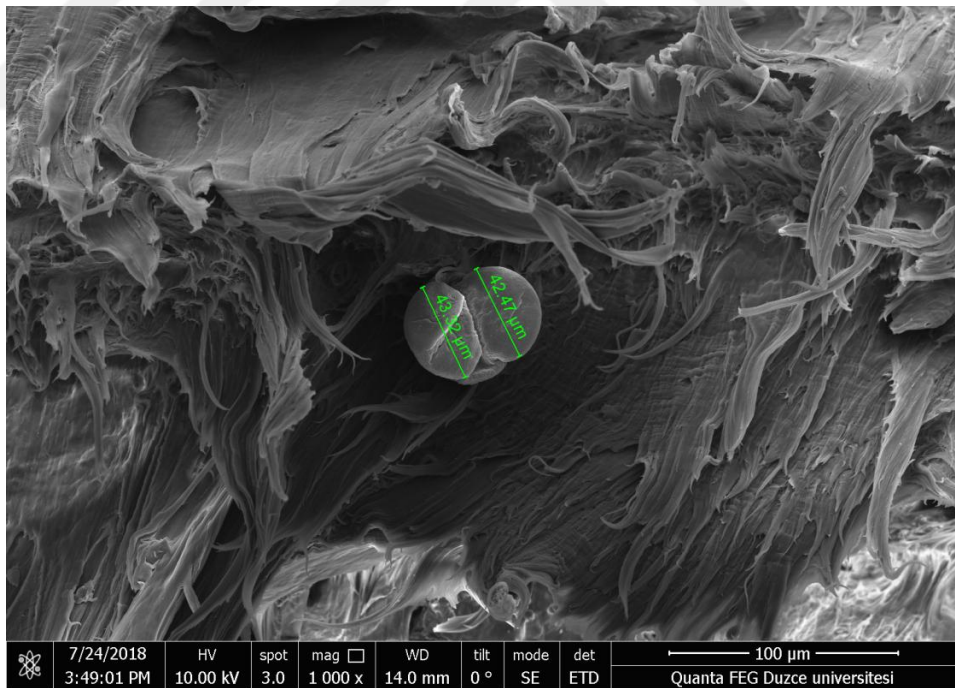


**Figure 6.91.** SEM micrograph of the blend containing 7% crosslinked poly(ABCF13) microsphere, Tensile Test.
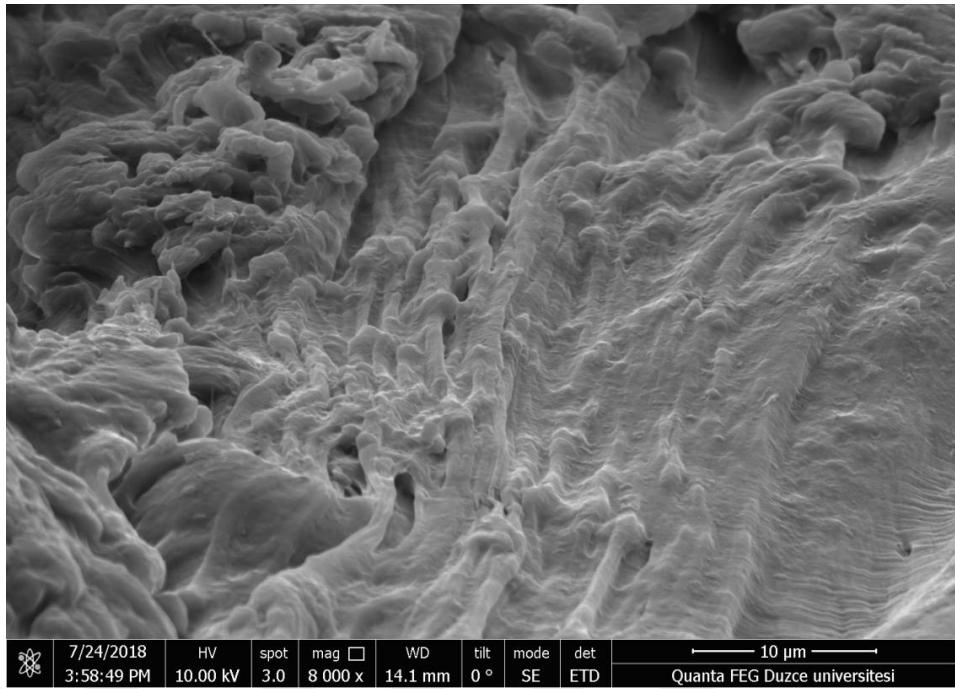
**Figure 6.92**. SEM micrograph of the blend containing 7% crosslinked poly(ABCF13) microsphere, Tensile Test.
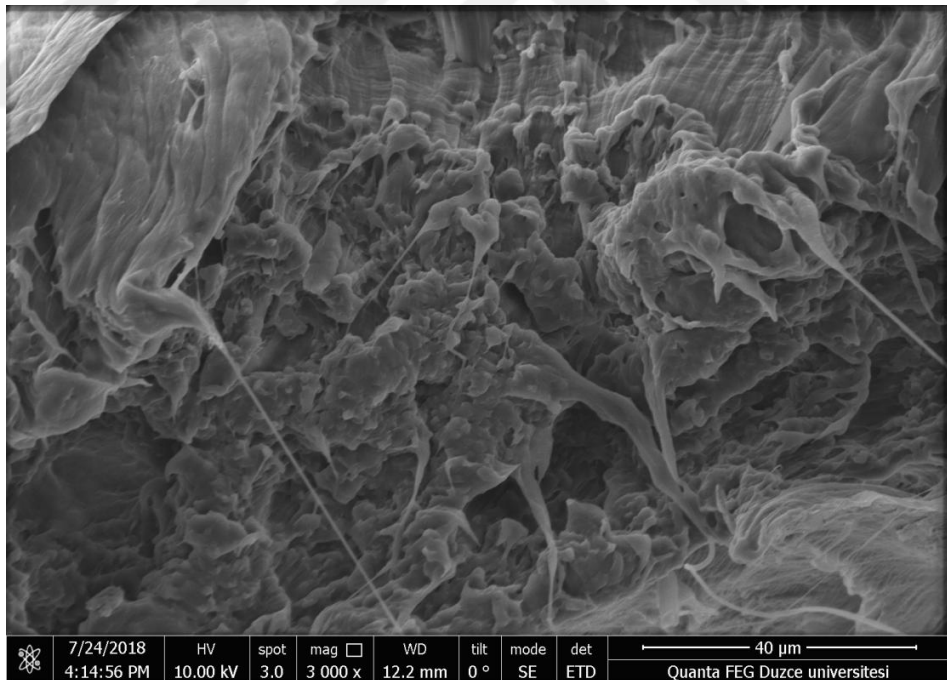


**Figure 6.93.** SEM micrograph of the blend containing 10% crosslinked poly(ABCF13) microsphere, Tensile Test.
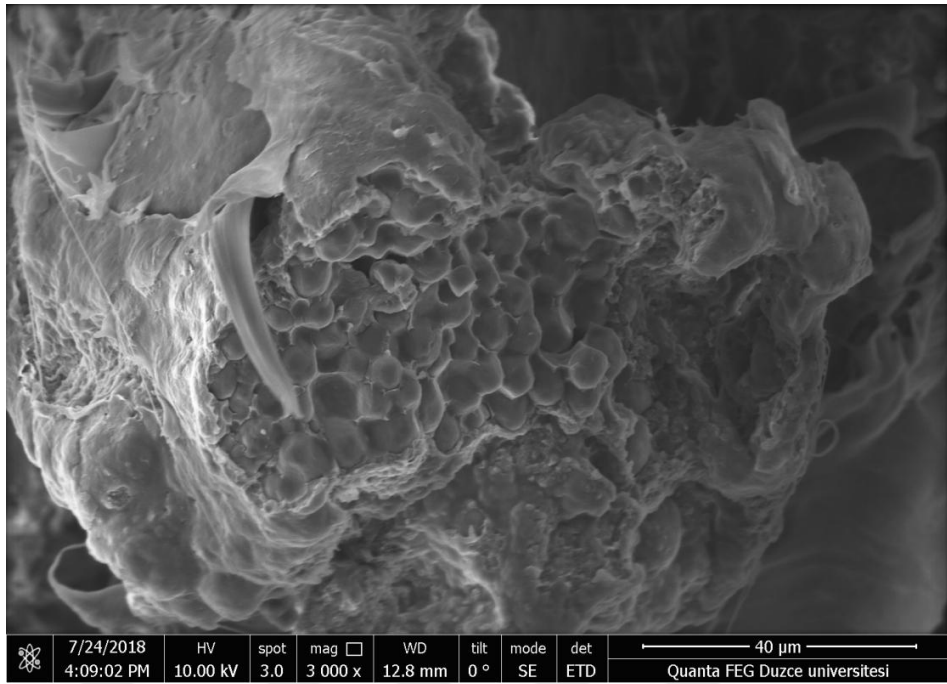
**Figure 6.94.** SEM micrograph of the blend containing 10% crosslinked poly(ABCF13) microsphere, Tensile Test.

# 7. CONCLUSIONS

✸ Homopolymerization of ABCF13 and thermally initiated graft copolymerization of ABCF13 onto HDPE were successfully conducted by bulk-melt polymerization method and using benzoyl peroxide initiator at constant temperature of 140°C in vacuum for an hour. The grafting was studied in detail with the reaction mixtures prepared at six different percentages of ABCF13 in the medium. The percent conversion of poly(ABCF13) depicted rising trend with the increase of ABCF13 concentration. This was probably due to the increase of initiator content with the raise of monomer percentage in the reaction mixture since the amount of initiator in the mixture was 2% of the weight of the monomer.

✸ The graft copolymerization brought about the significant increments in the melting temperature of HDPE crystalline domains. The initial increases were believed to arose from the improvements in the packing order of the chains due to the attractive interactions between the polar groups belonging to graft units. After maximum, the a sharp decreases in crystalline melting temperature of HDPE were observed in the products. The decrease following the maximum presumably resulted from that the assisting function of the graft units with polar groups in more ordered packing of HDPE chains might be lost with the increase of poly(ABCF13) percentage in the products

✸ The first weight loss of poly(ABCF13) was observed at about 226°C in both air and nitrogen atmosphere. The degradation primarily took place by decomposition of the side chains groups of the poly(ABCF13). These groups were mostly fluorinated, phenolic and vinylic parts and carbon dioxide. In the graft coproducts, the increasing of percentage of poly(ABCF13) in the matrix (meaning the decrease in HDPE percentage) led to the easier and earlier decomposition of the products in both air and nitrogen atmosphere. At further contents, it was observed that the retardation effect of HDPE weakened.

✸ Considerable lateral expansions were recorded in *a* and *b* unit cell parameters of the HDPE orthorhombic structure with the increasing of poly(ABCF13) content in the matrix. These increments in *a* and *b* unit cell parameters were probably caused

from that the grafted polar units probably forced the HDPE chains apart laterally to expanded lateral dimensions. After the maxima, the contraction trends in the dimensions were observed, which probably arose from the compressing effect of the graft units. The c parameter remained almost unchanged since the chain axis of HDPE molecular segments was parallel with the unit cell axis.

✻        The graft copolymerization brought about the increment in the crystal size of HDPE crystal domains in matrix with the increasing of the poly(ABCF13) content in matrix. The growth of HDPE grains presumably caused from not only the increment in the conformational freedom of HDPE chains arising from the increase in the free volume but also the enlargement in the basal area of the unit cells. Moreover, at high contents, the accumulation of the graft units with the presumable rigid, rod-like characteristics of the fluorinated segments affected negatively the crystals growing and also probably played the blocking role in the growth of the crystals to larger sizes.

✻        The grafting onto HDPE gave rise to linearly increasing of the free volumes in consistence with the percentage of poly(ABCF13). The poly(ABCF13) units with voluminous side groups bearing rigid, rod-like fluorinated segments presumably led to the formation of larger holes, cavities or openings in the materials. Furthermore, the ungrafted homopolymer molecules with glassy and amorphous properties with local kinks brought about the larger free volumes by playing a hindering role in compact packing of the polymer chains. In addition, The weak secondary molecular interactions between polar groups of poly(ABCF13) units and nonpolar HDPE chains might have additionally contributed to the reduction in close packing of the chains in the matrix, and thus to larger free volumes.

✻        The fluctuation in the free volume fraction values of the products was recorded with the increasing of poly(ABCF13) content in matrix. The reduction in the fraction probably due to the fact that the graft units occupied the free volume holes between the HDPE chains rather than creating new gaps and holes. The potential weak interactions between the polar groups of the graft units and the nonpolar HDPE chains may have played a role in filling these holes. On the other

hands, the voluminous side groups presumably preventing the close packing of the chains in the material might have played an efficient role in the increase of the fraction at that percentage.

✷    Extreme mechanical improvements were achieved in the especially tensile strength and Young's modulus of the graft coproducts. But, yield stress and percent elongation were lost with the increasing of poly(ABCF13) content in matrix and the products exhibited increasing brittleness in the characters. The mechanical characters of the products were largely governed by free volume. The enlargements in the free volume probably gave rise to increase in the conformational freedom of the chains in the material, conducing to a significant alignment and orientation of the chains in the draw direction. Moreover the formation of high level of extensive fibrillation probably led to the improvements of mechanical properties of the produts. On the other hand, as the poly(ABCF13) content increased, the loss of fibrillation in the products was accompanied with reduction in the tensile properties in spite of the increases in the free volume. The presence of poly(ABCF13) chains composed of voluminous side groups bearing rigid, rod-like fluorine segments might play a role in preventing the orientation and alignment of the chains in the draw direction. Additionally, the impact strengths (absorbed energies in the tests) of the products increased initially and then the energy exhibited a decrease trend as the content increased further. The initial increase might be caused from that the increased conformational freedom and mobility of the chains accompanied with the enlargements in the free volume probably resulted in the more absorbed energy because of more effective delocalization of the loaded energy on the material in the test.

✷    There existed no phase separation in all products, and the samples had completely homogeneous structure although HDPE with nonpolar structure has a different nature from poly(ABCF13) comprising polar groups. The findings depicted not only the formation of the chemical bonds between HDPE chains and poly(ABCF13) units but also the compatibilizing agent behaviour of poly(ABCF13)-g-PE units by providing good interfacial adhesion between ungrafted poly(ABCF13) and HDPE. At low contents, the products exhibited ductile behavior with the formation of large, thick and long fibrillar structures formed probably as a

consequence of the orientations and alignments of the chains of the matrix. But, as the content increased further, layered structures with holes, openings and microcracks began to appear and the microstructural defects with rarely seen small extensions were found to be high in the products.

✳     The synthesis conditions to prepare the crosslinked poly(ABCF13) microspheres were optimized by depending on crosslinking agent (EGDMA), the monomer (ABCF13), the initiator (KPS) concentrations and stirring rates. It was observed that all parameters had significant roles in the production of the microspheres. After optimization, the well-defined, desired and well-shaped microspheres with smooth surfaces and good roundness were obtained and the size of the fabricated microspheres ranged approximately from 10 to 100 μm. The optimum parameters in order to prepare well-defined crosslinked poly(ABCF13) microsphere were depicted as followings;

- ✓ 0.2 g of ABCF13 monomer as dispersed phase,
- ✓ 1% of crosslinking agent (EGDMA) with respect to weight monomer,
- ✓ 1.3% l of water soluble initiator (KPS) with respect to weight of monomer,
- ✓ 150 mL of pure water as the continuous phase,
- ✓ 70°C reaction temperature,
- ✓ 500 rpm agitation rate,
- ✓ 24 hours reaction time.

✳     The blends were prepared by directly mixing of HDPE in powder form with the fabricated crosslinking poly(ABCF13) microspheres with varying compositions. The melting temperature of the HDPE decreased from 131°C to about 129°C, but there existed no significant change in the melting point of the blends at all contents and melting points remained constant at about 129°C. I was presumed that the increment in orderly arrangements of PE chains led to increasing of the orientation, mobility and free movement of PE chains, which resulted that PE chains started to melt easier.

✸      The *a* and *b* unit cell parameters of PE crystals increased initially and reached to maximum value with the blend sample including 5% crosslinked poly(ABCF13) microspheres. *a* and *b* unit cell parameters of this sample showed expansion of 1.66 and 1.82%, respectively. The crosslinked poly(ABCF13) particles could partially penetrate into nearest and folded neighbor chains of PE in crystal regions or may be expelled out and rejected from lamellar stacks in spherulite domain due to thermal mobility. After the maximum of *a* and *b* unit cell parameters, the decrements were observed with the increasing of the crosslinked poly(ABCF13) contents. This may be attirubuted that the growing unit cell fronts of the crystals could be damaged, hindered and disturbed since the lamellae of the PE was surrounded by the amorphous crosslinked poly(ABCF13) microsheres defined as inclusions in PE matrix phase. was no considerable effect of the crosslinked poly(ABCF13) content on *c* unit cell parameter and it remained relatively unchanged at all contents. It may be derived from the chain dimension of the molecular segments of PE was the parallel with the *c* axis.

✸      The grain sizes of PE increased initial contents and the impressive increment from the 16.42 to 24.42 (48.72%) was obtained in the blend containing 5% the crosslinked poly(ABCF13) microspheres. When the PE cooled from the melts, the PE crystal presumably had effective primary nucleation and grew on the surface of the dispersed particles possessing the three-dimensional spherical shapes, which resulted in the larger crystal sizes. This behavior of the samples resembled the dendritic growth of polymer crystals. After maximum, the fall of crystal sizes was recorded as the increasing of the crosslinked poly(ABCF13) microspheres content. , the reason of decrements in the crystal size at higher contents may be that the crystal growing in PE matrix impinged on crystal growth of each other and created not only restriction effect on crystal growth but also the borders due to impingements.

✸      Considerable improvements were recorded in the mechanical characteristics of the products composed of varying content of crosslinked poly(ABCF13) microspheres and HDPE. However, as the crosslinked poly(ABCF13) content increased, the dramatic decrements was also observed in percentage strain and yield stress and the brittle nature became more   dominant in blends. The mechanical

properties of the products were highly depended on the microsphere content in blends. The maximum value in tensile strength and modulus was recorded with 5% microsphere content. The ball bearing behavior of the microspheres in matrix probably led to remarkable dimensional stability by improving flatness and stress distribution, which resulted in the increment in directional micro-orientations and ideal alignments of the HDPE chains. After maxima, the dramatic decreasing was detected in mechanical characters of the products due to the losses and restriction of the HDPE chain mobility. Moreover, the impact behaviors of the products depicted the similar trend. The increasing of microspheres content in matrix made the product more brittle and this effect probably caused that the products had the lower withstanding and resistance against deformation when the load was applied.

✸    All the blends containing varying percent poly(ABCF13) depicted non-homogeneous structure. The extensions decreased with the increase of the microsphere content although there existed fibrillar formations in all samples. While ductile behavior was observed with the formation of long-bulky extensions at low contents, brittleness started to prevail at high contents with some short and thin fibrils.

# 8. REFERENCES

Abdelrahman AI, Thickett SC, Liang Y, Ornatsky O, Baranov V and Winnik MA (2006) "Surface Functionalization Methods to Enhance Bioconjugation in Metal-Labeled Polystyrene Particles" Macromolecules, 44:4801-4813.

Abrakhi S, Peralta S, Fichet O, Teyssie D and Cantin S (2013) "Poly(azobenzene acrylate-co-fluorinated acrylate) Spin-Coated Films: Influence of the Composition on the Photo-Controlled Wettability" Langmuir, 29:9499-9509.

Ahmad H, Upin D, Armes SP and Lewis AL (2009) "Synthesis of Biocompatible Sterically-Stabilized Poly(2-(methacryloyloxy)ethyl posphorylcholine) Latexes via Dispersion Polymerization in Alcohol/Water Mixtures" Langmuir, 25:11442-11449.

Akdeniz G, Yahsi U and Tav C (2010) "Viscous Behavior of PS, PP and ABS in terms of Temperature and Pressure Dependent Hole Fraction" J. Appl. Polym. Sci., 117:110.

Akhtar S, Shukla D and Kumar V (2008) "Studies on Effect of Nano-Talc Filler on Nucleation, Crystal Morphology and Crystallization Behaviour of Semi-Crystalline Plastics" Solid State Phenom., 136:161-174.

Alothman OY (2012) "Processing and Characterization of High Density Polyethylene/Ethylene Vinyl Acetate Blends with Different VA Contents" Adv. Mater. Sci. Eng., 635693.

Altaweel AMAM, Ranganathaiah C and Kothandaraman B (2009) "Mechanical Properties of Modified Epoxies as Related to Free Volume Parameters" J. Adhes., 85:200-215.

Ameduri B and Sawada H (2017) Fluorinated Polymer Volume 2: Applications, The Royal Society of Chemistry, Cambridge.

Andruzzi L, Chiellini E, Galli G, Li X, Kang SH and Ober CK (2002) "Engineering Low Surface Energy Polymers Through Molecular Design: Synthetic Routes to Fluorinated Polystyrene-Based Block Copolymers" J. Mater. Chem.,12:1684-1692.

Andruzzi L, D'Apollo F, Galli G and Gallot B (2001) "Synthesis and Structure Characterization of Liquid Crystalline Polyacrylates with Unconventional Fluoroalkylphenyl Mesogens" Macromolecules, 34:7707-7714.

Aoki Y (1999) "A Novel Liquid Crystal Showing Antiferroelectric Smectic C* and Twist Grain Boundary Phases" Liq. Cryst., 26:97-100.

Aramoon A, Breitzman TD, Woodward C and El-Awady AJ (2017) "Correlating Free-Volume Hole Distribution to the Glass Transition Temperature of Epoxy Polymers" J. Phys. Chem. B., 121:8399-8407.

Arshady R (1988) "Preparation of Polymer Nano and Microspheres by Vinyl Polymerization Techniques" J. Microencapsul., 5:101-114.

Arshady R (1992) "Suspension, Emulsion and Dispersion Polymerization: A Methodological Survey" Colloid. Polym. Sci., 270:717-732.

Azapagic A, Emsley A and Hamerton L (2003) Polymers; The Environment and Sustainable Development, Wiley Inc., Chichester.

Badaire S, Cottin-Bizonne C and Stroock AD (2008) "Experimental Investigation of Selective Colloidal Interactions Controlled by Shape, Surface Roughness, and Steric Layers" Langmuir, 24(20):11451-11463.

Bai F, Li R, Yang X, Li S and Huang W (2006) "Preparation of Narrow-Dispersion or Monodisperse Polymer Microspheres with Active Hydroxyl Group by Distillation–Precipitation Polymerization" Polym. Int., 55:319-325.

Baker AME and Windle AH (2001) "An X-ray Diffraction and Modelling Study of Short Chain Branch Location Within the Structure of Polyethylene" Polymer, 42:681-698.

Baker AME and Windle AH (2001) "Evidence for a Partially Ordered Component in Polyethylene from Wide-Angle X-ray Diffraction" Polymer, 42:667-680.

Bamford D, Dlubek G and Reiche A (2001) "The Local Free Volume, Glass Transition, and Ionic Conductivity in a Polymer Electrolyte: A Positron Lifetime Study" J. Chem. Phys., 115(15):7260-7270.

Bartczak Z, Argon AS, Cohen RE and Weinbergb M (1999) "Toughness Mechanism in Semi-Crystalline Polymer Blends: II. High Density Polyethylene Toughened with Calcium Carbonate Filler Particles" Polymer, 40:2347-2365.

Batra D, Kakar S, Singh R and Nautiyal U (2012) "Magnetic Microspheres as a Targeted Drug Delivery System:An Overview" J.D.D.R., 1:1-17.

Bharali DJ, Sahoo SK, Mozumdar S and Maitra A (2003) "Cross-linked Polyvinylpyrrolidone Nanoparticles: a Potential Carrier for Hydrophilic Drugs" J. Colloid. Interf. Sci., 258:415-23.

Bhattacharya A and Misra BN (2004) "Grafting: a Versatile Means to Modify Polymers Techniques, Factors and Applications" Prog. Polym. Sci., 29:767-814.

Bilchak CR, Buenning E, Asai M, Zhang K, Duming CJ, Kumar SK, Huang YC, Benicewicz BC, Gidley DW, Cheng SW, Sokolov AP, Minelli M and Doghieri F (2017) "Polymer-Grafted Nanoparticle Membranes with Controllable Free Volume" Macromolecules, 50:7111-7120.

Billmeyer FW (1984) Textbook of Polymer Science, Wiley Inc., New York.

Bitz C and Doelker E (1996) "Influence of the Preparation Method on Residual Solvents in Biodegradable Microsphere" Int. J. Pharm., 131:171-181.

Breed DR, Thibault R, Xie F, Wang Q, Hawker CJ and Pine DJ (2009) "Functionalization of Polymer Microspheres Using Click Chemistry" Langmuir, 25:4370-4376

Broer DJ, Crawford GP and Zumer S (2011) The Liquid Crystal Book Series: Crosslinked Liquid Crytalline System from Rigid Polymer Networks to Elastomer, CRC Press:Taylor and Francis Group, New York.

Brooks BW (2010) "Suspension Polymerization Processes" Chem. Eng. Technol., 33:1737-1734.

Brusa RS, Naia MD, Margoni D and Zecca A (1995) "Positron Mobility in Polyethylene in the 60-400 K Temperature-Range" Applied Physics a-Materials Science & Processing, 60(5):447-453.

Burgessa SK, Lee JS, Mubarak CR, Kriegel RM and Korosa WJ (2015) "Caffeine Antiplasticization of Amorphous Poly(Ethylene Terephthalate): Effects on Gas Transport, Thermal, And Mechanical Properties" Polymer, 65:34-44.

Cai S, Weng Z, Zheng Y, Zhao B, Gao Z and Gao C (2016) "High Porosity Microspheres with Functional Groups Synthesized by Thiol–yne Click Suspension Polymerization" Polym. Chem., 7:7400-7407.

Callander DB (2005) Molecular Modeling of Polymer Free Volume Distribution, Doctor of Philosophy Thesis, Georgia Institute of Technology, Chemical and Biomolecular Engineering, Georgia.

Caykara T, Alaslan SS, Gürü M, Bodugöz H and Güven O (2007) " Preparation and Characterization of poly(isobutyl methacrylate) Microbeads with Grafted Amidoxime Groups" Radiat. Phys. Chem., 76:1569-1576.

Cengiz U, Gengec NA , Kaya NU, Erbil HY and A. Sezai Sarac (2011) "Mechanical and Thermal Properties of Perfluoroalkyl Ethyl Methacrylate–Methyl Methacrylate Statistical Copolymers Synthesized in Supercritical Carbon Dioxide" J. Fluorine Chem., 132:348-355.

Cetin S (2004) Graft Copolymerization of p-Acryloyloxybenzoic Acid and p-Methacryloyloxybenzoic Acid onto Isotactic Polypropylene, Doctor of Philosophy Thesis, METU, Graduate School of the Natural and Applied Sciences, Ankara.

Chae D, Kim KJ and Kim BC (2006) "Effects of Silicalite-1 Nanoparticles on Rheological and Physical properties of HDPE" Polymer, 47:3609-3615.

Chai Z, Zheng X and Sun X (2003) "Preparation of Polymer Microspheres from Solutions" J. Polym. Sci. B Polym. Phys., 41:159-165.

Chen CC and White JL (1993) "Compatibilizing Agents in Polymer Blends - Interfacial-Tension, Phase Morphology, and Mechanical-Properties" Polym. Eng. Sci., 33:923-930.

Chen CW, Chen CY and Cioul ZH (2010) "Preparation of Monodisperse Functional poly(styrene-co-acrylamidoxime) Microsphere with Chelating Amidoxime Group" Colloid. Polym. Sci., 288:665-672.

Chen Y, Zou HW, Liang M and Cao Y (2014) "Melting and Crystallization Behavior of Partially Miscible High Density Polyethylene/Ethylene Vinyl Acetate Copolymer (HDPE/EVA) Blends" Thermochim. Acta., 586:1-8.

Chen Z, Fang PF, Wang HM and Wang SJ (2008) "Effect of the Graft Yield of Maleic Anhydride on the Rheological Behaviors, Mechanical Properties, Thermal Properties, ond Free Volumes of Maleic Anhydride Grafted High-Density Polyethylene" J. Appl. Polym. Sci., 107:985-992.

Choi D, Yeom EH, Park M, Kim JK and Kim BC (2004) "Preparation and Properties of Methyl Methacrylate and Fluoroacrylate Copolymers for Plastic Optical Fiber Cladding" J. Appl. Polym. Sci., 93:2082-2089.

Chu H and Pan Q (2015) "Preparation of Micron-sized Monodisperse Poly (Styrene-co-Methyl Methacrylate) Microspheres by Dispersion Copolymerization" C.M.S.E., 428-433.

Cohen MH and Turnbull D (1959) "Molecular Transport in Liquids and Glasses" J. Chem. Phys., 31(5):1164-1169.

Coleman MM, Graf JF and Painter PC (1991) Specific Interaction and the Miscibility of Polymer Blends, Technomic Publishing Company Inc., Pennsylvania.

Colling PJ and Hird M (2009) Introduction to Liquid Crystals Chemistry and Physics, Taylor and Francis Ltd., London.

Dinarvand R, Moghadam SH, Mohammadyari-Fard L and Atyabi1F (2003) "Preparation of Biodegradable Microspheres and Matrix Devices Containing Naltrexone" AAPS Pharm. Sci. Tech., 4:3.

Dinc FS, Sedlacek T, Tav C nad Yahsi U (2014) "On the Non-Newtonian Viscous Behavior of Polymer Melts in Terms of Temperature and Pressure-Dependent Hole Fracation" J. Applied Polymer Sci., 131 (15), 40540.

Denizli A, Ozkan G and Arıca MY (1999) "Preparation and Characterization of Magnetic Polymethylmethacrylate Microbeads Carrying Ethylene Diamine for Removal of Cu(II), Cd(II), Pb(II), and Hg(II) from Aqueous Solutions" J. Appl. Polym. Sci., 78:81-89.

Dullens RPA, Claesson EM and Kegel WK (2004) "Preparation and Properties of Cross-Linked Fluorescent Poly(methyl methacrylate) Latex Colloids" Langmuir, 20(3):658-664.

Durmaz YY, Sahkulubey EL, Yagci Y, Martinelli E and Galli G (2012) "A Novel Poly(p-phenylene) Containing Alternating Poly(perfluorooctylethyl acrylate-co-methyl methacrylate) and Polystyrene Grafts by Combination of Atom Transfer Radical Polymerization and Suzuki Coupling Processes" J. Polym. Sci. Pol. Chem., 50:4911-4919.

Ebnesajjad S (2003) "Properties of Fluoropolymers" Melt Processible Fluoroplastics, 375-447.

Ebnesajjad S (2013) Introduction to Fluoropolymers; Materials, Technology and Applications, Elsevier, Waltham.

Eldrup M, Lightbody D and Sherwood JN (1981) "The Temperature-Dependence of Positron Lifetimes in Solid Pivalic Acid" Chemical Physics, 63:51-58.

El-Nashar D, Gomaa E and Abd-El-Messieh S (2009) "Study of Electrical, Mechanical, and Nanoscale Free-Volume Properties of Nbr and Epdm Rubber Reinforced by Bentonite or Kaolin", Journal of Polymer Science: Part B: Polymer Physics, 47:1825-1838.

Eriman B (2008) Effect of the Polyethylene Graft Copolymer to Structures and Mechanical Properties of Polyethylene/Clay Nanocomposites, Master Degree Thesis, İTÜ, Institute of Science and Technology, İstanbul.

Erol I, Sen O, Dedelioglu A and Ciftci C (2009) "Synthesis and Characterization of Novel Fluorine-Containing Methacrylate Copolymers: Reactivity ratios, Thermal properties and Antimicrobial activity" J. Appl. Polym. Sci., 114:3351-3359

Fialkov YA, Shelyazhenko SV and Yagupol'skii LM (1983) "Liquid-Crystals Containing Fluorine .8. 4-Perfluoroalkyl-4'-Alkylaminodiphenyls" Zh. Org. Khim., 19: 1048-1053.

Filipe S, Cidade MT and Maia JM (2006) "Uniaxial Extensional Flow Behavior of Immiscible and Compatibilized Polypropylene/Liquid crystalline Polymer Blends" Rheol. Acta., 45:281-289.

Fouad H (2010) "Experimental and Numerical Studies of the Notch Strengthening Behaviour of Semi-crystalline Ultra-High Molecular Weight Polyethylene" Mater. Des., 31:1117-1129.

Freiberg S and Zhu XX (2004) "Polymer Microspheres for Controlled Drug Release" Int. J. Pharm., 282:1-18.

Fu M, Deng LR, Zhao AL, Wang YS and He DW (2010) "Fabrication and Optical Properties of Alq(3) Doped PMMA microsphere Arrays Templated by ZnO Inverse Opal Structure" Opt. Mater., 32:1210-1215.

Genzer J, Sivaniah E, Kramer EJ, Wang J, Körner H, Char K, Ober CK, DeKoven BM, Bubeck RA, Fisher DA and Sambasivan S (2000) "Temperature Dependence of Molecular Orientation on the Surfaces of Semifluorinated Polymer Thin Films" Langmuir, 16:1993-1997.

Genzer J, Sivaniah E, Kramer EJ, Wang J, Körner H, Xiang M, Char K, Ober CK, DeKoven BM, Bubeck RA, Chaudhury MK, Sambasivan S and Fisher DA (2000) "The Orientation of Semifluorinated Alkanes Attached to Polymers at the Surface of Polymer Films" Macromolecules, 33:1882-1887.

Giannetti E (2001) "Featured ArticleSemi-Crystalline Fluorinated Polymers" Polym. Int., 50:10-26.

Giunchedi P, Alpar HO and Conte U (1998) "PDLLA Microspheres Containing Steroids: Spray-Drying, o/w and w/o/w Emulsifications as Preparation Methods" J. Microencapsul., 15:185-195.

Gomaa E, Mostafa N, Mohsen M and Mohammed M (2003) "Correlation Between Free-Volume Parameters and Physical Properties of Polyethylene-Nitrile Rubber Blend" Journal of Materials Engineering and Performance, 13:583-587.

Guittard F, Taffin de Givenchy E, Geribaldi E and Cambon A (1999) "Highly Fluorinated Thermotropic Liquid Crystals: An Update" Fluorine Chem., 100:85-96.

Guo HL, Zhao XP and Wang JP (2005) "Synthesis of Functional Microcapsules Containing Suspensions Responsive to Electric Fields" J. Colloid. Interf. Sci., 284:646-51.

Guo N, Wu DC, Pan XH and Lu ML (2009) " Magnetic Polymer Microspheres with Azidocarbonyl Groups: Synthesis, Characterization and Application in Protein Immobilization" J. Appl. Polym. Sci., 112: 2383-2390.

Hamad K, Kaseem M, Deri F and Ko YG (2016) "Mechanical Properties and Compatibility of Polylactic acid/Polystyrene Polymer Blend" Mater. Lett., 164:409-412.

Hamielec A and Tobita EH (1992) Polymerization Processes. Ullmann's Encyclopedia of Industrial Chemistry, VCH Publishers, Inc., New York.

Han LM, Suo QL and Hong HL (2008) "Applications of Polymer Microsphere in Electrochemistry" Prog. Chem., 20:931-935.

Hartmann PC, Collet A, Viguier M and Blanc C (2004) "Acrylic Monomers and Polymers with Perfluoroalkylatedbiphenyl Side Groups: Synthesis and Phase Transitions" J. Fluorine Chem., 125:1909-1918.

Haraguchi N, Nishiyama A and Itsuna S (2010) " Synthesis of Polymer Microspheres Functionalized with Chiral Ligand by Precipitation Polymerization and their Application to Asymmetric Transfer Hydrogenation" J. Polym. Sci. Part A:Polym. Chem., 4:3340-3349.

He AH, Ou YC, Fang XP, Liu HZ and Yang GS (2004) "Effect of Maleic Anhydride Grafted Thermoplastic Eastomer on PP/PA6 Bends" Acta. Polym. Sin., 4:534-540.

He J and Liu J (1997) "Compatibilization by Sulfonate Ionomers in Polyblends with Thermotropic Liquid Crystalline Polymers" J. Appl. Polym. Sci., 67:2141-2151.

Henton DE, Powell C and Reim RE (1996) " The Decomposition of Sodium Persulfate in the Presence of Acrylic Acid" J. Appl. Polym. Sci., 64:591- 600.

Hsieh TT, Tiu C, Hsieh KH and Simon GP (2000) "Characterization of Thermotropic Liquid Crystalline Polyester/Polycarbonate Blends: Miscibility, Rheology, and Free Volume Behavior" J. Appl. Polym. Sci., 77(10):2319-2330

Hirao A, Sugiyama K and Yokoyama H (2007) "Precise Synthesis and Surface Structures of Architectural Per- and Semifluorinated Polymers with Well-Defined Structures" Prog. Polym. Sci., 32:1393-1438.

Hird M (2007) "Fluorinated Liquid Crystals-Properties and Applications" Chem. Soc. Rev., 36:2070-2095.

Hird M and Toyne KJ (1988) "Fluoro Substitution in Thermotropic Liquid Crystals" Mol. Cryst. Liq. Cryst., 323:1-67.

Honda K,  Morita M, Otsuka H and Takahara A (2005) "Molecular Aggregation Structure and Surface Properties of Poly(fluoroalkyl acrylate) Thin Films" Macromolecules., 38:5699-5705.

Hong SJ, Yu HS and Kim HW (2009) "Preparation of Porous Bioactive Ceramic Microspheres and in Vitro Osteoblastic Culturing for Tissue Engineering Application" Acta. Biomater., 5:1725-1731.

Horak D and Shapoval P (2000) "Reactive Poly(glycidyl methacrylate) Microspheres Prepared by Dispersion Polymerization" J. Polym. Sci. Part A: Polym. Chem., 38:3855-3863.

Hosseinabadi HG, Bagheri R, Gigl T, Hugenschmidt C, Raps D and  Altstadt V (2018) "Interrelation Between Mechanical Response, Strain Field, And Local Free Volume Evolution In Glassy Polymers: Seeking The Atomistic Origin Of Post-Yield Softening"  Express. Polym. Lett., 12:2-12.

Howard PR and Crist B (1989) "Unit-Cell Dimensions in Model Ethylene Butene-1 Copolymers" J. Polym. Sci. Pol. Phys., 27:2269-2282.

Hsieh TT, Tiu C, Hsieh KH and Simon GP (1998) "Rheological, Thermal And Free Volume Studies of Blends Containing Two Thermotropic Liquid Crystalline Polymers" Korea Polym. J., 6:44-52.

Hsu TC, Lichkus AM and Harrison IR (1993) "Liquid Crystal Polymer/ Polyethylene Blends for Thin Film Applications" Polym. Eng. Sci., 33: 860-863.

Huang B, Bai F, Yang X and Huang W (2010) "Synthesis of Monodisperse Hollow Polymer Microspheres with Functional Groups by Distillation Precipitation Polymerization" Chin. J. Polym. Sci., 28:277-28.

Hwisa NT, Kataham P, Chandu BR and Adiki SK (2013) "Solvent Evaporation Techniques as Promising Advancement in Microencapsulation" VRI. Biol. Med. Chem., 1:8.

Iacono ST (2008) Semifluorinated Polymers via Cycloaddition and Nucleophilic Addition Reactions of Aromatic Trifluorovinyl Ethers, Doctor of Philosophy Thesis, Graduate School of Clemson University, Clemson.

Ivanova T, Zicans J, Elksnite I, Kalnins M and Maksimov R (2011) "Mechanical Properties of Injection-Molded Binary Blends of Polyethylene with Small Additions of a Liquid-Crystalline Polymer" J. Appl. Polym. Sci., 122:3564-3568.

Janulis EP, Osten DW, Radcliffe MD, Novack JC, TristaniKendra M, Epstein KA, Keyes M, Johnson GC, Savu PM and Spawn TD (1992) "Fluorinated Liquid Crystals: an Update" Liq. Cryst. Mater. Devices Appl., 665:146-153.

Jasso-Gastinel CF and Kenny JM (2017) Modification of Polymer Properties, Matthew Deans Elsevier, Oxfrod.

Jean YC, Mallon PE and Schrader DM (2003) Principles and Applications of Positron&Positronium Chemistry, World Scientific Publishing Co. Pte. Ltd., Singapore.

Yuan J, Li WN, Gomez S and Suib SL (2003) "Shape-Controlled Synthesis of Manganese Oxide Octahedral Molecular Sieve Three-Dimensional Nanostructures" J. Am. Chem. Soc., 127:14184-14185.

Kahraman M and Uçar T (2016) "Enhanced Mechanical Properties of Low-Surface Energy Thin Films by Smultaneous Plasma Polymerization of Fluorine and Epoxy Containing Polymers" Appl. Surf. Sci., 362:210-216.

Kalyan S, Sharma PK, Garg VK, Kumar N and Varshney J (2010) "Recent Advancement In Chitosan Best Formulation And Its Pharmaceutical Application" Pelagia Research Library, 1:195-210.

Kamiyama M, Koyama K, Matsuda H and Sano Y (1993) "Micron-Sized Polymeric Microsphere by Suspension Polymerization" J. Appl. Polym. Sci., 50:107-113.

Kansy J (2008) "A Comparison of Different Theoretical Models of Positron Lifetime Spectra for Polymers" Acta Phys. Pol. A., 113(5):1397-1407.

Karagoz B, Gunes D and Bicak N (2010) "Preparation of Crosslinked Poly(2-bromoethyl methacrylate) Microspheres and Decoration of Their Surfaces with Functional Polymer Brushes" Macromol. Chem. Phys., 211:1999-2007.

Krishnan S, Kwark YJ and Ober CK (2004) "Fluorinated Polymers: Liquid Crystalline Properties and Applications in Lithography" Chem. Rec., 4:315-330.

Kawaguchi H (2000) "Functional Polymer Microspsheres" Prog. Polym. Sci., 25:1171-1210.

Kayaisang K, Amornsakchai T and Saikrasun S (2009) "Influence of Liquid Crystalline Polymer and Recycled PET as Minor Blending Components on Rheological Behavior, Morphology, and Thermal Properties of Thermoplastic Blends" Polym. Advan. Technol., 20:1136-1145.

Kenig S (1987) "Orientability of Liquid Crystal Polymers in Elongational Flow" Polym. Eng. Sci., 27:887–892.

Khairuddean M (2008) Synthesis of Fluorinated Liquid Crystals, Doctor of Philosophy Thesis, Kent State University, Graduate School of the Natural and Applied Sciences, Ohio.

Kharitonov AP, Maksimkin AV, Mostovaya KS, Kaloshkin SD, Gorshenkov MV, D'yachkova TP, Tkachev AG and Alekseiko LN (2015) "Reinforcement of Bulk Ultrahigh Molecular Weight Polyethyleneby Fluorinated Carbon Nanotubes Insertion Followed by Hot Pressing and Orientation Stretching" Compos. Sci. Technol., 120:26-31.

Kirkegaard P, Eldrup M, Mogensen OE and Pedersen NJ (1981) "Program System for Analyzing Positron Lifetime Spectra and Angular-Correlation Curves", Comput. Phys. Commun., 23(3):307-335.

Kitazume T, Kaneko S and Yamazaki T (1993) "A Convenient Synthesis of Ferroelectric Liquid Crystals Bearing the Trifluoromethyl Group" J. Fluorine Chem., 60:135-140.

Kobayashi T, Sato M, Takeno N and Mukaida N (1994) "Compatibilizing Effect of a Thermotropic Liquid-Crystalline Compatibilizer on Liquid-Crystalline Polycarbonate Poly(P-Phenylene Oxide) Blends" Macromol. Chem. Phys., 195:2771-2777.

Kobayashi Y, Zheng W, Meyer EF, Mcgervey JD, Jamieson AM and Simha R (1989) "Free Volume and Physical Aging of Poly(Vinyl Acetate) Studied by Positron Annihilation", Macromolecules, 22:2302-2306.

Kocsis JK (1995), Polypropylene Structure, Blends and Composites, Copolymers and Blends, Chapman and Hall, London.

Koden M, Nakagawa K, Ishii Y, Funada F, Matsuura M and Awane K (1989) "The Effect of Fluorinated Alkyl Group on Mesophase Thermal Stabilities" Mol.Cryst. Liq. Crysr. Lett., 6:185-190.

Kumar A, Jha S, Rawal R, Chauhan PS and Maurya S. D (2013) "Mucoadhesive Microspheres for Novel Drug Delivery System: A Review" Am. J. Pharm. Tech. Res., 3:197-213.

Kumar H, Siddaramaiah, Kumaraswamy GN, Ravikumar HB and Ranganathaiah C (2005) "Free Volume and The Physico-Mechanical Behaviour of Polyurethane /Polyacrylonitrile Interpenetrating Polymer Networks: Positron Annihilation Results" Polym. Int., 54:1401-1407.

Kurt O (2010) Preparation of Cross-linked Poly (vinylamine) Microspheres and Their Phosphometylated Derivative as Efficient Chelating Material, Master Degree Thesis, İTÜ, Graduate School of the Natural and Applied Sciences, İstanbul.

Kozlowski M and LaMantia FB (1997) "Study on Compatibilization of Polypropylene Liquid Crystalline Polymer Blends" J. Appl. Polym. Sci., 66:969-980.

Lee MW, Hu X, Li L, Yue CY,Tam KC and Cheong LY (2003) "PP/LCP Composites: Effects of Shear flow, Extensional Flow and Nanofillers" Compos. Sci. Technol. 63:1921-1929.

Lima EV, Wood PE and Hamielec AE (1997) "An Updated Review on Suspension Polymerization" Ind. Eng. Chem. Res., 36:939-965.

Li M, Rouaud O and Poncelet D (2008) "Microencapsulation by Solvent Evaporation: State of the Art for Process Engineering Approaches" Int. J. Pharm., 363:26-39.

Lin M, Zhao Q, Dang S, Wang Y, Wang Y and Wang X (2015) "Preparation and Properties of Terpolymeric Microspheres for Deep Profile Control in Oilfields" Mater. Res. Innov., 19:574-579.

Lue SJ, Lee DT, Chen JY, Chiu CH, Hu CC, Jean YC and, Lai JY (2008) "Diffusivity Enhancement Of Water Vapor In Poly(Vinyl Alcohol)-Fumed Silica Nano-Composite Membranes: Correlation With Polymer Crystallinity And Free-Volume Properties" J. Membrane. Sci., 325:831-839.

Machiels AGC, Denys KFJ, Dam JV and De Boer AP (1997) "Effect of Processing History of the Morphology and Properties of Polypropylene/Thermotropic Liquid Crystalline Polymer Blends" Polym. Eng. Sci. 37:59-72.

Ma G and Su Z (2013) Microspheres and Microcapsules in Biotechnology: Design, Preparation and Applications, Taylor&Francis Group LLC, New York.

Mahler W, Guillon D and Skoulios A (1985) "Evidence for Two Coexisting Nematic Phases in Mixtures of Rod-Like and Disc-Like Nematogens" Mol. Cryst. Liq. Crysr. Lett., 2:111-116.

Mahmoud KR, Al-Sigeny S, Sharshar T and El-Hamshary H (2006) "Positron Annihilation Study on Free Volume of Amino Acid Modified, Starch-Grafted Acrylamide Copolymer" Radiat. Phys. Chem., 75:590-595.

Mandal PK, Bandyopadhyay D and Chakrabarty D (2004) "Studies on Morphology, Mechanical, Thermal, and Rheological Behavior of Extrusion-Blended Polypropylene and Thermotropic Liquid Crystalline Polymer" J. Appl. Polym. Sci., 88:767-774.

Mane S, Ponrathnam S and Chavan N (2015) "Effect of Chemical Cross-linking on Properties of Polymer Microbeads: A Review" Can. Chem. Trans., 3:473-485.

Mao SR, Shi Y, Li L, Xu J, Schaper A and Kissel T (2008) "Effects of Process and Formulation Parameters on Characteristics and Internal Morphology of poly(D,L-lactide-co-glycolide) Microspheres Formed by the Solvent Evaportion Method" Eur. J. Pharm. Biopharm., 68:214-223.

Marchionni G, Ajroldi G, Righetti MC and Pezzin G (1993) "Molecular Interactions in Perfluorinated and Hydrogenated Compounds: Linear Paraffins and Ethers" Macromolecules, 26:1751-1757.

Margel S, Nov E and Fisher I (1991) "Polychloromethylstyrene Microspheres: Synthesis and Characterization" J. Polym. Sci. Polym. Chem., 29:347-355.

Mayoux C, Dandurand J, Ricard A and Lacabanne C (2000) "Inverse Suspension Polymerization of Ssodium Acrylate: Synthesis and Characterization" J. Appl. Polym. Sci., 77:2621-2630

Meouche W, Branger C, Beurroies I, Denoyel R and Margaillan A "Inverse Suspension Polymerization as a New Tool for the Synthesis of Ion-Imprinted Polymers" Macromol. Rapid. Comm., 33:928-932.

Mills JT, Gleeson HF, Goodby JW, Hird M, Seed A and Styring P (1998) "X-ray and Optical Studies of the Tilted Phases of Materials Exhibiting Antiferroelectric, Ferrielectric and Ferroelectric Mesophases" J. Mater. Chem., 8:2385-2390.

Moly KA, Radusch HJ, Androsh R, Bhagawan SS and Thomas S (2005) " Nonisothermal Crystallisation, Melting Behavior and Wide Angle X-Ray Scattering Investigations on Linear Low Density Polyethylene (LLDPE)/Ethylene Vinyl Acetate (EVA) Blends:Effects of Compatibilisation and Dynamic Crosslinking" Eur. Polym. J., 41:1410-1419.

Mostafa N, Ali EH and Mohsen M (2009) "Dynamic Study of Free Volume Properties in Polyethylene/Styrene Butadiene Rubber Blends by Positron Annihilation Lifetime Method", J. Appl. Polym. Sci., 113(5):3228-3235.

Mukund JY, Kantilal BR and Sudhakar RN (2012) "Floating Microspheres:A Review" Braz. J. Pharm. Sci., 48:17-30.

Murphy J (2001) Additives for Plastics Handbook, Second Addition, Elsevier Science Ltd., Oxford.

Nagai K, Tanaka S, Hirata Y, Nakagawa T, Arnold ME, Freeman BD, Leroux D, Betts DE, Desimone JM and DiGiano FA (2001) " Solubility and Diffusivity of Sodium Chloride in Phase-Separated Block Copolymers of Poly(2-dimethylaminoethyl methacrylate), poly(1,1′-dihydroperfluorooctyl

methacrylate) and poly(1,1,2,2-tetrahydroperfluorooctyl acrylate)" Polymer, 42:9941-9948.

Nakanishi H and Jean YC (1990) Positron and Positronium Chemistry. Amsterdam: Elsevier (Chapter 5).

Nakanishi H and Jean YC (1988) "Positron Annihilation Studies of Fluids" Paper presented at the Word Scientific Singapore, Singapore.

Ningaraju S, Hegde VN, Prakash APG and Ravikumar HB (2018) "Free Volume Dependence on Electrical Properties of Poly (Styrene-co-Acrylonitrile)/Nickel Oxide Polymer Nanocomposites" Chem. Phys. Lett., 698:24-35.

Nunes RCR, Fonseca JLC and Pereira MR (2000) "Polymer–Filler Interactions and Mechanical Properties of a Polyurethane Elastomer" Polym. Test., 19:93-103.

Nwabunma D and Kyu T (2008) Polyolefin Blends, Second Edition, Wiley Inc., New Jarsey.

Odian G (2004) Principles of Polymerization, Fourt Edition, John Wiley & Sons, Inc., Hoboken, New Jersey.

Odonnell HJ and Baird DG (1995) "In-Situ Reinforcement of Polypropylene with Liquid-Crystalline Polymers - Effect of Maleic Anhydride-Grafted Polypropylene" Polymer., 36:3113-3126.

Omidian H, Zohuriaan-Mehr MJ and Bouhendi H (2003) "Polymerization of Sodium Acrylate in Inverse-Suspension Stabilized by Sorbitan Fatty Esters" Eur. Polym. J., 39:1013-1018.

Ou YC, Lei YG, Fang XP and Yang GS (2004) "Maleic Anhydride Grafted Thermoplastic Elastomer as an Interfacial Modifier for Polypropylene/Polyamide 6 Blends" J. Appl. Polym. Sci., 91:1806-1815.

Ozturk B (2018) Preparation And Characterization Of Some Side Chain Liquid Crystalline Polymer Graft Copolymers Of High Density Polyethylene And Isotactic Polypropylene, Doctor of Philosophy Thesis, Bolu Abant Izzet Baysal University, Bolu, Turkey.

Park KY, Jeong WW and Suh KD (2006) "Monodisperse Crosslinked Microsphere Polymer Particles by Dispersion Copolymerization of Glycidyl Methacrylate and Divinylbenzene" J. Macromol. Sci. Pure. Appl. Chem., 40:617-627.

Peacock AJ (2000) Handbook of Polyethylene: Structures, Properties and Applications, Marcel Dekker Inc., New York.

Peng B and Imhof A (2015) "Surface Morphology Control of Cross-linked Polymer Particles via Dispersion Polymerization" Soft Matter., 11:3589.

Peng M, Wang L, Wei Z, Wang X, Zhang Q, Long S and Yang J (2014) "Structure Controlling and Adsorption Application of Polyethersulfone Porous Microspheres Prepared via Electrospraying" Chin. J. Polymer. Sci., 32:1390-1399.

Pereira RA, Mona EB and Dias ML (1997) "WAXS Study on Orthorhombic Crystalline Phases in Hot-Drawn High Density Polyethylene" Poly. Test., 16: 589-601.

Petrusic S, Jovancic P, Lewandowski M, Giraud S, Bugarski B, Djonlagic J and Koncar V (2012) "Synthesis, Characterization and Drug Release Properties of Thermosensitive poly(N-isopropylacrylamide) Microgels" J. Polym. Res., 19:9979.

Piorkowska E and Rutledge GC (2013) Handbook of Polymer Crystallization: Crystallization in Polymer Composites and Nanocomposites, John Wiley & Sons Inc., Hoboken.

Piskin E, Tuncel A, Denizli A and Ayhan H (1994) "Monosize Microbeads Based on Polystyrene and Their Modified Forms for Some Selected Medical and Biological Applications" J. Biomater. Sci. Polym. Ed., 5:451-471.

Ponnamma D, Ramachandran R, Hussain S, Rajaraman R, Amarendra G, Varughese K and Thomas S (2015) "Free-Volume Correlation with Mechanical and Dielectric Properties of Natural Rubber/Multi Walled Carbon Nanotubes Composites" Composites: Part A, 77:164-171.

Postema AR and Fennis PJ (1997) "Preparation and Properties of Self-reinforced Polypropylene/Liquid Crystalline Polymer Blends" Polymer, 38:5557-5564.

Pracella M (2013) Handbook of Polymer Crystallization: Crystallization of Polymer Blends, John Wiley & Sons Inc., Hoboken.

PrasanthVV, Moy AC, Mathew ST and Mathapan R (2011) "Microspheres-An Overview" Int. J. Pharm. Biomed. Res., 2:332-338.

Qi N, Chen ZQ, & Uedono A (2015) "Molecular Motion and Relaxation Below Glass Transition Temperature in Poly(methyl methacrylate) Studied by Positron Annihilation" Radiat. Phys. Chem., 108:81-86.

Ramteke KH, Jadhav VB and Dhole SN (2012) "Microspheres: as Carrieres Used for Novel Drug Delivery System" I.O.S.R.P.H.R., 4:44-48.

Ravi S, Peh KK, Darwis Y, Murthy KB, Singh TRR and Mallikarjun C (2008) "Development and Characterization of Polymeric Microspheres for Controlled Drug Release Protein Loaded Drug Delivery System" Indian. J. Pharm. Sci., 70:303-309.

Ren Y, Shoichet MS, McCarthy TJ, Stidham HD and Hsu SL (1995) "Spectroscopic Characterization of Polymer Adsorption at the Air–Solution Interface" Macromolecules, 28:358-364.

Reno CO and Motisuke M (2016) "Optimizing the Water-Oil Emulsification Process for Developing CPC Microspheres" Mat. Res., 19:1388-1392.

Riande E, Diaz-Calleja R, Prolongo M, Masegosa R, and Salom C (2000) Polymer Viscoelasticity-Stress and Strain in Practice, Marcel Dekker, New York.

Robeson LM (2007) Polymer Blends: A Comprehensive Review, Carl Hanser Verlag GmbH & Co. KG., Münich.

Roussel F (1999) "Nematic Ordering and Crystal Structure of Liquid Crystals Containing a 4-Chlorophenyldifluoroethylene Unit" Liq. Cryst., 26:251-260.

Roussenova M, Hughes DJ, Enrione J, Diaz-Calderon P, Sivaniah E, Song Q, Ubbink J, Beavis P, Swain A and Alam MA (2014) "Free Volume, Molecular Mobility and Polymer Structure: Towards the Rational Design of Multi-Functional Materials" Acta. Phys. Pol A., 125:801-805.

Ruckenstein E and Hong L (1995) "Sedimentation Polymerization" Polymer, 36:2857-2860.

Ruckenstein E and Sun Y "Preparation and Characteristics of Polymer-Based Large Adsorbent Particles" J. Appl. Polym. Sci., 61:1949-1956.

Saengsuwan S, Bualek-Limcharoen S, Mitchell GR and Olley RH (2003) "Thermotropic Liquid Crystalline Polymer (Rodrun LC5000)/Polypropylene in situ Composite Films: Rheology, Morphology, Molecular Orientation and Tensile Properties" Polymer., 44:3407-3415.

Sahil K, Akanksha M, Premjeet S, Bilandi A and Kapoor B (2011) " Microsphere: a Review" Int. J. Res. Pharm. Chem., 4:1184-1198.

Sahin F, Dinc A, Sorrentino A, Tav C and Yahsi U (2015) "The Effect of Hole Fraction on Viscosity in Atactic and Syndiotactic Polystyrenes" Int. J. Thermophys, 36 (9):3239-3254.

Sahin F, Tav C and Yahsi U (2006) "Linking the Viscous and Vacancy Behavior of Mixtures of High-Molecular-Weight Hydrocarbons" Int. J. of Thermophysics, 27 (5):1501.

Sainath AVS, Rao AK and Reddy AVR (2000) "Synthesis, Characterization and Liquid Crystalline Properties of Polyacrylates and Polymethacrylates Containing Aryl Ester Pendant Unit" J. Appl. Polym. Sci., 75:465-474.

Santos GC, Carmo DM, Rezende CGF, Zattera AJ, Oliveira MG and Oliveira PJ (2011) "Use of EPDMSDD as Compatibilizer Agent for EPDM/EPDMR Blends: Rheologic, Mechanical, and Morphologic Properties" J. Appl. Polym. Sci., 122:948-955.

Saralidze K, Aldenhoff YBJ, Knetsch MLW and Koole LH (2003) "Injectable Polymeric Microspheres with X-ray Visibility. Preparation, Properties, and Potential Utility as New Traceable Bulking Agents" Biomacromolecules, 4:793-798.

Saralidze K, Koole LH and Knetsch MLW (2010) "Polymeric Microspheres for Medical Applications" Materials., 3:3537-3564.

Scheirs J (1997) Modern Fluoropolymers: High Performance Polymers for Diverse Applications, Wiley Inc., Chichester.

Schulte MD , Clarson SJ, Natarajan LV, Tomlin DW and Bunning TJ (2000) "The Effect of Fluorine-Substituted Acrylate Monomers on the Electro-Optical and Morphological Properties of Polymer Dispersed Liquid Crystals" Liq. Cryst., 27:467-475.

Senel S, Isıkyuruksoy I and O Guven (1996) "A Kinetic Study of Homogeneous Bulk Polymerization of Ethyl Methacrylate Initiated by Benzoyl Peroxide and an N,N'-Dimethylaniline Redox Pair" Turk. J. Chem., 20:62-68.

Sharma J, Tewari K  and Arya RK (2017) "Diffusion in Polymeric Systems–A Review on Free Volume Theory" Prog. Org. Coat., 111:83-92.

Sharma SK and Pujari PK (2017) "Role of Free Volume Characteristics of Polymer Matrix in Bulk Physical Properties of Polymer Nanocomposites: A Review of Positron Annihilation Lifetime Studies" Prog. Polym. Sci., 75:31-47.

Shelyazhenko SV, Dronkina MI, Fialkov YA and Yagupolskii  LM (1988) " Fluorine-Containing Liquid-Crystals .11. Electron Effects of Terminal Groups on Mesomorphism of 4'-Substituted 4-Perfluoroalkyldiphenyls" Zh. Org. Khim., 24: 619-625.

Sherrington DC and Hodge P (1988) Syntheses and Separations Using Functional Polymers, Wiley, Chichester.

Shi X, Jin J, Chen S and Zhang J (2009) " Multiple Melting and Partial Miscibility of Ethylene-Vinyl Acetate Copolymer/Low Density Polyethylene Blends" J. Appl. Polym. Sci., 113:2863-2871.

Singh V and Chaudhary AK (2011) "Preparation of Eudragit E100 Microspheres by Modifed Solvent Evaporation Method" Acta. Pol. Pharm., 68:975-80.

Sivakumar M. Panduranga R.K. (2002) "Synthesis, Characterization, and in Vitro Release of Ibuprofen From poly(MMA-HEMA) Copolymeric Core-Shell Hydrogel Microspheres for Biomedical Applications" J. Appl. Polym. Sci., 83:3045-3054.

Solomon TW (1996) Graham Organic Chemistry, Wiley Inc., New York.

Song T, Zhou M, Liu W, Bian G, Qi Y, Bai F and Yang X (2015) "Preparation of Polymer Microspheres with Reactive Epoxy Group and Amino Groups as Stabilizers for gold Nanocolloids with Recoverable Catalysis" Colloid. Polym. Sci., 293:187-197.

Soykan U (2013) Graft Copolymerization of p-Benzophenoneoxycarbonylphenyl Acrylate Onto High Density Polyethylene, Master Degree Thesis, BAIBU, Graduate School of the Natural and Applied Sciences, Bolu.

Soykan U and Cetin S (2015) "Reinforcement of High Density Polyethylene with a Side Chain LCP by Graft Copolymerization-Thermal, Mechanical and Morphological Properties" J. Polym. Res., 22:204.

Soykan U, Cetin S, Ozturk B, Karaboga F, Zalaoglu Y, Dogruer M, Yildirim G and Terzioglu C (2013) "Synthesis and Characterization of p-Benzophenone oxycarbonylphenyl Acrylate by Means of Experimental Measurements and Theoretical Approaches, and Bulk Melt Polymerization" J. Mol. Struct., 1049:479-487.

Sperling LH (2006) Introduction to Physical Polymer Science (Fourth Edition), John Wiley & Sons, Inc., Hoboken, New Jersey.

Steinke KHG, Dunkin IR and Sherrington DC (1996) "Transparent Macroporous Polymer Monoliths" Macromolecules, 29:5826-5834.

Steller R and Zuchowska D (1999) "Free-Volume Effects on Rheological and Thermal-Properties of Polymers and Polymer Blends" J. Appl. Polym. Sci., 43:1411-1419.

Strathmann JL and Lipson JEG (1999) "Miscibility of Polyolefin Blends" Macromolecules, 32:1093-1102.

Struik LC (1977) "Physical Aging in Plastics and Other Glassy Materials" Polym. Eng. Sci., 17:165.

Suzuki T, Oki Y, Numajiri M, Miura T and Kondo K (1996) "Radiation Effect on Polypropylene Studied by the Relaxational Behaviour at Low Temperature Using Positron Annihilation" Polymer, 37:5521-5524.

Swift G, Carraher CE and Bowman CN (1997) Polymer Modification, Plenum Press, New York.

Tao SJ (1972) "Erratum: Positronium Annihilation in Molecular Substance" J. Chem. Phys., 56:5499.

Teegarden D (2004) Polymer Chemistry: Introduction to Indispensible Science, National Science Teacher Association Press, Virginia.

Thraenert S, Hassan EM and Krause-Rehberg R (2006) "Ortho-positronium Lifetime Measurement-Positron Source Activity and Statistics" Nucl. Instrum. Methods. Phys. Res. B., 248(2):336-339.

Thomas RR, Anton DR, Graham WF, Darmon MJ, Sauer BB, Stika KM and Swartzfager DG (1997) "Preparation and Surface Properties of Acrylic Polymers Containing Fluorinated Monomers" Macromolecules., 30:2883-2890.

Thurber CM, Xu Y, Myers JC, Lodge TP and Macosko CW (2015) "Accelerating Reactive Compatibilization of PE/PLA Blends by an Interfacially Localized Catalyst" ACS. Macro. Lett., 4:30-33.

Tummar AV, Kyada CR, Kalyanvat R and Shreevastva B (2013) "A Review on Mucoadhesive Microspheres as a Novel Drug Delivery Dystem", I.J.P.R.S., 2:188-200.

Tjong SC (2006) "Structural and Mechanical Properties of Polymer Nanocomposites" Mater. Sci. Eng. R. Rep., 53:73-197.

Tjong SC and Meng Y (1997) "The Effect of Compatibilization of Maleated Polypropylene on a Blend of Polyamide-6 and Liquid Crystalline Copolyester" Polym. Int., 42:209-217.

Uguzdogan E (2013) "Synthesis and Characterization of Hydrophilic and Spherical poly(glycerol dimethacrylate-co-glycerol-1,3-diglycerolate diacrylate) Microbeads" Des. Monomers. Polym., 16:250-262.

Utracki LA and Sedlacek T (2007) "Free Volume Dependence of Polymer Viscosity" Rheol. Acta., 46:479-494.

Vasile C (2000) Handbook of Polyolefins (Revised and Expanded), Second Edition, Marcel Dekker Inc., New York.

Vasile C and Pascu M (2005) Practical Guide to Polyethylene, Rapra Technology Limited, Shropshire.

Vasile C and Kulshreshtha AK (2003) Handbook of Polymer Blends and Composites, Volume 3, Rapra Tecnology Ltd., Shropshire.

Verweire I, Schacht E, Qiang BP, Wang K and Scheerder ID (2000) "Evaluation of Fluorinated Polymers as Coronary Stent Coating" J. Mater. Sci., 11:207-212.

Wang C, Podgorski M and Bowman CN (2014) "Monodisperse Functional Microspheres from Stepgrowth "Click" Polymerizations: Preparation, Functionalization and Implementation" Mater. Horiz., 1:535-539.

Wang J, Mao G, Ober CK and Kramer EJ (1997) "Liquid Crystalline, Semifluorinated Side Group Block Copolymers with Stable Low Energy Surfaces: Synthesis, Liquid Crystalline Structure, and Critical Surface Tension" Macromolecules, 30:1906-1914.

Wang XJ and Zhou QF (2004) Liquid Crystalline Polymers, World Scientific Publishing Co. Pte. Ltd., Singapore.

Watts PJ, Davies MC and Melia CD "Microencapsulation Using Emulsification/Solvent Evaporation:an Overview of Techniques and Applications" Crit. Rev. Ther. Drug Carrier Syst., 7:235-259.

White RP and Lipson JEG "Polymer Free Volume and Its Connection to the Glass Transition" Macromolecules., 49:3987-4007.

Witschi C and Doelker E (1998) "Influence of the Microencapsulation Method and Peptide Loading on Poly(lactic acid) and Poly(lactic-co-glycolic acid) Degradation During in Vitro Testing" J. Control. Release., 51:327-341.

Wunderlich B (2005) Thermal Analysis of Polymeric Materials ,Springer-Verlag, Berlin.

Xia Z, Trexler M, Wu F, Jean YC and David Van Horn J (2014) "Free-volume Hole Relaxation in Molecularly Oriented Glassy Polymers" Phys. Rev. E., 89: 022603.

Xiang M, Li X , Ober CK, Char K, Genzer J, Sivaniah E, Kramer EJ and Fischer AD (2000) "Surface Stability in Liquid-Crystalline Block Copolymers with Semifluorinated Monodendron Side Groups" Macromolecules, 33:6106-6119.

Yahsi U, Coskun A, Yumak K, Baubakir K and Tav C (2015) "Relaxation Time Of Polypropylene Glycol and Polypropylene Glycol Dimethylether-Like Polymers in Terms Of Fluid-Phase Temperature and Pressure Dependent Hole Fraction" European Polymer Journal, 68:226-232.

Yahsi U, Deligoz H, Tav c, Ulutaş K, Deger D, Yılmazturk S, Erdemci G, Coskun B, Yılmazoglu M and Yakut S (2018) "Ionic Conductivity of PVdF-co-HFP with LiClO4: Free Volume Effects Probing by Positron Annihilation Lifetime Spectroscopy" Radiation Effects and Defects in Solids.

Yahsi U and Sahin F (2004) "Linking the Viscous and Vacancy Behavior of High Molecular Weight Hydrocarbons" Reology Acta, 43(2):189.

Yahsi U, Ulutas K, Tav C and Deger D (2008) "On the Ionic Conductivity of Polymer Electrolytes in terms of Hole Fraction" J. Polym. Sci. B Polym. Phys., 46(20):2249-2254.

Yampolskii YP, Korikov AP, Shantarovich VP, Nagai K, Freeman BD, Masuda T, Teraguchi M and Kwak G (2001) "Gas Permeability And Free Volume Of Highly Branched Substituted Acetylene Polymers" Macromolecules, 34: 1788-1796.

Yang C, Guan Y, Xing J, Shan G and Liu H (2008) "Preparation and Characterization of Monodisperse Superparamagnetic poly(vinyl alcohol) Beads by Reverse Spray Suspension Crosslinking" J. Polym. Sci. Part A: Polym. Chem., 46:203-210.

Yang XY, Chen LT, Huang B, Bai F and Yang XL (2009) "Synthesis of pH-sensitive Hollow Polymer Microspheres and Their Application as Drug Carriers" Polymer, 50:3556-63.

Yang Y (2011) Positron Annihilation Lifetime Spectroscopy Studies of Amorphous and Crystalline Molecular Materials", (PhD. Thesis), Martin-Luther-Universität Halle-Wittenberg.

Yang YY, Chung TS and Ng NP (2001) "Morphology, Drug Distribution and Vitro Release Profiles of Biodegradable Polymeric Microspehres Containing Protein Fabricated by Double-Emulsion Solvent Extraction/Evaporation Method" Biomaterials, 22:231-241.

Yao W, Li Y and Huang X (2014) "Fluorinated poly(meth)acrylate: Synthesis and Properties" Polymer, 55:6197-6211.

Yaparpalvi R, Loyalka SK and Tompson R (1994) "Production of Spherical ZrO$_2$-Y$_2$O$_3$ and ZnO Particles" J. Biomed. Mater. Res., 28:1087-1093.

Yener MY, Basturk E, Madakbas S, Kahraman V, Dumludg F, Umer MA, Yahsi U and Tav C (2018) "Effects of Boron Nitrite in Thermoplastic Polyurethane on Thermal, Electrical and Free Volume Properties" Polymer Bulletin.

Yin J, Han X, Cao Y and Lu C (2014) "Surface Wrinkling on Polydimethylsiloxane Microspheres via Wet Surface Chemical Oxidation" Sci. Rep., 4:5710.

Yin YJ, Xu MX, Chen XL and Yao KD (1996) "Drug Release Behavior of Chitosan/Gelatin Network Polymer Microsphere" Chinese. Sci. Bull., 41:1266-1270.

Yu L, Shi ZZ and Li CM (2015) "Atom Transfer Radical Polymerization to Fabricate Monodisperse poly[glycidyl methacrylate-co-poly (ethylene glycol) methacrylate] Microspheres and Its Application for Protein Affinity Purification" J. Colloid. Interface. Sci., 453:151-158.

Yu Z, Yahsi U, McGervey JD, Jamieson AM and Simha R (1994) "Molecular-weight Dependence of Free Volume in Polystyrene Studied by Positron Annihilation Measurements" J. Polymer Science B: Polymer Physics, 32, 2637-2644.

Zekriardehani S, Jabarin SA, Gidley DR and Coleman MR (2017) "Effect of Chain Dynamics, Crystallinity, and Free Volume on the Barrier Properties of Poly(ethylene terephthalate) Biaxially Oriented Films" Macromolecules, 50: 2845-2855.

Zhang HJ, Sellaiyan S, Kakizaki T, Uedono A, Taniguchi Y and Hayashi K (2017) "Effect of Free-Volume Holes on Dynamic Mechanical Properties of Epoxy Resins for Carbon-Fiber-Reinforced Polymers" Macromolecules, 50:3934-3943.

Zhang J and He JS (2001) "The Interfacial Compatibilization for PSF/LCP Blends by a Maleic Anhydride Modified Polysulfone" Chem. J. Chinese. U., 22:1419-1424.

Zhang M, Lan Y,Wang D,Yan R,Wang S, Yang L and Zhang W (2011) "Synthesis of Polymeric Yolk−Shell Microspheres by Seed Emulsion Polymerization" Macromolecules, 44:842-847.

Zhao XY, Du XY, Liu DS and Zhou QX (2000) "Compatibilization of PPO/LCP Blends by Semi-Interpenetrating Liquid Crystalline Polymer Networks LCP/PS" Macromol. Mater. Eng., 274:36-41.

Zheng Z ,Ma J, Li W , Song J , Liu Y and Xuan L (2008) "Improvements in Morphological and Electro-optical Properties of Polymer-Dispersed Liquid Crystal Grating Using a Highly Fluorine-Substituted Acrylate Monomer" Liq. Cryst., 35:885-893.

Zhuang P, Kyu T and White JL (1988) "Characteristics of Hydroxybenzoic Acid-Ethylene Terephthalate Copolymers and Their Blends with Polystyrene, Polycarbonate, and Polyethylene Terephthalate" Polym. Eng. Sci., 28:1095-1106.

Zhou M, Zhao JZ, Pu WF, Wang X and Yang Y (2012) "Synthesis and Characterization of Salt Resistance Hydrogel Microspheres by Inverse Suspension Polymerization" E-Polymers, 084.

# CURRICULUM VITAE

**Name SURNAME**  **:** Uğur SOYKAN

**Place and Date of Birth** **:** AYDIN- 27.07.1988

<u>**Universities**</u>

**Bachelor's Degree**  **:** Abant İzzet Baysal University

**MSc Degree**    **:** Abant İzzet Baysal University

**e-mail**      **:** ugursoykan@ibu.edu.tr

**Address**     **:** Abant İzzet Baysal University

         Yenicaga Yasar Celik Vocational High School.

**Work and Workplace**  **:** Lecturer, Yenicaga Yasar Celik Vocational High

         School, Food Quality Control and Analysis

         Program.

<u>**List of International Publications**</u>

<u>**a) International Refereed Articles (SCI or SCI-Expanded)**</u>

✓ Cetin S, Sen BO, **Soykan U,** Firat EE and Yildirim G **(2016)** "Experimental and Theoretical Approaches for Structural and Mechanical Properties of Novel Side Chain LCP-PP Graft Coproducts" Turk. J. Chem., 40:467-83.

✓ **Soykan U** and Cetin S **(2015)** "Reinforcement of High Density Polyethylene with a Side Chain LCP by Graft Copolymerization-Thermal, Mechanical and Morphological Properties" J. Polym. Res., 22(11).

✓ Cakir I, **Soykan U**, Cetin S, Karaboga F, Zalaoglu Y, Dogruer M, Terzioglu C and Yildirim G **(2014)** "Electrochemical and Spectroscopic Characteristics of p-Acryloyloxybenzoyl Chloride and p-Acryloyloxybenzoic Acid and Antimicrobial Activity of Organic Compounds" Spectrochim. Acta. A., 132:502-13.

✓ **Soykan U**, Cetin S, Ozturk B, Karaboga F, Zalaoglu Y, Dogruer M, Yildirim G and Tezioglu C **(2013)** "Synthesis and Characterization of p-Benzophenone oxycarbonylphenyl Acrylate by Means of Experimental Measurements and Theoretical Approaches, and Bulk Melt Polymerization" J. Mol. Struct., 1049:479-87.

- ✓ Karaboga F, **Soykan U**, Dogruer M, Ozturk B, Yildirim G, Cetin S and Terzioglu C **(2013)** "Experimental and Theoretical Approaches for Identification of p-Benzophenoneoxycarbonylphenyl Acrylate" Spectrochim. Acta. A., 113:80-91.

## b) Proceeding of International Conferences

- ✓ Behiye Ozturk Sen, Ugur Yahsi, Sedat Cetin, Cumali Tav, Murat Yavuz Yener, **Ugur Soykan (2018) "** Correlation Between Free Volume Holes and Mechanical Properties of Side Chain LCP-HDPE Graft Products" Oral Presentation, International Conference on Application In Chemistry And Chemical Engineering (ICACCHE**)**, 10-14 October 2018.

- ✓ **Soykan U** and Cetin S **(2017)** "Synthesis And Characterization Of Micron-size Crosslinked Microspheres By Inverse Suspension Polymerization Of N-vinylpyrrolidone/Novel Rod Like Diacrylate" Oral Presentation, 1. International Advanced Research and Engineering Congress, 16-18 November 2017.

- ✓ **Soykan U** and Cetin S **(2017)** "Extreme Improvements in The Mechanical Behaviour of High Density Polyethylene with a Semi Fluorinated Novel Compound by Graft Copolymerization" Poster Presentation, Turkish Physical Society, 33rd International Physics Congress, 06-10 September.

- ✓ Karaboga S, **Soykan U**, Yildirim G and Karaboga F **(2017)** "Quantum Chemical Calculations on The Identification of N-(5-acetyl-2-methylphenyl) Quinoline-2-carboxamide", Oral Presentation, Turkish Physical Society 33rd International Physics Congress, 06-10 September.

- ✓ **Soykan U**, Karaboğa S, Yildirim G and Karaboğa F **(2017) "**Solvent Polarity Effect on Self-consistent Field (SCF) Energy, Dipole Moment and Charge Distributions Of N-(5-acetyl-2-bromo¬phen¬yl) Quinoline-2-carboxamide, Oral Presentation, Turkish Physical Society 33rd International Physics Congress, , 06-10 September.

- ✓ Ozturk Sen B, Yahsi U, Tav C, **Soykan U** and Cetin S **(2017)** "Free Volume Properties of Side Chain LCP-HDPE Graft Coproducts Probed by Positron Annihilation Lifetime Spectroscopy" Poster Presentation, The International Joint Science Congress of Materials And Polymers, 25-28 August.

- ✓ Ozturk Sen B, **Soykan U** and Cetin S **(2016)** "Thermal Mechanical And Microstructural and Morphological Properties Of Side Chain LCP-HDPE Graft Coproducts, Poster Presentation, 46th Iupac World Polymer Congress (MACRO 2016), 17-21 July.

- Cetin S, **Soykan U**, Ozturk Sen B and Yildirim G **(2015)** "Experimental and Theoretical Approaches for Identification of 3,3,4,4,5,5,6,6,7,7,8,8,8 Dodecafluoro 5-Methyloctyl 4-Acryloyloxy Benzoate, Poster Presentation, 9th International Physics Conference of The Balkan Physical Union, 24-28 August.

### c) Proceeding of National Conferences

- Ozturk Sen B, **Soykan U** and Cetin S **(2015)** "p-Bifeniloksikarbonilfenil Akrilat ve p-Bifeniloksikarbonilfenil Metakrilatın Izotaktik Polipropilen Üzerine Aşı Kopolimerleşmesi" Poster Presentation, 27. International Chemistry Congress, 23-28 August.

- **Soykan U**, Oztürk Sen B and Cetin S **(2014)** "Aşı Polimerleşmeyle Yüksek Yoğunluklu Polietilenin Yan Zincir Sıvı Kristal Polimer Ile Güçlendirilmesi" Poster Presentation, V. International Polymer Science and Technology Congress, 01-04 September.

- Cakir I, Karaboga F, Zalaoglu Y, **Soykan U**, Dogruer M, Cetin S and Yildirim G **(2014)** "p-Acryloyloxybenzoil Klorür ve p-Akriloyloksibenzoik Asit Moleküllerinin Gıda Kaynaklı Patojen Bakteri ve Biyofilm Oluşturan Mikroorganizmalar Üzerine Antimikrobiyal Etkisi", Oral Presentation, Food Enginering 5. Student Congress, 24-25 April.